

Sec61 interactor analysis by chemical crosslinking

Dissertation

zur Erlangung des Grades

des Doktors der Naturwissenschaften

der Naturwissenschaftlich-Technischen Fakultät

der **Universität des Saarlandes**

von

Fábio A.P. Pereira

Saarland University
Saarbrücken, Germany
2019

Tag des Kolloquium:	22.07.2019
Dekan:	Prof. Dr. Guido Kickelbick
Berichterstatter:	Prof. Dr. Karin Römisch
	Prof. Dr. Dr. Richard Zimmermann
Vorsitzender:	Prof. Dr. Volkhard Helms
Akad. Mitarbeiter:	Dr. Jens Neunzig

Contents

Listing of figures	v
Listing of tables	viii
List of abbreviations	ix
Abstract	xiii
Zusammenfassung	xiv
0 Introduction	1
0.1 Secretory Pathway	2
0.2 Protein Translocation	7
0.2.1 Sec61 channel	7
0.2.2 Targeting	11
0.2.3 Translocation	13
0.2.3.1 Co-translational Translocation	13
0.2.3.2 Post-translational Translocation	16
0.3 Protein Folding and ER Quality Control	18
0.3.1 Folding	18
0.3.2 Quality control	23
0.3.3 UPR	27
0.4 ERAD	29
0.4.1 Recognition and Targeting	30
0.4.2 Ubiquitin ligases - Doa10 and Hrd1	34
0.4.3 Ubiquitination	36
0.4.4 Cdc48	37
0.4.5 Proteasome	39
0.4.6 Retrotranslocon	40
0.5 Protein Interaction and Chemical Crosslinking	45
0.5.1 Protein interaction	45
0.5.2 Crosslinking	47
0.5.3 Mass Spectrometry	49
0.6 Aim of this Study	52

1	Material and Methods	53
1.1	Materials	54
1.1.1	Laboratory equipment and their Suppliers	54
1.1.2	Reagents, Chemicals and their Suppliers	56
1.1.3	Software	62
1.1.4	<i>E. coli</i> Strains	63
1.1.5	<i>S. cerevisiae</i> Strains	64
1.1.6	Plasmids	68
1.1.7	Primers	70
1.1.8	Antibodies	74
1.1.9	Enzymes	75
1.1.10	Media and Buffers	76
1.2	Methods	78
1.2.1	Sterilization	78
1.2.2	Growth of <i>S.cerevisiae</i>	79
1.2.3	Growth of <i>E.coli</i>	79
1.2.4	Polymerase Chain Reaction	79
1.2.4.1	Splice Overlap Extension (SOE) PCR	81
1.2.4.2	Colony PCR	83
1.2.5	Small Scale DNA Extraction	85
1.2.5.1	Isolation of Plasmidic DNA from <i>E.coli</i>	85
1.2.5.2	Isolation of Plasmidic DNA from <i>S.cerevisiae</i>	85
1.2.5.3	Isolation of <i>S.cerevisiae</i> total DNA	86
1.2.6	Agarose Gel Electrophoresis	87
1.2.7	Recovery of DNA Fragments	87
1.2.8	Restriction Digestion of PCR Products and Plasmid DNA	88
1.2.8.1	DNA cleaning	89
1.2.9	Dephosphorylation of Vector DNA	89
1.2.10	Phosphorylation of insert DNA	90
1.2.11	Ligation of Vector DNA and Insert DNA	90
1.2.12	Transformation of <i>E.coli</i> Cells with Plasmidic DNA	91
1.2.12.1	Preparation of Chemically Competent <i>E.coli</i> Cells	91
1.2.12.2	Transformation of chemically competent <i>E. coli</i> cells	91
1.2.13	DNA Sequencing	92
1.2.14	Preparation of Lyticase	92
1.2.15	Transformation of <i>S.cerevisiae</i>	93
1.2.16	Verification of <i>S.cerevisiae</i> Transformants	94
1.2.17	<i>S.cerevisiae</i> Growth on Plates (Drop Test)	94
1.2.18	Isolation of <i>S.cerevisiae</i> RNA	95
1.2.19	Protein Gel Electrophoersis and Western Blot Analysis	96
1.2.19.1	Preparation of Cell Extracts	96

1.2.19.2	Protein Gel Electrophoresis	96
1.2.19.3	Coomassie Staining (Normal)	97
1.2.19.4	Coomassie G-250 Staining (Normal)	97
1.2.19.5	Coomassie Staining for Mass Spectrometry	98
1.2.19.6	Western Blot Analysis	98
1.2.20	Preparation of Rough Microsomal Membranes	99
1.2.21	Small Scale Preparation of Hot Rough Microsomal Membranes	100
1.2.22	<i>HAC1</i> mRNA Splice Assay	101
1.2.23	Cycloheximide chase	103
1.2.24	Pulse-Chase Experiments	103
1.2.24.1	Pulse Labeling	103
1.2.24.2	Chasing	104
1.2.24.3	Immunoprecipitation	105
1.2.25	Chemical Crosslinking	106
1.2.26	Extraction of Luminal and Cytosolic Microsome-Associated Proteins	107
1.2.27	Purification of Sec61	107
1.2.28	Mass Spectrometry	108
1.2.28.1	Sample preparation	108
1.2.28.2	LC-MS/MS	109
1.2.28.3	Data analysis	110
1.2.28.4	Statistical Analysis	110
1.2.29	Mutant Construction	111
1.2.29.1	<i>sec61ΔL7</i> integration in the genomic DNA	111
1.2.29.2	14His-Tagged constructs	113
1.2.29.3	<i>SEC61</i> Loop 5 deletion mutants	113
1.2.29.4	<i>MPD1</i> HA-Tagging	114
1.2.30	Detection of Sec61 Interactors in Radiolabeled Membranes	115
2	Results	117
2.1	Determination of Sec61 and Sec61ΔL7 DSS crosslink pattern	118
2.2	Immunoblotting analysis of Sec61 SDAD crosslink pattern	122
2.3	Immunoblotting analysis of Sec61 SMPH crosslink pattern	130
2.4	Sec61-crosslinked-complex Purification and Analysis	138
2.4.1	Sec61 N-Terminal 14His-tagging	139
2.4.2	Characterization of the 14His-tagged Sec61 forms	144
2.4.3	Crosslink to His ₁₄ -tagged Sec61 and Sec61S353C	151
2.4.4	14His-tagged Crosslink Purification Setup	155
2.5	Liquid Chromatography-tandem Mass Spectrometry and Statistical Analysis	163
2.5.1	Crosslinked Peptide Analysis	172
2.6	Sec61 Interactors Analysis	176

2.6.1	Characterization of Sec61 Interactor Mutants	177
2.6.1.1	She2	183
2.6.1.2	Asi3	187
2.7	Sec61 Hinge Mutants to Evaluate Function of Sec61-Mpd1 Interaction .	189
2.7.1	Sec61 Hinge Deletion Mutant Construction	191
2.7.2	Sec61 Hinge Deletion Mutant Characterization	195
2.8	Mpd1 interaction	203
2.8.1	MPD1 HA tagging	203
2.8.2	Mpd1 interaction with Sec61	206
2.9	Genomic Integration of <i>sec61</i> Δ L7	208
3	Discussion	212
3.1	Crosslinking Setup	214
3.2	Sec61 Purification	220
3.3	Mass Spectrometry Analysis	223
3.4	Functional Analysis	226
3.5	Crosslinked Peptides Identification	230
3.6	Sec61, Mpd1 and ERAD	236
3.7	Concluding Remarks	242
	References	244
	Publication	284
	Acknowledgments	286
	Appendix A Supplements	288

Listing of figures

1	Overview of the secretory machinery	2
2	ER to Golgi and Golgi to ER system representation.	5
3	SNARE mediated Vesicle Fusion	6
4	Sec61 Structure	8
5	Sec61 trimeric complex	9
6	Sec heptameric complex	10
7	Steps of translocation	11
8	Translocation process	14
9	Trans-membrane segments membrane insertion scheme	16
10	Pos-translational translocation scheme	17
11	Nascent chain interaction with luminal chaperones	20
12	Quality control in the ER	23
13	Glycan trimming	25
14	Calnexin/calreticulin cycle	26
15	UPR in yeast	28
16	ERAD pathway scheme	30
17	De-manosilation as foldingsignal	32
18	ERAD L-, M- and C scheme	33
19	Ubiquitin ligases complexes	35
20	Ubiquitylation cascade	37
21	26S Proteasome schematic	39
22	Sec61 retrotranslocon model	42
23	Hrd1 retrotranslocon model	44
24	Scheme of typical setup for mass spectrometry analysis of affinity purified chemical crosslinked samples	47
25	Workflow of standard analysis procedure of mass spectrometry data analysis	51
1.1	General SOE-PCR schematic	82
2.1	DSS structure.	119
2.2	Sec61 DSS crosslink pattern determination.	121
2.3	SDAD structure.	122
2.4	Sec61 SDAD crosslink pattern determination.	124
2.5	Effect of the absence of different protein populations on SDAD crosslink pattern.	127

2.6	Multi-antibody analysis of SDAD crosslink pattern.	128
2.7	SMPH structure.	131
2.8	Sec61 SMPH crosslink pattern determination	132
2.9	Effect of the absence of different protein populations on SMPH crosslink pattern.	133
2.10	Multi-antibody analysis of SMPH crosslink pattern.	134
2.11	Analysis of Δ hrd3 SMPH crosslink and Δ hrd1 and Δ hrd3 Δ gp α F ERAD.	137
2.12	His ₁₄ -tagging Vector.	139
2.13	Constructs obtained by cloning into pRS426-GAL-His ₁₄	141
2.14	Constructs obtained by subcloning 14His-tagged constructs into pRS315.	142
2.15	His ₁₄ -tagged constructs expression confirmation.	143
2.16	Growth rate of 14His-tagged mutants	145
2.17	Temperature and tunicamycin sensitivity of 14His-tagged strains.	147
2.18	UPR activation in the 14His-tagged mutants.	149
2.19	14His-tagged Sec61 forms half life determination.	150
2.20	LC-SPDP structure.	152
2.21	LC-SPDP crosslink pattern determination.	153
2.22	His ₁₄ -Sec61 solubilization test.	156
2.23	Purification system scheme.	159
2.24	Immunoblot and gel staining analysis of purified fractions	162
2.25	Volcano Plot	167
2.26	Interaction Grid	170
2.27	Protein abundance/Enrichment	171
2.28	xQuest/xProphet pipeline analysis scheme	172
2.29	xQuest/xProphet Sec61xMpd1 crosslink report	175
2.30	Temperature and tunicamycin sensitivity test of Δ asi3, Δ ynr021w, Δ psg1, and Δ she2 mutants.	177
2.31	Import dynamics in Δ asi3, Δ ynr021w, Δ psg1, and Δ she2.	179
2.32	Translocation defect assay	181
2.33	Kww and Khn ERAD dynamics in Δ asi3, Δ ynr021w, and Δ psg1 backgrounds.	183
2.34	SMPH crosslink pattern determination in <i>sec61S353C</i> / Δ she2	184
2.35	Mid2 import and maturation analysis.	185
2.36	Erg11 degradation dynamics analysis.	188
2.37	Structure of Sec61 channel in closed and opened state.	189
2.38	Alignment of loop 5 hinge region	190
2.39	Hinge mutants construction scheme	192
2.40	Hinge mutants constructs scheme	193
2.41	Hinge mutants correct expression test	194
2.42	Growth rate of <i>sec61</i> hinge mutants mutants	195

2.43	Temperature and tunicamycin sensitivity of <i>sec61</i> hinge mutants strains.	196
2.44	UPR activation in the <i>sec61</i> hinge mutants.	197
2.45	Protein steady state levels	198
2.46	Analysis of ER import in <i>sec61</i> hinge mutants	199
2.47	KWW and KHN ERAD dynamics determination.	201
2.48	$\Delta gp\alpha F$ and Cpy* ERAD dynamics determination.	202
2.49	<i>MPD1</i> gene scheme	204
2.50	<i>MPD1</i> HA-tagging cassette	205
2.51	Mpd1-HA expression test	206
2.52	Mpd1-Sec61 direct interaction determination.	208
2.53	Chromosomal integration of <i>sec61</i> $\Delta L7$	210
2.54	Chromosomal integration of <i>sec61</i> $\Delta L7$	211
3.1	Structure of Sec61, Sec71 and Sec72 when in complex	217
3.2	Sec61 and Sec63 structure	233
3.3	Structure of Mdp1 compared to Pdi1	240
3.4	Mpd1-Sec61 interaction model	242
A.1	Sec61 SDAD crosslinking pattern determination	289
A.2	SDAD conditions titration	289
A.3	Sec61 SDAD crosslinking pattern determination	290
A.4	Immunoprecipitation of crosslinked samples	290
A.5	SMPH concentration titration	291
A.6	SMPH crosslinking pattern determination by multi-antibody immunoprecipitation	291
A.7	SMPH crosslinking pattern determination in permeated cells	292
A.8	Constructs obtained by cloning into pRS426-GAL-His ₁₄ (continuation).	292
A.9	Constructs obtained by subcloning 14His-tagged constructs into pRS315.	293
A.10	Growth rate of 14His-tagged mutants in minimal medium	293
A.11	Protein total amount after purification	294
A.12	Purification buffers test	295
A.13	Purification system test	296
A.14	MA plot	297
A.15	Secondary comparisons Volcano plots	298
A.16	Secondary comparisons MA plots	299
A.17	Nsg1 degradation dynamics analysis.	299
A.18	Erg11 degradation dynamics analysis by cyclohexemide chase	300

Listing of tables

1.1	Laboratory Equipment	54
1.2	Reagents, chemicals and consumables	56
1.3	Software used in this study	62
1.4	<i>E. coli</i> strains	63
1.5	<i>S. cerevisiae</i> strains	64
1.6	Plasmids	68
1.7	Primers	70
1.8	Antibodies	74
1.9	Enzymes used in this study and their sources	75
1.10	<i>S.cerevisiae</i> growth media routinely used in this study	76
1.11	Composition of Synthetic Complete amino acid drop-out mixture for <i>S.cerevisiae</i>	77
1.12	<i>E.coli</i> growth media routinely used in this study	78
1.13	Standard reaction mixture for PCRs	80
1.14	Standard thermal cycler program for PCRs	81
1.15	Genral setup of SOE-PCR for the generation of the <i>sec61</i> mutants.	83
1.16	Standard colony PCR reaction mixture	84
1.17	Standard thermal cycler program for colony PCRs	84
1.18	Standard reaction mixture for the restriction of DNA.	88
1.19	Reaction mixture for the dephosphorylation of digested vector DNA.	89
1.20	Reaction mixture for the dephosphorylation of digested vector DNA.	90
1.21	Standard reaction mixture for the ligation of vector and insert DNNA.	91
1.22	Reverse transcription reaction mixture.	102
1.23	Standard reaction mixture for PCRs	115
2.1	Tested purification Buffers	157
2.2	Purification program.	160
2.3	List of samples analysed by LC-MS/MS	164
2.4	Shortlisted hits	168

List of abbreviations

3gpαF	Triply glycosylated pro alpha factor
A	Alanine
AAA-ATPase	ATPase associated with diverse cellular activities
Ade	Adenine
Asn	Asparagine
Atf6	Activating transcription factor 6
ATP	Adenosine triphosphate
BiP	Immunoglobulin binding protein
C	Cysteine
C-terminal	Carboxy terminal
C-terminus	Carboxy terminus
CaCl₂	Calcium chloride
Cdc48	Cell division control protein 48
Cne1	Calnexin and calreticulin homolog
ConA	Concanavalin A
COPI/II	Coat protein complex I/II
CPY	Carboxypeptidase Y
Cryo-EM	Cryo-electron microscopy
D	Aspartic acid
DEPC	Diethyl pyrocarbonate
Der1/3	Degradation in the ER protein 1/3
DMSO	Dimethyl sulfoxide
DNA	Deoxyribonucleic acid
Doa10	Degradation of alpha 2 protein 10
DPAPB	Diaminopeptidase B
DSS	Disuccinimidyl suberate
DTT	Dithiothreitol
E	Glutamic acid
E. coli	Escherichia coli
E3	Ubiquitin-protein ligase
EDTA	Ethylene diamine tetraacetic acid
eIF2α	Eukaryotic translation initiation factor 2 subunit alpha
ELISA	Enzyme-linked immunosorbent assay
Eq	Equivalent
ER	Endoplasmic reticulum

ERAD	ER-associated degradation
ERES	ER exit sites
ERGIC	ER-Golgi intermediate compartment
ERp57	ER-resident protein 57
ERQC	ER quality control
F	Phenylalanine
G	Glycine
GlcNAc2-Man9-Glc3	N-acetylglucosamine-2-Mannose-9-Glucose-3
GTP	Guanosine triphosphate
h	Hour(s)
H	Histidine
HA	Hemagglutinin A
Hac1	Homolog to Atf/Creb1
HCl	Hydrochloric acid
HDEL	His-Asp-Glu-Leu
HEPES	4-(2-hydroxyethyl)-1-piperazineethanesulfonic acid
His	Histidine
Hrd1/3	HMG-CoA reductase degradation protein 1/3
Hsp70	70 kilodalton heat shock protein
Htm1	Homolog to ER mannosidase 1
I	Isoleucine
IMAC	Immobilized metal ion affinity chromatography
IP	Immunoprecipitation
IPTG	Isopropyl-β-D-thio-galactopyranoside
Ire1	Inositol-requiring protein 1
K	Lysine
KAc	Potassium acetate
Kar2	Karyogamy protein 2
KCl	Potassium chloride
kD	Kilodalton
KOAc	Potassium acetate
L	Leucine
LB	Lysogeny broth
LC-SPDP	succinimidyl 6-[3'-(2-pyridyldithio)-propionamido] hexanoate
Leu	Leucine
LiAc	Lithium acetate
Lys	Lysine
M	Methionine
MES	2-(N-morpholino)ethanesulfonic acid
Mg(OAc)₂	Magnesium acetate

MgSO₄	Magnesium sulphate
min	Minute(s)
MnCl₂	Manganese chloride
MOPS	3-(N-morpholino)propanesulfonic acid
MQ H₂O	ultrapure water
mRNA	Messenger RNA
N	Asparagine
N-terminal	Amino terminal
N-terminus	Amino terminus
Na₂CO₃	Sodium carbonate
NaAc	Sodium acetate
NaCl	Sodium chloride
NHS	N-hydroxysuccinimide
OD	Optical density
ORF	Open reading frame
OST	Oligosaccharyl transferase
PCR	Polymerase chain reaction
Pdi1	Protein disulfide isomerase
PEG	Polyethylene glycol
PERK	Protein kinase RNA-like ER kinase
PMSF	Phenylmethylsulfonyl fluoride
Pmt 1-7	Protein O-mannosyltransferase
ppαF	Prepro alpha factor
PPI	Protein-protein interaction
PTM	Post-translational modification
Q	Glutamine
QC	Quality control
RING	Really interesting new gene
RNC	Ribosome-nascent chain complex
RP	Regulatory particle
Rpt2	Regulatory Particle Triphosphatase 2
RT	Room temperature
S	Serine
<i>S. cerevisiae</i>	<i>Saccharomyces cerevisiae</i>
Sar1	Secretion-Associated, Ras-related
Sbh1	Sec61 beta homolog 1
SDS	Sodium dodecyl sulfate
SDS-PAGE	SDS-polyacrylamide gel electrophoresis
SEC	Size exclusion chromatography
Sec61/62/63/71/72	Protein transport protein Sec61/62/63/71/72
sec	Second(s)

Ser	Serine
SMPH	Succinimidyl-6-[(β -maleimidopropionamido)hexanoate]
SNARE	Soluble NSF Attachment Protein Receptor
Snd1/2/3	SRP-independent targeting protein 1/2/3
SP	Signal peptide
SR	SRP receptor
SRP	Signal recognition particle
Ssh1	Sec sixty-one homolog 1
Sss1	Sec sixty-one suppressor 1
T	Threonine
TAP	Tandem-affinity purification
TAE	Tris, acetate, EDTA
TBS	Tris-buffered saline
TBS-T	0.1% Tween 20 TBS
TCA	Trichloroacetic acid
TE	Tris-EDTA
tER	Transitional ER
TGN	Trans-Golgi network
Thr	Threonine
Tm	Tunicamycin
TMD	Transmembrane domain
Tm [°C]	Melting temperature
TPR	tetratricopeptide
tRNA	Transfer RNA
Trp	Tryptophan
Ts	Temperature sensitivity
Ubx2	Ubiquitin regulatory X domain-containing protein 2
Ufd1	Ubiquitin fusion degradation protein 1
UPR	Unfolded Protein Response
UPRE	UPR element
Ura	Uracyl
Usa1	U1 Snp1-associating protein
V	Valine
XBP1	X-box binding protein 1
Y	Tyrosine
Yos9	Yeast OS-9 homolog
YP	Yeast peptone
YPD	Yeast peptone dextrose
YPGal	Yeast peptone galactose

Sec61 interactor analysis by chemical crosslinking

Abstract

The Sec61 complex is a heterotrimeric complex responsible for the translocation of secretory proteins through the endoplasmic reticulum (ER) membrane. Sec61, the pore forming subunit of the channel, is a transmembrane protein with 10 transmembrane domains. Its luminal loops are mostly short, with the exception of L5, which is the hinge that allows channel opening, and a large luminal loop (L7). Proteins that misfold in the endoplasmic reticulum are transported back to the cytosol for ER-associated degradation (ERAD). The Sec61 channel is also one of the candidates for the retrograde transport conduit.

In this work I developed and optimized a chemical crosslinking setup using ER membranes. Upon purification and mass spectrometry analysis of crosslinked samples I was able to identify new Sec61 interactors. In addition to known interactors I detected new interactions with ERAD factors including Cue1, Ubc6, Ubc7, Asi3, and Mpd1. I show that a substrate dependent on Asi3 for degradation (Erg11), is also Sec61 dependent. Moreover, I show that the CPY* ERAD factor Mpd1 binds to the luminal Sec61 hinge region. Deletion of the Mpd1 binding site reduced the interaction between both proteins and caused an ERAD defect specific for CPY* without affecting protein import into the ER or ERAD of other substrates. My data suggest that Mpd1 binding to Sec61 is a prerequisite for CPY* ERAD and confirm a role of Sec61 in ERAD of misfolded secretory proteins

Sec61 interactor analysis by chemical crosslinking

Zusammenfassung

Der Sec61-Komplex ist ein heterotrimerer Proteinkomplex, der sekretorische Proteine ins Endoplasmatische Retikulum (ER) transloziert. Die porenbildende Untereinheit des Komplexes, Sec61, hat 10 Transmembrandomänen. Die meisten ER-luminalen Loops von Sec61 sind kurz, bis auf L5, das die Verbindung oder Angel zwischen der N- und der C-terminalen Hälfte des Kanals bildet, um die sich die N-terminale Hälfte bei der Kanalöffnung bewegt, und den langen L7. Proteine, die im ER fehlfalten, werden zum Abbau zurück ins Zytosol transportiert (ER-assoziierte Degradation, ERAD). Der Sec61 Kanal ist einer der Kanal-Kandidaten für den retrograden Proteintransport.

In meiner Arbeit habe ich eine chemische Crosslinking-Methode für Sec61-Interaktoren ausgearbeitet und optimiert für Mikrosomen. Ich reinigte die Sec61-Komplexe und analysierte ihre Komponenten durch Massenspektrometrie. Es gelang mir, neue ER-lumenale Interaktionspartner von Sec61 zu identifizieren. Zusätzlich zu bekannten Sec61-bindenden Proteinen detektierte ich ERAD-Faktoren in den Sec61-Komplexen wie Cue1, Ubc6, Ubc7, Asi3 und Mpd1. Ich habe gezeigt, dass der Ubiquitinligase Asi3-abhängige Abbau von Erg11 ebenfalls abhängig ist von Sec61. Weiterhin habe ich gezeigt, dass der CPY*-spezifische ERAD-Faktor Mpd1 an den luminalen L5 von Sec61 bindet. Deletion der Mpd1-Bindestelle in L5 reduzierte die Interaktion zwischen Sec61 und Mpd1 und führte zu einem ERAD-Defekt für CPY* ohne ER-Import oder ERAD anderer Substrate zu beeinträchtigen. Meine Daten zeigen, dass Mpd1-Interaktion mit Sec61 eine Voraussetzung für CPY*-ERAD ist, und bestätigen eine Beteiligung von Sec61 am ERAD fehlgefalteter sekretorischer Proteine.

0

Introduction

0.1 Secretory Pathway

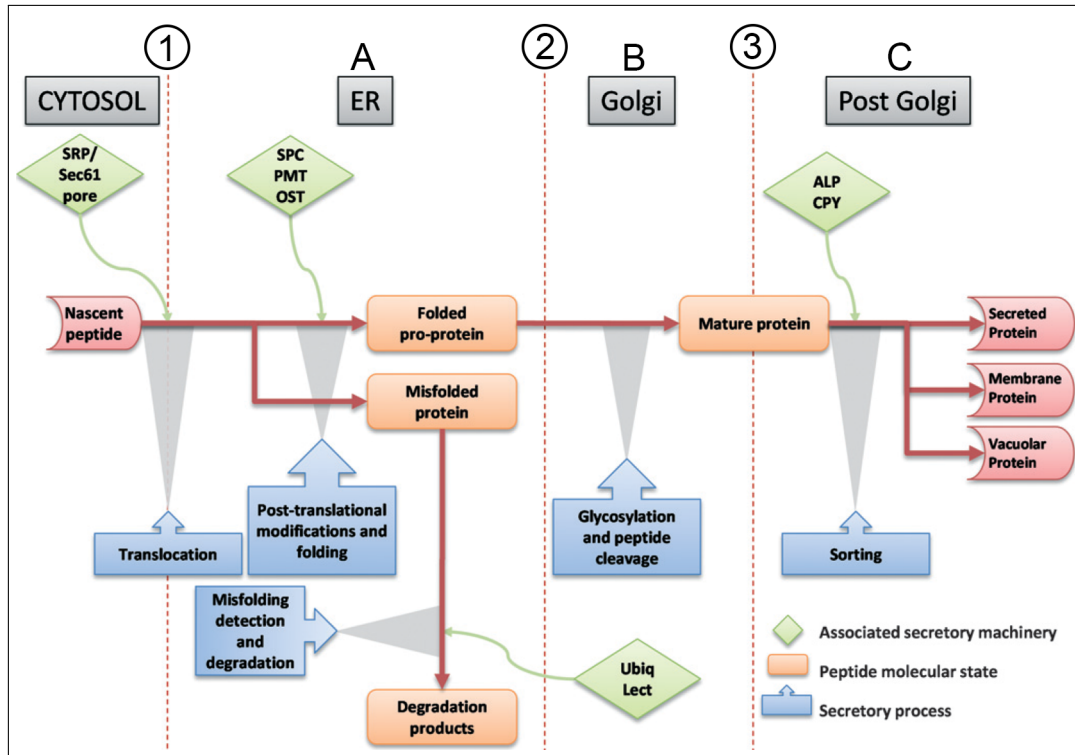


Figure 1: Overview of the secretory machinery. Figure from Hou et al. [165]. The nascent peptide is folded and modified through different mechanisms until it reaches an appropriate structure to perform its functions as a protein. SRP, signal recognition particle; SPC, signal peptidase complex; PMT, protein O-mannosyl transferase; OST, oligosaccharyl transferase; Ubiquitin, Ubiquitin; Lectin, Lectin; ALP, arginine transporter pathway; CPY, carboxypeptidase Y pathway.

Protein secretion is an essential process in both prokaryotes and eukaryotes. Unlike prokaryotes that only secrete proteins into the periplasmic space or exterior of the cell, eukaryotic cells possess a complex endomembrane system (i.e. organelles) that is functionally interconnected [414]. This means that in practice the cell is compartmentalized into multiple organelles, with different structures and local environments that are associated with different functions, protein contents and redox conditions [91]. Loosely speaking a cell might be compared to a factory. As any factory, it possesses

different departments (i.e organelles) that communicate between each other and that possess their unique machinery and function (e.g proteins).

Although this compartmentalization brings numerous advantages, it also creates the necessity for a shuttling system of products and effectors between compartments, as well as with the exterior. The pathway responsible for this process is the Secretory Pathway. It is estimated that in an eukaryotic cell approximately 30 % of all protein produced go through at least one step of this pathway [76].

The scheme depicted in Figure 1 shows the general structure of the secretory pathway and its main checkpoints and events, where vertical dotted lines represent membrane barriers that have to be transposed either by translocation (cytosol to ER; Figure 1, step 1) or vesicle budding and fusion events (ER to Golgi and Golgi to downstream; Figure 1, step 2 and 3, respectively).

The secretory pathway starts with protein translocation into the endoplasmic reticulum (ER), either co- or post-translationally (Figure 1, step 1). In *S. cerevisiae*, the ER presents two morphologies: the perinuclear ER or nuclear envelope and the peripheral or cortical ER. Perinuclear ER is formed by membrane sheets that enclose the nucleus, while the cortical ER is a highly dynamic network of interconnected tubules that lines the cell periphery [300]. Protein translocation across the ER membrane is mediated mainly by the Sec61 channel, either the Sec61 trimeric complex (Sec61, Sbh1 and Sss1) when done co-translationally or by the heptameric Sec complex (Sec61 trimeric complex plus Sec63 heptameric complex -Sec62, Sec63, Sec71 and Sec72) when done post-translationally. In both cases the pore forming sub-unit of the complex is Sec61 [469, 258]. This subject will be addressed more thoroughly further ahead (Section 0.2).

After translocation into the ER lumen, proteins are targeted by a series of chaper-

ones that facilitate folding, like Kar2, or processed by glycosylation (oligosaccharyl-transferase (OST) complex) and disulfide bond formation (Pdi1) [76] (Figure 1, stage A). The matter will be discussed in more detail in Section 0.3.2. At this stage, proteins enter a long process of processing and quality control (QC) steps that ensures correct folding as misfolded proteins have an extremely toxic effect [80, 392]. In fact, many of the chaperones involved in protein maturation serve themselves as checkpoints where any signal of misfolding, like delay in processing, ensues either remediation or degradation of the misfolded form [449]. If proteins are deemed irreversibly incorrectly folded, they must be degraded. This degradation is done by a process called endoplasmic reticulum associated degradation (ERAD) that recognizes and retrotranslocates this misfolded protein to the cytoplasm for proteasome-dependent degradation [296] (subject delft in more detail in Section 0.4).

Some proteins are ER resident, and after translocation and processing they do not need to go any further. Soluble or membrane proteins targeted for other cellular compartments or for secretion, however, must continue further through this pathway and enter the Golgi apparatus (Figure 1; step 2). Once deemed correctly processed by ER QC, they became available for further traffic through the secretory pathway (Figure 2, step 2). In ER to Golgi transport, proteins meant for transport accumulate at discrete sites called transitional ER (tER) or ER exit sites (ERES) [324, 359]. *Saccharomyces cerevisiae* lacks discrete tER sites and cargo proteins leave the ER membrane from many small tER which are distributed all over the ER [324, 57].

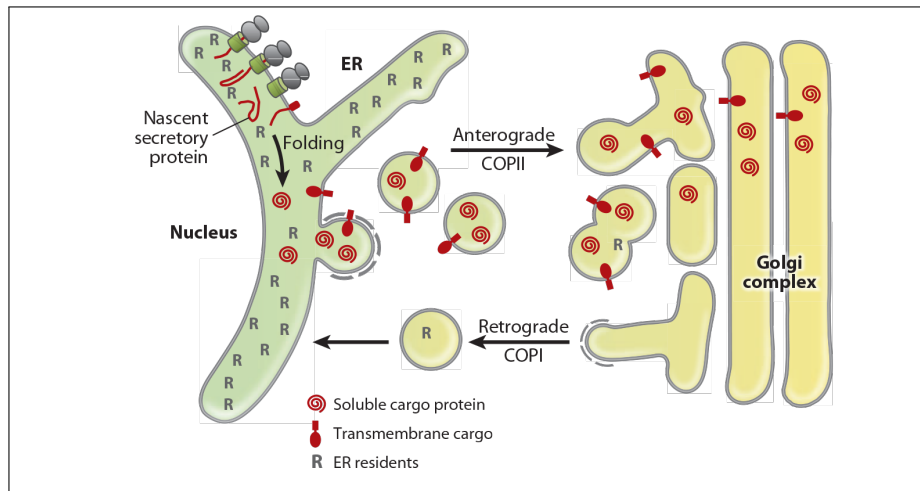


Figure 2: ER to Golgi and Golgi to ER system representation. Figure extracted from Dancourt & Barlowe [71]. Model depicting bidirectional transport between the endoplasmic reticulum (ER) and Golgi compartments. COPI and COPII- coat protein complex I and II. R- ER resident proteins.

Transport is then done by means of a vesicle-shuttling system. These vesicles are responsible for moving secretory proteins forward in the secretory pathway without perturbing the functional segregation conferred by organelles [129, 414] (Figure 2). In anterograde transport, COPII-coated vesicles are responsible for transport. COPII coat comprises five subunits: Sar1–GTP, dimeric Sec23/Sec24, and tetrameric Sec13/Sec31 [13, 378]. This complex is responsible not only for the budding of the cargo vesicle but also by the selective incorporation of correctly folded and assembled secretory and membrane proteins into the formed vesicles [13, 27, 93].

After ER-budding, vesicles must fuse with the target downstream organelle, the Golgi. In mammalian cells, an intermediary structure called ERGIC is formed between ER and the *cis*-Golgi [167]. This structure results from the fusion of multiple COPII vesicles [167, 414]. In yeast, however, COPII vesicles fuse directly with the *cis*-Golgi cisternae [414]. Vesicle fusion with the membranes depends on a set of membrane-bound Soluble NSF Attachment Protein Receptor (SNARE) proteins [373, 53]. When

SNARE proteins associate into a complex, they form elongated four-helical bundles with a high degree of stability that mechanically pull the membranes closer together and results in the formation of a fusion pore (Figure 3)[174, 98].

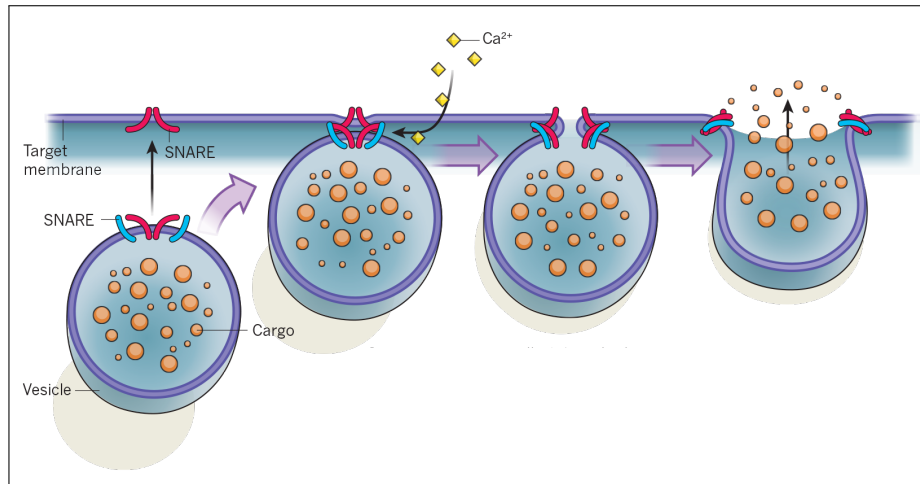


Figure 3: SNARE mediated Vesicle Fusion. Based on figure from Ferro-Novick & Brose [98]. Illustration of SNARE mediated vesicle fusion.

Unlike most eukaryotic cell types, *S. cerevisiae*'s Golgi complex is not arranged in coherent stacks. Instead, its composed of a collection of single, isolated cisternae scattered throughout the cytoplasm that can only occasionally associate with one another [300, 323]. Based on protein content, these cisternae can be classified as *cis*, *medial*, *trans* or *trans-Golgi Network (TGN)* [360, 228]. In the different Golgi cisternae, secretory proteins undergo processing in compartment-specific manner (e.g outer-chain carbohydrate modifications, proteolytic processing) (Figure 1, stage B). For glycoproteins, for example, the core carbohydrate is extended by addition of α -1,6-mannose in the *cis*-Golgi and of α -1,2- and α -1,3-mannose in the medial compartment [76]. Once the *trans*-Golgi cisternae are reached, and secretory proteins are deemed correctly folded, the Golgi is also responsible for sorting them to their correct

location by vesiculation (Figure 1, stage C) [414] .

This vesicle-shuttling system, however, is characterized by its bidirectionality, meaning that not only vesicles migrate in the ER-Golgi direction in COPII-coated vesicles (i.e anterograde transport) for further processing and secretion, but also in the Golgi-ER direction (i.e retrograde transport) by COPI-coated vesicles (Figure 2) [129, 414]. The COPI complex, or coatomer, is composed by seven subunits (α , B , B' , γ , δ , ϵ , and ζ -COP), which are recruited as an intact complex to membranes [143]. One of the main roles of the COPI-coated vesicles is the retrieval to the ER or to previous Golgi cisternae (*trans* to *cis* transport) of transport machinery and escaped ER residents [129, 414, 87]. The COPI-mediated retrieval of ER resident proteins uses specific sorting signals, namely the retrieval motifs HDEL (His-Asp-Glu-Leu) for luminal cargo and K(X)KXX for membrane proteins [64].

Ultimately, the cell maintains its organelle structure, function, and homeostasis by modulating early secretory pathway flux of proteins and lipids [14].

0.2 Protein Translocation

0.2.1 Sec61 channel

As mentioned in the previous section, about one third of the eukaryotic proteome, namely secretory and transmembrane proteins, reside within the endomembrane system [59], and thus cycle through the ER. For this purpose, proteins have to either cross or integrate into the ER membrane [353, 270]. This is achieved in either a co- or posttranslational manner, mainly, with the help of a proteinaceous aqueous channel, the Sec61 channel [281].

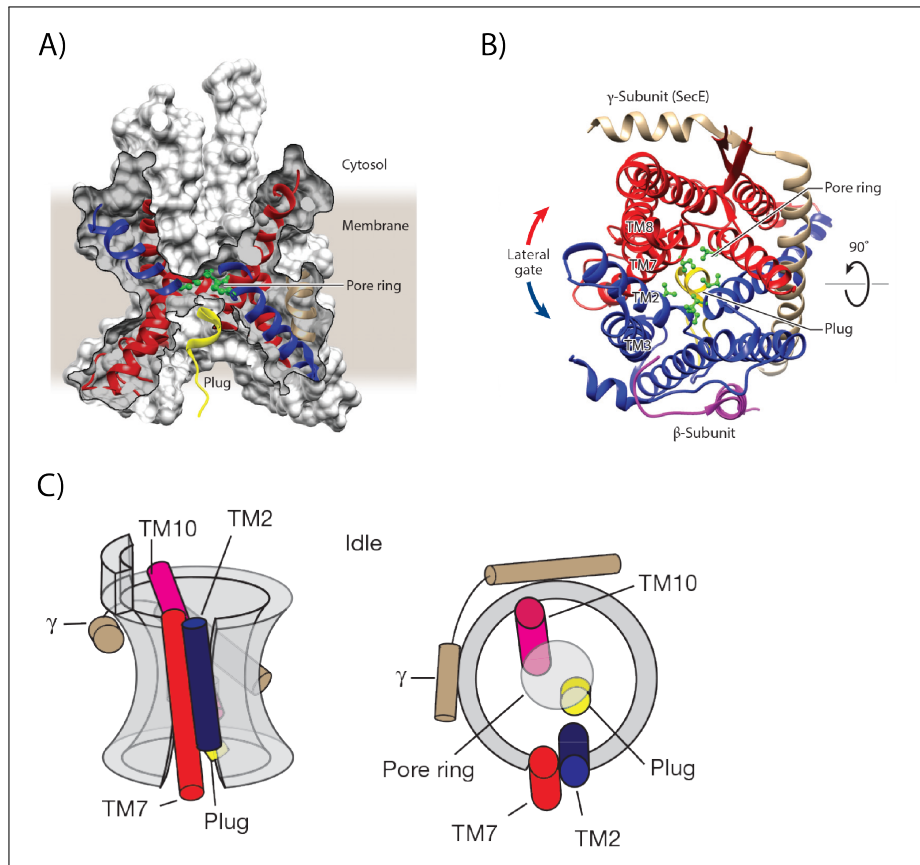


Figure 4: Sec61 Structure. A) Cutaway side view of a space-filling model of the idle SecYE β channel from *Methanocaldococcus jannaschii* (PDB code 1RH5) in the membrane. Pore ring in green and Plug domain in yellow. TM7/TM8 and TM2/TM3 in red and blue, respectively. Figure from Rapoport et al. [310] B) Crystal structure of the idle SecY channel from *Methanocaldococcus jannaschii* (PDB code 1RH5) as seen from above. Same colour code as in A. SecE (brown) and Sec β (purple) are also visible. Figure from Rapoport et al. [310]. C) Schematic representation of the channel as seen from the side (left) and from above (right). Same colour code as A and B with the addition of TM10 being represented in Magenta. Figure from Gogala et al. [127].

A breakthrough on the mechanistic insights into the Sec complex function were obtained by the resolution of the x-ray structure of the archaeal-bacterial SecY complex which revealed that SecY (Sec61 in yeast and Sec α in mammals) is divided into two bundles of five transmembrane domains (TMD). These two bundles form an hourglass-shaped pore, in which the loop between TMD5 and TMD6 serves as a hinge [404, 400, 84] (Figure 4 A).

The middle constriction, called the pore ring (Figure 4 A; green), consists of conserved hydrophobic residues. On the luminal side the pore is sealed by a short helical plug domain (TMD2a) (Figure 4 A; yellow) [313, 310]. This two structures (the pore ring and plug) guarantee that the channel is sealed, preventing ion and metabolite leakage, thus maintaining membrane integrity [280]. The plug was also shown to be important for efficient protein translocation, signal anchor protein orientation, and Sec61 complex stability [184, 183].

Another interesting structure of the channel is its lateral gate, located opposite to the hinge, and formed by TMD2b and TMD7. It is bordered by segments of TMD2 and TMD3 on one side and by segments of TMD7 and TMD8 on the other (Figure 4 B and C; blue and red, respectively) [404, 234]. This lateral gate serves as signal peptide binding site during translocation early stages and allows TMDs of nascent chains to partition into the lipid bilayer [292, 149, 127].

Translocation through the Sec61 channel can happen either co-translationally (i.e concomitant with protein synthesis) or post-translationally (i.e after termination of protein synthesis).

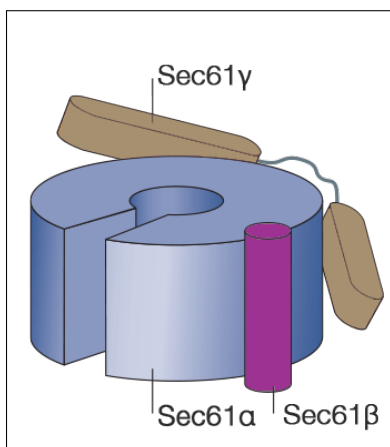


Figure 5: Sec61 trimeric complex. Schematic representation of the Sec trimeric complex. Figure from Cross et al. [69].

For co-translational translocation, Sec61 associates in a trimeric complex with Sbh1 (Sec61 β in mammals) and Sss1 (SecE in bacteria, Sec61 γ in mammals) [278, 442, 188, 153]. Sss1 contains an amphipathic helix that lies flat on the cytosolic surface of the ER membrane, and a TMD that diagonally crosses the membrane, holding the two halves of the Sec61 together (Figure 4 B and C, and 5; brown). It has been proposed to act as a “clamp” that holds both halves of the SecY/Sec61 together, thus stabilizing the open or closed state [90, 404]. Sbh1 is a tail anchored protein with an unstructured cytosolic domain (Figure 4 B and 5; purple) [404, 424]. Both its trans-membrane helix and its cytosolic domain interact with Sec61 [424, 465].

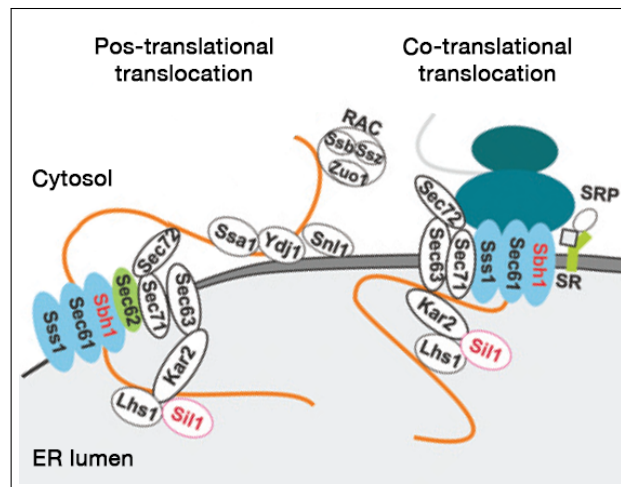


Figure 6: Sec heptameric complex. Schematic representation of the Sec complex during both post-translational (heptameric complex; left) and co-translational (trimeric complex; right) translocation. Figure from Delic et al. [76].

In eukaryotes, a requirement for post-translational transport is the association of the Sec61 complex with the Sec63 complex [248, 277], which consists of Sec63, Sec62, Sec71, and Sec72 [79, 44], forming the heptameric Sec complex (Figure 6, left). Indeed, gating of the Sec61 translocon by Sec63 in a precursor dependent fashion is hypothesized [214]. Also, over-expression of Sec63 decreases steady-state

levels of multi-spanning membrane proteins, pointing to a potential regulatory function [232].

0.2.2 Targeting

The first step of protein translocation, either co- or post-translational, is the recognition of the to-be translocated peptide and its targeting to the translocon (Figure 7). Both processes depend on the recognition of a N-terminal signal peptide (SP) composed by three domains: a net positive charge in the N-terminal region; a central hydrophobic H-region; and a polar C-terminal region defining the signal peptidase cleavage site [417, 147]. The general architecture of signal peptides is conserved [416]. Their primary sequence and length, however, vary substantially [418]. After translocation the signal peptide is removed by signal peptidase.

For the movement of signal peptides into the phospholipid bilayer, the hydrophobicity of the H region is recognized by a hydrophobic patch of the lateral gate [423].

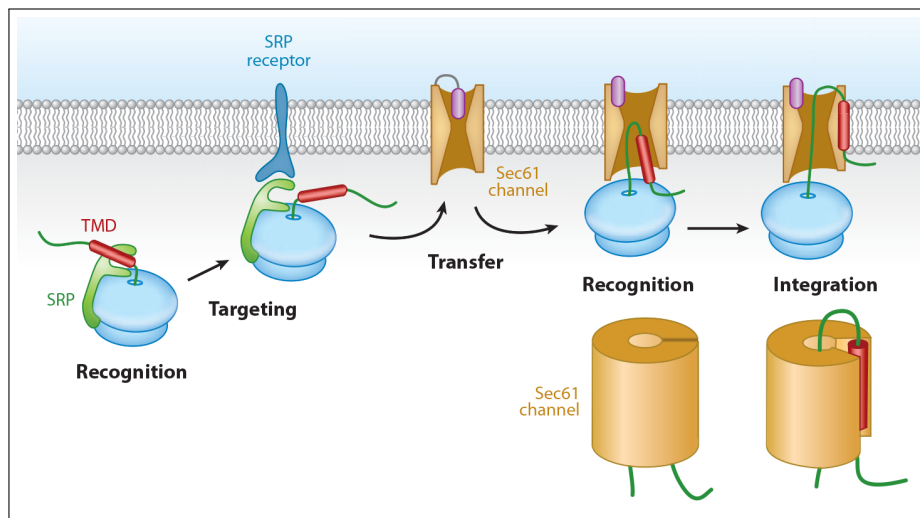


Figure 7: Steps of translocation. Schematic representation of the steps necessary for co-translational translocation. SRP - Signal Recognition Particle. TMD - Transmembrane Domain. Figure from Shao & Hegde [353].

The targeting for the co-translational translocation route begins in the cytosol when the first hydrophobic element in the nascent polypeptide, either an N-terminal signal peptide or the first TMD is recognized by the signal recognition particle (SRP) (Figure 7; Recognition) [426, 352, 136]. This recognition causes high affinity binding of SRP to the ribosome and an arrest of chain elongation, increasing the time during which the nascent chain remains competent for translocation [426, 447]. Targeting of the ribosome/nascent-chain/SRP complex to the translocon occurs via an initial interaction between SRP and the ER-localized SRP receptor (SR) (Figure 7; Targeting) [123, 247] encoded by SRP101 and SRP102 in yeast [271]. This interaction causes SRP displacement from the signal peptide and a concomitant release of the elongation arrest [121]. The ribosome-SR complex then transfers the nascent chain to Sec61 and translation resumes (Figure 7; Transfer and Recognition) [440]. Supporting this hypothesis, is the biochemical and genetic evidence showing that the SR directly interacts with the Sec61 complex [180, 376].

In this model, the Sec61 complex acts as a receptor for the ribosome via its cytosolic loops [60] and the alignment of the ribosomal tunnel with the central pore of the translocon allows direct movement of the nascent chain from the ribosomal tunnel exit across or into the membrane (Figure 7; Recognition and Integration) [18, 19]

Generally speaking, membrane proteins and SP preferentially engage the SRP-dependent pathway due to their high hydrophobicity. SP of lower hydrophobicity, however, depend on a Sec complex-mediated post-translational translocation [258].

The targeting of proteins for post-translational translocation is less well understood. They escape recognition by SRP, either because they are too short to engage SRP before their synthesis is completed, or due to less hydrophobic signal peptides [310]. Indeed, the heptameric Sec complex subunit Sec62 has been suggested to act as

a targeting receptor for small presecretory proteins with comparatively short and apolar signal peptides [212, 214]. Likewise, the Sec72 component, which possesses a tetratricopeptide repeat (TPR) domain, was also shown to interact with an Hsp70, suggesting it may act as a target receptor [398].

However, signal peptides have a dual function: they do not only target pre-secretory proteins to the Sec61 complex; they also trigger the opening of the Sec61 pore forming subunit for passage of the nascent polypeptide [445, 404, 63].

0.2.3 Translocation

In the quiescent state, the Sec channel is closed both axially across the membrane and laterally toward the lipid bilayer [422, 423]. Nevertheless, for both co- and post-translational import the channel must open longitudinally.

0.2.3.1 Co-translational Translocation

During co-translational import the initial trigger for channel priming is ribosome arrival. The cytosolic loops 6 and 8 of Sec61 interact with the RNC at the polypeptide exit site on the large ribosomal subunit [60, 17, 422]. Ribosomal interaction induces shifting of these transmembrane helices, resulting in a cracking of the cytosolic half of the lateral gate. This both destabilizes the interaction between helices 2 and 7 (responsible for the closed state of the lateral gate) and exposes a seam of hydrophilic residues to the hydrophobic bilayer. Thus, ribosome binding, constrains Sec61 in a destabilized state relative to the quiescent channel [424]. Structural analysis of the mammalian translocon also suggested that simple ribosome binding was sufficient to induce lateral gate opening [284]. Alternative data, however, showed that in the SecY channel ribosome binding causes only minor alterations, and that it is the SP binding that causes struc-

tural modifications [279, 215].

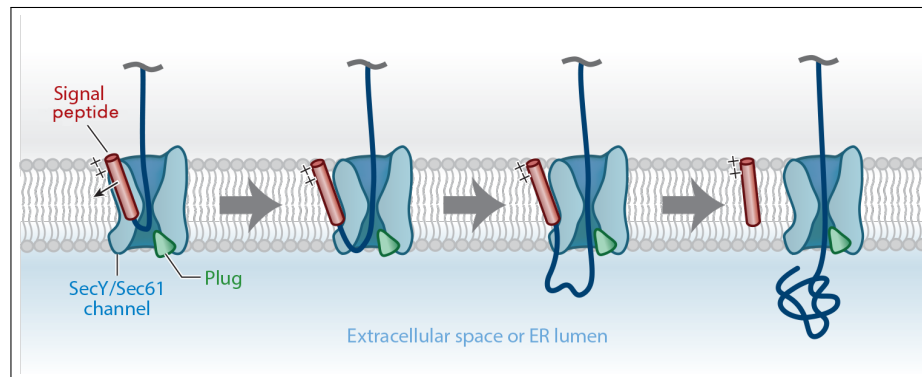


Figure 8: Translocation process. Schematic representation of the stages of protein translocation through the Sec61 channel. Based on figure from Rapoport et al. [310].

As the hydrophobic signal peptide approaches the channel, it is faced with a predominantly hydrophilic environment: the aqueous pore of Sec61 and the polar head-groups of the lipid bilayer [423]. Due to the conformational changes caused by the ribosome binding, the hydrophobic patch belonging to TMD2 and TMD7, is also exposed, creating thus a binding site for the hydrophobic H region of the signal peptide [292, 423]. After SP binding, translocation is initiated by insertion of the nascent-chain into the channel in loop-like manner. While the SP remains bound to the channel hydrophobic patch, the downstream section resides in the pore (Figure 8, left) [354, 292, 310].

If the signal is sufficiently hydrophobic, it displaces TMD2, destabilizing further the lateral gate, while simultaneously widening the central pore to dislodge the plug by movement of TMD7 towards TMD10 [423, 160, 279]. This allows the intercalation of the hydrophobic signal (or TMD) into the lipidic bilayer in an energetically favorable fashion (Figure 8, middle) [42, 241, 423].

The Sec61 channel is a passive pore with an aqueous interior; a polypeptide chain

located in the channel can slide in either direction. To achieve unidirectional transport (i.e., export from the cytosol into the ER lumen or extracellular space), the channel associates with partners that provide a driving force. In cotranslational translocation, the channel partners with the translating ribosome, which feeds the growing polypeptide into the channel [310]. In post-translational translocation in eukaryotes, the Sec61 channel partners with the Sec63 complex and the luminal chaperone Kar2 (Bip in mammals), a member of the Hsp70 family of ATPases [310, 235]

During the entire process, the SP is thought to remain bound to the Sec61 complex until a translocon associated signal peptidase cleaves it, releasing the translocated peptide into the ER lumen (Figure 8, right) [181, 5, 145].

Most membrane proteins, however, lack a SP and their highly hydrophobic N-terminal TMDs serve as a recognition signal instead [419]. Nevertheless, most of them use the cotranslational pathway for their integration [258, 8, 335].

Translocation of hydrophilic peptides requires only slightly rearrangement of the channel, where the lateral gate displays an essentially closed state. Membrane insertion of a hydrophobic domain, on the other hand, requires Sec61 lateral gate to open and a rearrangement of its plug to guarantee maintenance of ion permeability barrier [127]. Structural rearrangements of helices 2b and 3 on one side and 7 and 8 on the other, allow partition of the TMDs into the lipid bilayer [160, 313]. This partitioning is mainly determined by the TMD hydrophobicity [156] and follows the “positive-inside rule” [420] (Figure 9). Depending on the peptide sequence, this might happen only once (Figure 9 A and B) or multiple times (Figure 9 C) until all TMDs have been inserted into the membrane [353].

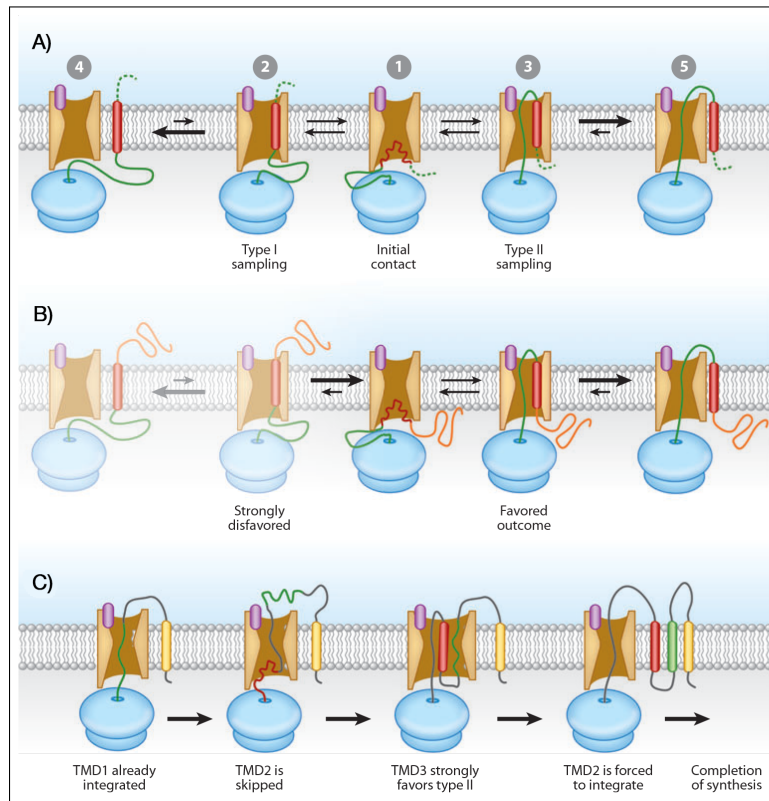


Figure 9: Trans-membrane segments membrane insertion scheme. Models of transmembrane domain (TMD) insertion. A) Generic model for TMD-translocon interactions. B) Depending on any of various parameters, the sequence of events in panel a can be biased toward one or the other outcome. Lengthy N-terminal domains strongly disfavor their translocation into the lumen. Consequently, type II orientation is the favored. C) Example of non-sequential insertion of TMDs in a polytopic integral membrane protein (IMP). Figure from Shao & Hegde [353].

0.2.3.2 Post-translational Translocation

Although alternate post-translational pathways to the ER are used by specialized subclasses of proteins [353, 148, 8], most post-translational translocation is done by the heptameric Sec complex (Figure 10).

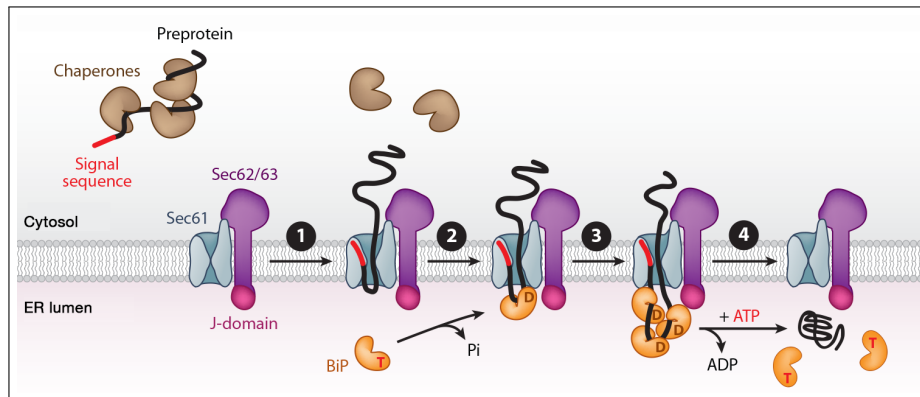


Figure 10: Pos-translational translocation scheme. Model of pos-translational translocation in eukaryotes. The scheme shows different steps in the pos-translational translocation of a eukaryotic secretory protein. Figure from Park & Rapoport [280].

Current models for post-translational translocation suggest that the Sec63 complex recognizes and binds the SP of soluble, fully translated substrates. Through conformational changes, it then transmits information to the translocon and Kar2, which is lumenally associated [14, 145, 280]. As in co-translational translocation, SP binds to the channel near the lateral gate and induces pore opening, allowing the hydrophilic polypeptide to transverse the membrane (Figure 10, step 1) [292, 423]. The secretory protein then associates with Kar2 which promotes directed movement of the polypeptide (Figure 10, steps 2 and 3) [235, 277]. In fact, the Kar2/Sec63 (through its J domain) interaction is responsible for the coordinated and directed anterograde peptide movement [94, 250]. Additional data suggests that this interaction might also play a role in co-translational translocation [43, 309, 411]. It has been suggested that the Kar2 drives import by promoting folding, which serves as the driving force [130, 307].

0.3 Protein Folding and ER Quality Control

0.3.1 Folding

As polypeptides emerge from the translocon, they are unfolded. They must, therefore, undergo a folding process until their native conformation is achieved. Since the ER lumen is an aqueous environment, hydrophobic peptides and protein domains would be bound to aggregate if left in a free, unstructured form. To tackle this problem, molecular chaperones immediately engage the nascent polypeptides at the pore exit. Chaperones can help in the actual translocation, like Kar2 [309, 43], and promote protein folding [116, 37, 7]. Moreover, chaperone interaction guarantees that any given protein stays in the ER until it is correctly folded [456].

In fact, the ER provides an optimized environment for protein folding and maturation. This is mainly due to the high concentration of ER-resident chaperones [85]. With their help both soluble and membrane proteins can acquire their native conformations [461].

Chaperones perform their functions by non covalently binding to the surface-exposed hydrophobic patches of the unfolded or misfolded peptides, thus preventing protein aggregation. In some cases they even provide secure (i.e protected) environment for protein folding [329, 47].

One of the main families of chaperones is the heat shock proteins of 70 kDa (Hsp70s) family [236, 73]. This family is quite prolific and versatile. They are not only present in nearly every cellular compartment in eukaryotes and in most prokaryotes, as their functions span protein folding, transport, and degradation [411]. In general, Hsp70 proteins, like BiP (Figure 11, top, in purple), catalyze ATP hydrolysis when binding to exposed hydrophobic segments of unfolded proteins (Figure 11, top) , remaining

bound until ADP is released, thus facilitating protein folding. Due to a weak ATPase activity, Hsp70s need DNAJ/Hsp40 co-chaperones (ERdj: ER-resident DNAJ protein) to accelerate ATP hydrolysis and promote maximal chaperone activity (Figure 11, bottom, in brown) [245, 154, 425, 68]. For ADP and ATP release and re-fuelling, respectively, nucleotide-exchange factors (NEFs) are necessary (Figure 11, top, in red)[144, 46, 20].

In yeast, one of the most prominent Hsp70 is the already mentioned Kar2, having an important role in ER folding besides its role in translocation. For Kar2, the known co-chaperones are Sec63, Scj1, and Jem1 [337, 266]. Sec63 is transmembrane (3 TMDs) with a luminal J-domain, Jem1 is ER membrane-associated, and Scj1 is a soluble ER-luminal protein [366, 266, 94]. Although Kar2 interacts with Sec63 also during translocation, its interaction with Jem1 and Scj1 seems to be exclusively to maintain aberrant proteins soluble [267]. As for its nucleotide exchange factors, Kar2 seem to partner with the Hsp70 Lhs1, as well as with Sil1, a GrpE family member [15, 379, 135]. Additionally, Kar2 has also been described as having prominent roles in protein degradation via ERAD and UPR regulation [267, 239].

Due to its roles in recognizing and binding of unfolded proteins and in maintaining said protein in the ER, Kar2 activity represents a major ER quality control (ERQC) stage.

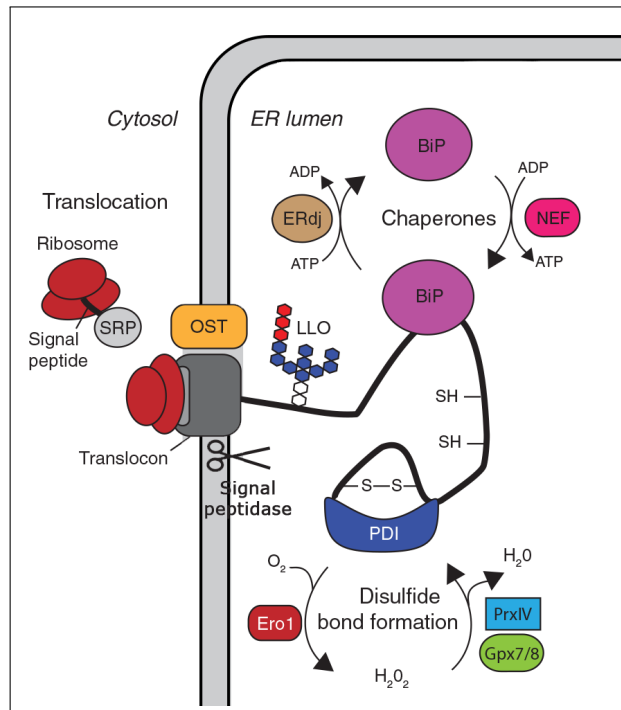


Figure 11: Nascent chain interaction with luminal chaperones. Model of protein folding and misfolding at the ER. Co-translational glycosylation mediated by OST catalyses followed by chaperone action. BiP binds nascent chains in an ATP-dependent manner assisted ERdjs and NEFs. Pdi1 promotes disulfide-bond formation oxidizing cysteine residues, being kept oxidized by Ero1 and ER peroxidases PrxIV and Gpx7/8. Based on figure from McCaffrey & Braakman [239].

Another essential folding catalyst and chaperone of the ER is Pdi1, the better known member of the PDI family [119, 104]. Pdi1 has a dual role. It serves as a chaperone, interacting with portions of the substrate that would normally self-associate, and thus inhibiting the aggregation of misfolded proteins [301, 51], and is responsible for disulfide bond formation (Figure 11, bottom, in dark blue). Disulfide bonds are crucial for protein folding, function and stability [6]. Since the ER lumen possesses an oxidizing environment, protein disulfide isomerases, with their thioredoxin-like domains, can catalyze the formation, isomerization, and reduction of disulfide bonds [14, 239]. Pdi1 is one of such proteins. Besides Pdi1, four other ER-resident PDI homologs have been identified: Mpd1, Mpd2, Eug1, and Eps1 [269].

Pdi1 has five domains: a, b, b', a', and c [72]. The a and a' domains are those containing the thioredoxin-like active sites and responsible for its oxidative role [97]. The b and b' domains have a fold similar to a and a' domains but do not contain active sites [193]. The c domain represent a highly negatively charged sequence that was related to its low affinity, high capacity calcium-binding properties [231, 403]. The presence of these activity devoided domains confers Pdi1 the capacity to bind peptides or proteins [268, 200], leading to its chaperone role [401]. Some data seems to suggest that the critical function of Pdi1 may be the isomerization of non-native disulfide bonds [133], and its chaperone activity is thought to depend on this isomerase function [190, 441, 346]. Indeed, Pdi1 is involved in the folding of even proteins that lack disulfide bonds [427, 51, 375]. Moreover, recent reports show that members of the PDI family (including Pdi1) interact with components of the ER folding machinery (e.g calnexin and Kar2) [120, 199], as well as with Htm1, a QC mannosidase enzyme [112].

Interestingly, only a subset of members of the PDI family are able to catalyse disulfide bond isomerization efficiently, whereas others are probably not directly involved in native disulfide bond formation [86]. Growing evidence suggests that the variation of domain architectures in the PDI family [415] might account for their different affinity for specific chaperones, which would allow shepherding of a broad range of proteins into either their folded forms or into ERAD pathways [14].

Together, Kar2 and Pdi1 represent preponderant QC sensors. Any incomplete folding or misfolding ensues binding of one or more of this factors promoting ER retention [103, 151, 152].

Of all the post-translational modifications (PTMs) happening in the ER, the most prevalent is the attachment of carbohydrates, which is essential for the maturation

of many proteins [150]. Attachment of oligosaccharides to newly synthesized polypeptides not only increases their solubility but also their processing serves as ER-resident lectin chaperone recruitment signals, regulating glycopolypeptide folding and turnover [430, 448, 189]. Although the mechanism for protein glycosylation is well studied, its direct role in folding and quality control was only recently understood. To the moment, only two forms of glycosylation capable of serving this role were identified: N-linked glycosylation and O-mannosylation [456].

In case of N-linked glycosylation, oligosaccharides are added to consensus Asn-X-Ser/Thr sites (sometimes NXC, NXV or NG) where X is any amino acid except proline [468]. This addition, which can be concomitant with polypeptide translocation, is catalyzed by the oligosaccharyl transferase (OST) enzyme using a lipid-linked glycan donor. The OST complex is composed by Ost1, Ost2, Ost3 or Ost6, Ost4, Ost5, Wbp1, Swp1, and Stt3, all of which are integral membrane proteins [192], and was described as directly interacting with the Sec61 translocon [334, 192, 226].

Besides N-linked glycosylation, there are proteins that undergo O-linked mannosylation. This happens by attachment of residues of mannose to serines or threonines by protein O-mannosyltransferases (Pmts) [383, 226]. *S.cerevisiae* expresses seven integral membrane mannosyltransferases (Pmt1–Pmt7) that are able to link mannose residues to proteins using a lipidic-linked mannose donor [383, 444]. A recent study also reported that the O-mannosyltransferase associates with the Sec61 translocon, allowing co-translational O-mannosylation [226].

This initial glycosylation, which was attached *en bloc* to nascent polypeptides, will then help protein folding and ER QC as it is sequentially processed by glycosylhydrolases in a protein conformation-dependent manner [150, 7].

0.3.2 Quality control

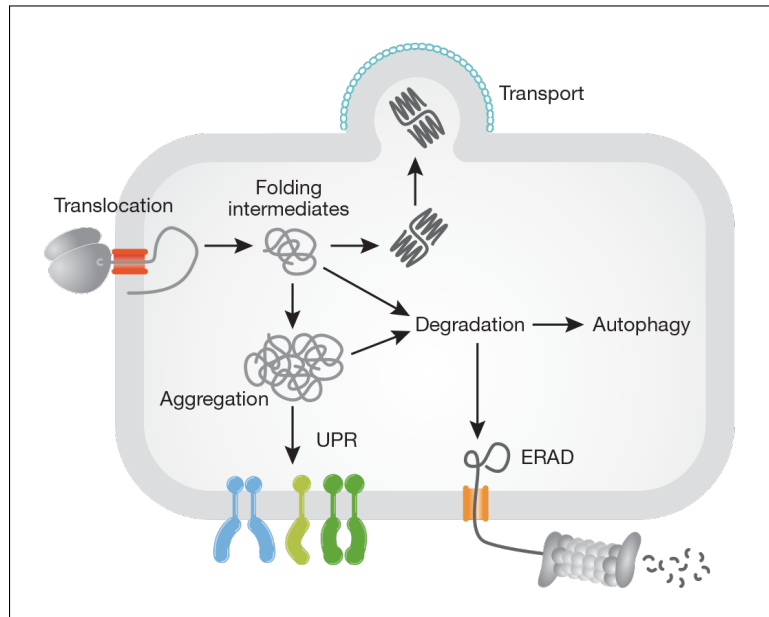


Figure 12: Quality control in the ER. Schematic representation of the different pathways involved in ER quality control from entrance in the ER until ER exit. Figure from Cyr & Hebert [70].

It has long been known that many eukaryotic newly synthesized proteins misfold during biogenesis [344]. Although estimations about protein biogenesis efficiency vary, it represents a high-fidelity process [82, 128]. Nonetheless, due to mutations, transcription and translation errors, cell stress, etc., a small proportion of proteins always misfold [225, 400]. The accumulation of aberrant proteins, without countermeasures, can seriously compromise cell function [205, 80, 320]. In order to circumvent this issue, the cell possesses sophisticated QC mechanisms that recognize, segregate, and degrade misfolded proteins (Figure 12). Therefore, proteins are subject to stringent quality control. For secretory proteins, such quality control begins at their site of biogenesis, the ER, which possesses perhaps the most elaborated QC environment. High concentration of chaperones and protein-modifying enzymes ensures that only

mature proteins exit the ER [399, 85, 7, 456].

At its essence, ER QC encompasses a series of pathways that integrate folding, traffic control, sorting and disposal of misfolded proteins (Figure 12). Understanding the system requires the characterization of individual pathways, the identification of components and their organization, the precise dissection of the sequential events, and how individual factors fit into each step. [189]

Proteins that do not fold properly must be retained and targeted to ERAD for turnover [391, 274, 328]

For the purpose of maintaining a tight QC system, the cell uses intrinsic structural signals to detect unfolding or misfolding. Many of these are PTMs, as mentioned in Section 0.3.1, as any lack or delay in the acquisition of said modification may serve as a signal of misfolding.

The cell distinguishes native from non-native protein conformations by using various sensor molecules, mainly molecular chaperones, since these inherently interact with incompletely folded proteins. Besides assisting in protein folding, chaperones are often involved in the recognition and dispatching of misfolded proteins for degradation [85, 36, 239, 381]. The conformation-sensing system depends on selective and covalent "tagging" of misfolded proteins, allowing their recognition by the machinery responsible for folding and degradation. The best described tags are ubiquitin and glucose. Ubiquitin, a small protein, is cytosolically attached to lysines as a signal for degradation [125]. Glucose, in turn, is attached at the ER lumen to the N-glycans of glycoproteins, functioning as a retention signal (Figure 13) [137, 283]. By preventing exit from the ER of folding intermediates, it extends their exposure to the ER folding machinery, thus improving the chance of correct maturation [249].

In both mammals and yeast, the rapid removal of terminal glucose and mannose

residues from protein-bound oligosaccharides and the regulated addition of a specific glucose residue dictates the sequential schedule of events occurring during maturation and selection for degradation (Figure 13) [388]. A series of carbohydrate trimming events begin with the removal of the terminal glucose residue by glucosidase I (Gls1/ Cwh41). Glucosidase II (Gls2/Rot2) removes the next two progressively (Figure 13, top panel, left). This process, which is quick in *S.cerevisiae*, can be slowed in other organisms for the calnexin folding cycle [150, 7].

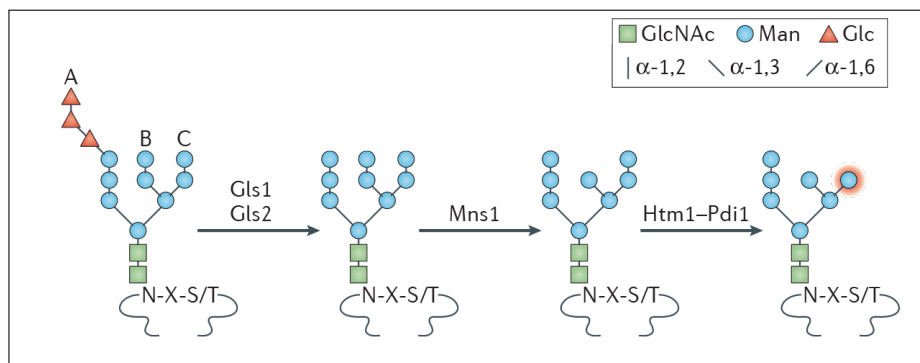


Figure 13: Glycan trimming. Upper panel depicts yeast pathway of glycan trimming, and the lower panel depicts the mammalian pathway. The blue sphere outlined in red (Man7GlcNAc2 glycan; right) indicates the terminal α -1,6-linked mannose ligand of the yeast Yos9 (OS-9 and XTP3-B in mammals), an ERAD receptor. Glc, glucose; GlcNAc, N-acetylglucosamine; Gls, glucan synthase of *cerevisiae* protein; Man, mannose; Mns1, mannosidase I; Pdi1, protein disulfide isomerase. Figure from Xu & Ng [456].

One of such primary QC systems, the mammalian calnexin/calreticulin cycle, is particularly well-characterized (Figure 14). This system retains in the ER non-native glycoproteins, thus promoting their folding or, in some cases, targeting misfolded glycoproteins for degradation [275, 432, 223, 409]. Calnexin and calreticulin interact with the intermediates of the N-linked core glycans trimming pathway of newly synthesized glycoproteins (Figure 14, middle) [137, 432, 146]. Both calnexin and calreticulin interact also with ERp57, a thiol-disulphide oxidoreductase [273, 272], forming a protected space where the substrate can bind. Glucosidase II hydrolyses a glucose from the core glycan of the substrate glycoprotein, promoting its dissociation from calnexin or

calreticulin. The UDP-glucose:glycoprotein glucosyltransferase (UGGT), however, catalyzes the inverse reaction, re-glycosylating the substrate and promoting reassociation with calnexin or calreticulin. UGGT works as a folding and re-glycosylation sensor only if the glycoprotein is incompletely folded [283]. Only when UGGT fails to re-glycosylate it, does a protein exit the cycle. In this way, glucose acts as a selective tag for incomplete folding. Cycles of glycosylation and de-glycosylation end when the glycoprotein either reached its native conformation or is targeted for degradation (Figure 14, right and top, respectively) [85].

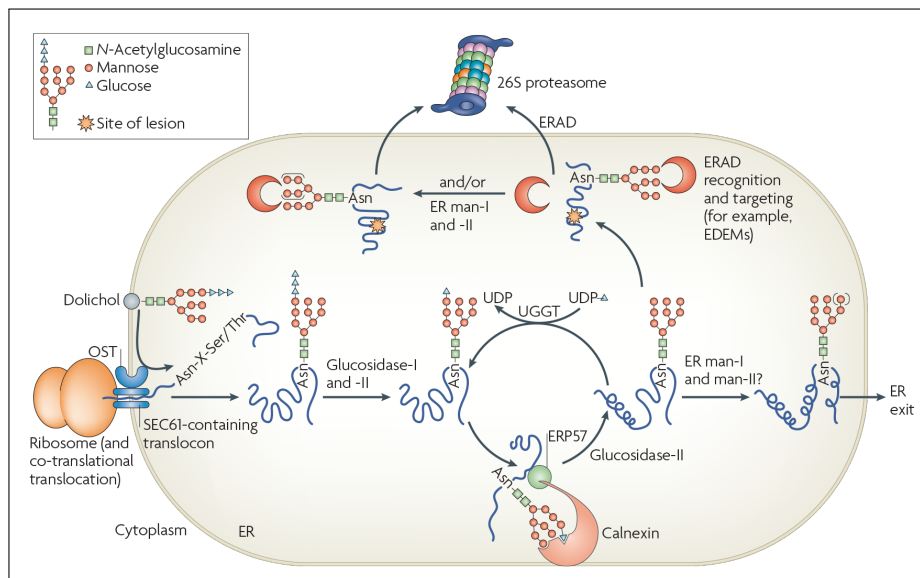


Figure 14: Calnexin/calreticulin cycle. N-linked glycosylation and the degradation of glycosylated proteins. After co-translational glycosylation, glycan is sequentially trimmed by glucosidase-I and glucosidase-II enabling substrate recognition by calnexin and calreticulin, which facilitate folding. ERP57 (disulphide isomerase homologue) catalyses disulphide bond formation. If glycoproteins have adopted their native conformations, they can be de-mannosylated (denoted by the use of parentheses around the mannoses) by ER mannosidases I and II (ER man-I and man-II) and exit the ER. If not, proteins are re-glycosylated by UGGT, which promotes re-entry into the folding cycle. Terminally misfolded glycoproteins might also be targeted for ER-associated degradation (ERAD). Based on figure from Vembar & Brodsky [409].

In *S.cerevisiae*, however, there is no UGGT and a role for calnexin in protein folding remains to be determined (Figure 13, top versus lower panel) [240].

Yeast also possesses two additional ER mannosidases (Mns1 and Htm1) that trim mannose residues from the glycan moiety (Figure 13, middle and right) [49, 189]. Mns1 and Htm1, two related enzymes, have distinct specificities. Mns1 removes the terminal mannosyl residue of Man9GlcNAc2 processing it into Man8GlcNAc2, which is the typical glycan of exported proteins (i.e fully folded glycoproteins) [176]. Htm1 is thought to interact with terminally misfolded proteins, after Mns1 [62]. The resulting Man7GlcNAc2 glycan is recognized by Yos9, an ER lectin that targets the protein for ERAD (Figure 13, right, circled in red) [55, 77].

0.3.3 UPR

Retention of unfolded or misfolded proteins in the ER as a result of the action of the ER QC machinery activity can cause ER-proteostasis stress. In yeast, ER proteostasis stress elicits the unfolded protein response (UPR) [24, 107]. Use of ER protein folding inhibitors (e.g., tunicamycin, dithiothreitol) or overexpression of misfolded proteins can also experimentally induce UPR [24].

The UPR triggers an adaptive response to restore ER homeostasis by coordinating a reduction in the quantity of protein produced, increased synthesis of molecular chaperones to deal with buildup of misfolded protein, as well as an increase in ERAD to remove misfolded proteins [396, 343]. In fact, much of the folding and biogenesis machinery in the ER was found to be under the transcriptional control of the UPR. By genetic screening *IRE1*, *HAC1*, and *RLG1* were found to be essential for robust UPR [67, 363].

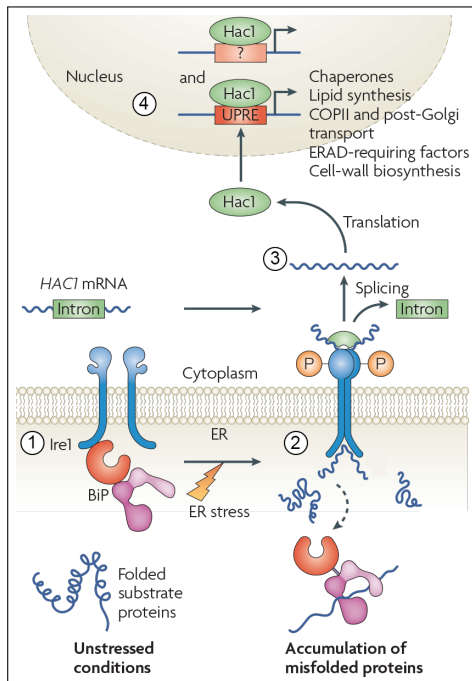


Figure 15: UPR in yeast. General yeast UPR schematic. Under unstressed conditions, BiP binds to Ire1 maintaining it inactive. When the ER is stressed, BiP can be titrated away to bind to misfolded substrates, in turn inducing Ire1 dimerization and activation. Ire1 activation triggers its endoribonuclease activity which in turn causes *HAC1* (a dedicated UPR transcriptional activator) mRNA splicing. After re-ligated and translated, Hac1 translocates into the nucleus, binds to UPR elements (UPREs) upregulation target-genes expression. Figure from Vembar & Brodsky [409].

Posterior studies revealed that *IRE1* encodes an ER transmembrane protein that has a cytosolic domain with kinase/ribonuclease activity and a luminal domain that senses and transduces unfolded protein levels. *HAC1* encodes a transcription factor with a leucine zipper that binds to specific unfolded protein response element (UPRE) sequences, typically 22bp long, inducing their expression. *RLG1* encodes a tRNA ligase that is required for the ligation of the Ire1-spliced *HAC1* pre-mRNA [67]. Current models indicate that the luminal domain of Ire1 interacts with Kar2 and unfolded proteins, thus sensing the protein folding status (Figure 15, step 1) [25, 290, 108]. When unfolded proteins accumulate in the ER, Kar2 interaction is compromised and Ire1 oligomerizes, thus activating its cytoplasmic kinase and ribonuclease domains (Figure

15, step 2). Activated Ire1 ribonuclease splices *HAC1* pre-mRNA and the the Rlg1 ligates the intermediate product, producing mature *HAC1* mRNA (Figure 15, step 3). Hac1 protein will then act as a potent transcriptional activator of UPR target genes (i.e UPRE-containing) (Figure 15, step 4) [24, 364, 191]. Besides Kar2, other ER folding key components are under UPR induction, like Pdi1 and Eug1 [66, 252]. Interestingly, Ire1 has been shown to form a complex with the Sec61 translocon, which it needs to efficiently cleave its mRNA substrates [298].

The mechanism of Ire1 activation and signal transduction is conserved from yeast to mammals [431, 356, 220]. However, while in yeast the only mechanism for UPR induction is the one mediated by Ire1, in mammals there are three classes of ER stress sensors: inositol-requiring enzyme 1 α (IRE1 α) and IRE1 β ; protein kinase RNA-like ER kinase (PERK); and activating transcription factor 6 (ATF6; both α and β isoforms) [157, 70].

When a protein has attained its native conformation, it is targeted to its final destination. If an aberrant conformation arises or folding is delayed, the substrate is subjected to additional folding cycles, or if deemed terminally misfolded, shepherd for ERAD [47, 240].

0.4 ERAD

ER-associated degradation (ERAD) is the process by which misfolded ER proteins are detected by ER-resident factors and directed for retro-translocation into the cytosol, where they undergo ubiquitin- and proteasome-dependent degradation (Figure 16) [430, 409]. This highly conserved process prevents accumulation and eventual aggregation of defective secretory proteins, thus promoting ER homeostasis and a normal cellular physiology [159, 45, 370].

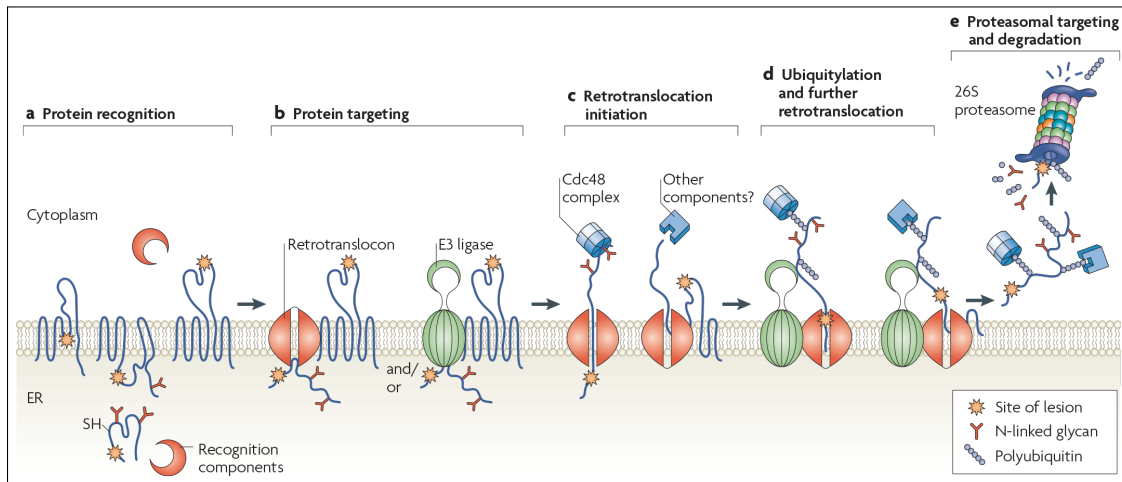


Figure 16: ERAD pathway scheme. Step-by-step illustration of endoplasmic reticulum-associated degradation. Based on figure from Vembar & Brodsky [409].

0.4.1 Recognition and Targeting

The first step in ERAD of misfolded proteins is their recognition by the cell (Figure 16, step A). ERAD substrate recognition and targeting (Figure 16, step B) can become indistinguishable as growing evidence suggests that the recognition factors belong to multiprotein complexes that are required for targeting as well [409].

The association of ER chaperones with unfolded and misfolded proteins suggests dual function in protein folding and quality control. While chaperones transiently bind unfolded polypeptides to aid folding in the ER [114, 260, 137, 291], irreversibly misfolded proteins seem to exhibit stable interactions with ER chaperones [169, 259]. This dynamic is best understood in the well characterized mammalian calnexin/calreticulin cycle [150]. Indeed in the ER lumen, the chaperones Kar2, Pdi1 and its homologue Eps1, and the semi-redundant J-domain containing proteins Scj1 and Jem1 proteins are required for ERAD [267, 366, 120, 185, 429]. This process seems logical as, in order to be translocated across the ER membrane to the cytosol, ERAD substrates

need to be soluble and dissociated from oligomeric complexes, and their disulfide bonds need to be reduced [393, 120, 92, 267, 350]. Substrates that present misfolded cytosolic domains and contain short or folded luminal segments seem to depend on the cytoplasmic Hsp42, Hsp26, Hsp70 and its co-chaperones Ydj1 and Hlj1 for ERAD in a way that can be substrate-specific [172, 2, 282, 410, 460].

Prolonged chaperone association, however, does not appear to be a sufficient trigger for ERAD. There are numerous examples of misfolded proteins stably retained in the ER [224, 208, 202, 377]. Indeed the actual targeting into the ERAD pathway may be mediated by chaperones that do not interact with normal folding intermediates [321]. Furthermore, recent studies indicate specific “signals” must be displayed to activate degradation [454].

One of this signals is de-mannosylation, which has been identified as a requirement for degradation of misfolded N-glycosylated proteins (Figure 17) [150, 452]. After trimming by Glc1, Glc2 and Mns1, the resulting Man8-GlcNAc2 is indicative of a protein ready for export (Figure 17, number 1). Delay in this stage, allows this structure to be processed by a mannosidase-related lectin in the ER (Htm1/Mnl1 in yeast; EDEM in mammalian cells) [150] whose action seems to be determinant for ERAD (Figure 17, number 2) [175, 251]. Work with CPY* and PrA* (standard glycosylated substrates) suggested that formation of a local structure adjacent to the glycan is dependent on the overall folding of the polypeptide and that the full determinant is as simple as a Man7GlcNAc2 glycan attached to an unfolded/disordered structure. Its positioning seems to effectively generate an intrinsic sensor for the overall folding of the polypeptide [453, 454]. Presently, an elegant mechanism where a protein-linked carbohydrate chain is transformed into an intrinsic timer for folding is widely accepted [303, 62, 454].

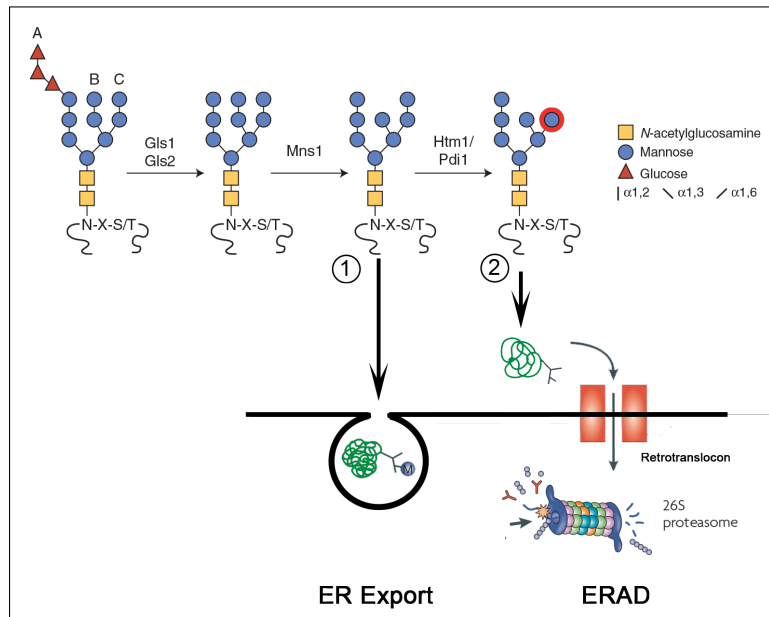


Figure 17: De-mannosilation as folding signal. Schematic representation of the glycan moiety of glycoproteins and of how its length serves as signal for protein fate. Enzymes responsible for each of the trimming steps are represented at the proper steps. Red circle highlights the α 1,6-linked mannose residue that serves as the Yos9 ligand. Based on figure from Thibault & Ng [391] and Ellgaard & Helenius [85].

In both yeast and mammals, multiple glycoprotein-recognizing ER-resident factors were characterized recently. These include the ER degradation-enhancing α -mannosidase-like (EDEMs) and the mannose-6-phosphatereceptor-like domain containing (Yos9 in yeast, OS9 in mammals) lectins. These factors are thought to be responsible for ERAD-substrate delivery to the retrotranslocon [189]. Suggesting a chaperone like activity, Yos9 was shown to bind even unglycosylated misfolded substrates. Moreover, Yos9 associates with BiP and the Hrd1 complex, where it may regulate Hrd1 selectivity for misfolded substrates [77, 55, 111]

Work in *Saccharomyces cerevisiae* resulted in a simple model of three core ERAD pathways depending on the localization of the misfolded domain. They were named ERAD-L, -M, or -C depending if the substrate lesion was in the ER lumen, within the

membrane, or on the cytosolic side of the ER membrane, respectively (Figure 18) [77, 55, 407, 172, 113]. These pathways involve distinct ubiquitin ligases (Hrd1 and Doa10) which associate with specific adapter molecules to form hetero oligomeric complexes that associate with misfolded proteins [96, 159].

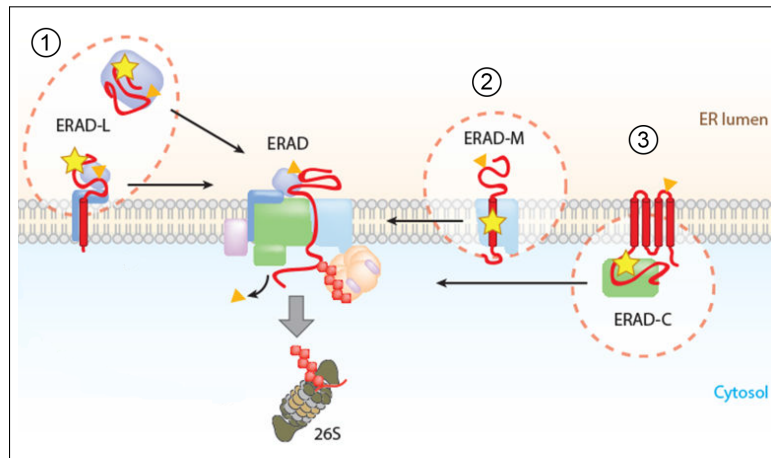


Figure 18: ERAD L, M- and C scheme. Schematic depiction of the different ERAD pathways. Figure from Stevenson et al. [381].

ERAD-L substrates (Figure 18, number 1) use the Hrd1 complex [34, 55], being recognized by Kar2, Jem1 and Scj1. These chaperones, assisted by Pdi1 and Yos9, associate with Hrd3 and thus recruit substrates to the Hrd1 complex [111]. Substrates of ERAD-M and ERAD-C (Figure 18, numbers 2 and 3, respectively) are directly recognized by Hrd1 and Doa10, respectively, with the latter acting together with Ssa1, Ydj1 and Hlj1 [254]. Doa10, however, also recognizes some ERAD-M substrates [134]. In this model, ERAD specificity is mainly assured by the ubiquitin-ligase complexes accessory proteins, that function as substrate-recruitment factors. They bind misfolded proteins selectively, and promote their targeting for downstream processing [101, 246].

Besides this well established pathways, a fourth pathway responsible for the degradation of misfolded inner nuclear membrane proteins was recently identified [102]. It

instead utilizes a ubiquitin ligase-complex consisting of three proteins, Asi1, Asi2, and Asi3 [102, 194].

The ERAD-C, ERAD-L and ERAD-M pathways, however, have been defined only in yeast. In mammals, the bigger assortment of ERAD-requiring components, led to an increased complexity of the evolved secretory-pathway residents, which may have caused a blurring of the distinctions between pathways. Even in yeast the ERAD-C and ERAD-L pathways can overlap, as certain membrane substrates require both the Doa10 and Hrd1 ubiquitin ligases for degradation [172, 207, 255]. This probably increases degradation efficiency and allows for compensation in case of substrate overload of one or the other pathway [409].

Rather surprisingly, soluble substrates (but not transmembrane ERAD substrates) also rely on genes required for ER-Golgi vesicle budding and anterograde transport (SEC12, SEC18, ERV29, ERV14, SEC23, SEC13, UFE1, SED5) [52, 390, 105] which suggests that some proteins are subject to one round of transport to the Golgi complex followed by recycling to the ER [52, 406].

0.4.2 Ubiquitin ligases - Doa10 and Hrd1

All ERAD pathways converge on the ER cytosolic face, where they require other components of the ubiquitination machinery and an ATPase complex consisting of the AAA+ ATPase Cdc48 (called p97 or VCP in mammals) and a heterodimeric cofactor, composed of Ufd1 and Npl4 [16, 40, 178, 305, 457, 458].

Central components of this process are the multimeric protein complexes containing membrane bound ubiquitin ligases. There are two main E3 ligase complexes in the yeast ER: Doa10 and Hrd1, both multi-spanning membrane proteins [138]. They also have in common the fact that they partner with substrate-recognition, targeting

and retrotranslocation components, and assemble in large protein complexes. Mainly, they coordinate protein quality-control activities with cytoplasmic substrate ubiquitylation, the Cdc48 action, and the proteasome action [101, 246].

Of both these complexes, Doa10 is the simpler (Figure 19 A). Besides Doa10 (green), it contains Ubc7 (E2 ubiquitin conjugating enzyme; cyan), which is attached to Doa10 via Cue1 (grey) [29]. In addition, the Cdc48 subcomplex (Cdc48/Ufd1/Npl4; purple, magenta and yellow, respectively), which provides the driving force for substrate extraction [16, 457, 178, 305], is linked to it through Ubx2 (orange) [257, 345].

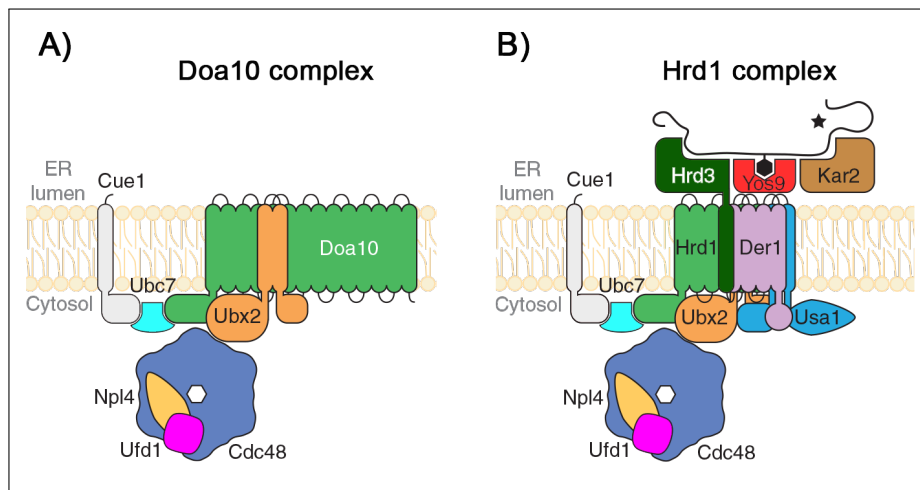


Figure 19: Ubiquitin ligases complexes. Schematic depiction of the two main cellular ubiquitin ligase complexes. A) Doa10 complex. B) Hrd1 complex. Figure from Thibault & Ng [391].

Hrd1 (Figure 19 B, light green), a ER-membrane protein with a cytosolic RING finger domain [159, 74], forms a complex with Hrd3 (dark green), which acts as a substrate recruitment factor [113]. Despite little similarity between the two E3 enzymes, the Hrd1 complex also includes Cue1, Ubc7, Ubx2, Cdc48, Ufd1, and Npl4 (grey, cyan, orange, purple, magenta, and yellow respectively), which explains why mutating any of these component results in broad ERAD defects [389, 55]. Additionally,

Usa1 bridges Der1 (lilac) to the complex. Lastly, Yos9 (red) is bound to the luminal domain of Hrd3 [48, 26, 197, 385] (Figure 19 B). Because Hrd3's luminal domain can bind proteins with or without glycans, these factors are believed to work together in substrate recognition [111].

0.4.3 Ubiquitination

Most known ERAD substrates need to be ubiquitylated for proteasome-mediated degradation. This process needs the action of a set of enzymes that include an E1 ubiquitin-activating enzyme, an E2 ubiquitin-conjugating enzymes and an E3 ubiquitin ligases. In some cases, action of E4 ubiquitin-chain-extension enzymes was shown to facilitate ERAD [255, 314, 204].

The ubiquitin conjugation process happens in a cascade of E1–E2–E3 enzymes (Figure 20) [304]. It is initiated by E1 enzymes, like Uba1 (Figure 20, step 1). Activated ubiquitin can then be transferred to an E2 (or Ubc) enzyme by trans-esterification (Figure 20, step 2). Finally, E3 enzymes (ubiquitin ligases) catalyze the protein-ubiquitylation, by covalently binding ubiquitin to lysine residues (Figure 20, step 3 or 4) [78, 405]. Although lysines are the most common acceptor for ubiquitylation, ubiquitylation of serine, threonine, or cysteine has been observed in both yeast and mammals [50, 358] and of N-terminal amino groups in higher eukaryotes [32, 21]. The conjugation machinery shows hierarchical organization. In yeast, only one E1 exists, while it has 11 E2s and a large family of E3s (60–100). The admirable selectivity of E3s ubiquitylation is mediated by their direct interaction with the substrate [101].

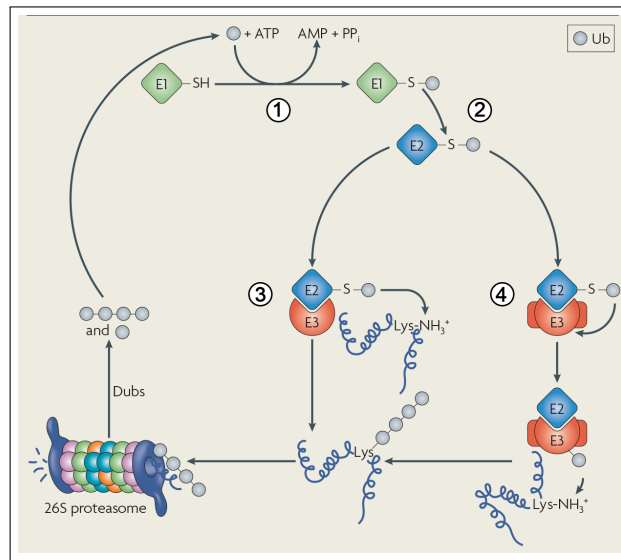


Figure 20: Ubiquitylation cascade. Scheme illustrating the ubiquitylation cascade necessary for ERAD. The sequential action of E1-E2-E3 enzymes guarantee specificity and versatility of the ubiquitylation system. Based on figure from Vembar & Brodsky [409].

The E3 ubiquitin ligases, like Hrd1 and Doa10, mediate only the initial oligo-ubiquitylation of ERAD substrates; polyubiquitylation, which is required for degradation by proteasomes, is catalyzed by so-called E4 enzymes such as Ufd2 [203, 314]. Ufd2, Cdc48, the 19S proteasome regulatory particle (RP) subunits Rpn10 and Rpt5, Rad23 and Dsk2, all bind ubiquitin conjugates and may transport substrates to the proteasome proteolytic core, but their respective roles are unclear [203, 213, 242, 413].

It must be highlighted that since ubiquitylation takes place in the cytosol it cannot be involved in initiating the export of soluble proteins from the ER [138].

0.4.4 Cdc48

After polyubiquitylation, and prior to or during targeting to the proteasome, proteins must be extracted from the membrane. Although the proteasome being able, in a few cases, to retrotranslocate substrates [237, 216], another cytoplasmic protein complex,

the cell-division cycle-48 (Cdc48) complex, was shown to be involved in substrate retrotranslocation [179]. In yeast, the complex consists of Cdc48, a hexameric AAA+ ATPase, and Ufd1 and Npl4. Recruitment of the complex to the ER membrane might happen through its interaction with Ubx2 (vIMP in mammals) [257, 345, 459], by its binding to Sec61 [41], or through its binding to Hrd1 [11].

The Cdc48/Ufd1/Npl4 complex has been described as being both a “dislocase”, capable of exerting force and extracting substrates from the retrotranslocon [457, 458], and a “segregase,” recognizing and binding ubiquitinated proteins, thus selecting them from non-ubiquitinated ones, facilitating their availability to the proteasome for degradation [308, 40]. As Cdc48 associates with the proteasome cap [412], substrates might be transferred directly from the Cdc48 complex to the proteasome for degradation [413].

Increasing evidence suggests that other factors may have decisive roles in substrate degradation [304], as is the case of Uba domain- and Ubl domain-containing proteins, which interact with the proteasome and with ubiquitylated substrates [409], and Rad23 and Dsk2, which increase ERAD efficiency [314, 242]. Curiously, one Cdc48- and Rad23-associated protein is Png1, a deglycosylating enzyme [219, 196] indicating that glycosilation may sterically hinder substrate access to the catalytic chamber of the proteasome. Whether these factors are static or mobile members of the Cdc48 complex, responsible for binding and escorting ERAD substrates to the proteasome is unknown [409].

0.4.5 Proteasome

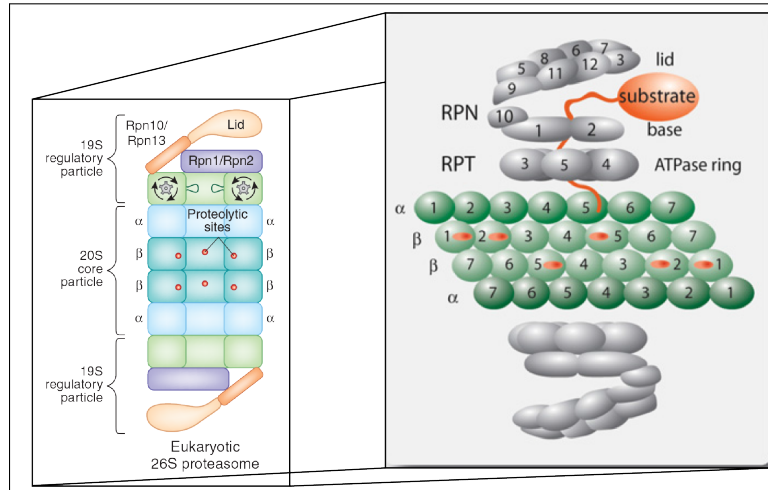


Figure 21: 26S Proteasome schematic. The overall structure of the eukaryotic proteasome. A) Side-on cross-section of the eukaryotic 26S proteasome. The 20S core particle is flanked by 19S regulatory particles, and the proteolytic sites are located in the β -rings of the 20S core particle. The scaffold proteins Rpn1 and Rpn2, the ubiquitin receptors Rpn10 and Rpn13 and the loops lining the ATPase ring are depicted. B) More detailed subunit composition scheme showing a in-process substrate. Figures from Schrader et al. [342] and Raasi & Wolf [304].

The proteasome, highly conserved in evolution and found in all eukaryotes, is the most complex protease known, having 33 distinct subunits [100]. Its best investigated function is that of degrading ubiquitin–conjugated proteins, being organized into two sub assemblies: the 19S regulatory particle (RP) and the 20S core particle (CP) (Figure 21) [304]. The 19S RP participates in substrate recognition, while the 20S CP contains the proteolytically active sites, which are protected within its cavity, ensuring strict access control and minimal nonspecific proteolysis [342, 304]. Substrates are driven from the 19S RP to the 20S CP through a narrow interconnecting tunnel. To allow the access of globular proteins to the channel, the six ATPases that form the hexameric ring complex of the 19S RP (Rpt1–Rpt6) are able to actively unfold them and feed them into the 20S CP [342, 304]. This hexameric ring complex also contributes

to substrate export from the ER [438, 126, 327, 216]. For the non-ubiquitinated ERAD substrate p α F, the 19S RP is indeed the only cytosolic factor required for export from the ER (*in vitro*) [216].

The 19S RP also contains ubiquitin receptors, like regulatory particle non-ATPase-13 (Rpn13), Rpn10 and regulatory particle ATPase-5 (Rpt5). Data suggests that Rpn13 mediates the highest affinity binding, while its positioning supports a key role in substrate selection [170], and that Rpn10 binds to and drives substrates into the 20S CP for degradation [409]. Other components of the RP base, like the large subunits Rpn1 and Rpn2, serve as scaffolds that allow recruitment of multiple factors, such as ubiquitin–protein conjugates [101].

As it is, a significant fraction of cellular proteasome population was found to be associated with the ER [88, 318, 317], and a direct interaction of the AAA-ATPase containing base of the 19S RP with Sec61 channels has been shown [187, 186].

0.4.6 Retrotranslocon

A central aspect of ERAD is the fact that luminal ER proteins have to be translocated to the cytosol to be ubiquitinated and proteasome degraded. This process, mostly referred to as retrotranslocation, would therefore be dependent, in most cases, on a conducting channel for ER membrane crossing, although in some cases the proteins may be pulled directly out of the bilayer during ERAD [297]. For the majority of proteins that are subject to ERAD-L, the evidence suggests that retrotranslocation occurs through one or more distinct retrotranslocation channels. The identity of these channels is still under debate but the candidates are Sec61, Der1 and Hrd1 [439, 221, 56].

The first proposed retrotranslocation channel was the Sec61 translocon, when

two transmembrane ERAD substrates (HC and US2) were found to associate with the heterotrimeric Sec61 complex prior to degradation [439]. Following this discovery, various mutations in the *S. cerevisiae* Sec61 protein were reported to cause defects in retrotranslocation and degradation of ERAD-L substrates, while their anterograde transport into the ER was unaffected [293, 289, 28, 443]. Indeed, Sec61 mutations have profound defects on ERAD of mutant p α F, causing its prolonged association with Sec61 and with PDI [289, 288, 120]. More recently, Sec61 was reported to associate with the ERAD substrates CPY* and Deg1:Sec62ProtA just preceding degradation [333] and to form disulphide bonds with an ERAD substrate that was trapped in the channel during export [348]. Further supporting the idea of Sec61 as the retrotranslocon is the fact that direct blockade of the Sec61 channels with ribosome nascent chain complexes in ER-derived vesicles abrogated the retrotranslocation of cholera toxin and amyloid beta-peptide from the ER lumen [339, 340]. Also, strains that are unable to induce the expression of SEC61 upon overexpression of CPY* develop an ER protein import defect that is alleviated upon overexpression of SEC61, suggesting that the protein translocation channel becomes limiting for import into the ER if there is a high demand for export [261]. Direct interaction between Sec61 and the proteasome [262, 187], and the fact that a mutation in *SEC61* that reduces affinity for 19S RP also impairs ERAD of a 19S RP-dependent substrate [187] provided yet other indications that Sec61 might be involved in ERAD.

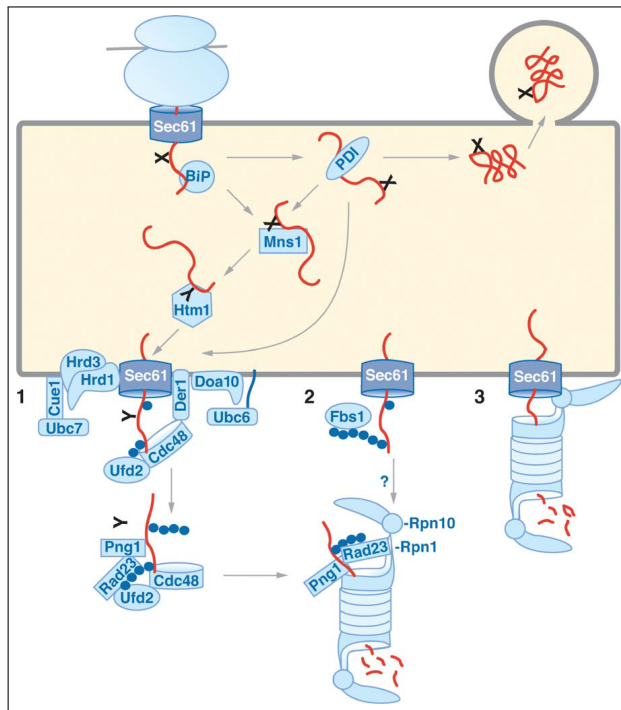


Figure 22: Sec61 retrotranslocon model. Schematic representation of potential Sec61-containing retrotranslocon structures. Based on figure from Römisch [321].

Although the Sec63 complex is not required for ERAD, the role of Sec63 itself is controversial [289, 293]. Recently Servas et al. demonstrated that mutations in the DnaJ-domain of Sec63 causes a defect in ERAD, whereas mutations in the BrI, acidic, and transmembrane domains only affect protein import into the ER [349].

An interesting piece of data shows that the Hrd1 ligase itself is unstable in cells lacking Hrd3; however, a *sec61* retrograde mutant can restore Hrd1 levels in this background [294].

Taken together, the data provides compelling evidence that protein export from the ER is mediated by a channel containing Sec61 (Figure 22).

However, experimental data exists supporting the idea that the other candidates are also responsible for the formation of retrotranslocation channels that are respon-

sible for the retrograde transport of either a subpopulation of substrates, or of some substrates under some specific conditions.

The gene encoding the yeast homologue of Derlin-1, *DER1*, was identified in a screen for mutants that stabilize CPY* [201]. Der1 has 4 TMs, which are not enough to form a channel, but it has been found to oligomerize [243]. In contrast to *SEC61*, *DER1* is a non-essential gene, and its deletion completely blocks ERAD of two soluble substrates (CPY* and PrA*) in yeast [201]. For other substrates, however, there is either only a modest effect (a twofold increase in the half life of KHN, KWW, pαF) or none at all (Pdr5*, Sec61-2) [201, 407, 295]. Moreover, some organisms (e.g *Hansenula polymorpha*) have no *DER1/DFM1* homologues making it unlikely that Der1 is a general ERAD export channel [76]. Its transmembrane domains, however, have been shown to associate with both Hrd1 and in transit ERAD substrates [463, 243].

The third candidate, and perhaps the most popular retrotranslocation channel candidate in the present days, is Hrd1. Initial evidence for Hrd1 forming a channel came from the observation that its overexpression in yeast makes the other components of the Hrd1 complex dispensable for the degradation of ERAD-L and -M substrates, while all downstream components, such as the ubiquitination machinery and the Cdc48 ATPase complex were still required [56, 109, 294]. *HRD1*, as *DER1*, is also a non-essential gene, and its deletion in yeast leads to ERAD defects for several substrates. The fact that the 6 transmembrane domains in Hrd1 are sufficient to form a pore led to the proposal that it is the ERAD channel [454]. Its role in retrotranslocation was also supported by photocrosslinking of ERAD substrates to Hrd1 during retro-translocation [56]. Like Sec61 and Der1, Hrd1 was found to associate with ERAD substrates via its transmembrane domains and to polyubiquitinate soluble ERAD-L substrates [380]. Indeed, *in vitro* retrotranslocation seems to have been reconstituted in proteoliposomes

that contained both Hrd1 and a single-spanning substrate protein with a large misfolded domain [11]. These experiments, however, might have some conceptual and experimental artifacts as discussed by a recent review [322].

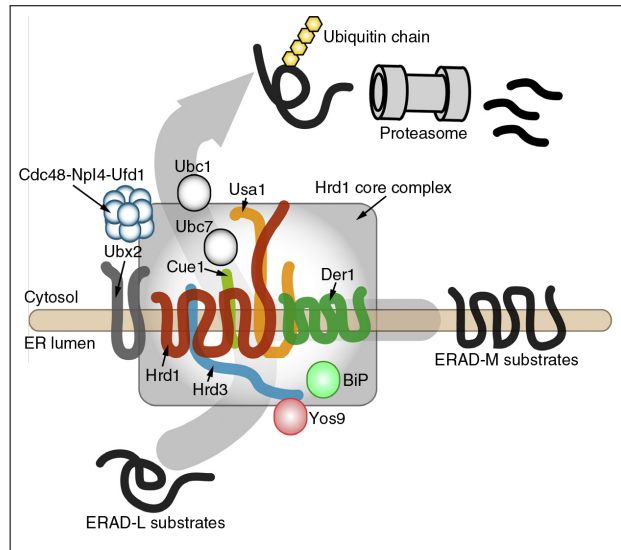


Figure 23: Hrd1 retrotranslocon model. Scheme representing a model for the process of retrotranslocation through a Hrd1-based retrotranslocon channel. Based on figure from Vembar & Brodsky [409].

According to Rapoport's lab, auto-ubiquitination of Hrd1 was postulated to be the trigger for retrotranslocation of the substrate. The crucial modification seems to occur in the RING finger of Hrd1, as mutation of lysines in this domain prevented retrotranslocation *in vitro* and the degradation of ERAD-L substrates *in vivo* [11]. These results led to a model in which auto-ubiquitination of Hrd1 opens the channel for ERAD-L substrates [11]. Unidirectionality of the transport would be guaranteed by the attachment of a polyubiquitin chain that could prevent its back-sliding into the ER lumen (Figure 23). Interestingly, the lysine mutations in the RING finger domain do not have a strong effect on ERAD-M substrates [451]. There is, however, another line of investigation that suggests that no auto-ubiquitination is needed [139].

Consequently, although much effort has been spent in the sense of identifying the retrotranslocon, its identity remains unclear. Due to the amount of data supporting each one of the alternatives, however, the most probable scenario is that depending on the substrate and cellular state, either one or a combination of these potential retrotranslocating channels might serve the purpose of retrograde transport of misfolded proteins out of the ER.

0.5 Protein Interaction and Chemical Crosslinking

0.5.1 Protein interaction

Almost all cellular functions depend on and are executed by complex protein-protein interactions (PPIs) [455]. Over 80% of the proteins were estimated to operate in complexes, their interactions being regulated by multiple mechanisms (e.g metal-binding or PTMs) that alter the affinity, co-operativity and kinetic parameters of the interaction [23].

Generally, PPIs can be classified into either domain–domain or domain–motif interactions. Domain–domain interactions involve the binding of two large contact interfaces (≈ 2000 Å), with relatively strong affinities, while domain–motif interaction form much smaller contact interfaces (≈ 300 – 500 Å), being short linear motifs (up to 20–30 amino acid residues) that interact with its partner with low affinity [256, 466]

Due to their great biological impact, PPIs have been the object of intense study across the years using a panoply of techniques [286]. The advent of gene fusion and protein labeling, together with the engineering of fluorescent probes, provided the initial spark for a technological revolution in the study of PPIs [39]. A variety of experimental methods, based on either biophysical, genetic, or biochemical principles, have also been developed to aid in their study. Each type of method has its own strengths

and limitations in terms of sensitivity and specificity [466].

State of the art techniques to study PPIs include yeast two-hybrid systems [99], affinity purification procedures based on immunoprecipitation (IP) or a single or double affinity tag (e.g. FLAG tag and TAP tag, respectively [162, 315, 302]) associated with protein identification by mass spectrometry, microarray technology [467, 306], and computational prediction methods [332, 4].

One of the most widely used methods to analyze PPIs is the two-hybrid system but, although its exact rate of false-positive results is unknown, it has been estimated as high as 50% [75]. Another widely used technique is affinity chromatography, a biochemical separation technique for purification of a specific molecule from complex mixtures, based on highly specific interactions between two molecules, like receptor and ligand or antibody and antigen. It greatly enhances the speed and efficiency of protein purification and also provides the technology platform to perform PPI studies, such as pull-down, tandem affinity purification (TAP), and antibody-based methods including co-immunoprecipitation (Co-IP) and enzyme-linked immunosorbent assay (ELISA) [466]. Since in affinity fusion-based protein purification a tag has been genetically fused to the target protein, a selective binding is possible, making it an excellent method to purify and identify multiprotein complexes [23].

Affinity-based techniques, however, are biased towards high abundance and/or slow dissociation kinetics proteins. Therefore, when detecting transient PPIs, affinity chromatography-based procedures may not be optimal, particularly if stringent washing steps are used [421, 23].

0.5.2 Crosslinking

The main challenge that affinity-based methods face is the inherent difficulty in maintaining protein and complex integrity during removal of non specific interactors by washing steps. These washing steps must be often harsh, especially when dealing with membrane proteins, as these commonly require high levels of detergent in order to guarantee solubility [124, 312]. To circumvent this issue, affinity-based methods have been successfully combined with cross-linking strategies for protein-protein interaction characterization, and became a standard method [466, 402].

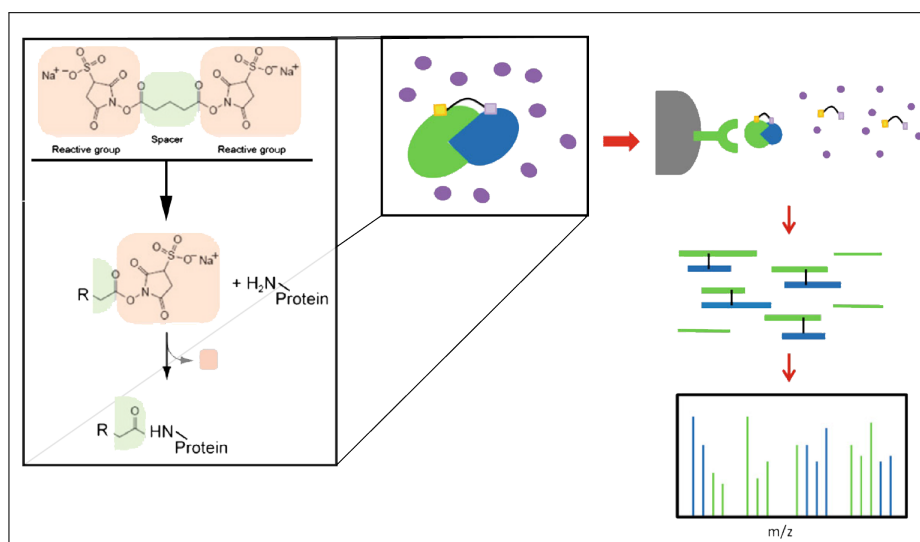


Figure 24: Scheme of typical setup for mass spectrometry analysis of affinity purified chemical crosslinked samples. Scheme depicting a general setup for identification of protein interactions. Cross-linking using a cross-linker composed of one or two reactive groups separated by a spacer arm. Here bis(sulfosuccinimidyl)glutarate (BS2G) which reacts with primary amines (lysine side chain, protein N-terminus). Part of the cross-linker, the leaving group, is replaced by the primary amine. R can stand for either the rest of the cross-linker or another protein, if the cross-linker had already reacted on its other end. After complex stabilization by crosslinking, it can be isolated by affinity purification, digested and identified by mass spectrometry. Figure from Turriziani et al. [402] and Rappsilber [311].

Chemical crosslink is able to stabilize and lock PPIs by forming covalent bonds between proteins in the native cellular environment [256, 435, 198]. This is achieved using chemicals that possess two terminal reactive elements (i.e bifunctional) that re-

act with specific functional groups (such as primary amines and sulfhydryls) of amino acids [83]. The crosslinked protein complexes remain intact during cell lysis and stringent washes and can capture transient and/or low-affinity interactions (Figure 24) [244, 132].

Overall, four protein functional groups account for most of the crosslinking techniques:

- Primary amines (–NH₂): Present in the N- terminus of all polypeptides and in lysine (Lys, K) side chains.
- Carboxyls (–COOH): Present in the C-terminus of all polypeptides, as well as in aspartic acid (Asp, D) and glutamic acid (Glu, E) side chains.
- Sulfhydryls (–SH): Group present in cysteine (Cys, C) side chains.
- Carbonyls (–CHO): Aldehyde groups created by oxidation of carbohydrate groups in glycoproteins.

(Source: www.piercenet.com)

Identifying the crosslinked residues/peptides can point towards the contact/binding interfaces among protein complexes, potentially helping mapping the topology of proteins and protein complexes [124, 10, 368, 394, 464].

Crosslinkers can be either homo- or hetero-bifunctional reagents. This means they can possess identical or different reactive groups, respectively, allowing the establishment of inter- and intra-molecular crosslinks [368]. The most widely used crosslinkers belong to the homobifunctional class of cross-linkers and contain two NHS esters. NHS esters present a high reaction efficiency, yield a stable amide bond and react at physiological conditions (pH 7-8) [38, 227, 369]. Moreover, NHS esters crosslink to lysine residues, which is a frequent amino acid [470]. However, hetero bifunctional crosslinkers present a more versatile character as they also allow sequential (two-step) conjugations than can help minimize self-conjugation and unwanted polymerization[83].

Crosslinker choice is not only based on chemical reactivities but also on other chemical properties that allow their use in the desired conditions:

1. Spacer arm length - will it detect only close interaction or will it be more flexible?
2. Spacer arm cleavability - can the linkage be reversed or broken when desired?
3. Water-solubility and cell membrane permeability - can it cross lipid bi-layers and/or crosslink hydrophobic within transmembrane domains?
4. Reaction induction - reagent acts upon addition or activation needed?

Chemical crosslinking is an ideal strategy to demonstrate protein-protein interactions, since if two proteins are close enough to physically interact, then they can be covalently linked by crosslinking. Thus crosslink of two distinct proteins is direct and convincing evidence of their close proximity and can reveal the regions of contact between them [83]. Although the rate of false positive is low, the cross-linking has to be well calibrated in order to decrease the amount of unspecific links [311, 402]

0.5.3 Mass Spectrometry

With the increased capacity of "locking" both transient as well as low-abundance interactors to their partners, the need for more sensitive methods of downstream detection arose. Chemical cross-linking methods in combination with mass spectrometry have become increasingly important tools for mapping of protein topology and for studying protein-protein interactions [10, 394, 368, 408]. Mass spectrometric analysis of cross-linked protein complexes allows identification of the protein interacting partners and in principle, could lead to identification of interaction regions between proteins provided that the crosslinked sites are identified. However, the identification of the sites of interaction or crosslinker labeling sites are highly challenging due to the complexity of

linked peptides inherent to cross-linking approaches [387, 311]. In crosslinking reactions, excessive amounts of crosslinker are often used, as to increase reaction rate and product yield, thus resulting in highly complex mixtures. Proteolysis results in a population of peptides that might or might not be crosslinker-associated, or even associated to other peptide(s) through the crosslinker. All these factors result in a spectral complexity that precludes peptide/protein identification (Figure 25, top) [464].

The abundance estimation of detected protein interactions also yields valuable information for structural biologists. Stoichiometry data can be obtained in experiments with isotope-labeled reference peptides [436, 22, 338] or less labor-intensive label-free quantification methods [436, 371]. However, due increased equipment sensitivity, quantitative filters need to be introduced to distinguish contaminants from real interactors. These filters typically rely on either isotope labels or normalization algorithms for label-free quantitation [12, 372].

Prioritizing detected PPIs is not trivial, and this remains a major challenge in biological follow-up studies. Recently, a more direct measure of the importance of these interactions was developed by determining the stoichiometry of all of the interactors in single-step affinity purifications [436, 371]. Wepf et al. implemented isotope labeled-reference peptides to quantify proteins, and used the resulting calibrated ion signal intensities for label-free quantification in reciprocal pulldowns [436]. Smits et al. reported a fully label-free stoichiometry quantitation method [371], which applies the intensity-based absolute quantitation (iBAQ) algorithm [347] and does not require isotope-labeled reference peptides. Importantly, this method can be directly applied to affinity purification mass spectrometry (AP-MS) data of a single protein of interest and a matched control. These measurements are performed on protein complex populations that might be heterogeneous and stoichiometry values represent the average

complex composition. Additional quantitative information can directly be used to distinguish core interactors from those that are substoichiometric [372].

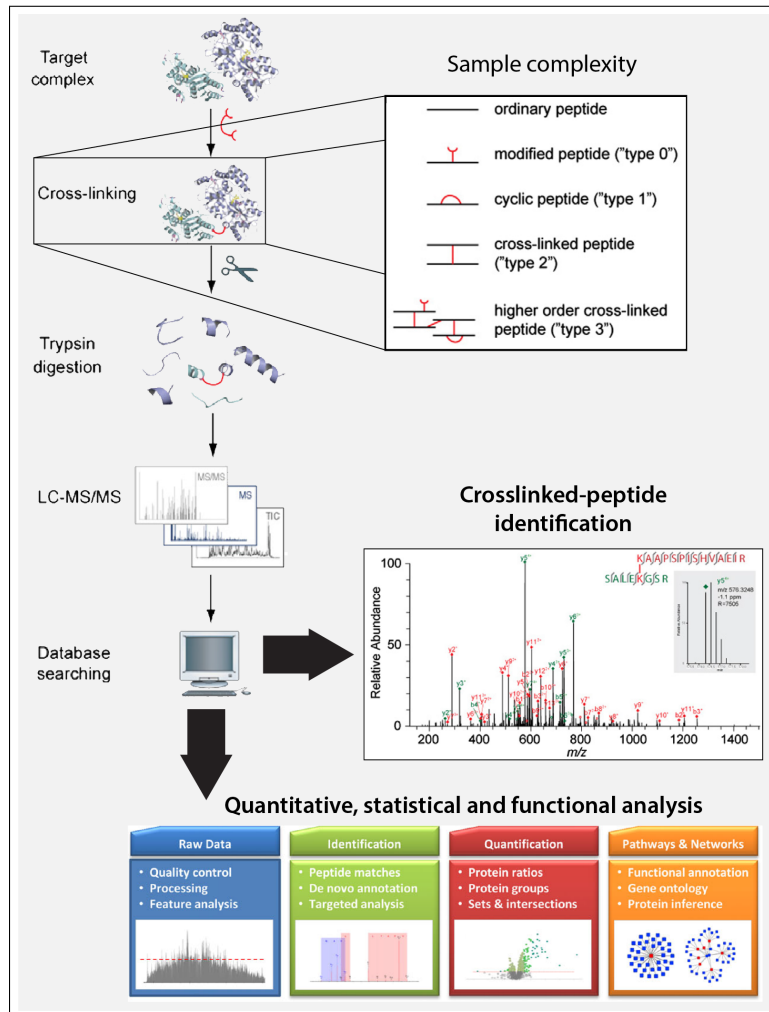


Figure 25: Workflow of standard analysis procedure of mass spectrometry data analysis. Outline of a typical cross-linking/mass spectrometry setup. Target complex is cross-linked and digested with trypsin. The peptides are analysed by liquid chromatography coupled high-resolution mass spectrometry (LC-MS/MS). Peptide fragmentation spectra are subjected to database searching to identify cross-linked peptides. Peptides types that can be observed after cross-linking and trypsin digestion. Proteomics data can then be analyzed and visualized, as well as interpreted through different approaches (bottom panels). Based on figure from Rappsilber [311] and Oveland et al. [276].

This information is especially valuable in combination with the recently developed

crosslinking mass spectrometry (XL-MS) workflows [462, 163], which allow identifying neighboring protein complex subunits (Figure 25, middle). Developments in crosslinking reagents, instrumentation, and analysis software have resulted in a broader use of XL-MS [218, 311, 155]. This methodology was recently optimized to be compatible with single-step affinity purification and can be performed parallel to label-free PPI identification and quantitation [357, 233]. Recently, the XL-MS approach was extended to crude lysates for global topology analysis using an MS-cleavable crosslinker [222]. Combination of high-confidence PPI data and the stoichiometry and topological information derived from XL-MS data facilitates modeling the architecture of protein complexes. A modeling approach based on interactor identification and interaction weights based on reported contacts has even recently been reported (Figure 25, bottom) [1, 299].

0.6 Aim of this Study

The main objectives of this study are:

- Establish a chemical crosslinking setup for Sec61 crosslinking to known and new interactors
- Establish a setup for crosslinked-complex enrichment and analysis
- Functional characterization of Sec61 interactions

Throughout the project, the primary goal was the identification of Sec61 luminal interactors that might be involved in ERAD, as these could validate the hypothesis that Sec61 is part of the retrotranslocon.

As most Sec61 interaction studies in the past focused on nascent chain-Sec61 interactions, my crosslinking studies also provided a more comprehensive picture of Sec61 interactors with new proteins in both ER membrane and ER lumen.

1

Material and Methods

1.1 Materials

1.1.1 Laboratory equipment and their Suppliers

The laboratory equipment used in this study is listed in Table 1.1.

Table 1.1: Laboratory Equipment

Company	Product
AGFA Healthcare GmbH	CP1000 X-ray film processor
Beckman Coulter Inc.	Optima L-90K ultracentrifuge
	Optima MAX-XP benchtop ultracentrifuge
	Avanti® J-E high-speed centrifuge
Bio-Rad Laboratories Inc.	583 gel dryer
	PowerPac HC power supply
	Trans-Blot electrophoretic transfer cell
	BioLegend LP Purification system
BioSpec Products Inc.	Mini-BeadBeater -24
Eppendorf AG	Microcentrifuge 5415R
	Thermomixer Comfort
GE Healthcare	Amersham autoradiography Hypercassettes
	Amersham Ultrospec 2100 pro UV/VIS Spectrophotometer
	ImageQuant TL software
	Storage Phosphor Screens and cassettes
	Typhoon TRIO phosphorimager
	Amersham Imager 600

Company	Product
Gilson Inc.	Pipette set
Hellma Analytics	Quartz cuvettes
Hirschmann Gmbh & Co. KG	Pipet-Aid pipette controller
IKA-Werke GmbH	EUROSTAR power-b overhead stirrer RCT basic magnetic stirrer
Infors AG	Multitron Standard incubation shaker
Merck KGaA	Millipore MilliQ water purification system
neoLab Migge gmbH	Overhead rotator Rocking shaker
Roth GmbH & Co. KG	Neubauer Hemocytometer
Sartorius AG	Analytical balance
Scientific Industries Inc.	Vortex-Genie 2
Singer Instruments	MSM 300 tetrad dissection microscope
Sigma Laborzentrifugen GmbH	4K15 refrigerated centrifuge
Systec	DX-150 autoclave
	XCell SureLock Mini-Cell electrophoresis system
Thermo Fisher Scientific Inc.	Sorvall Evolution RC centrifuge 3UV-Lamp
VWR/PEQLAB	E-BOX VX2 gel documentation system peqSTAR 2X gradient thermocycler PerfectBlue Gelsystem Mini S

Company	Product
Zeiss Microscopy & GmbH	Axioskop microscope
Wheaton	55 ml tissue grinder, Potter-ELV

1.1.2 Reagents, Chemicals and their Suppliers

All reagents, consumables and chemicals are listed in Table 1.2.

Table 1.2: Reagents, chemicals and consumables

Company	Product
AGFA HealthCare GmbH	Agfa Developer G153 Agfa Fixer G354
Applichem GmbH	Ampicillin Sodium Salt (BioChemica)
	DEPC (BioChemica)
	Kanamycin Sulfate (BioChemica)
	Tunicamycin
	HEPES-Sodium Salt
	Sodium Chloride
	Magnesium Chloride
	Sodium Acetate
BD	Magnesium Acetate
	Ammonium Acetate
	Bacto™ Casamino Acids
	Bacto™ Peptone
	Bacto™ Yeast Extract

Company	Product
BD	Difco™ Yeast Nitrogen Base without Amino Acids & Ammonium Sulfate
	Difco™ Yeast Nitrogen Base without Amino Acids
Beckman Coulter GmbH	Polycarbonate Bottles, thick-walled, 70 ml (rotor type 45 Ti)
	Polyallomer Tubes, thin-walled, 4.4 ml (rotor type SW 60 Ti)
	Polycarbonate Tubes, thick-walled, 1.0/1.4 ml (TLS-55)
Bio-Rad Laboratories Inc.	Polycarbonate Tubes, thick-walled, 3.0/3.5 ml (TLA-100.3)
	Microfuge® Tubes, Polyallomer, 1.5 ml
	Nitrocellulose Membrane (0.2 µM, 0.45 µM pore size)
Carl Roth GmbH	Precision Plus Protein™ All Blue Standards
	PMSF (≥99%)
	Roti®-Aqua-Phenol (RNA extraction)
	Rotiphorese® Gel 30 (37,5:1)
	β-Mercaptoethanol (99 %, p.a.)
	TEMED (99 %, p.a.)
	Roti®-Phenol/Chloroform/Isoamyl-Alcohol (Nucleic acid extraction)
Peptone (from Casein)	
	Yeast Extract

Company	Product
Carl Roth GmbH	Glycine (PUFFERAN®, ≥99 %, p.a.)
	Agar-Agar, Kobe I
	Ammonium Peroxydisulfate (≥98 %, p.a.)
	SDS Pellets (≥99 %)
	RNase AWAY®
	Glycerol (≥98 %)
	Triton X 100, pure
	Sodium Carbonate
	Urea
	Potassium Acetate
2-Nitrophenyl-β-D-Galactopyranoside	
Fermentas	Conventional and FastDigest® Restriction Enzymes
	T4 DNA Ligase
	FastAP™ Thermosensitive Alkaline Phosphatase
	GeneRuler™ 1 kb DNA Ladder
	GeneRuler™ 1 kb Plus DNA Ladder
	PageRuler™ Prestained Protein Ladder
	PageRuler™ Plus Prestained Protein Ladder
	RNase A, DNase and Protease-free (10 mg/ml)
5-Fluoroorotic Acid	
Formedium™	Synthetic Complete Drop-Out Mixture, (SC) (-Ade, -His, Leu, -Lys, -Trp, -Ura), (Kaiser Mixture)
FujiFilm	Medical X-ray Film (Super HR-E30)
GE Healthcare	Protein A Sepharose™ CL-4B

Company	Product
GE Healthcare	Con-A Sepharose® 4B HisTrap FF crude 1mL
Invitrogen™	NuPAGE® Novex 4-12 % Bis-Tris Gel 1.5 mm, 10 Well (Novex®) NuPAGE® MOPS SDS Running Buffer (20X) (Novex®)
Calbiochem®	Cycloheximide
New England Bio-Labs® (NEB)	Conventional Restriction Enzymes
PEQLAB Biotechnologie GmbH	KAPA HiFi™ PCR Kit
PerkinElmer Inc.	EXPRE ³⁵ S ³⁵ S Protein Labeling Mix, [³⁵ S]-, 50mM Tricine (pH 7.4), 10mM 2-mercaptoethanol COUNT-OFF Liquid Concentrate
Promega GmbH	Recombinant RNasin® Ribonuclease Inhibitor
Rockland™	HRP-conjugated anti-rabbit
Sartorius AG	Minisart® Plus Syringe Filters (0.2, 0.45 µm pore size)
Sigma-Aldrich®	Adenine (≥99 %) L-Cysteine (≥98 %) L-Histidine (Sigma) Uracil (≥99 %) L-Leucine (≥98.5 %) L-Tryptophan (≥98 %)

Company	Product
	L-Methionine ($\geq 99\%$)
	L-Cysteine ($\geq 99\%$)
	DL-Dithiothreitol, BioUltra, $\geq 99.0\%$
	Sucrose BioXtra, $\geq 99.5\%$
	Tryptone, enzymatic digest from casein
	D-(+)-Glucose ($\geq 99.5\%$)
	Deoxyribonucleic Acid Sodium Salt
	Absolute Ethanol
	Bromophenol Blue Sodium Salt
	Trizma® Base, for molecular biology, $\geq 99.8\%$
	Urea
	Sodium Azide, BioUltra, $\geq 99.5\%$
	Tween® 20
	DMSO
	Glass Beads, acid-washed 425-600 μm
	EDTA, anhydrous, $\geq 99\%$
	Lithium Acetate Dihydrate, BioXtra
	Polyethylene Glycol, BioXtra, average mol wt 3,350
	D-(+)-Galactose ($\geq 99\%$)
	Sodium Chloride, for molecular biology ($\geq 98\%$)
	GenElute™ PCR Clean-Up Kit
	GenElute™ Gel Extraction Kit
	Corning® Cryogenic Vials, internal thread (2.0 mL)
	Tunicamycin

Company	Product
Sucofin	Skimmed Milk Powder
	Pierce 660 nm Protein Assay Reagent
	SuperSignal West Dura Extended Duration Chemiluminescent Substrate (ECL)
	Filter Units – 115/250/500 ml capacity, MF75™ Series, 0.45 µm pore size
	DMSO
Thermo Fisher Scientific	DSS (disuccinimidyl suberate)
	SDAD (succinimidyl 2-[(4,4'-azipentanamido)ethyl]- 1,3'-dithiopropionate)
	SMPH (Succinimidyl-6-[(β- maleimidopropionamido)hexanoate])
	LC-SPDP (succinimidyl 6-[3'-(2-pyridyldithio)- propionamido] hexanoate)
VWR® International	Cloridric acid 99 % GPR RECTAPUR®
	Ethanol Absolut AnalaR NORMAPUR®
ZChL	All other chemicals not mentioned above but men- tioned in the respective sections of this chapter

1.1.3 Software

In Table 1.3 is listed all the software used throughout this work.

Table 1.3: Software used in this study

Name	Use
BibDesk	Bibliography Software
ChemSketch	Draw chemical structures
GraphPad Prism	Data plotting
Illustrator	Image editing
ImageQuant	Band intensity quantitation
Lightroom	Image managing
MaxQuant	Mass spectrometry data analysis (Mandy Rettel)
MsConvert	Convert mass spectrometry spectrums to the .mzXML format for xQuest analysis
Photoshop	Image editing
PyMOL	3D structure analysis
R	Mass spectrometry statistical analysis (Frank Stein)
SnapGene	DNA sequence editing
TexMaker	Text Editor (\LaTeX)
xQuest/xProphet	Crosslinked peptide analysis

1.1.4 *E. coli* Strains

All *E. coli* strains used and generated throughout this study are listed in Table 1.4 or- ganized by their Strain Collection code.

Table 1.4: *E. coli* strains

Strain	Genotype	Source
DH5 α	F- endA1 glnV44 thi-1 recA1 relA1 gyrA96 deoR nupG Φ 80dlacZ Δ M15 Δ (lacZYA-argF)U169,hsdR17(rK- mK+), λ -	Hanahan [140]
KRB3	Lyticase expressing <i>E. coli</i> (in DH5 α)	Shen et al. [355]
KRB351	p416 p Δ gpaF (in DH5 α)	Mumberg et al. [253]
KRB356	pBW11 (SEC61 WT in pRS315)(in DH5 α)	Stirling et al. [382]
KRB842	pRS315 in DH5 α	M. Schmitt, Sikorski & Hieter [365]
KRB856	pRS313-PHO8-URA3 (in DH5 α)	Ng et al. [258]
KRB863	pRS315-sec61-S353C (in DH5 α)	Kaiser & Römisch [186]
KRB866	pRS306-truncsec61-S353C (in DH5 α) (in DH5 α)	Kaiser & Römisch [186]
KRB882	pSM70 KHN-HA (URA3)(in DH5 α)	D. Ng, Vashist et al. [406], Vashist & Ng [407]
KRB883	pSM101 KWW-HA (URA3) (in DH5 α)	D. Ng, Vashist & Ng [407]
KRB951	pRS315-sec61 Δ L7 (in DH5 α)	Tretter et al. [397]
KRB966	pRS305-truncsec61 Δ L7 (in DH5 α)	This work

Strain	Genotype	Source
KRB1060	pRS426	Stein et al. [380]
KRB1055	pRS426-14His-SEC61	This work
KRB1056	pRS426-14His-sec61S353C	This work
KRB1057	pRS426-14His-SBH1	This work
KRB1058	pRS426-14His-SSS1	This work
KRB1090	pRS315-14His-SEC61	This work
KRB1091	pRS315-14His-sec61S353C	This work
KRB1093	pRS316-NSG1-HA	Carvalho lab, Foresti et al. [102]
KRB1094	pRS316-ERG11-HA	Carvalho lab, Foresti et al. [102]
KRB1113	pRS315-sec61Δ201-216	This work
KRB1114	pRS315-sec61Δ230-236	This work
KRB1115	pRS315-sec61Δ201-216/Δ230-236	This work

1.1.5 *S. cerevisiae* Strains

Listed in Table 1.5 are all *S. cerevisiae* strains used and generated throughout this study organized by their Strain Collection code.

Table 1.5: *S. cerevisiae* strains

Name	Genotype	Source/Reference
KRY37	<i>MATa his4 trp1-1 leu2-3,112 ura3-52 hoc1-1 sec61-3</i>	Schekman lab Stirling et al. [382]
KRY47	<i>MATa leu2-3,112 ura3-52</i>	Pilon et al. [289]

Name	Genotype	Source/Reference
KRY153	<i>MATα can1-100 leu2-3,112 his3-11,15 trp1-1 ura3-1 ade2-1 sec61::HIS3 [pDQ SEC61]</i>	R. Schekman, Pilon et al. [288]
KRY157	<i>MATα can1-100 leu2-3,112 his311,15 trp1-1 ura3-1 ade2-1 sec61::HIS3 [pDQ sec61-32]</i>	R. Schekman, Pilon et al. [288]
KRY160	<i>MATα eu2-3,112 his3-11,15 trp1-1 ura3-1 ade2-1 can1-100 leu23,112::LEU+ UPRE-lacZ MET+ ire1::TRP1 pRS304</i>	Sidrauski/Peter Walter, Shamu & Walter [351]
KRY161	<i>MATα ade2-1 ura3-1 his3-11,15 leu23,112 trp1-1 can1-100 prc1</i>	D. Wolf, [201]
KRY461	<i>MATα sec61::HIS3 leu2 trp1 prc1-1 his3 ura3 [pGAL-SEC61-URA3]</i>	Römisch Lab
KRY486	<i>MATα/α can1-100 ura3-1 trp1-Δ1 ade2-1 leu2-3,112 his3-11,15 can1-100 ura3-1 trp1-Δ1 ade2-1 leu2-3,112 his3-11,15</i>	Schekman lab, [35]
KRY850	<i>BMA38a, kanr-pGAL-Sec61, his3Δ200 leu2-3.112 trp1-Δ1 ura3-1 ade2-1 can1-100</i>	Kaiser & Römisch [186]
KRY853	<i>MATα leu2-3,112 ura3-52 [pRS306-truncsec61-S353C]</i>	Kaiser & Römisch [186]
KRY896	<i>MATα sec61::HIS3 leu2 trp1 prc1-1 his3 ura3 pRS315-sec61ΔL7</i>	Tretter et al. [397]
KRY897	<i>MATα sec61::HIS3 leu2 trp1 prc1-1 his3 ura3 pRS315-SEC61</i>	Tretter et al. [397]

Name	Genotype	Source/Reference
KRY956	<i>can1-100 ura3-1 trp1-Δ1 ade2-1 his3-11,15</i> <i>SEC61::trunc.sec61ΔL7(LEU2)</i>	This work
KRY962	<i>MATα his3Δ1 leu2Δ0 lys2Δ0 ura3Δ0</i>	Euroscarf
KRY963	<i>MATα his3Δ1 leu2Δ0 lys2Δ0 ura3Δ0</i> <i>hrd1::kan</i>	Euroscarf
KRY964	<i>MATα his3Δ1 leu2Δ0 lys2Δ0 ura3Δ0</i> <i>hrd3::kan</i>	Euroscarf
KRY1005	<i>MATα ura3-52 leu2-3,112 sec61::truncsec61-</i> <i>S353C(URA3) hrd3::KanMX</i>	This work
KRY1061	<i>MATα sec61::HIS3 leu2 trp1 prc1-1 his3 ura3</i> <i>ade2 [pGal-14His-sec61S353-LEU2]</i>	This work
KRY1081	<i>MATα sec61::HIS3 leu2 trp1 prc1-1 his3 ura3</i> <i>ade2 [pGal-14His-SEC61-LEU2]</i>	This work
KRY1097	<i>MATα his3Δ1 leu2Δ0 lys2Δ0 ura3Δ0</i> <i>ASI3::Kan</i>	Euroscarf
KRY1098	<i>MATα his3Δ1 leu2Δ0 lys2Δ0 ura3Δ0</i> <i>YNR021w::Kan</i>	Euroscarf
KRY1099	<i>MATα his3Δ1 leu2Δ0 lys2Δ0 ura3Δ0</i> <i>PSG1::Kan</i>	Euroscarf
KRY1100	<i>MATα his3Δ1 leu2Δ0 lys2Δ0 ura3Δ0</i> <i>SHE2::Kan</i>	Euroscarf
KRY1116	<i>MATα sec61::HIS3 leu2 trp1 prc1-1 his3 ura3</i> <i>ade2 [pRS315-sec61Δ201-216]</i>	This work

Name	Genotype	Source/Reference
KRY1117	<i>MATα sec61::HIS3 leu2 trp1 prc1-1 his3 ura3 ade2 [pRS315-sec61Δ230-236]</i>	This work
KRY1118	<i>MATα sec61::HIS3 leu2 trp1 prc1-1 his3 ura3 ade2 [pRS315-sec61Δ201-216/Δ230-236]</i>	This work
KRY1119	<i>MATα his3Δ1 leu2Δ0 lys2Δ0 ura3Δ0 [pRS426-MID2-HA]</i>	This work
KRY1120	<i>MATα his3Δ1 leu2Δ0 lys2Δ0 ura3Δ0 SHE2::kanM [pRS426-MID2-HA]</i>	This work
KRY1121	<i>MATα his3Δ1 leu2Δ0 lys2Δ0 ura3Δ0 pmt2::LEU2 [pRS426-MID2-HA]</i>	This work
KRY1122	<i>MATα can1-100 leu2-3,112 his3-11,15 trp1-1 ura3-1 ade2-1 sec61::HIS3 [pDQ sec61-32] [pRS426-MID2-HA]</i>	This work
KRY1124	<i>MATα his3Δ1 leu2Δ0 lys2Δ0 ura3Δ0 SHE2:Kan SEC61::trunc.sec61S353C-URA</i>	This work
KRY1130	<i>MATα can1-100 leu2-3,112 his3-11,15 trp1-1 ura3-1 ade2-1 sec61::HIS3 [pDQ SEC61] [Nsg1-HA-Trp]</i>	This work
KRY1131	<i>MATα can1-100 leu2-3,112 his3-11,15 trp1-1 ura3-1 ade2-1 sec61::HIS3 [pDQ SEC61] [Erg11-HA-Trp]</i>	This work

Name	Genotype	Source/Reference
KRY1132	<i>MATα can1-100 leu2-3,112 his3-11,15 trp1-1 ura3-1 ade2-1 [pDQ sec61-32] [Nsg1-HA-Trp]</i>	This work
KRY1133	<i>MATα can1-100 leu2-3,112 his3-11,15 trp1-1 ura3-1 ade2-1 [pDQ sec61-32][Erg11-HA-Trp]</i>	This work

1.1.6 Plasmids

Listed in Table 1.6 are all plasmids used in this study.

Table 1.6: Plasmids

Plasmid	Strain cat. #	Use/Description	Source/ Reference
pBW11	KRB356	<i>SEC61</i> expression	Stirling et al. [382]
p416p Δ gpaf	KRB351	Overexpression of p Δ gpaf (URA3)	Mumberg et al. [253]
pRS315	KRB842	Cloning vector	M. Schmitt, Sikorski & Hieter [365]
pRS313- <i>PHO8-URA3</i>	KRB856	Expression of the chimeric Pho8-Ura substrate	Ng et al. [258]
pRS315- <i>sec61S353C</i>	KRB863	Expression of Sec61S353C	Kaiser & Römisch [186]

Plasmid	Strain cat. #	Use/Description	Source/ Reference
pRS306- <i>truncsec61-S353C</i>	KRB866	Genomic integration of <i>sec61S353C</i>	Kaiser & Römisch [186]
pSM70 KHN-HA (URA3)	KRB882	KHN-HA	D. Ng, Vashist & Ng [407]
pSM101 KWW-HA (URA3)	KRB883	Expression of KWW-HA	D. Ng, Vashist & Ng [407]
pRS315- <i>sec61ΔL7</i>	KRB951	Expression of Sec61ΔL7	Tretter et al. [397]
pRS305- <i>truncsec61ΔL7</i>	KRY966	Genomic integration of <i>sec61ΔL7</i>	This work
pRS426	KRB1060	14His gene tagging	Stein et al. [380]
pRS426-14His- <i>SEC61</i>	KRB1055	Sec61 tagging with a 14His-tag	This work
pRS426-14His- <i>sec61S353C</i>	KRB1056	Sec61S3534C tagging with a 14His-tag	This work
pRS426-14His- <i>SBH1</i>	KRB1057	Sec61 tagging with a 14His-tag	This work
pRS426-14His- <i>SSS1</i>	KRB1058	Sec61 tagging with a 14His-tag	This work
pRS315-14His- <i>SEC61</i>	KRB1090	Expression of His ₁₄ -Sec61	This work

Plasmid	Strain cat. #	Use/Description	Source/ Reference
pRS315-14His- sec61S353C	KRB1091	Expression of His ₁₄ - Sec61S3534C	This work
pRS315-sec61Δ201- 216	KRB1113	Expression of sec61del1	This work
pRS315-sec61Δ230- 236	KRB1114	Expression of sec61del2	This work
pRS315-sec61Δ201- 216/Δ230-236	KRB1115	Expression of sec61del1/del2	This work
pRS316-NSG1-HA	KRB1093	Expression of HA tagged Nsg1	Foresti et al. [102]
pRS316-ERG11-HA	KRB1094	Expression of HA tagged Nsg1	Foresti et al. [102]

1.1.7 Primers

Listed in Table 1.7 are all plasmids used in this study.

Table 1.7: Primers

Name	Sequence (5' → 3')	T _m [°C]*	Application
16	GGATCCGCGCATTGCTTAAGCAA- GGATAC C	60	SEC61 downstream. Hinge mutants con- struction

Name	Sequence (5' → 3')	Tm [°C]*	Application
24	GTAAAACGACGGCCAGT	53	M13 primer (Frw). Used in sequencing or Colony PCR
25	CAGGAAACAGCTATGAC	47	M13 primer (Rev). Used in sequencing or Colony PCR
51	CTAGGGGGTCCGTCTTCTC	56	<i>HRD3</i> upstream. Hrd3 deletion
52	CCAATTGTATCACCTTCGCC	55	<i>HRD3</i> downstream. Hrd3 deletion
61	ATGTCAAGCCCAACTCC	52	<i>SBH1</i> ATG. Cloning into pRS426-14His
62	CTTCTATAGAAgCTTGAATC	40	<i>SBH1</i> downstream. Cloning into pRS426- 14His
63	ATGCCTCCAACCGTGT	54	<i>SEC61</i> ATG. Cloning into pRS426-14His
64	CAACTTCCTaaGCTTCACGCC	51	<i>SEC61</i> downstream. Cloning into pRS426- 14His. Hinge mutants construction
66	ATGGCTAGAGCTAGTGAAAAAGGTG- AAGAG	61	<i>SSS1</i> ATG. Cloning into pRS426-14His

Name	Sequence (5' → 3')	T _m [°C]*	Application
73	GTTGGAAAGCTTTCCATG	43	<i>SSS1</i> downstream. Cloning into pRS426-14His
85	GCAAATTAAGCCTTCGA	49	<i>CYC</i> . Subcloning of 14His-construct into pRS315
93	GCTGGAGCTCTAGTACG	52	<i>pGAL</i> . Subcloning of 14His-construct into pRS315
95	GTATATTCATGTTAAACGCCTTT	60	<i>PSG1</i> upstream. Deletion confirmation
100	AAATTCGGTACTATCAGCTTTCC	64	<i>YNR021W</i> upstream. Deletion confirmation
101	TTTGTTGTAGTTATGCTCCACGA	64	<i>SHE2</i> upstream. Deletion confirmation
102	ATATCACTAAACGACGCTCAAAA	62	<i>ASI3</i> upstream. Deletion confirmation
103	ATACTCTCACACAATATTCCCAA	51	<i>HRD1</i> upstream. Deletion confirmation
104	TTTAAACTTAATACTAGGGGGTC	50	<i>HRD3</i> upstream. Deletion confirmation
105	CTGCAGCGAGGAGCCGTAAT	62	<i>KanB</i> . Deletion confirmation

Name	Sequence (5' → 3')	Tm [°C]*	Application
106	GGAAAAAGGCAGGAGCAAACGCTC- TCCAG	90	deletion1. SOE PCR of <i>sec61del1</i>
107	CGTTTGCTCCTGCCTTTTTCCATCTT- TTGGCTG	98	deletion1. SOE PCR of <i>sec61del1</i>
108	GGACAAGAAATACCGTACCAATCTA- CCTAATATGTTCC	106	deletion2. SOE PCR of <i>sec61del2</i> (and <i>sec61del1/2</i>)
109	TGGTACGGTATTTCTTGTCTTTCTG- ACAGCC	94	deletion2. SOE PCR of <i>sec61del2</i> (and <i>sec61del1/2</i>)
110	GCCAATTA AAAAGAACCATTCTCC TCAGGAAACAAGCACGAC- GAATTGCGTACGCTGCA GGTC- GAC		S3-MPD1. MPD1 HA genomic tagging
111	CATATGTTGTGTTTAATTAGATAATC- ATTGAATGAGGAAACGTACCA CTAATCGATGAATTCGAGC TCG		S2-MPD1. MPD1 HA genomic tagging
114	GGATACAAGTCGACGCAAATTTCTC	72	MPD1 upstream. Sub-cloning of genomic <i>MPD1-HA</i> into pRS426

Name	Sequence (5' → 3')	Tm [°C]*	Application
115	CAATTTTGGATGGGAATTCAATTAT- AC	72	MPD1 downstream. Subcloning of genomic <i>MPD1-HA</i> into pRS426.
118	GTGGTGAACGATAGATGGAC	60	<i>ACT1. HAC1</i> mRNA splicing assay
119	ATTCTGAGGTTGCTGCTTTG	58	<i>ACT1. HAC1</i> mRNA splicing assay
120	CTGGCTGACCACGAAGACGC	66	<i>HAC1. HAC1</i> mRNA splicing assay
121	TTGTCTTCATGAAGTGATGA	54	<i>HAC1. HAC1</i> mRNA splicing assay
124	TTTTTTTTTTTTTTTTTT	36	Oligo-dT. cDNA synthesis

*Tm as given by SnapGene Software.

1.1.8 Antibodies

Listed in Table 1.8 are all antibodies used in this study.

Table 1.8: Antibodies

Antibody	Use & Dilution	Source
Anti-Sec61(N-terminus)	Western Blot 1: 2.500; IP 1:100	KB Römisch
Anti-Sec61(C-terminus)	Western Blot 1: 2.500; IP 1:100	KB Römisch
Anti-Sec63	Western Blot 1: 2.500; IP 1:100	Schekman lab

Antibody	Use & Dilution	Source
Anti-Sss1	Western Blot 1: 2.500; IP 1:100	Schekman lab
Anti-Sec62	Western Blot 1: 2.500; IP 1:100	Schekman lab
Anti-Sec71	Western Blot 1: 2.500; IP 1:100	Schekman lab
Anti-Rpn12	Western Blot 1:2.500	Römisch lab
Anti-Rpl24	Western Blot 1:2.500	Ng lab
Anti-Hrd1	Western Blot 1:10.000	T. Sommer lab
Anti-Hrd3	Western Blot 1:10.000	T. Sommer lab
Anti-HA	Western Blot 1:5.000 ; IP 1:200	BioLegend
Anti-CPY	Western Blot 1:2.000; IP 1:100	KB Römisch lab
Anti-pp α F	Western Blot 1:2.000; IP 1:100	KB Römisch lab
Anti-DPAPB	IP 1:100	Stevens lab
Anti- rabbit (HRP)	Western Blot 1:10.000	Rockland™
Anti- rat (HRP)	Western Blot 1:10.000	SIGMA
Anti-She2	Western Blot 1: 200; IP 1:100	Jansen lab
Anti-Asi3	Western Blot 1: 5000; IP 1:100	Carvalho lab
Anti-Pdi1	Western Blot 1: 5000; IP 1:100	Römisch lab
Anti-Kar2	Western Blot 1: 5000; IP 1:100	Römisch lab

1.1.9 Enzymes

Listed in Table 1.9 are all enzymes used in this study.

Table 1.9: Enzymes used in this study and their sources

Class	Enzyme	Company
Restriction Enzymes	BamHI	New England Biolabs (NEB)

Class	Enzyme	Company
Restriction Enzymes	BglI	New England Biolabs (NEB)
	EcoRI	
	HindIII	
	MscI	
	NheI	
	SalI	
	SmaI	
	SfiI	
Polymerases	OneTaq	NEB
	Crimson Taq	
	KAPA HiFi™	Peqlab
Reverse Transcriptase	Maxima® RT	Fermentas
Ligase	T4 DNA Ligase	Fermentas
Other enzymes	FastAP™	Thermo Fisher Scientific
	Lyticase	Römisch Lab

1.1.10 Media and Buffers

Routinely used media in the course of this study for both *S.cerevisiae* and *E.coli* growth are listed in Table 1.10 and Table 1.12, respectively.

Table 1.10: *S.cerevisiae* growth media routinely used in this study

Medium	Composition
YP (Yeast Extract, Peptone)	1 (w/v) % Yeast Extract, 2 (w/v) % Peptone (For solid media: 2 (w/v) % Agar-Agar)

Medium	Composition
YPD* (Yeast Extract, Peptone, Dextrose)	1 (w/v) % Yeast Extract, 2 (w/v) % Peptone, 2 (w/v) % Glucose (For solid media: 2 (w/v) % Agar-Agar)
Minimal Medium**	0.67 (w/v) % Yeast Nitrogen Base without Amino Acids, 0.13 (w/v) % Synthetic Complete Drop-Out Mixture*** (-Ade, -His, -Leu, -Lys, -Trp, -Ura), 2 (w/v) % Glucose, Amino Acids according auxotrophies (Table 1.11) (For solid media: 2 (w/v) % Agar-Agar)
Sporulation Medium	1% Potassium Acetate, 0.1% Yeast Extract, 0.05% Glucose (For solid media: 2 (w/v) % Agar-Agar)

*Glucose (50 %) filtrated and added to the YP solution prior to use.

**Sterilized by filtration. Auxotrophic amino acids added as listed in Table 1.5. For solid media, MQ water with agar-agar was autoclaved and other components filtered in before plate-pouring.

***composition of the complete synthetic "drop-out" mixture used is listed in Table 1.11.

Table 1.11: Composition of Synthetic Complete amino acid drop-out mixture for *S.cerevisiae*

Compound	mg/l	Compound	mg/l
Adenine	18	L-Leucine	380
L-Alanine		L-Lysine	76
L-Arginine HCl		L-Methionine	
L-Asparagine	76	<i>para</i> -Aminobenzoic acid	8
L-Aspartic Acid		L-Phenylalanine	
L-Cysteine		L-Proline	76
L-Glutamine		L-Serine	

Compound	mg/l	Compound	mg/l
L-Glutamic acid		L-Threonine	
Glycine		L-Tryptophan	
L-Histidine	76	L-Tyrosine	76
<i>myo</i> -inositol		Uracil	
L-isoleucine		L-Valine	

Table 1.12: *E.coli* growth media routinely used in this study

Medium	Composition
LB (Lysogeny Broth)	0.5 % (w/v) Yeast Extract, 1 % (w/v) Tryptone, 0.05 % (w/v) NaCl, 1.0 mM NaOH (For solid media: 2 % Agar-Agar)
LB-Amp	LB with 100 µg/ml Ampicillin* (For solid media: 2 % Agar-Agar)
LB-Kan	LB with 50 µg/ml Kanamycin*

*Antibiotics stock solutions were sterile filtered, and added to the media prior to use at the designated concentration.

All buffers composition is described at the appropriate section of use.

1.2 Methods

1.2.1 Sterilization

All glassware and media were sterilized by autoclaving at 100 kPa and 121 °C for 20 min if not stated otherwise.

1.2.2 Growth of *S.cerevisiae*

S. cerevisiae cells were grown at 30°C in YPD or in SC medium with continuous shaking at 220 rpm. Cells on solid medium were also grown at 30°C if not stated otherwise. To test temperature sensitivity, cells were counted and serial dilutions were prepared. A volume of 5 µl of each dilution (containing 10⁴ – 10 cells) was pipetted onto YPD plates. To test tunicamycin (Tm) (SIGMA) sensitivity, cells were grown on YPD plates supplemented with 0, 0.25, 0.5, or 0.75 µg/ml Tm. Plates were incubated at indicated temperatures for 3 days (Table 1.10 and 1.11).

1.2.3 Growth of *E.coli*

E.coli cells were grown at 37 °C in LB medium with continuous shaking at 160 rpm or on LB medium plates. When necessary, both liquid and solid media were supplemented with adequate concentration of appropriate antibiotic (Table 1.12).

1.2.4 Polymerase Chain Reaction

Polymerase Chain Reaction (PCR) is a technique that allows the amplification (i.e exponential increase of the copy number) of a targeted DNA sequence. For this purpose, three key elements are necessary: template DNA (containing region to be amplified); flanking primers (short single-stranded oligonucleotides, which are designed to specifically bind to the template DNA at the 5' and 3' end of the target sequence); and a DNA polymerase, which will be the responsible for the actual polymerization of the new DNA copies.

A standard PCR reaction consist of a 20-35 cycle (depending on the polymerase used) of three steps: denaturing, primer annealing, and primer extension. During the first step, the PCR mix (Table 1.13) is heated at a high temperature (also poly-

merase dependent) so as to denature the double-stranded DNA and allow access of primers to their area of homology. Primer annealing (step 2) is performed at a lower, sequence-specific temperature to ensure specific binding of the primer pair to the template DNA. During the extension, or elongation step, the DNA polymerase extends the primers and adds nucleotides complementary to the template DNA. Since these three step are repeated in cycle, when in non-limiting concentration of dNTPs and primers, will result in an exponential increase of the copy number of the target sequence.

During this study PCR was performed in order to amplify multiple DNA targets. Unless stated otherwise, Kapa HiFi (Peqlab) was used for all cloning-purpose amplifications (Section 1.1.9, Table 1.9). The standard reaction composition and program used is described in Tables 1.13 and 1.14, respectively. Temperature and duration of each step (Table 1.14) were optimized for each reaction/sequence. Gene-specific primers (Table 1.7) were designed using the sequences acquired on www.yeastgenome.org.

The peqSTAR 2X Gradient Thermocycler (Peqlab) was used routinely for PCRs. The correct size of each PCR product was verified by agarose gel electrophoresis (Section 1.2.6). Resulting PCR products were either cloned into a vector or used to directly transform *S.cerevisiae*.

Table 1.13: Standard reaction mixture for PCRs

Component	Volume (µl)	Final concentration/
5X KAPAHiFi™ Reaction Buffer	10	1X
KAPA dNTP Mix (10 mM each)		
Forward primer (10 µM)	1.5	0.3 mM
Reverse primer (10 µM)		
Template DNA	1	10ng plasmid DNA

Component	Volume (μ l)	Final concentration/ Quantity
KAPAHiFi™ Polymerase		0.02 U/ μ l
dH ₂ O	to 50	–

Table 1.14: Standard thermal cycler program for PCRs

N° of Cycles	Operation	Temperature (°C)	Duration
1	Initial denaturation	95°C	5sec
35	Denaturation	98	20sec
	Primer annealing	58*	15sec
	Primer extension	72	30 sec/kb
1	Final extension	72	5 min
1	Store	4	∞

*Primer annealing for the great majority of the PCR reactions was 58°C. For all other PCRs (eg. HAC1 mRNA splice assay) primer annealing tempera-

ture is mentioned in the Methods section when specific protocol is described.

1.2.4.1 Splice Overlap Extension (SOE) PCR

PCR-driven overlap extension was used for site-directed mutagenesis during this study. During SOE-PCR, overlapping gene fragments are generated (Figure 1.1, 1st round). These overlapping fragments will, upon annealing of the homologous regions, generate a continuous unit, that is used as template in a new PCR reaction, generating the fused (full-length) product (Figure 1.1, 2nd round). By choosing appropriate internal primers that overlap each other and flank the mutagenesis-targeted se-

quence, one can either delete, add or exchange a given sequence. The intermediate fragments can then be fused together in a final PCR using flanking primers [161, 164]

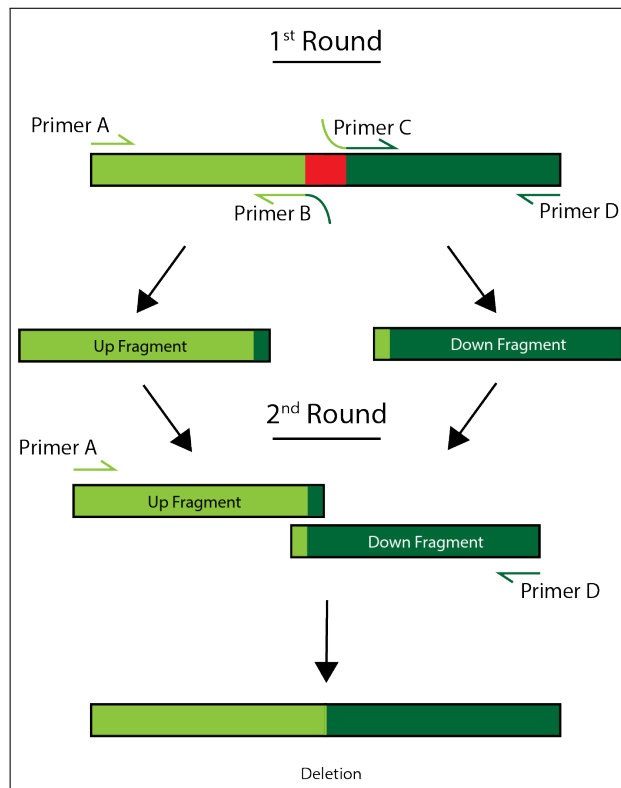


Figure 1.1: General SOE-PCR schematic.

For generation of the *sec61* hinge mutants, SOE PCR setup was as described in Table 1.15

In between reactions, samples were resolved in agarose gel 1% for size confirmation and cleaned out of the gel using the GeneElute Gel extraction Kit as described in Section 1.2.7. The amplification reactions were done as described in Section 1.2.4 using the KAPA HiFi (Peqlab), an annealing temperature of 58°C, and an adequate extension period. During the second round of PCR, as template, equal amounts of each complementary fragments (i.e both halves of the gene) were used (100ng).

Table 1.15: Genral setup of SOE-PCR for the generation of the *sec61* mutants.

	1 st round				2 nd round			
	Template	Reaction (#)	Primer (Frw)	Primer (Rev)	Template	Reaction (#)	Primer (Frw)	Primer (Rev)
<i>sec61</i> <i>deletion</i>	<i>SEC61</i>	1	64	106	<i>1st round</i> <i>products</i>	1	64	16
		2	107	16				
1	<i>SEC61</i>	1	64	108	<i>1st round</i> <i>products</i>	1	64	16
		2	109	16				
1/2	<i>sec61del1</i>	1	64	108	<i>1st round</i> <i>products</i>	1	64	16
		2	109	16				

1.2.4.2 Colony PCR

Colony PCR is a variation of the traditional PCR reaction, in which cell crude extract is used as source of template DNA. To obtain this crude extract, a sample of each transformant colony to be screen was resuspended in 50 µl of MQ water, and denatured at 95°C for 5min. After debris sedimentation (16.000 x g, 1 min), 10 µl of the supernatant was used as "template DNA" in a PCR reaction. In this study, colony PCRs were done in a total volume of 25 µl and using the OneTaq® DNA polymerase (Table 1.9). Reaction composition and programs used with this setup are described in Table 1.16 and 1.17, respectively. Whenever possible, the M13 primers were used for these reaction (Table 1.7) .

Table 1.16: Standard colony PCR reaction mixture

Component	Volume (μ l)	Final concentration/ Quantity
2X OneTaq Master Mix	12.5	1X
Forward primer (10 μ M)	0.5	0.2 μ M
Reverse primer (10 μ M)	0.5	0.2 μ M
Template DNA	10 (of crude extract)	x
dH ₂ O	1.5	–

Table 1.17: Standard thermal cycler program for colony PCRs

N° of Cycles	Operation	Temperature ($^{\circ}$ C)	Duration
1	Initial denaturation	94	5min
30	Denaturation	94	30sec
	Primer annealing	45-68*	30sec
	Primer extension	68	1 min/kb
1	Final extension	68	5 min
1	Store	4	∞

* Primer annealing temperature was optimized according to the primer pair used.

Full volume of the reaction was then resolved in an agarose gel of appropriate concentration as described in Section 1.2.6, and positive clones selected by band-size confirmation. Positive clones were then further confirmed by sequencing.

1.2.5 Small Scale DNA Extraction

1.2.5.1 Isolation of Plasmidic DNA from *E.coli*

To isolate plasmidic DNA from *E.coli*, the Plasmid Isolation Kit (Sigma) was used. Cellular mass of 2 ml of an over-night culture of *E.coli* grown as described in Section 1.2.3, and collected. Pellet was then resuspended in 250 µl Solution A, 250 µl of Solution B was added, and sample incubated at room temperature for 5 min. This step is responsible for the cell lysis. After incubation, 250 µl of Solution C was added, as to stop the lysis process. Sample was then centrifuged at 14.000 x g for 5 min, supernatant applied to a minispin column and respective collector tube, and submitted to new centrifugation step. Flow-through was discarded, as DNA stays trapped in the cellulose-based membrane. DNA is then washed with Washing solution, flowthrough discarded, and membrane properly dry. After fitting column into clean collector tube, DNA was eluted by applying 50 µl of warm MQ-water onto the membrane and spinning it for 1 min at 14.000 x g. Plasmid DNA was quantified using the NanoDrop spectrophotometer (Thermo Scientific) and stored at – 20 °C.

1.2.5.2 Isolation of Plasmidic DNA from *S.cerevisiae*

For isolation of plasmidic DNA from *S.cerevisiae* strains, no kits were used, and instead a manual phenol/chloroform extraction protocol was applied. To this end, cells were grown overnight on YPD as described in Section 1.2.2, in 10 ml cultures. Entire cell mass was collected by low speed centrifugation (5 min at 3000rpm), supernatant discarded, and pellet disrupted by vortexing. Cells were re-suspend in 200 µL of Breaking Buffer (10 mM Tris Hcl, pH 8.0 / 2 % Tx-100 / 1 % SDS / 100 mM NaCl / 1 mM EDTA, pH 8.0) and ≈200 µl volume of glass beads and 200 µl phenol/chloroform/isoamyl alcohol was added. Sample was then submitted to 3 min of bead-beating (4°C) and

centrifuged for 5 min at 13.000rpm (RT). Supernatant was transferred to new tube, and 1/10 of the total volume of cold sodium acetate (3 M, pH 5.2) and 3 volumes of cold 100 % ethanol were added. Sample was incubated for 1 h at -80°C, centrifuged at 16.000 x g for 30 min (4°C), supernatant discarded and tube rinsed with 70 % ethanol. After another step of centrifugation (15min, 16.000 x g), supernatant was discarded and pellet air dried. Finally, pellet was resuspended in 100 µl of TE Buffer (10 mM Tris-HCl, pH 7.5 / 1 mM EDTA) and quantified using a NanoDrop spectrophotometer (Thermo Scientific) and stored at 4 °C.

1.2.5.3 Isolation of *S.cerevisiae* total DNA

For isolation of total DNA from *S.cerevisiae*, cells were grown overnight on YPD as described in Section 1.2.2, in 10 ml cultures. Cells were collected at 3000rpm for 5 min (RT) and washed with 0.5 ml of distilled water. After a quick sedimentation step (5 sec at 16.000 x g, RT), supernatant was discarded, pellet disrupted by vortexing, and resuspended in 200 µl of Breaking Buffer (10 mM Tris Hcl, pH 8.0 / 2 % Tx-100 / 1 % SDS / 100 mM NaCl / 1 mM EDTA, pH 8.0). After adding ≈200 µl and 200 µl phenol/chloroform/isoamyl alcohol, sample was vortexed at highest speed for 3 min. At this point, 200 µl of TE Buffer (10 mM Tris-HCl, pH 7.5 / 1 mM EDTA) were added and sample was vortexed briefly, followed by a centrifugation at 16.000 x g for 5 min (RT). Aqueous layer was transferred to new tube, 1 ml of 100 % ethanol was added, and sample mixed by inversion. After new sedimentation step (16.000 x g for 3min, RT), pellet was resuspend in 400 µl TE Buffer and 15 µl of DNase-free RNase A (10 mg/ml, Sigma) was added, sample mixed and incubated for 15min at 37°C. After incubation, 10 µl of 4 M ammonium acetate and 1 ml of 100 % ethanol were added, sample mixed by inversion and centrifuged at 16.000 x g for 3 min (RT). Pellet was

washed with 15 % ethanol, air dried, resuspended in 100 µl of TE Buffer and quantified using a NanoDrop spectrophotometer.

1.2.6 Agarose Gel Electrophoresis

Agarose gel electrophoresis was performed to separate, identify and purify DNA fragments. In general, DNA samples were mixed with DNA Loading Dye (6X: 50 % (w/v) Sucrose / 0.15 % (w/v) Bromophenol Blue / 0.02 M EDTA) and loaded onto a 1 % Agarose Gel (1 % (w/v) Agarose / 2 % (v/v) 50X TAE / 90 % (v/v) dH₂O) containing 0.5 µg ml⁻¹ Ethidium Bromide (EtBr). The gel was placed in a Peqlab gel tank containing 1X TAE buffer (Tris Acetate EDTA / 50X: pH 8.4 / 20 M Tris- HCl / 10 M Acetic Acid / 0.05 M EDTA). Electrophoresis was then carried out at 100 - 120 V for 1-2 hr. GeneRuler™ 1 kb DNA ladder (Fermentas) was used as the size standard (0.5 µg loaded). The gel was placed over a transilluminator for visualization of the DNA, which was photographed using the E-Box VX2 Gel Documentation System (Peqlab).

1.2.7 Recovery of DNA Fragments

In order to recover DNA from agarose gels, the GenElute™ Gel Extraction Kit (Sigma-Aldrich) was used. The appropriate DNA band was excised from the agarose gel using a sterile scalpel, and then transferred into a 2 ml microcentrifuge tube. The gel slice was resuspended in 3 gel volumes of Gel Solubilization Solution. The mixture was incubated at 60 °C until the gel was dissolved followed by the addition of 1 gel volume of 100 % isopropanol. The gel solution was loaded onto an equilibrated binding column and spun for 1 min at full speed in a benchtop centrifuge (MiniSpin®, Eppendorf). The flow-through liquid was discarded each time. Next, 700 µl of Wash Solution were added to the binding column and the column centrifuged for 1 min at RT,

full speed. Once all of the solution had been passed through the binding column, the column was centrifuged as before in order to remove residual Wash Solution. The DNA was eluted by addition of 50 μ l warm MQ water to the membrane of the binding column and incubated for 1 min at RT followed by centrifugation for 1 min at full speed. DNA was stored at $-20\text{ }^{\circ}\text{C}$ until needed.

1.2.8 Restriction Digestion of PCR Products and Plasmid DNA

All endonuclease restriction digestions were carried out in a 50 μ l reaction mixture containing the appropriate buffer, as recommended by the supplier (NEB, if not stated otherwise), and 10 units of enzyme per μ g of DNA. Reaction mixtures were incubated for 1-2 hr at $37\text{ }^{\circ}\text{C}$ (SmaI: $25\text{ }^{\circ}\text{C}$) and afterwards either heat-inactivated as recommended or cleaned with the PCR cleaning Kit (Sigma). DNA was then analyzed by gel electrophoresis (Section 1.2.6). In the case of two enzymes being used, the buffer in which both enzymes exhibit the highest efficiency was used at the appropriate concentration. The standard reaction mixture is outlined in Table 1.18. For digestions of larger amounts of DNA, the amounts of enzymes and buffer were increased and the amount of water adjusted accordingly.

Table 1.18: Standard reaction mixture for the restriction of DNA.

Component	DNA	Buffer*	Restriction Enzyme	dH ₂ O
Volume (μ l)	x (1 μ g)	5	1 (10U)	to 50

* The buffers were those recommended by the suppliers.

1.2.8.1 DNA cleaning

For linearized DNA cleaning after processing (either by PCR or by enzymatic treatment) the GenElute™ PCR Clean-Up Kit was used. Briefly, mini-spin columns supplied in the kit were prepared by adding 500 µl of Column Preparation Solution and centrifuging at 14.000xg for 1 min. Flowthrough was discarded. DNA sample was then diluted by adding 5 volumes of Binding Solution to 1 volume of the DNA sample, mixed, applied to the column, centrifuged at 14.000xg for 1 min and flowthrough discarded. Column was washed with 750 µl of Washing Solution, centrifuged twice at 14.000xg (once for 1 min and once for 2 min, exchanging collector tube in between), and left to dry for some minutes. DNA elution was done by adding 50 µl of warm MQ water to the center of the column, letting it sit for a couple of minutes, and then centrifuge the column at 14.000xg for 1 min in a clean eppendorf. Sample was then quantified using a NanoDrop spectrophotometer (Thermo Scientific).

1.2.9 Dephosphorylation of Vector DNA

FastAP™ Thermosensitive Alkaline Phosphatase (Thermo Fisher Scientific) was used to hydrolyze 5' phosphate group prior to ligation in case of double blunt end cloning, in order to avoid re-ligation of the digested vector. The reaction mix (Table 1.19) consisted of 1 unit of FastAP™ Thermosensitive Alkaline Phosphatase, 1/10 volume of 10X FastAP™ buffer and 1 µg of vector DNA. The sample was incubated at 37 °C for 10 min and heat-inactivated at 65 °C for 15 min.

Table 1.19: Reaction mixture for the dephosphorylation of digested vector DNA.

Component	DNA	Buffer	FastAP	dH ₂ O
Volume (µl)	x (1 µg)	2	1	to 20

1.2.10 Phosphorylation of insert DNA

T4 Polynucleotide Kinase (PKN) (NEB) was used to add a 3' phosphate group to the insert prior to ligation, in case of double blunt end cloning, in order to allow ligation with the dephosphorilated digested vector. The reaction mix (Table 1.20) consisted of 1 unit of FastAP™ Thermosensitive Alkaline Phosphatase, 1/10 volume of 10X FastAP™ buffer and 1 µg of vector DNA. The sample was incubated at 37 °C for 10 min and heat-inactivated at 65 °C for 15 min.

Table 1.20: Reaction mixture for the dephosphorylation of digested vector DNA.

Component	DNA	Buffer	T4 PKN	dH ₂ O
Volume (µl)	x (1 µg)	2	1	to 20

1.2.11 Ligation of Vector DNA and Insert DNA

In general, following digestion of vector and insert DNA with the appropriate enzyme(s) to create matching sticky ends, the ligation was carried out for 10 min at 22 °C in a water bath using the T4 DNA ligase (Fermentas). The reaction mixture contained 10X T4 DNA ligase buffer, 2 units of T4 DNA ligase (2 U/µl) and a 3:1 ratio of insert to vector. Ligations were prepared according to the reaction mixture presented in Table 2.17. Generally, 10 µl of the ligation were used to transform E. coli cells.

Table 1.21: Standard reaction mixture for the ligation of vector and insert DNNA.

Component	Buffer	Vector DNA	Insert DNA	dH ₂ O	T4 DNA Ligase
Volume (µl)	2	x (50 ng)	y (3:1*)	to 20	1

* Molecular ratio insert : vector

1.2.12 Transformation of *E.coli* Cells with Plasmidic DNA

1.2.12.1 Preparation of Chemically Competent *E.coli* Cells

E.coli DH5α cells were grown to an OD₆₀₀ of approximately 0.5-0.7 and subsequently centrifuged at 4000 rpm at 4°C for 6 min (Sorvall Evolution RC centrifuge, SLA3000 rotor). The pellet was resuspended in 8.5 ml of cold and sterile TFPI buffer at pH 5.8 (30 mM KOAc / 100 mM KCl / 10 mM CaCl₂ / 50 mM MnCl₂ / 10 % glycerol) and incubated on ice for 10 min. After centrifugation at 4000 rpm at 4°C for 6 min, the pellet was resuspended in 1 ml of cold and sterile TFPII buffer at pH 6.5 (10 mM KCl / 75 mM CaCl₂ / 10 % glycerol / 10 mM MOPS) and incubated on ice for 30 min. The sample was then divided into 50 or 100 µl aliquots that were flash frozen in liquid nitrogen and stored at -80°C until use.

1.2.12.2 Transformation of chemically competent *E. coli* cells

To generate recombinant bacteria, 10-100 ng of plasmid DNA were added to 100 µl of chemically competent *E.coli* DH5α cells. Cells were incubated for 20 min on ice and subsequently heat-shocked at 42°C for 2 min. Next, 700 µl of pre-warmed LB medium were added and cells were incubated for 1 h at 37°C under shaking. After centrifugation (1 min, 10000 rpm; Eppendorf 5415 R microcentrifuge), the supernatant was discarded by decanting and cells were resuspended in the residual LB

medium. Cells were finally plated onto LB agar plates containing the appropriate selection marker (ampicillin, kanamycin, etc.).

1.2.13 DNA Sequencing

In order to analyze DNA sequences all plasmids were sequenced. Miniprep DNA samples of all transformants of interest were sent for sequencing. Sequencing (single read sequencing) was performed by GATC Biotech AG (Konstanz) according to the sequencing method by Sanger et al. [330]. For the great majority of sequencings the M13 primers were routinely used if not stated otherwise. The results were analyzed with the Snapgene® software.

1.2.14 Preparation of Lyticase

Lyticase preparation was done according to a protocol from R. Schekman's laboratory. Briefly, from a 200 ml overnight culture of the strain RSB805, 10 L (8 x 1.25 L) of LB-Amp medium were inoculated with 15 ml of the culture. Cells were grown at 37 °C, 200 rpm to an OD₆₀₀ of 0.5. The cultures were then induced with 0.5 mM IPTG for 5 hr at 37 °C, 200 rpm. Cells were then harvested (4200 rpm for 10 min, 4 °C) (Sorvall Evolution® RC Centrifuge, SLA3000 rotor). Pellets were resuspended with 400 ml 25 mM Tris, pH 7.4 and pooled. The resulting pellet was centrifuged for 5 min, 4 °C at 8000 rpm. The supernatant was discarded and the pellet resuspended with 200 ml 25 mM Tris, pH 7.4 / 2 mM EDTA. An equal volume of 25 mM Tris pH 7.4 / 40 % sucrose was slowly added to the suspension which was stirred very slowly for 20 min at RT on a magnetic stirrer (RH basic 2 IKAMAG®, IKA®). The suspension was then centrifuged as before and the supernatant discarded carefully (in the cold room) as the resulting pellet was very soft. The pellet was resuspended with 150 ml of ice-

cold 0.5 mM MgSO₄, slowly stirred in the cold room for 20 min and centrifuged as before. The supernatant containing the lyticase was aliquoted in 15 ml falcon tubes, snap-frozen in liquid nitrogen and stored at – 80 °C. Lyticase activity was determined using the yeast strain KRY49 (Table 1.5). Cultures (50 ml) were grown in YPD to an OD₆₀₀ of 2, harvested for 5 min at 4200 rpm (Sorvall Evolution® RC Centrifuge, SS34 rotor), RT and resuspended in 50 mM Tris-HCL pH 7.4/ 10 mM DTT to an OD₆₀₀ of 2 (OD₆₀₀START). Aliquots (1 ml) of the yeast culture (duplicates or triplicates) were incubated with various concentrations of lyticase (0.01, 0.02, 0.5, 1, 2 µl). Samples were incubated at 30 °C for 30 min and the OD₆₀₀ was immediately measured. The lyticase activity was determined based on the principle that a 10 % decrease of OD₆₀₀ corresponds to 1U of lyticase activity. The higher the lyticase activity, more shifted to the low lyticase-amount range will the activity linearity zone be.

1.2.15 Transformation of *S.cerevisiae*

S. cerevisiae transformations were done using the Lithium Acetate method (LiAc/SS-DNA/PEG) [117, 118]. Briefly, a 25 ml culture of *S.cerevisiae* was grown overnight at 30 °C as described in Section 1.2.2. For each transformation reaction, 2 ml of cells were harvested (3000 rpm for 2 min at RT) (Minispinner Table top) and washed with 1 ml of sterile LiAc/TE Solution (10 mM Tris -HCl, pH 7.5 / 100 mM LiAc / 1 mM EDTA). The pellet was resuspended in 100 µl of LiAc/TE Solution, and 20 µl of carrier DNA (DNA from salmon testes, 10 mg/ml (Sigma), boiled for 5 min prior to use), 1 µg of DNA (previously linearized if it is an integrative vector), 600 µl of PEG solution (10 mM Tris -HCl, pH 7.5 / 100 mM LiAc / 1 mM EDTA / 40 % PEG₄₀₀₀), and 50 µl of 1 M LiAc were added (all solution were filter-sterilized). Sample was mixed gently and incubated for 1 hr at 30 °C, followed by 15 min at 42 °C after adding 20 µl of DMSO.

Cellular fraction was collected (3000 rpm for 2 min) and pellet washed in 1 ml of TE (10 mM Tris-HCl pH 8.0 / 1 mM EDTA pH 8.0). After one last resuspension in 100 μ l of TE Solution, cells were plated onto the appropriate minimal medium plates or antibiotic supplemented plates and incubated at 30 °C for 2-4 days. The LiAc method was applied to transform all *S. cerevisiae* strains in this work with the appropriate plasmid DNA or linear DNA (Table 1.6) to create the desired strains.

1.2.16 Verification of *S.cerevisiae* Transformants

Positive transformants were picked and plated onto minimal medium plates lacking the auxotrophic aminoacid followed by isolation of their genomic DNA (Section 1.2.5.3) which was used as template in a PCR reaction (Section 1.2.4) with target-gene specific primers to confirm proper integration of the desired sequence into the yeast genome. The PCR product was further sequenced to guarantee gene identity and quality. Transformants in the KRY461 (pGAL-SEC61) background were verified by plating onto minimal medium without LEU (2 % (w/v) Galactose/ 0.2 % (w/v) Glucose) after the transformation. Plates were incubated at 30 °C for 2-4 days. Transformants were plated onto 5-FOA plates (0.002 % (w/v) Uracil, supplements according to auxotrophies (lacking Uracil) / 0.67 % (w/v) YNB w/o Amino Acids / 2 % (w/v) Glucose / 2 % (w/v) Agar / 0.1 % (w/v) 5-Fluoroorotic acid (Fermentas)). Real positive transformants were able to grow.

1.2.17 *S.cerevisiae* Growth on Plates (Drop Test)

YPD Cultures (5 ml) were inoculated with a single colony and grown overnight at 30 °C and 220 rpm. In the next day the cells were counted in a hemocytometer (Neubauer chamber) and the cell number per ml was determined. For each strain serial dilutions

in sterile MQ water were prepared and 5 µl of each dilution were dropped onto YPD or minimal medium (concentrations on plate: 10^4 – 10^1). For temperature sensitivity assays, the plates were incubated at various temperatures (20, 30 or 37 °C) for at least 3 days. For tunicamycin sensitivity, the plates were supplemented with 0.25, 0.5 or 0.75 µg/ml of tunicamycin and incubated at 30 °C for at least 3 days.

1.2.18 Isolation of *S.cerevisiae* RNA

The preparation of yeast total RNA was done according to Current Protocols in Molecular Biology. Briefly, 10 ml of a yeast culture were grown to an OD_{600} of 1 at 30 °C, 220 rpm. Cells were harvested for 5 min at 4 °C, 7000 rpm (Sigma 4K15 Refrigerated Centrifuge, 11140 rotor). The supernatant was discarded and the pellet was resuspended in 1 ml of ice-cold RNase-free water (DEPC-treated) and transferred to clean RNase-free microcentrifuge tube. The cells were centrifuged at full speed, 4 °C for 10 sec. The supernatant was discarded and the pellet resuspended with 400 µl TES Solution (10 mM Tris-HCl, pH 7.7 / 10 mM EDTA / 0.5 % (w/v) SDS). Next, 400 µl of Acid Phenol (Roti®-Aqua-Phenol, Carl Roth) were added and the sample vortexed for 10 sec and incubated at 65 °C for 1 hour with occasional vortexing. After the incubation step, the sample was placed on ice for 5 min, followed by a centrifugation at full speed, 4 °C for 5 min. The aqueous (top) phase was transferred to a clean microcentrifuge tube. 400 µl Roti®-Aqua-Phenol were added and the sample was vortexed for 20 sec, incubated on ice for 5 min and centrifuged as before. The resulting aqueous phase was transferred to a clean microcentrifuge tube and mixed with 400 µl chloroform, vortexed for 20 sec and centrifuged as before. The aqueous phase was transferred to a clean microcentrifuge tube and 40 µl of 3 M NaAc (pH 5.3) and 1 ml of ice-cold 100 % ethanol were added. The sample was vortexed and centrifuged as

before. The resulting pellet was washed with 1.5 ml 70 % (v/v) ethanol, centrifuged as before and resuspended in 50 μ l RNase-free dH₂O (DEPC-treated). RNA concentration was determined using a NanoDrop spectrophotometer (Thermo Scientific), and RNA was stored at – 20 °C.

1.2.19 Protein Gel Electrophoresis and Western Blot Analysis

1.2.19.1 Preparation of Cell Extracts

For the preparation of yeast cell extracts fresh overnight cultures were used to inoculate 25 ml YPD. Cells were grown to an OD₆₀₀ of 1 at 30 °C, 220 rpm. Next, 2 OD₆₀₀ of cells were harvested at 8000 rpm for 1 min (MiniSpin® Centrifuge, Eppendorf) and the supernatant was discarded. The pellet was washed with 1 ml of sterile MQ water, resuspended in 200 μ l 2X SDS Sample Buffer (100 mM Tris-HCl, pH 6.8 / 4 % SDS / 0.2 % bromophenol blue / 20 % glycerol / 200 mM DTT). About 100 μ l of glass beads (acid washed, 1 mm, Sigma) were added and the cells disrupted in the cold room using a bead beater (Mini-Beadbeater-16; Bio Spec Products Inc.). Disruption was conducted over 3 cycles of 2 min (with 1 min of disruption followed by 1 min of rest). The samples were heated for 10 min at 65 °C and centrifuged at 14.000 x g for 1 min. Samples were then ready to be resolved by SDS-PAGE (Section 1.2.19.2).

1.2.19.2 Protein Gel Electrophoresis

Protein gel electrophoresis (SDS-PAGE) was routinely conducted using NuPAGE® Novex® Pre-Cast Bis-Tris gels (generally 4-12 % gels, 1.5 mm, 10 wells) and the XCell SureLock™ Mini-Cell (both Invitrogen) if not stated otherwise. Prior to loading an appropriate volume of the protein sample onto the gel, samples were prepared by adding the appropriate volume of 2X SDS-Sample Buffer and heating samples at 95

°C (65 °C for membrane proteins) for 5 min (10 for membrane proteins). The samples were run in 1X NuPAGE® MOPS SDS Running Buffer (Invitrogen) at 80-160 V, RT using a Bio-Rad PowerPac™ HC power supply, until the gel front ran off the bottom of the gel. The PageRuler™ Prestained Protein Ladder or the PageRuler™ Plus Prestained Protein (both Fermentas) were used as the size standard according to the supplier's instructions.

1.2.19.3 Coomassie Staining (Normal)

For Coomassie gel staining, after SDS-PAGE, the gels were incubated with 50-100 ml of staining solution (0,025 % CBB G-250) in a lid containing box, the box was closed, and the gel was incubated for 20 min at 65 °C. After incubation, gel was rinsed multiple times with destaining solution (30 % methanol / 10 % acetic acid), and incubated in it (under shaking) until adequate background was reached. After destaining, gel was rinsed with MQ Water two times.

1.2.19.4 Coomassie G-250 Staining (Normal)

For Coomassie G-250 gel staining, after SDS-PAGE, the gels were incubated under shaking with 50-100 ml MQ Water (3X10min). After disposing of all the water, 50-100 ml of staining solution (0,02 % CBB G-250 / 5 % Aluminum Sulfate Hydrate / 10 % Ethanol / 2 % Orthophosphoric acid) were added to the gel in a lid containing box, the box was closed, and the gel was incubated overnight under shaking. After incubation, gel was rinsed twice with MQ Water and incubated with destaining solution (10 % Ethanol / 2 % Orthophosphoric acid) for 60min. After destaining, gel was rinsed with MQ Water two more times.

1.2.19.5 Coomassie Staining for Mass Spectrometry

After SDS-PAGE the gel was placed into staining solution (0.08 % Coomassie Brilliant Blue G250 / 10 % citric acid / 8 % ammonium sulfate / 20 % methanol) for 6h to overnight. Gel was de-stained with distilled water (several changes) until the background was clear. Protocol suggested by the EMBL Proteomics Core Facility.

1.2.19.6 Western Blot Analysis

Western Blotting was employed to identify target proteins using appropriate antibodies. The first part of the Western Blot protocol consists on the transfer of proteins from the protein gel (Section 1.2.19.2) onto nitrocellulose (NC) membranes (0.45 μm pore size, Bio-Rad). To this end, a "sandwich" containing the acrylamide gel and the NC membrane, as well as 3 MM Chromatography Paper (Whatman®) and sponges soaked in Transfer Buffer (25 mM Tris / 200 mM Glycine / 20 % (v/v) Methanol / 0.2 % (w/v) SDS) were assembled. The protein transfer was then conducted in Transfer Buffer for 2 hr at 100 V in the cold room using a Trans-Blot® Electrophoretic Transfer Cell (with plate electrodes and super cooling coil, Bio-Rad).

For the the second part of the Western Blot protocol, the immunoblot and detection phase, the membrane was blocked in Blotto (50 mM Tris-HCl, pH 7.4 / 150 mM NaCl / 2 % (w/v) Milk Powder / 0.1 % (v/v) Tween-20 / 5 mM Sodium Azide) for 1 hr under shaking (RT). The membrane was then incubated under shaking with the primary antibody (Section 1.8) diluted in Blotto for 2h at RT or overnight in the cold room. The membrane was then washed twice (10 min) in Blotto followed by 2 washes (also of 10 min) in 1X TBS-T (50 mM Tris-HCl, pH 7.4 / 150 mM NaCl / 0.1 % (v/v) Tween-20 / 5 mM Sodium Azide). For the last step, the membrane was incubated with the secondary antibody (Table 1.8) diluted in 1X TBS-T shaking for 1 hr at RT. The mem-

brane was washed 4 times for 10 min with TBS-T. The blot was prepared for detection using the SuperSignal™ West Dura Extended Duration Chemiluminescent Substrate (Pierce) according to the supplier's instructions. Signals were detected using the Amersham Imager 600 (GE Healthcare).

1.2.20 Preparation of Rough Microsomal Membranes

The isolation of rough microsomal membranes from *S. cerevisiae* was performed according to Lyman & Schekman [230] and Pilon et al. [289]. Briefly, 2.5-10 L of a yeast culture were grown overnight in YPD at 30 °C and 200 rpm to an OD₆₀₀ of ≈2. The cells were harvested at 5.000 rpm and RT for 3 min (Sorvall Evolution® RC centrifuge, SLA3000 rotor), the pellet was resuspended in 100 mM Tris-HCl pH 9.4 / 10 mM DTT to 100 OD₆₀₀/ml and then incubated for 10 min at RT in order to weaken the cell walls. Cells were pelleted for 5 min at 5.000 rpm, RT and then resuspended in Lyticase Buffer (50 mM Tris-HCl, pH 7.5 / 0.75 X YP / 700 mM Sorbitol / 0.5 % Glucose / 10 mM DTT) to 100 OD₆₀₀/ml. Lyticase was added to a final concentration of 40 U per OD₆₀₀ of cells, and sample incubated for 20 min at 30 °C, 80 rpm (Multitron Standard Incubation Shaker, Infors HT). Following the incubation, the cells were chilled on ice for 2 min and then pelleted for 5 min at 5000 rpm, 4 °C. The supernatant was carefully discarded and the pellet washed with 2X JR Buffer (40 mM Hepes-KOH, pH 7.4 / 400 mM Sorbitol / 100 mM KOAc / 4 mM EDTA) to 250 OD₆₀₀/ml and centrifuged at 10.000 rpm and 4 °C for 10 min (Sorvall Evolution® RC centrifuge, SS34 rotor). The resulting pellet was resuspended in 2X JR buffer to 500 OD₆₀₀/ml and frozen at – 80 °C for at least 1 hr. The spheroplasts were thawed in an ice-cold water bath and mixed with an equal volume of cold MQ water. PMSF and DTT were added to a final concentration of 1 mM and the spheroplasts were disrupted with ten

strokes of a motor-driven Potter Elvehjem homogenizer (EUROSTAR power basic, IKA®) in the cold room. The lysate was centrifuged for 5 min at 3.000 rpm, 4 °C (Sorvall Evolution® RC Centrifuge, SS34 rotor) and the supernatant transferred to a clean polycarbonate SS34 tube and centrifuged at 17.500 rpm, 4°C for 15 min to pellet the membranes. The sample was placed on ice and the pellet was resuspended in a minimum volume (≈ 0.5 ml) of B88 (20 mM Hepes-KOH, pH 6.8 / 250 mM Sorbitol / 150 mM KOAc / 5 mM Mg(OAc)₂) and gently homogenized on ice using a small teflon pestle and carefully resuspended using a Gilson® pipette. The sample was loaded onto a 1.2 M/1.5 M Sucrose Gradient (20 mM Hepes-KOH, pH 7.5 / 50 mM KOAc / 2 mM EDTA / 1 mM DTT / 1.2 M or 1.5 M Sucrose) and centrifuged at 44.000 rpm, 4 °C for 1 hr (Optima™ L-90 K Ultracentrifuge, SW 60 Ti rotor). For the sucrose gradient, 1.5 ml of each sucrose solution (1st: 1.5 M, 2nd: 1.2 M) was layered into an SW60Ti tube (Beckman Coulter). ER-derived microsomes were collected at the interphase of the 1.2 M/1.5 M sucrose gradient and washed with 25 ml of cold B88. The sample was centrifuged at 17.500 rpm, 4 °C for 15 min (Sorvall Evolution® RC Centrifuge, SS34 rotor). The microsome pellet was carefully resuspended in the appropriate volume of B88. Membrane concentration was measured at OD₂₈₀ in 2 % (w/v) SDS at a 1:200 dilution. The concentration was adjusted to an OD₂₈₀ of ≈ 30 with B88 and the samples aliquoted (50 μ l), snap-frozen in liquid nitrogen and stored at – 80 °C.

1.2.21 Small Scale Preparation of Hot Rough Microsomal Membranes

To prepare radiolabeled ER vesicles, 7 OD₆₀₀ of early log-phase cells were incubated in synthetic minimal media supplemented appropriately and lacking methionine, cysteine, and ammonium sulfate for 30 min at 30°C, 220 rpm. Cells were labelled with 6,5 MBq [³⁵S] methionine/cysteine (Express Labeling, PerkinElmer) mix for 30 min. Af-

ter labelling, cells were immediately washed twice with Tris-Azide Buffer (20 mM Tris-HCl, pH 7.5 / 20 mM sodium azide). Cells were then incubated in 100 mM Tris-HCl, pH 9 / 10 mM DTT for 10 min at room temperature, sedimented, and resuspended in 300 μ l of 2 x JR Lysis Buffer (40 mM Hepes-KOH, pH 7.4 / 400 mM sorbitol / 100 mM KOAc / 4 mM EDTA / 1 mM DTT / 1 mM PMSF) [289]. Acid-washed glass beads (1/2 volume) were added and the sample submitted to 2 cycles of 1 min bead-beating (Mini-beadbeater-16, BioSpec) with 2 min of incubation on ice after each cycle. From this point on, all samples were kept at 4°C. Beads were washed 3 times with 300 μ l of B88, pH 7.2 (20 mM Hepes-KOH, pH 6.8 / 250 mM sorbitol / 150 mM KOAc / 5 mM Mg(OAc)₂). Washes were pooled and sedimented for 2 min at 1.500 x g and the microsome-containing supernatant was transferred to a clean tube. Microsomes were then sedimented at 16.000 x g for 10 min, washed and resuspended in 200 μ l B88, pH 7.2. Crude radiolabelled ER vesicles were then aliquoted (50 μ l), flash frozen in liquid nitrogen, and stored at -80°C.

1.2.22 *HAC1* mRNA Splice Assay

Upon induction of the UPR the *HAC1* mRNA is spliced. Thus, the comparison of the two species, *HAC1_u* and *HAC1_i* (u = uninduced; i = induced), allows for the evaluation of the UPR status of various yeast strains. Cultures of the appropriate strains were prepared in minimal medium and grown at 30 °C, 220 rpm to an OD₆₀₀ of 1. For positive controls each strain was grown in the presence of tunicamycin (Tm). In this case, when an OD₆₀₀ of 1 was reached, 2 μ g/ml Tm were added to the cultures. The cultures were then incubated for another 3 hr at 30 °C, 220 rpm. A volume of 10 ml of each culture was pelleted, and used to isolate yeast RNA according to Section 1.2.18. RNAs were then diluted to a final concentration of 0.1 μ g/ μ l, and used in reverse tran-

scription reactions to generate cDNA using the Maxima® Reverse Transcriptase (Fermentas). The reaction setup was as shown in Table 1.22. The samples were incubated for 30 minutes at 50 °C, followed by an inactivation at 85 °C for 5 minutes.

Table 1.22: Reverse transcription reaction mixture.

Component	Volume (µl)	Final concentration
RNA	1	0.1 µg
Oligo(dT ₁₈ -primer (100 mM)	1	100 pmol
dNTP mix (10 mM)	1	0.5 mM
RNase-free dH ₂ O	to 14.5	to 14.5 µl
5X RT Buffer	4	1X
RNasin (40 U/µl)	0.5	20U
Maxima® RT	1	200U

* Molecular ratio insert: vector

Each cDNA (0.1 µg) was used in a PCR using the *HAC1* as well as the *ACT1* specific primers (Table 1.7). The PCR setup was as described in Table 1.13. The thermal cycler program was as described in Table 1.14 with the following exceptions: primer annealing (step 3) was at 50 °C, primer extension (step 4) was for 45 sec, final primer extension was for 3 min and steps 2 to 4 were cycled 24 times. The PCR products (10 µl) were resolved on a 1 % Agarose Gel in 1X TAE Buffer (50X TAE pH 8.4 / 20 M Tris-HCl / 10 M Acetic Acid / 0.05 M EDTA) at 100 V and RT for 1 hr (Section 1.2.6). Bands were visualized and photographed using the E-BOX VX2 gel documentation system (Peqlab).

1.2.23 Cyclohexemide chase

For cycloheximide chases, cultures were grown to a maximum OD_{600} of 1 and were treated with 200 $\mu\text{g/ml}$ cyclohexemide (Merck), time at which the 0 time points were taken, cells sedimented and flash-frozen. After all time points had been taken in similar fashion, samples were thawed on ice, washed with Tris-Azide Buffer (20 mM Tris-HCl, pH 7.5 / 20 mM Sodium Azide), resuspended in 50 μl of 2x SDS-buffer (100 mM Tris-HCl, pH 6.8 / 4 % SDS / 0.2 % bromophenol blue / 20 % glycerol / 200 mM DTT) and lysed with glass beads (Sigma) in a Mini-Beadbeater-16 (BioSpec; three 1 min disruption cycles at 4°C with 1 min of incubation at 4°C between cycles). Lysates were heated for 10 min at 65°C before Western Blot analysis as described in Section 1.2.19.6.

1.2.24 Pulse-Chase Experiments

1.2.24.1 Pulse Labeling

Pulse experiments were performed as described by Gillece et al. [120] and Verma et al. [412]. Briefly, cells were grown overnight at 30 °C, 220 rpm in Growth Medium (0.67 % (w/v) Yeast Nitrogen Base (YNB) w/o Amino Acids (AA) / 0.13 % (w/v) SC drop-out mix / 0.2 % (w/v) Casamino Acids (CAA) / 5 % (w/v) Glucose, Supplements as required by the strain's auxotrophies) to an OD_{600} of 0.5–1. Cells were harvested at 3000 rpm, RT for 5 min, washed twice with Labeling Medium (0.67 % (w/v) YNB w/o AA and Ammonium Sulfate / 5 % (w/v) Glucose, Supplements as required by the strain's auxotrophies), and resuspended in Labeling Medium to an OD_{600} of 6. Aliquots of 1.5 OD_{600} were transferred to clean 2 ml microcentrifuge tubes. The samples were pre-incubated at 30 °C, 800 rpm for 15 or 30 min (Thermomixer® comfort, Eppendorf). Cells were then pulsed with 0.35 mCi/ml Express Protein Labeling Mix

(Perkin Elmer) and incubated for 5, 10 or 30 min (depending on the substrate) at 800 rpm, 30 °C or 20 °C (if at the restrictive temperature). Following the pulse, cells were immediately transferred to ice killed by adding 750 µl of cold Tris-Azide Buffer (20 mM Tris-HCl, pH 7.5 / 20 mM Sodium Azide). The cells were then sedimented for 1 min at full speed, the pellets resuspended in 1 ml of Resuspension Buffer (100 mM Tris-HCl, pH 9.4 / 10 mM DTT / 20 mM Ammonium Sulfate) and incubated for 10 min at RT. The samples were centrifuged as before and resuspended in 150 µl of Lysis Buffer (20 mM Tris-HCl, pH 7.5 / 2 % (w/v) SDS / 1 mM PMSF / 1 mM DTT). Acid washed glass beads (≈150 µl, 1 mm, Sigma) were added and the cells disrupted in a Mini-Beadbeater-24 (Bio Spec Products Inc.) for 2 x 1 min with 1 min pause in between cycles. Samples were then denatured at 90 °C for 5 min (10 min at 65 °C for membrane proteins). Beads were washed 3 times with 250 µl of IP Buffer w/o SDS (15 mM Tris-HCl, pH 7.5 / 150 mM NaCl / 1 % (v/v) Triton X-100 / 2 mM Sodium Azide), the samples vortexed and centrifuged as before, each time and the supernatants pooled in a clean 2 ml microcentrifuge tube. The sample was then submitted to immunoprecipitation as described in Section 1.2.24.3 and resolved by SDS-PAGE (Section 1.2.19.2).

1.2.24.2 Chasing

For pulse-chase experiments, after labeling, two aliquots per sample were immediately killed and set aside, while to the other time points 250 µl of 2x Chase Mix (0.008 % Met / 0.006 % Cys / 20 mM ammonium sulphate) was added and incubation continued until they reached desired incubation time. Samples were then treated as for normal pulses (Section 1.2.24.1)

1.2.24.3 Immunoprecipitation

The samples were precleared by adding 60 μ l of 20 % (w/v) Protein A Sepharose™ CL-4B (GE Healthcare) in IP Buffer (15 mM Tris-HCl, pH 7.5 / 150 mM NaCl / 1 % (v/v) Triton X-100 / 2 mM Sodium Azide / 0.1 % (w/v) SDS) incubating for 30 min under rotation at RT. After pre-clear, sample was centrifuged for 2 min at full speed, RT and each supernatant was transferred to a clean microcentrifuge tube containing 60 μ l of 20 % (w/v) Protein A Sepharose™ CL-4B as well as the appropriate antibody/antiserum (Table 1.8). The samples were then incubated either overnight at 4 °C (cold room) or at RT for 2 hours on a rotating wheel. Samples were centrifuged for 2 min at full speed, RT, washed with 1 ml of IP Buffer with SDS and 1 ml of Urea Wash (2 M Urea / 200 mM NaCl / 1 % (v/v) Triton X-100 / 100 mM Tris-HCl, pH 7.5 / 2 mM Sodium Azide) three times each, and washed once with 1 ml of ConA Wash (500 mM NaCl / 1 % (v/v) Triton X-100 / 20 mM Tris-HCl, pH 7.5 / 2 mM NaN₃) and 1 ml of Tris-NaCl Wash (50 mM NaCl / 10 mM Tris-HCl, pH 7.5 / 2 mM NaN₃). Samples were centrifuged for 1 min at full speed, RT, and the supernatants discarded. After the washes, 20 μ l of 2X SDS-PAGE Protein Sample Buffer (125 mM Tris-HCl, pH 6.8 / 4 % (w/v) SDS / 10 % (v/v) β -Mercaptoethanol / 0.002 % (w/v) Bromophenol Blue / 20 % (v/v) Glycerol) were added and the samples incubated at 95 °C for 5 min (10 min at 65 °C for membrane proteins). Samples were centrifuged for 10 sec at full speed, RT and the supernatant carefully loaded onto a protein gel using a gel-loading tip to avoid transfer of sepharose. Generally, proteins were resolved using a 4-12 % Bis-Tris gel (NuPAGE® Novex® Pre-Cast gels) as described in Section 1.2.19.2. Following the electrophoresis protein gels were incubated in Fixator 1 (10 % (v/v) Acetic Acid / 40 % (v/v) Methanol / 2 % (v/v) Glycerol) for 15 min and in Fixator 2 (50 % (v/v) Methanol / 1 % (v/v) Glycerol) for 30 min, under shaking. Gels were then dried at 80

°C for 1 hour in a gel dryer (Model 583, Bio-Rad), exposed to phosphorimager plates and signal acquired in Typhoon Trio™ Variable Mode Imager, GE Healthcare. Signal were analyzed and quantified using the ImageQuant™ TL software (GE Healthcare).

1.2.25 Chemical Crosslinking

Microsomes (17 eq) were washed and resuspended in B88 (20 mM Hepes-KOH / 250 mM sorbitol / 150 mM KOAc / 5 mM Mg(OAc)₂). For SMPH and LC-SPDP crosslinking B88 was used at pH 7.2, for DSS and SDAD crosslinking pH was 7.9. The total reaction volume for subsequent detection by immunoblotting was 100 µl with appropriate amount of crosslinker (SMPH or LC-SPDP: 1 mM; SDAD: 1.5 mM; DSS: 0.8 mM). Control reactions were prepared with 5 µl of DMSO, but otherwise treated identically. For up-scaling, proportion of microsomes/total volume was maintained. After crosslinker addition, samples were incubated on ice for 30 min. For DSS crosslinking, incubation was at 20°C for 20 min. Then, Quenching Buffer (1M Tris-HCl, pH 8 / 100 mg/ml L-cys) was added (1/10 of total volume), and the sample incubated on ice for 15 min. For DSS, quenching was done by adding 7.5 µl of 8.4 M ammonium acetate for 20 min on ice. Samples were then washed twice (always in the presence of quenching buffer) with appropriate pH B88, membranes sedimented at 16.000 x g for 10 min, and resuspended in appropriate form for subsequent use. For LC-SPDP cleavage, membranes were incubated for 15 min at room temperature in the presence of 100 mM of DTT. For SDAD crosslinking, after the washes the sample was exposed, on ice, to a 15 min UV (365 nm) irradiation with a 3UV Lamp (115V, 60Hz) (ThermoFisher) at a distance of 3,6 cm.

1.2.26 Extraction of Luminal and Cytosolic Microsome-Associated Proteins

For extraction of cytosolic membrane-associated proteins, microsomes were resuspended in B88/Urea (20 mM Hepes-KOH, pH 6.8 / 250 mM sorbitol, 150 mM KOAc / 5 mM Mg(OAc)₂ / 2,5 M urea), incubated for 20 min on ice, followed by sedimentation and washing of the membranes with B88, pH 6.8. For extraction of ER-luminal proteins, microsomes were resuspended in 100 mM sodium carbonate, pH 11.5, incubated on ice for 20 min, followed by sedimentation (20 min at 346.000xg, 4°C) of the membranes through a sucrose cushion (200 mM sucrose / 100 mM sodium carbonate, pH 11.5), and resuspension in B88, pH 6.8. For mock extractions, samples were treated in same way, but in absence of either urea or sodium carbonate.

1.2.27 Purification of Sec61

ER membranes (500 eq) were treated as described in "Chemical Crosslinking", either with DMSO (control), SMPH, or LC-SPDP in a total volume of 1.5 ml. After washing, membranes were resuspended in 150 µl of Quenching Buffer (1 M Tris-HCl, pH 8 / 100 mg/ml L-cys) and diluted with 1 ml of IP Buffer (15 mM Tris-HCl, pH 7.5 / 150 mM NaCl / 1 % Triton X-100 / 0,1 % SDS) for solubilization (30 min at 4°C) followed by 10 min denaturation at 65°C. From this point on, all steps were done at 4°C. Sample was diluted with cold Binding Buffer (50 mM Tris-HCl, pH 7.4 / 300 mM KCl / 0,5 % Triton X- 100 / 40 mM imidazole) to a final volume of 5 ml and applied to an His-Trap FF crude (1 ml) column integrated into a BioLegend LP automated purification system (Biorad). After sample loading (0.5 ml/min for 10 ml), the column was washed with Binding Buffer (10 ml; 1 ml/min) and sample eluted along a step gradient of imidazole (100-500 mM, 15 ml per step, 1ml/min. Steps: 100; 200; 400; 500). Fractions (7,5 ml) were collected along the gradient with an automatic fraction collector. DTT

(100 mM) was added to each fraction. Each differently treated sample was applied to an independent column. Between purifications, the system was washed with 10 ml H₂O, 10 ml ethanol 20 %, 10 ml H₂O, and 20 ml Binding Buffer. Fractions where Sec61 was eluted (fraction 3-10 - 50 ml total) were pooled, proteins precipitated with 10 % TCA on ice for 2h and washed with ice-cold acetone. Each pellet was resuspended in 2 x Laemmli Buffer, and resolved for 5 cm on 4-12,5% NuPAGE gel. The gel was then stained by Coomassie Colloidal Staining (0.08% Coomassie Brilliant Blue G250 (CBB G250) / 10 % citric acid / 8% ammonium sulfate / 20 % methanol) overnight and destained with water as described in the EMBL online Proteomics Core Facility Protocols. The gels were then sealed in individual plastic bags with a few milliliters of water and shipped to the Mass Spectrometry Facility.

1.2.28 Mass Spectrometry

1.2.28.1 Sample preparation

The whole lane of each samples was cut out into small cubes and subjected to in-gel digestion with trypsin [331]. After overnight digestion, peptides were extracted from the gel pieces by sonication for 15 minutes, tubes were centrifuged, the supernatant removed and placed in a clean tube. Followed by a second extraction round with a solution of 50:50 water: acetonitrile / 1% formic acid (2 x the volume of the gel pieces), the samples were sonicated for 15 min, centrifuged and the supernatant pooled with the first extract. The pooled supernatants were then subjected to speed vacuum centrifugation. Samples were reconstituted in 96:4 water: acetonitrile / 0.1% formic acid and further processed using an OASIS® HLB μ Elution Plate (Waters) according the manufacturer's instructions.

1.2.28.2 LC-MS/MS

Peptides were separated using the nanoAcquity Ultra Performance Liquid Chromatography (UPLC) system (Waters) using a trapping (nanoAcquity Symmetry C18, 5 μm , 180 μm x 20 mm) as well as an analytical column (nanoAcquity BEH C18, 1.7 μm , 75 μm x 200 mm). The outlet of the analytical column was coupled to a Linear Trap Quadrupole (LTQ) Orbitrap Velos Pro (Thermo Fisher Scientific) using the Proxeon nanospray source. Solvent A consisted of water / 0.1% formic acid and solvent B consisted of acetonitrile / 0.1% formic acid. Sample was loaded with a constant flow of solvent A at 5 $\mu\text{l}/\text{min}$ onto the trapping column. Peptides were eluted over the analytical column with a constant flow of 0.3 $\mu\text{l}/\text{min}$. During elution the percentage of solvent B increased linearly from 3% to 7% in 10 min, then increased to 25% in 110 min and to 40% for the final 10 min. A cleaning step was applied for 5 min with 85% B followed by 3% B 20 min. The peptides were introduced into the mass spectrometer via a Pico-Tip Emitter 360 μm OD x 20 μm ID; 10 μm tip (New Objective), and a spray voltage of 2.2 kV was applied. Capillary temperature was 300 $^{\circ}\text{C}$. Full scan MS spectra were acquired with a resolution of 30000. The filling time was set at a maximum of 500 ms with a maximum ion target of 1.0×10^6 . The fifteen most intense ions from the full scan MS (MS1) were sequentially selected for sequencing in the LTQ. Normalized collision energy of 40% was used, and the fragmentation was performed after accumulation of 3.0×10^4 ions or after a maximum filling time of 100 ms for each precursor ion (whichever occurred first). Only multiply charged (2^+ , 3^+ , 4^+) precursor ions were selected for MS/MS. The dynamic exclusion list was restricted to 500 entries with maximum retention period of 30 s and a relative mass window of 10 ppm. In order to improve the mass accuracy, a lock mass correction using the ion (m/z 445.12003) was applied.

1.2.28.3 Data analysis

The raw mass spectrometry data was processed with MaxQuant (v1.5.2.8) [65] and searched against an Uniprot *Saccharomyces cerevisiae* proteome database. The search parameters were as follows: Carbamidomethyl (C) (fixed), Acetyl (N-term) and Oxidation (M) (variable) were used as modifications. For the full scan MS spectra (MS1) the mass error tolerance was set to 20 ppm, and for the MS/MS spectra (MS2) to 0.5 Da. Trypsin was selected as protease with a maximum of two missed cleavages. For protein identification a minimum of one unique peptide with a peptide length of at least seven amino acids and a false discovery rate below 0.01 were required on the peptide and protein level. The match between runs function was enabled, a time window of one minute was set. Label free quantification was selected using iBAQ (calculated as the sum of the intensities of the identified peptides and divided by the number of observable peptides of a protein) [347] with the log fit function enabled.

The xQuest/xProphet pipeline [217] was also used to identify crosslinked peptides in our samples. For this, we used the basic protocol and conditions used in Leitner et al. [217], correcting the meaningful parameters to fit our crosslinker (e.g. monoisotopic shift, only light chain, reactive groups, etc.). Databases of no more than 30 proteins were fed into the pipeline.

1.2.28.4 Statistical Analysis

The raw output data of MaxQuant (proteinGroups.txt file) was processed using the R programming language (ISBN 3-900051-07-0). As a quality filter, only proteins that were quantified with at least 2 unique peptides were allowed. Potential batch-effects were removed from the log₂ of the iBAQ values using the limma package [316]. Fur-

thermore, batchcleaned data was normalized with the vsn package (variance stabilization) [166]. Missing values were imput using the MSNbase package [110]. For conditions with at least 2 out of 3 identifications, the “knn” method was used. For less identifications, the “MinDet” method was applied. Finally, limma was used again to identify differentially expressed proteins. A protein was called a “hit” with a false discovery rate (fdr) smaller 5 % and a fold change of at least 3 and a “candidate” with a fdr smaller 20 % and a fold change of at least 3.

1.2.29 Mutant Construction

1.2.29.1 *sec61*Δ*L7* integration in the genomic DNA

In order to integrate the *sec61*Δ*L7* we subcloned the gene from pRS315-*sec61*Δ*L7* into pRS305. Plasmid pRS315-*sec61*Δ*L7* (1 μg) was digested with BglI in a standard restriction digestion as described in Section 1.2.8 using NEBuffer™ 3.1 and performing the reaction at 37 °C for 2h. This resulted in a truncation of the *sec61*Δ*L7* gene, which is necessary to assure the presence of a single copy of the gene after integration of the mutation into the genome. After enzyme inactivation (65°C for 20min) and cleaning as described in Section 1.2.8.1, sample was incubated with T4 DNA ligase in the absence of ATP, which resulted in a blunting of the overhang end generated by the BglI digestion. After new cleaning step by the same process used before, sample was digested again in a standard restriction digestion as described in Section 1.2.8, this time with Sall-HF in Cutsmart™ Buffer at 37 °C for 2h. This resulted in a 1705 bp fragment that was resolved in agarose gel, confirming its size, and recovered as described in Section 1.2.7. This fragment was then ligated as described in Section 1.2.11 into a SmaI/Sall digested pRS305. Half the ligation reaction was used to transform *E.coli* DH5α as described in Section 1.2.12.2. After overnight growth at 37°C,

positive clones were screened by colony PCR as described in Section 1.2.4.2 using the M13 primers for the reactions. Positive clones were further confirmed by sequencing. With this process, a truncated version of *sec61ΔL7* was subcloned into pRS305, originating pRS305-*trunc.sec61ΔL7*

For integration, pRS305-*trunc.sec61ΔL7* was linearized by MscI digestion as described in Section 1.2.8, and the full reaction volume was used to transform *S.cerevisiae* cells as described in Section 1.2.15. Screen of positive clones was done by isolating genomic DNA from the transformants as described in Section 1.2.5.3, and using it as template for a PCR using Sec61 flanking primers. Positive clones were detected by increased mobility of the *sec61ΔL7* in agarose gel when compared with that of *SEC61*. I started by transforming an haploid yeast strain. Although having sporadic positive clones, expression of Sec61ΔL7 was never achieved. I then tried integrating this construct in a diploid strain. After genomic integration of the mutation, I sporulated this diploid strains by growing them in Sporulation Medium (1% Potassium Acetate / 0.1% Yeast Extract / 0.05% Glucose) for 5 to 10 days at 25°C with slow shaking. As soon as spores were detected, samples (1 ml) of culture were collected, cells sedimented and washed with sterile MQ water. Cells were then resuspended in Tris-HCl, pH 5, 10 μl of β-Glucuronidase (SIGMA) were added, and sample was incubated at 37 °C. Different incubation times were tried until proper ascus digestion was obtained. Tetrads were then dissected using an MSM Tetrad Dissector, and spores were isolated. Positive clones were selected in the same way as previously. In this way, the integrant *sec61ΔL7* strain (KRY956) was generated.

1.2.29.2 14His-Tagged constructs

For His₁₄-tagging of *SEC61* and *sec61S353C*, both genes were amplified from pBW11 and pRS315-*sec61S353C*, respectively, using Primer 63 and Primer 64. The resulting PCR products were cloned into pRS426pGAL1 [380] using the SfoI and HindIII restriction sites. Correct cloning was confirmed by sequencing. The pGal-His₁₄-*SEC61*-CYC and pGal-His₁₄-*Sec61S353C*-CYC cassettes were then amplified using Primer 85 and Primer 93. The resulting PCR products were cloned into pRS315 (CEN, LEU2). Transformants in the JDY638 (pGAL-*SEC61*-URA3) *S. cerevisiae* background were first selected on SC -URA medium containing 2% (w/v) galactose and 0.2% (w/v) glucose lacking leucine. The pGAL-*SEC61* plasmid was selected against on SC 5-FOA plates containing 2% (w/v) galactose and 0.2% (w/v) glucose without leucine. Constructs were confirmed by sequencing.

1.2.29.3 *SEC61* Loop 5 deletion mutants

Mutations *sec61del1*, *sec61del2*, and *sec61del1/2* were generated by PCR-driven overlap extension (SOE PCR) [3, 164] as described in Section 1.2.4.1. SOE-PCR resulting fragments were then digested HindIII/BamHI as described in Section 1.2.8, as was the pRS315(CEN, *LEU2*) vector. After cleaning the digested DNA with a PCR cleaning Kit (Sigma), each mutant gene (*sec61del1*, *sec61del2*, and *sec61del1/2*) was ligated into the digested pRS315 as described in Section 1.2.11 and transformed into *E. coli* DH5 α as described in Section 1.2.12.2. After overnight growth at 37°C, positive clones were screened by colony PCR as described in Section 1.2.4.2 using the M13 primers for the reactions. Positive clones were further confirmed by sequencing. Correct pRS315-*sec61del1*, pRS315-*sec61del2*, and pRS315-*sec61del1/2* were then transformed into KRY461 as described in Section 1.2.15. Transformants into

JDY638 (*pGAL-SEC61-URA3*) were first selected on SC -URA medium containing 2% (w/v) galactose and 0.2% (w/v) glucose without leucine. The *pGal-SEC61* plasmid shuffle was done on SC 5'-FOA plates lacking leucine. All constructs were confirmed by sequencing.

1.2.29.4 *MPD1* HA-Tagging

In order to generate a detectable form of Mpd1, the *MPD1* gene was genomically tagged with a C-terminal HA-tag. For this purpose the protocol described in Janke et al. [177] was used. Briefly, the HA cassette was amplified from pYM24 (supplied by Michael Knop) using Primer 111 and Primer 112. The plasmid contains the HA-cassette as well as the hphNT1 marker for selection. The primers designed have the plasmid homology as described in the mentioned paper, so as to amplify the correct cassette/marker and also an homology with the appropriate regions of the gene of interest. The forward primer has to have homology with the last stretch of the coding region (in this case, *MPD1*) not including the STOP codon. The reverse primer has to have homology with the Stop codon and the region immediately downstream of the interest gene. Once adequate primers were designed, a PCR reaction as described in Table 1.23 was made. The resulting PCR product was cleaned, its size confirmed by gel electrophoresis (Section 1.2.6 and its sequence confirmed by sequencing (Section 1.2.13). Once the correct tagging was confirmed, the PCR product was used to transform KRY897, KRY1116, KRY1117, and KRY1117 as described in Section 1.2.15. Transformants were selected on YPD plates containing hygromycin (300µg/ml). Expression of Mpd1-HA was confirmed by making extract from mentioned strains as described in Section 1.2.19.1 and analyzing them by Western Blot as described in Section 1.2.19.6, where anti-HA antibodies were used for protein detection. Unfortunately

the expression level of the genomic *MDP1-HA* was very low. To circumvent this issue, the tagged *MPD1* form was cloned into a 2 μ plasmid, and therefore, of high copy number, in order to obtain higher tagged protein levels. *MPD1-HA* was amplified from the genomic DNA of one of the positive clones using Primer 114 and Primer 115, and cloned into pRS426 (2 μ , *URA3*) after *Sall*/*EcoRI* digestion (of both insert and vector). This plasmid was then used to transform the wildtype (KRY897) and hinge mutant strains (KRY1116, KRY1117, and KRY1118), originating strains KRY1162, KRY1163, KRY1164, and KRY1165, respectively.

Table 1.23: Standard reaction mixture for PCRs

Component	Volume (μ l)	Final concentration/ Quantity
5X KAPAHiFi™ Reaction Buffer	10	1X
KAPA dNTP Mix (10 mM each)		
Forward primer (10 μ M)	1.5	0.3 mM
Reverse primer (10 μ M)		
Template DNA	1	10ng plasmid DNA
KAPAHiFi™ Polymerase		0.02 U/ μ l
dH ₂ O	to 50	–

1.2.30 Detection of Sec61 Interactors in Radiolabeled Membranes

Crude radiolabeled ER vesicles (10 μ l) (Section 1.2.21) were crosslinked as described in Section 1.2.25 and submitted to two consecutive immunoprecipitations (Section

1.2.24.3. For the first precipitation, the membranes were solubilized in Lysis Buffer (20 mM Tris, pH 7.5 / 2% SDS / 1 mM PMSF) and denatured at 65°C for 10 min. Proteins were then diluted in Washing Buffer (15 mM Tris-HCl, pH 7.5 / 150 mM NaCl / 1% Triton X-100 / 2 mM NaN₃ / 1 mM PMSF). After pre-clearing, 60 µl of 20% Protein A-Sepharose beads (GE Healthcare) and saturating amount of Sec61 antibody were added. Samples were then incubated with rotation overnight at 4°C. After sedimentation, Protein A Sepharose pellets were washed as in standard immunoprecipitation sample (Section 1.2.24.3). For elution 20 µl of 20 mM Tris-HCl, pH 7.5 / 5% SDS / 50 mM DTT were added, sample was incubated for 15 min at room temperature and denatured for 10 min at 65°C. Eluted proteins were then diluted in Washing Buffer and the Mpd1-HA precipitated using anti-HA polyclonal antibody (BioLegend). Precipitation was done for 2h at room temperature followed by elution with 2 x Laemmli Buffer / 200 mM DTT. Proteins were denatured again as before, resolved on 4-12,5% NuPAGE gels exposed to Phosphorimager plates, and the signal acquired with a Typhoon PhosphorImager (GE Healthcare).

“Tis a lesson you should heed:

Try, try again.

If at first you don’t succeed,

Try, try again.”

William Edward Hickson

2

Results

The core objective of this project was to identify Sec61 luminal interactors by chemical crosslink. To achieve that, a setup that allowed efficient chemical crosslink of Sec61 to its interactors, as well as detection of these crosslinked forms and identification of their components had to be generated.

I devised and optimized a crosslink setup for different crosslinkers, to allow both immunoblotting and mass spectrometric analysis of Sec61 interactors.

2.1 Determination of Sec61 and Sec61 Δ L7 DSS crosslink pattern

The very first step in the establishment of a crosslink setup was the choice of crosslinker. Many crosslinkers with different reactivities, lengths, solubilities, etc., are commercially available, so a selection had to be made. Since my target (Sec61) is an ER-membrane protein, and my main interest was to identify luminal interactors, the use of a membrane permeable crosslinker was paramount. Another important consideration was the length of the crosslinker. Since I was interested in direct Sec61 interactions, the spacer-arm of the crosslinker would have to be short, to decrease the chance of crosslink to indirect interactors. It could not be too small, however, or else I risked missing direct interactions just due to the lack of crosslinkable amino acids in the interaction position or even by blockage of such crosslinkable amino acid by the actual interaction. Also, since this was still the initial setup phase, the better established and more efficient the reactivity of its reactive groups, better the chances of successfully finding conditions where Sec61 was efficiently crosslinked.

After careful crosslinker analysis, disuccinimidyl suberate (DSS) seemed to be a good first candidate. DSS is a water-insoluble, membrane permeable, homobifunctional N-hydroxysuccinimide ester (NHS ester), which is characterized by the presence of two reactive (i.e crosslinkable) groups (NHS esters) that, at pH 7 to 9, react

with primary amine groups (e.g NH₂ - Lysines, N-terminus) (Figure 2.1). DSS was chosen due to its standardized character. It is one of the most widely used and well established chemical crosslinkers. Also, its short spacer arm (11.4 Å), one of the shortest available, as well as the high crosslink efficiency associated to its reactive groups, seemed to make it the perfect candidate for this initial study. Since a DSS crosslink setup using microsomes had been tested previously in our lab (data not shown), there was no need for DSS titration and a working concentration of 0.8 mM was used for all crosslink reactions. Also, the conditions for the crosslink (e.g pH, incubation periods, incubation temperatures) were the same as previously used and stated in Section 1.2.25.

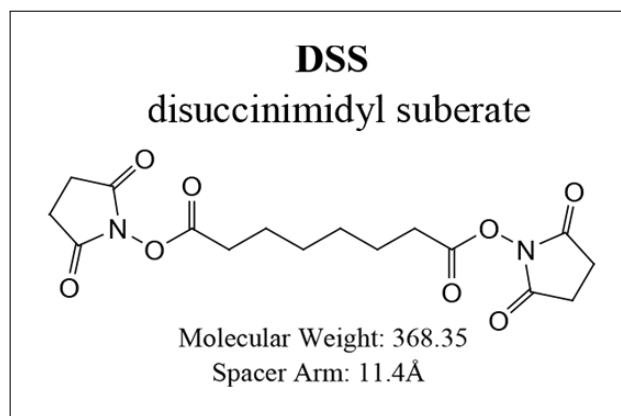


Figure 2.1: DSS structure. Scheme representing DSS structure. Molecular weight and spacer arm length also shown in figure.

Here I tested whether DSS treatment resulted in a crosslink-specific pattern for Sec61, but also whether such pattern, when present, was affected by the lack of the Sec61 luminal loop 7. In previous work, *sec61ΔL7* (the *sec61* mutant in which the Sec61 protein is lacking the full luminal loop 7), was shown to have an ERAD impairment, but it also displayed some import defects [397]. Since the lack of such prominent luminal loop might affect Sec61 luminal interactions, potentially with ERAD

factors, as well as cytosolic ones, I deemed that comparing the crosslink pattern of Sec61 versus Sec61 Δ L7 might yield some interesting results.

For this purpose, microsomes from two different backgrounds (*SEC61* and *sec61 Δ L7*) were crosslinked with 0.8 mM of DSS for 20 min at 20°C, quenched with ammonium acetate, resolved by SDS-PAGE, and immunoblotted against Sec61 (Figure 2.2 A). Comparing DSS untreated and treated samples (lane 1 versus lanes 2/3; lane 4 versus lanes 5/6), it could be observed that in the *SEC61* background a very distinct Sec61-containing band was present at around 50 kD, representing a shift or approximately 10 kD (Figure 2.2 A; lane 1 versus 2/3). In the *sec61 Δ L7* background a new crosslink-dependent Sec61 Δ L7-containing band can also be detected but at around 45 kD (Figure 2.2 A; lane 4 versus 5/6). This also represents a shift of around 10 kD, since the free Sec61 Δ L7, being smaller than Sec61, has an increased acrylamide gel mobility, running at around 35 kD (Figure 2.2 A; lanes 4-6). However, the 45 kD band detected in the *sec61 Δ L7* background showed a significantly lower intensity than the 50 kD band detected in the *SEC61* background (Figure 2.2 A; lanes 2/3 versus 5/6). Since the size of the shift in both backgrounds was the same, the probability of the non-Sec61-component of each band being the same seemed high. Its identity, however, had to be determined. Since the ER protein content is well known and I had access to several specific antibodies against ER proteins, I postulated that by identifying potential candidates based on the size of the shift, an immunoblotting approach could be used to identify the crosslinked-bands components. The reasoning was that if two different proteins could be detected (using their specific antibodies) showing the same uncharacteristic mobility (i.e co-localization of bands in a location different than their characteristic molecular size) only in crosslinked samples, a crosslink between both of them could be assumed.

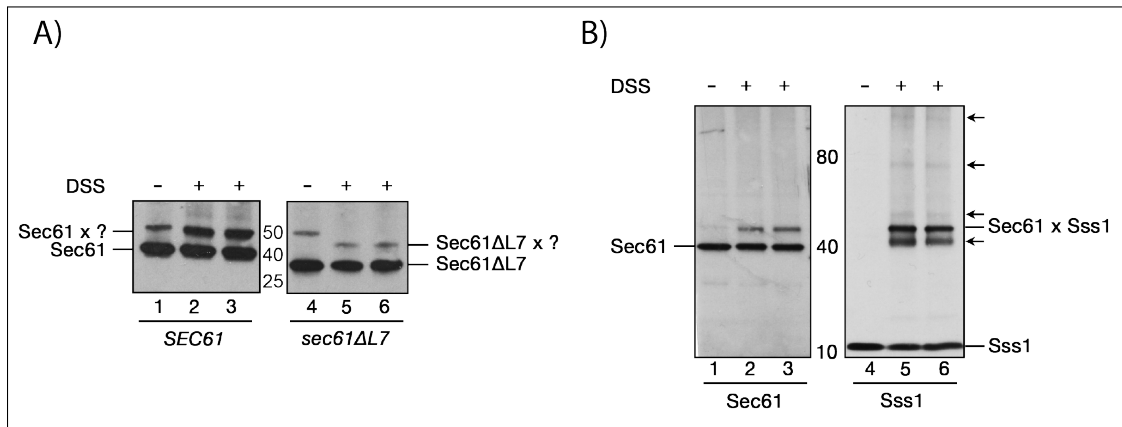


Figure 2.2: SEC61 DSS crosslink pattern determination. Immunoblot analysis of the DSS crosslink pattern. ER vesicles (17eq) were crosslinked with 0.8 mM of DSS and analyzed by SDS-PAGE on 4-12% Bis-Tris gels (NuPAGE® Novex® Pre-Cast gels, Invitrogen). Sec61 was detected by Immunoblotting and signal acquired on ECL film. A) Comparison of the crosslink pattern obtained on SEC61 and sec61ΔL7 backgrounds when Sec61 is detected. B) Immunoblot analysis of DSS crosslink pattern on a SEC61 background when both Sec61 and Sss1 are detected.

Since Sss1, one of the components of the Sec61 trimeric complex has a molecular weight compatible with the shift observed, I started by applying this approach to verify if the interaction detected was with Sss1. For that purpose, wild-type membranes were crosslinked with DSS and immunoblotted for both Sec61 and Sss1. By immunoblot analysis of the same reaction (resolved side-by-side) with both a Sec61- and a target protein-specific antibody, a potential co-migration of Sec61 and the target protein could be evaluated. As can be seen in Figure 2.2 B, the 50 kD band was detected with both Sec61 and Sss1 antibodies in a crosslink-dependent manner (Figure 2.2 B; lanes 2/3 and 5/6). This confirmed the hypothesis that the band at 50 kD represents a crosslink between Sec61 and Sss1 (Figure 2.2 B; lanes 5 and 6). It should also be noticed that several other crosslinker-dependent bands are detectable when immunoblotting against Sss1, showing that this setup might also be good to identify Sss1 interactors. Such study was beyond the scope of this work, however, and as was not pursued further.

Sbh1 was also present in the 50 kD band, although crosslink specific bands always presented weak intensities (data not shown) indicating a low accessibility of the crosslinked amino acids of either Sec61 or Sbh1 or of the antibody to Sbh1, due to epitope inaccessibility when in complexed form.

With these results, I could assess that a microsome-based chemical crosslink setup to identify Sec61-interactors was possible. Also, in doing so I was able to show that the Sec61 interaction with Sss1 was impaired when loop 7 was missing (data published in Tretter et al. [397]).

2.2 Immunoblotting analysis of Sec61 SDAD crosslink pattern

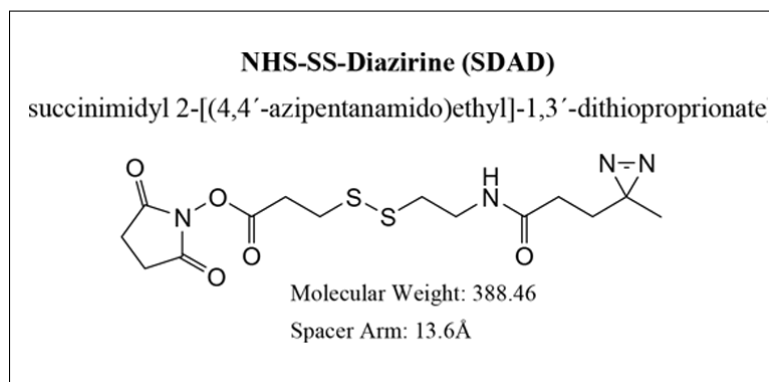


Figure 2.3: SDAD structure. Scheme representing SDAD structure. Molecular formula, molecular weight, and spacer arm length also shown in figure

Having been able to establish an efficient crosslink setup, a more broad approach was deemed necessary. My initial aim was to identify loop 7 interactions. DSS is only lysine-reactive and there are no lysines in loop 7. Therefore, the next step was to apply a crosslinker with an ampler reactivity. With this in mind, I chose succinimidyl 2-[(4,4'-azipentanamido)ethyl]-1,3'-dithiopropionate (SDAD). SDAD is a water-insoluble, membrane-permeable heterobifunctional crosslinker that contains an N-

hydroxysuccinimide (NHS) ester and a diazirine ring (Figure 2.3). NHS esters efficiently react with primary amino groups ($-NH_2$) to form stable amide bonds. Diazirine rings are photoactivatable with long-wave UV light, creating reactive carbene intermediates that form covalent bonds through addition reactions with any amino acid side chain or peptide backbone. SDAD has yet another characteristic: it is cleavable. As it possesses a disulfide bond in its spacer arm, crosslinked peptides can be cleaved upon sample reduction. Taking advantage of the more promiscuous reactivity of the diazirine ring when compared to the NHS-ester reactive group, as well as the slightly longer spacer arm, a more broad-spectrum crosslink setup was implemented.

The first step was to establish a crosslink protocol. Due to the intrinsically dynamic Sec61 environment, setting the reactions on ice was thought to slow down possible dissociation reactions, increasing the chance of effectively locking them by crosslink. Therefore, all reactions were done on ice, instead of the 20°C used for DSS crosslink. As stated before, SDAD has two reactive groups, an NHS-ester and a diazirine ring. Since the NHS-ester reactive group is the same as in DSS, the same reaction-pH (7.9) was used. The diazirine group, however, needed an extra UV-activation step. The optimal duration and distance of UV-irradiation had also to be tested along with an appropriate working concentration (Figure 2.4 A and B).

In this first assay, SDAD concentration was titrated from 0 to 2 mM (Figure 2.4 A). Microsomes of two wild-type strains were tested: one where *SEC61* is under the control of a galactose-inducible promoter (*GAL-SEC61*, left panel), and one where the *SEC61* is under the control of its endogenous promoter (right panel). To limit the number of variables to be assessed, maximum UV-exposure time suggested by the supplier (15 min) and a convenient UV-irradiation distance (3.6 cm - height of 1.5 ml Eppendorf tube) were used. An SDAD specific pattern was immediately observable

in all treated samples (Figure 2.4 A; lanes 2, 4, 6, 8, 10 and 12). Besides the Sec61 specific band at around 40 kD, at least two new Sec61-containing bands could be detected: one at around 50kD and another at around 80 kD, representing a shift of around 10 and 40 kD, respectively (Figure 2.4 A; lanes 2, 4, 6, 8, 10 and 12; Figure 2.4 B, "+" lanes).

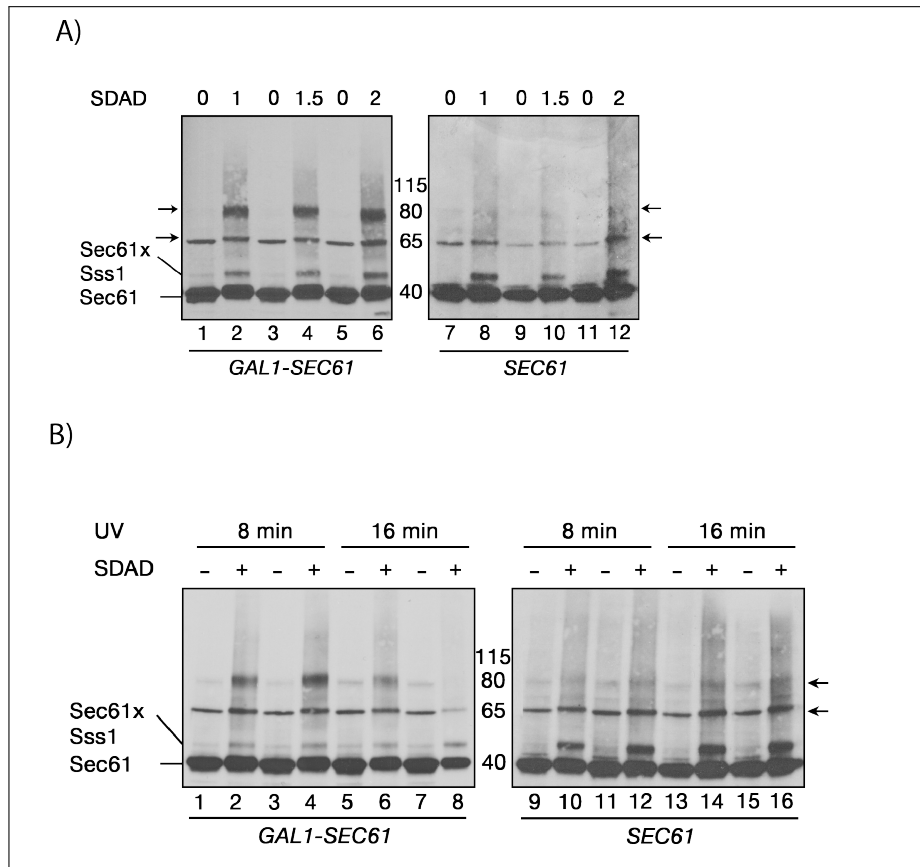


Figure 2.4: Sec61 SDAD crosslink pattern determination. Immunoblot analysis of the SDAD crosslink pattern. ER vesicles (17eq) were crosslinked with SDAD for 30 min on ice, quenched for 15min, UV-irradiated and analyzed by SDS-PAGE on 4-12 % Bis-Tris gels (NuPAGE® Novex® Pre-Cast gels, Invitrogen). Protein detection was done by Western Blotting using Sec61 N-terminal antibody and signal acquired on ECL film. **A)** SDAD concentration titration in wild-type microsomes. Microsomes from GAL1-SEC61 (left panel) and SEC61 (right panel) were used. UV irradiation distance was maintained constant (3.6 cm) as well as the duration of the irradiation (15min). **B)** Duration of UV irradiation test. Microsomes from GAL1-SEC61 (left panel) and SEC61 (right panel) were used. Concentration of SDAD used was 1.5 mM and the UV irradiation distance was also maintained constant (3.6 cm). Two different periods of irradiation were tested: 8 and 16 min.

As I have determined in Section 2.1, the 10 kD-shifted band corresponds to a crosslink between Sec61 and Sss1 (Figure 2.2 B; lanes 2/3 and 5/6). This crosslink pattern was visible independently of SDAD concentration used, although its intensity seemed to be higher at higher concentrations (lane 4, 6, 10 and 12). A third band at around 65 kD (25 kD shift) was also detected. Its intensities increased with SDAD treatment, but it was also present even in the absence of SDAD (Figure 2.4 A; lanes 1, 3, 5, 7, 9 and 11; Figure 2.4 B, "-" lanes). This might be the result of a co-migration of a Sec61-containing complex with this unspecific band, or just a stabilization of a complex that is unspecifically detected in the wild-type caused by the crosslink process. It became also obvious that the intensity of the 80 kD band was much higher and the intensity of the Sec61xSss1 band (50 kD) slightly lower in the samples where microsomes from the *GAL-SEC61* strain had been used (left versus right panels). Since the main objective of this project was to identify new Sec61 interactors, I chose to prioritize the quality of the 80 kD band instead of the Sec61xSss1 band. Hence, microsomes from a *GAL1-SEC61* strain were used for the remainder of this SDAD crosslink.

I also tested the effect of ATP during crosslink in both wild-type and *sec61 Δ L7* backgrounds, but observed no effect (Supplemental Figure A.3 B).

In addition, I tested the reactivity of N- *versus* C-terminal Sec61 antibodies after SDAD crosslink (Supplemental Figure A.1 A). The N-terminal antibody was better for Sec61-crosslinked-complexes detection. Interestingly, the 50 kD band had a lower intensity when detected with the C-terminal antibody (lane 2 to 5 versus lane 6 to 9). This might indicate that the interaction with Sss1 happens through Sec61's C-terminus, making access of the C-terminal antibody harder, resulting in a lower detectability.

Based on these results, 1.5 mM was deemed the best working SDAD concentration (Figure 2.4 A; lane 4).

After establishing a working concentration, titration of the duration of the UV irradiation was needed. I repeated the crosslink assays, varying the duration of the UV irradiation period (8 and 16 min) (Figure 2.4 B). No drastic difference in band intensity can be seen between both conditions, although a slightly higher intensity was obtained with higher irradiation periods (Figure 2.4; left panel, lanes 1-4 versus 5-4; right panel, lanes 9-12 versus lanes 13-16). The longer irradiation period (15min) was used for the remainder of the study.

Since the supplier suggested that shorter irradiation distances might yield better crosslink efficiencies, I also tested if reducing the distance of the irradiation to 1.6 cm (height of PCR tube) yielded better results (Supplemental Figure A.1 B). This assay was done with both *SEC61* and *sec61 Δ L7* microsomes, as a way of determining whether, as with DSS, the lack of loop 7 influences the crosslink pattern. The intensity of the crosslinked bands was lower when a shorter distance was used (Supplemental Figure A.1 B; left panel, lane 2 and 3). In the *sec61 Δ L7* background, independently of the distance of irradiation, the Sec61 Δ L7 specific band was detected at around 35 kD and only one other SDAD-dependent band at around 45 kD (Supplemental Figure A.1 B; right panel, lane 5-8). The latter represents the same 10 kD shifted band present in the *SEC61* background, although it seems to have a lower intensity than the Sec61-containing counterpart (Supplemental Figure A.1 B; lane 2 versus lane 7 or lane 3 versus lane 9).

Having identified at least two Sec61-containing complexes, the next step was trying to determine their components. To this end, different populations of proteins were extracted from the microsomes prior to crosslink. The reasoning behind this approach was that if extraction of a specific protein pool affected the crosslink pattern, then the Sec61-crosslinked partner would be either a protein from that pool or needed a

protein/cofactor from that fraction to interact with Sec61. Microsomes were either extracted with 2.5 M urea, with 100 mM sodium carbonate, pH 11.5, or high salt-treated. Carbonate treatment induces denaturation of soluble domains of transmembrane proteins, and sheeting of vesicles, resulting in a loss of luminal proteins [106]. Urea treatment removes the cytosolic proteins that are peripherally associated with the ER-membrane [122], as does the high-concentration salt treatment (Strip).

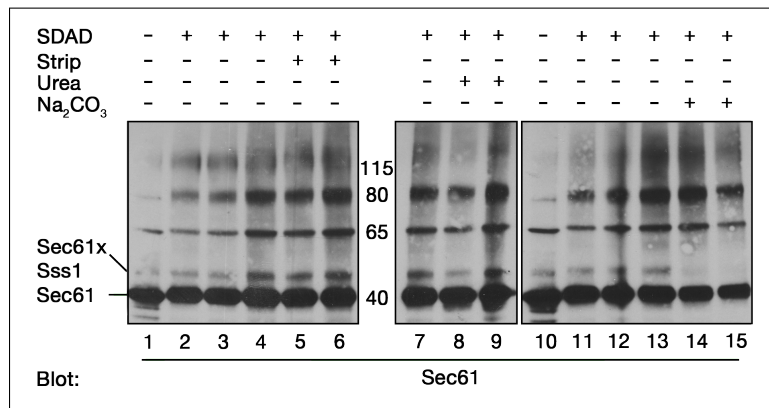


Figure 2.5: Effect of the absence of different protein populations on SDAD crosslink pattern. ER vesicles (17eq) were extracted with 2.5 M Urea (Urea), 100 mM of sodium carbonate (Na₂CO₃), or 500 mM potassium acetate (Strip) before SDAD crosslink, and analyzed by SDS-PAGE on 4-12% Bis-Tris gels (NuPAGE® Novex® Pre-Cast gels, Invitrogen). Protein detection was done by Western Blotting using Sec61 N-terminal antibody and signal acquired on ECL film.

As can be seen in Figure 2.5, all shifted bands are present independently of microsome-extraction protocol used, except for the Sec61xSss1 band, which was almost completely abolished by carbonate extraction (lanes 14/15 versus lane 13). Extraction of Sss1 by carbonate as been shown previously [90]. This strengthens the conclusion that this band represents in fact an Sec61xSss1 interaction. The fact that none of the other bands are affected by the treatment suggests that the detected potential interactions could only be with membrane proteins.

Sec61 forms both a trimeric complex with Sbh1 and Sss1, and an heptameric complex, where this trimeric complex joins the Sec63 complex [248, 277]. The Sec63

complex is composed by Sec62, Sec63, Sec71 and Sec72 [79, 44]. Since antibodies against Sec62, Sec63 and Sec71 were available from Rand Schekman's lab, I tried applying the same approach used to identify the Sss1 interaction in Section 2.1, and used these specific antibodies to detect a co-localization of Sec61 crosslinked bands and any of these targets. Wild-type membranes were crosslinked with 1 mM SDAD in three independent reactions (one untreated sample and two SDAD-treated samples). Each set was resolved by SDS-PAGE side-by-side, revealed with the specific antibody against one of the proteins mentioned above, and signal acquired on ECL film. In addition, one set was also developed using the Pdi1 antibody. Pdi1 is a protein disulfideisomerase which role in ERAD is well established [120].

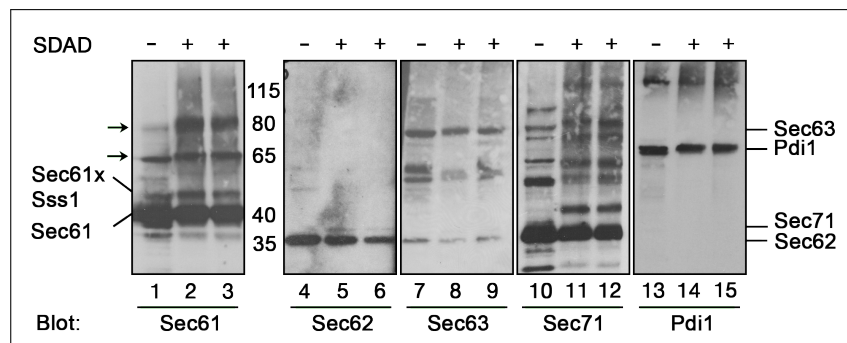


Figure 2.6: Multi-antibody analysis of SDAD crosslink pattern. ER vesicles (17 eq) were crosslinked with 1 mM SDAD crosslink for 30 min on ice, quenched for 15 min, UV-irradiated for 15 min (3.6 cm) and analyzed by SDS-PAGE on 4-12 % Bis-Tris gels (NuPAGE® Novex® Pre-Cast gels, Invitrogen). Protein detection was done by Western Blotting using either Sec61, Sec62, Sec63, Sec71 or Pdi1 antibody and signal acquired on ECL film. For each set of reactions (one untreated sample and two treated with SDAD), a different antibody was used for detection. 5 aligned panels are shown, each comprising a set. From left to right: anti-Sec61-N (40 kD), anti-Sec62 (32 kD), anti-Sec63 (73 kD), anti-Sec71 (35 kD) and anti-Pdi1 (65 kD).

As can be seen in Figure 2.6, no SDAD-specific bands with a migration pattern similar to the shifted bands observed in the anti-Sec61 revealed set (Figure 2.6; lanes 2 and 3) can be detected in the Sec62, Sec63 or Pdi1 immunoblotted samples (Figure 2.6; lanes 4-6, 7-9 and 13-15, respectively). In the anti-Sec71 revealed set, however, several shifted bands are detected upon SDAD treatment. Indeed, a shifted band

at round 80 kD can be detected (Figure 2.6; lanes 10-12), showing thus a band co-localization between anti-Sec61 and anti-Sec71 revealed, and SDAD treated samples (compare Figure 2.6; lanes 1-3 to lanes 10-12). This data suggests that an interaction between Sec61 and Sec71 could be identified by SDAD crosslink. It should also be noted that a series of other shifted bands can be detected in the anti-Sec71 revealed, SDAD treated samples (Figure 2.6; lanes 11 and 12). Namely, bands containing Sec71 (32 kD) can be detected at around 45, 65, 80 and 120 kD, representing a shift of 10, 30, 50 and 90 kD. Since Sec71 interactor determination was beyond the scope of this work, the identity of the interactors was not further investigated. Nevertheless, some Concanavalin A precipitations of SDAD treated samples were done (Supplemental Figure A.3 A), and the 80kD, Sec61-containing band was marginally precipitated, supporting the idea that Sec71 is one of its components, since Sec71 is glycosylated [95].

Interaction with another ERAD-relevant protein involved in targeting of ERAD-substrates for export to the cytosol, Yos9, was investigated. I used the same immunoblotting approach, in both wild-type and $\Delta yos9$ backgrounds, detecting with both Yos9 (35 kD) and Sec61 specific antibodies (Supplemental Figure A.2 A and B, respectively). Unfortunately the Yos9 antibodies were rather weak, so no obvious difference in crosslink pattern could be observed between wild-type and $\Delta yos9$ backgrounds (Supplemental Figure A.2 A). Also, upon Sec61 detection, no difference in crosslink patterns could be detected between wildtype and $\Delta yos9$ microsomes (Supplemental Figure A.2 B, respectively).

To further confirm whether the other subunits of the Sec complex were crosslinked to Sec61, immunoprecipitation of several of these proteins from SDAD crosslinked samples using specific antibodies was attempted. Unfortunately, the high levels of

background associated with the unfortunate co-migration of both linked and cleaved heavy and light antibody chains with several of the SDAD-specific bands (and also the free Sec61) made it impossible to obtain any useful data from these assays (data not shown; Supplemental Figure A.4).

Although multiple crosslinked bands had been detected with this SDAD crosslink/immunoblotting approach, I was able to identify only a single interactor, Sec71, which represents a known Sec61 interaction, since Sec71 is a component of the heptameric Sec complex. So, although SDAD crosslink showed itself as being a suitable setup to study Sec61-interactors, no novel information stemmed from this analysis.

2.3 Immunoblotting analysis of Sec61 SMPH crosslink pattern

Until this point I had only characterized potential interactions with known Sec61 interactors (Sss1 and Sec71). Trying to increase the chances of detecting luminal interactions, I idealized a new crosslink setup. In this setup, microsomes from a point mutant generated previously in our lab (*sec61S353C*) [186], where a serine in Sec61 loop 7 had been mutated to a unique cysteine, could be used in conjugation with a sulfhydryl-reactive crosslinker, in the hope of detecting primarily luminal crosslinks. This mutant has no ER import defects, with a decreased affinity to the 19S RP of the 26S proteasome, resulting in a Δ gpaF-specific ERAD defect, whose export from the ER is dependent on the 19S RP-Sec61 interaction [186].

For this purpose, a new crosslinker had to be chosen, tested and optimized. After careful consideration, Succinimidyl-6-[(β -maleimidopropionamido)hexanoate] (SMPH) was chosen. SMPH is a heterobifunctional crosslinker with N-hydroxysuccinimide (NHS) ester and maleimide groups that allow covalent conjugation of amine- and sulfhydryl-containing molecules. NHS esters react with primary amines at pH 7-9 to

form amide bonds, while the maleimides react with sulfhydryl groups at pH 6.5-7.5 to form stable thioether bonds. Unlike SDAD, SMPH is uncleavable. The main reason for choosing this crosslinker, besides its reactivity, was its spacer arm length (14.2 Å), which is in the range of the previously used crosslinkers.

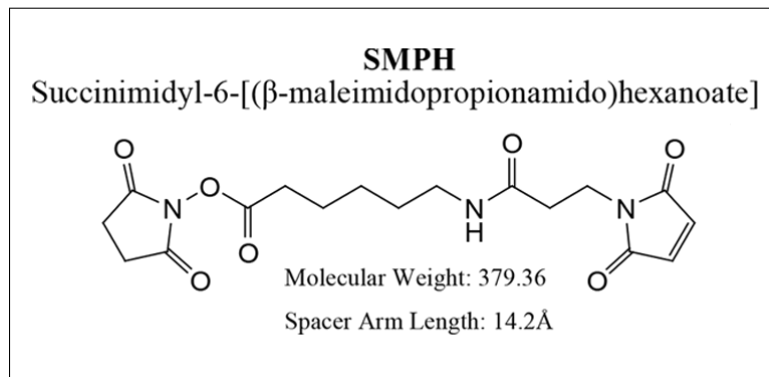


Figure 2.7: SMPH structure. Scheme representing SMPH structure. Molecular formula, molecular weight, and spacer arm length also shown in figure

Since the pH interval at which each one of the reactive groups reacts overlaps at pH 7-7.5, a working pH in that range seemed to be the optimal option. The possibility of allowing the reaction of each group in turns existed, by pH shift in between phases. I tested this approach, but it showed itself to be more technically demanding and without any gain in result quality (data not shown).

As before, the first step was to establish the best working SMPH concentration and pH. For this purpose, a series of SMPH concentrations were tested, always using pH 7.2 as the reaction pH. This screen was done with microsomes from a wild-type (*SEC61*) strain, a *sec61S353C* strain, and a *sec61ΔL7* strain (Supplemental Figure A.5 A and B). For simplicity sake, an image illustrating the best conditions found and henceforth used for standard SMPH crosslink reactions is supplied in Figure 2.8.

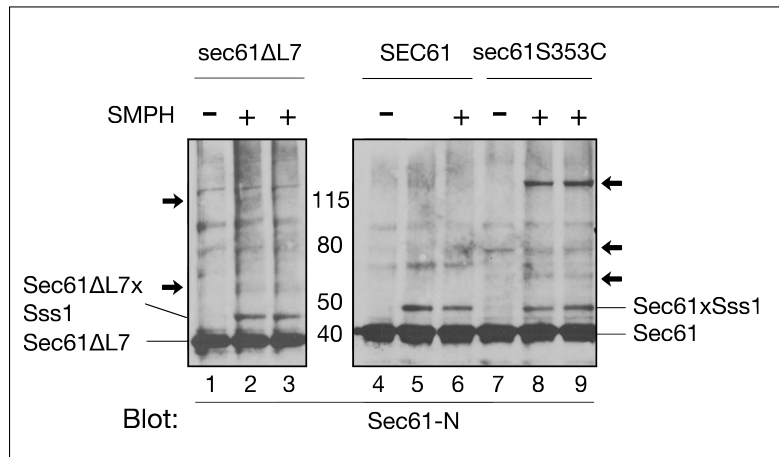


Figure 2.8: Sec61 SMPH crosslink pattern determination. Microsomes (17 eq) from *SEC61*, *sec61ΔL7*, and *sec61S353C* backgrounds were crosslinked with 1 mM SMPH for 30 min on ice, quenched for 15 min and analyzed by SDS-PAGE on 4-12 % Bis-Tris gels (NuPAGE® Novex® Pre-Cast gels, Invitrogen). Protein detection was done by Western Blotting using a specific Sec61 N-terminus antibody, and signal acquired on ECL film. Here the SMPH-specific Sec61-crosslink pattern obtained in either a *sec61ΔL7* background (left panels; lanes 1-3), a *SEC61* background (right panel; lanes 4-6) or a *sec61S353C* background (right panel; lanes 7-9) were compared.

In Figure 2.8 lanes 2/3, 5/6 and 8/9, it can be seen that besides the already characterized Sec61xSss1 interaction that can be detected in all three strains (band at 50 kD in *SEC61* and *sec61S353C* background; band at 45 kD in the *sec61ΔL7* background), in the *sec61S353C* background, three other shifted bands could be identified. This shifted bands migrated at 60, 80 and 120 kD representing, respectively, a shift of 20, 40 and 80 kD (Figure 2.8; lanes 8 and 9). In the *sec61ΔL7* background, however, besides the Sec61ΔL7xSss1 only two other bands could be detected: one around 55 kD and a faint one at around 110 kD (Figure 2.8; lanes 2 and 3), potentially the 120 kD Sec61S353C counterpart.

I also attempted SMPH crosslink in permeabilized cells, but it proved unsuccessful in shifted bands identification (Supplemental Figure A.7 A and B).

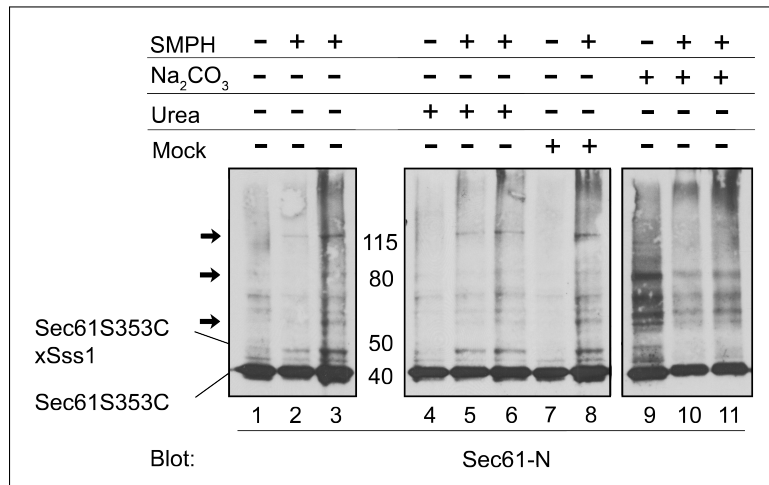


Figure 2.9: Effect of the absence of different protein populations on SMPH crosslink pattern. Microsomes of *sec61S353C* (17eq) were extracted with 2.5 M Urea (Urea) or 100 mM of sodium carbonate (Na₂CO₃) before crosslink with 1 mM of SMPH for 30 min on ice, quenched for 15 min, and analyzed by SDS-PAGE on 4-12 % Bis-Tris gels (NuPAGE® Novex® Pre-Cast gels, Invitrogen). Protein detection was done by Western Blotting using Sec61 N-terminal antibody and signal acquired on ECL film.

In order to narrow down the location of the detected crosslinked-partners, as in Section 2.2, cytosolic associated and luminal proteins were extracted prior to crosslink, by treating the microsomes with 2.5 M of urea or 100 mM sodium carbonate, pH 11.5.

As can be seen in Figure 2.9, the only treatment that resulted in band loss was the extraction of luminal proteins, as is evident by comparing lanes 8 to 6 and 11. In lane 6, all bands detected in the control lane 8 are present, suggesting that no cytosolically membrane-associated protein is involved in the detected crosslinks. But, in lane 11, none of the shifted bands seen in lane 8 are detected, not even the 50 kD, that as determined before, represents an interaction with Sss1 and is carbonate sensitive. The lack of all these crosslinks indicates that they represent interactions either with a luminal protein or with a transmembrane protein through its soluble domains, which was denatured upon carbonate treatment.

In an effort to identify the interactor partners that were SMPH-crosslinked to Sec61, immunoblot analysis using specific antibodies was applied. As it had already been de-

terminated that the SMPH crosslinks were carbonate-sensitive, I focused on luminal proteins.

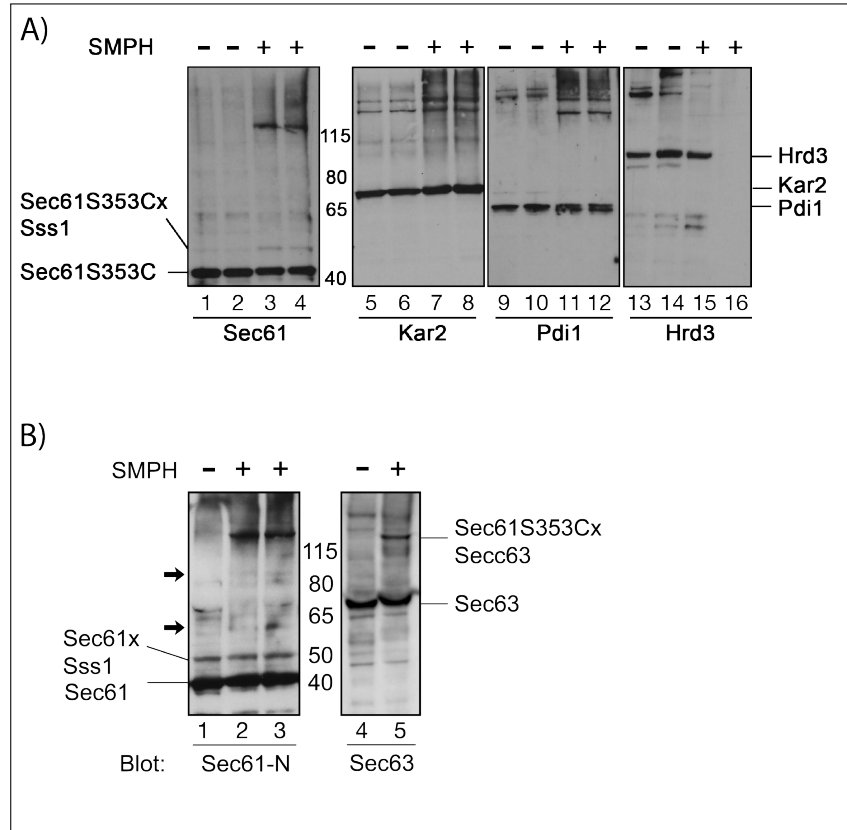


Figure 2.10: Multi-antibody analysis of SMPH crosslink pattern. Microsomes from *sec61S353C* (17eq) were crosslinked with 1 mM SMPH for 30min on ice, quenched for 15min, and analyzed by SDS-PAGE on 4-12% Bis-Tris gels (NuPAGE® Novex® Pre-Cast gels, Invitrogen). Protein detection was done by Western Blotting using specific antibodies and signal acquired on ECL film. For each set of reactions (one untreated sample and two treated with SMPH), a different antibody was used for detection. A) Protein detection done using either either Sec61, Bip, Pdi or Hrd3 antibody and. Figure shows 4 aligned panels, each comprising a set. From left to right: anti-Sec61-N (40 kD), anti-Bip (75 kD), anti-Pdi (65 kD), and anti-Hrd3 (95 kD). B) Protein detection done using either Sec61 N-terminal or Sec63 antibody.

In Figure 2.10 A, I analyzed the SMPH crosslink pattern in a *sec61S353C* background, blotting against Kar2 (75 kD), Pdi1 (60 kD) and Hrd3 (95 kD), all luminal proteins whose molecular weight would roughly fit with the size shifts observed in the SMPH crosslinked samples when Sec61 was detected. None of the immunoblots

with the tested antibodies resulted in the detection of a SMPH-dependent shifted band that showed the same migration as any of the shifted bands observed when Sec61S353C was detected.

Since a crosslink to Sec71 had already been established (Section 2.2), the probability of a crosslink to another element of the Sec63 complex also being detected seemed high. With this in mind, and encouraged by the fact that the observed shift (around 65 kD) would fit with a crosslink to Sec63, I used a Sec63 specific antibody for protein detection. A direct interaction with Sec63 seemed potentially interesting since this protein possesses a luminal domain that is involved in ERAD [349]. In Figure 2.10 B, two sets of crosslinked *sec61S353C* microsomes can be seen: one was immunoblotted against Sec61 and the other against Sec63. Comparing lanes 2 and 3 to lane 5, one can see that in both panels, a SMPH specific shifted band can be detected at around 120 kD. This suggested that a crosslink to Sec63 was identified, clarifying, at least partially, the composition of the corresponding shifted band. As this interaction was only present in the *sec61S353C* mutant and was carbonate-sensitive (Figure 2.9) it might represent a direct contact of Sec61 loop 7 with the luminal J-domain of Sec63.

An immunoprecipitation approach (as in Section 2.2) was also attempted, but as before, the quality of the Western Blots obtained from the immunoprecipitated samples did not allow proper data analysis due to the overlap of the IgG bands with the relevant bands (Supplemental Figure A.6).

To further probe whether there was any interaction with Hrd3, SMPH crosslink was attempted in microsomes from a *sec61S353C/Δhrd3* strain (Figure 2.11 A). The reasoning was that if any of the detected shifted bands had Hrd3 in their composition they would either disappear or shift size again if Hrd3 was absent. To this end,

the *sec61S353C/Δhrd3* strain was generated by deletion of the *HRD3* gene in the *sec61S353C* background by transformation of this strain with the *HRD3* deletion cassette amplified from a *Δhrd3* strain obtained from the Euroscarf strain collection. Primers 51 and 52 were used for the amplification and the resulting DNA fragment was directly transformed into yeast. This fragment was characterized by the *HRD3* flanking areas fused to the Kan (*KanMX4*) resistance cassette. Transformants were selected in YPD+G418 plates, potential positive clones screened by PCR using the above mentioned primers, followed by PCR-product sequencing. As can be seen in Figure 2.11 A, the bands detected when Hrd3 is present (lanes 3 and 4) are also detected when Hrd3 is absent (lanes 7 and 8).

Since the most popular hypothesis at the time of these experiments was that Hrd1/Hrd3 E3 ubiquitin ligase forms the ERAD channel for transport to the cytosol, I chose to investigate the effect of deletion of *HRD1* and *HRD3* on degradation of the non-ubiquitinated ERAD substrate pro- α -factor ($\Delta\text{gp}\alpha\text{F}$) [142, 326, 240]. The $\Delta\text{gp}\alpha\text{F}$ is a mutant form of the $\text{p}\alpha\text{F}$ peptide, that in turn is the precursor for of the α mating pheromone (αF) [367, 54]. In wild-type cells, the αF is translated as a precursor form called pre-pro- α -factor ($\text{pp}\alpha\text{F}$; ~ 18 kDa) and is rapidly post-translationally imported into the ER [326]. Upon import into the ER this peptide has its signal sequence cleaved, resulting in a ~ 16 kDa peptide denominated pro- α -factor ($\text{p}\alpha\text{F}$) [434]. This form is promptly glycosylated resulting in $3\text{gp}\alpha\text{F}$ (~ 26 kDa), which is transported to the Golgi where it is further processed [210, 182]. Like $\text{pp}\alpha\text{F}$, $\text{p}\Delta\text{gp}\alpha\text{F}$ (~ 18 kDa), which has 3 point mutations that prevent N-glycosylation, is post-translationally imported into the ER and has its signal sequence equally cleaved, maturing to $\Delta\text{gp}\alpha\text{F}$ (~ 16 kDa) [54]. Since this form lacks the glycosylation sites, it is not glycosylated, which results in retention in the ER and it becomes an ERAD substrate [54, 240]. Although $\Delta\text{gp}\alpha\text{F}$ retrotranslo-

cation onto the cytosol has been shown to be via the Sec61 channel [289], I thought it might be interesting to verify whether Hrd1 and/or Hrd3 had any role in this process.

Wild-type (*HRD1/HRD3*) cells, as well as $\Delta hrd1$ and $\Delta hrd3$ cells were labeled with [³⁵S]-met/cys and the ERAD dynamics of $\Delta gp\alpha F$ were evaluated by taking samples at different time points and immunoprecipitating $\Delta gp\alpha F$ (Figure 2.11 B)

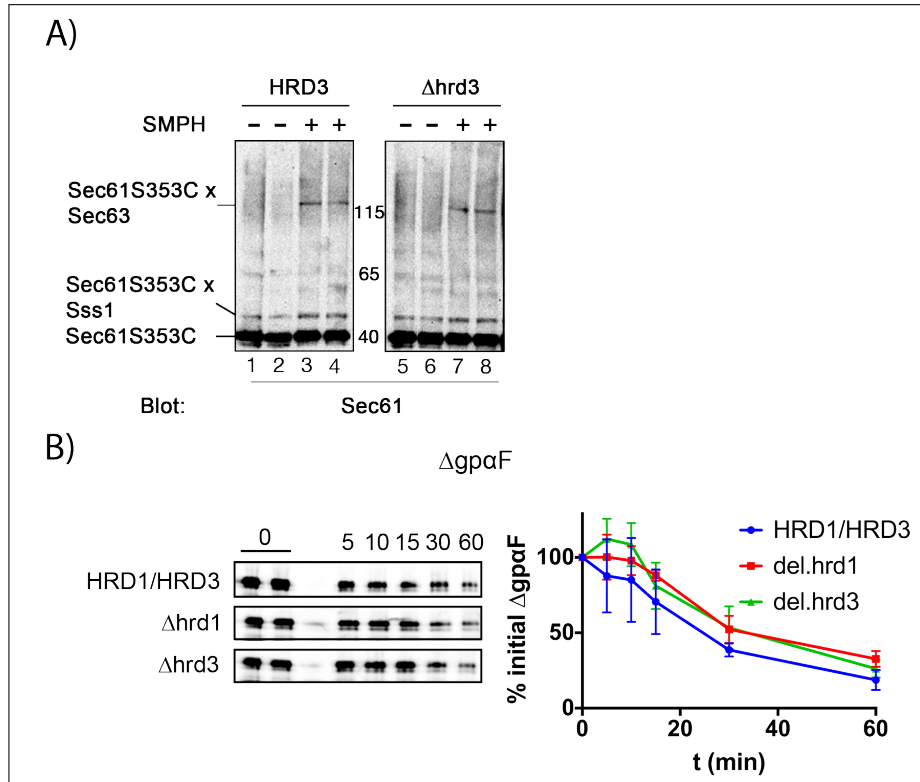


Figure 2.11: Analysis of $\Delta hrd3$ SMPH crosslink and $\Delta hrd1$ and $\Delta hrd3$ $\Delta gp\alpha F$ ERAD. A) Microsomes from *sec61S353C* and *sec61S353C/ $\Delta hrd3$* (17 eq) were crosslinked with 1 mM SMPH for 30 min on ice, quenched for 15 min, and analyzed by SDS-PAGE on 4-12 % Bis-Tris gels (NuPAGE® Novex® Pre-Cast gels, Invitrogen). Protein detection was done by Western Blotting using Sec61 N-terminal antibody and signal acquired on ECL film. B) Analysis of $\Delta gp\alpha F$ ERAD in $\Delta hrd1$ and $\Delta hrd3$ backgrounds. Early log-phase cells were pulse labeled (1.5 OD per sample) with [³⁵S]-met/cys, lysed, and mutant α -factor precursor ($\Delta gp\alpha F$ - post-translational imported, unglycosylated, ERAD substrate) immunoprecipitated. Starving and labeling were done at 30°C. Labeling was done for 5 min. Proteins were detected by phosphorimaging.

As can be seen in Figure 2.11 B, no significant $\Delta gp\alpha F$ ERAD defect could be observed in either the $\Delta hrd1$ nor the $\Delta hrd3$ mutants, but both mutants displayed a slight

delay in degradation of $\Delta gp\alpha F$. This delay may or may not be indirect due to the accumulation of ubiquitin-dependent ERAD substrates in the mutants, but it definitely excludes the Hrd1/Hrd3 complex as ERAD channel for $\Delta gp\alpha F$.

With this SMPH analysis, I could determine that SMPH was the better candidate for Sec61 luminal interactors crosslink, as I was able to detect a SMPH specific Sec61S353C-crosslink pattern that was mostly disturbed when luminal proteins were extracted prior to crosslink. I was able to identify an extremely consistent Sec61xSec63 crosslink, which is also carbonate sensitive. This, although not surprising, gives us not only a strong control for efficient S353C-dependent, luminal crosslink, but also tells us that the caught interaction between Sec61 and Sec63 might be through Sec63 J-domain, whose role in ERAD was previously described [349].

2.4 Sec61-crosslinked-complex Purification and Analysis

Since my immunoblotting analysis had limited success in identifying Sec61 partners, alternative approaches had to be considered. Until this point, only crosslinks to other elements of the Sec complex had been identified. Although these vouched for the efficiency of my crosslink setup, it did not result in any information about new luminal interactors of Sec61. Except for an interaction with the Sec63 J-domain, that might represent a link with ERAD, the most probable explanation for the detected interactions within the Sec complex is the fact that they are pretty stable, of very close proximity and of ubiquitous frequency, unlike luminal interactions, which by character, should be more transient and less stable. With this in mind, a viable approach seemed to be the enrichment of Sec61 and its crosslinked forms, to boost the amount of low frequency crosslinked forms representing more transient interactions. If in addition to this, a more sensitive form of protein detection (in alternative to immunoblotting)

was implemented, the detection of these less frequent, and consequently, less represented crosslinked forms might be possible.

To this end, and as a means of enriching the Sec61-crosslinked forms in my sample, I first tagged Sec61 with an 14-His N-terminal tag that could be used to enrich both the free and the crosslinked forms of Sec61 in my sample by affinity chromatography.

2.4.1 Sec61 N-Terminal 14His-tagging

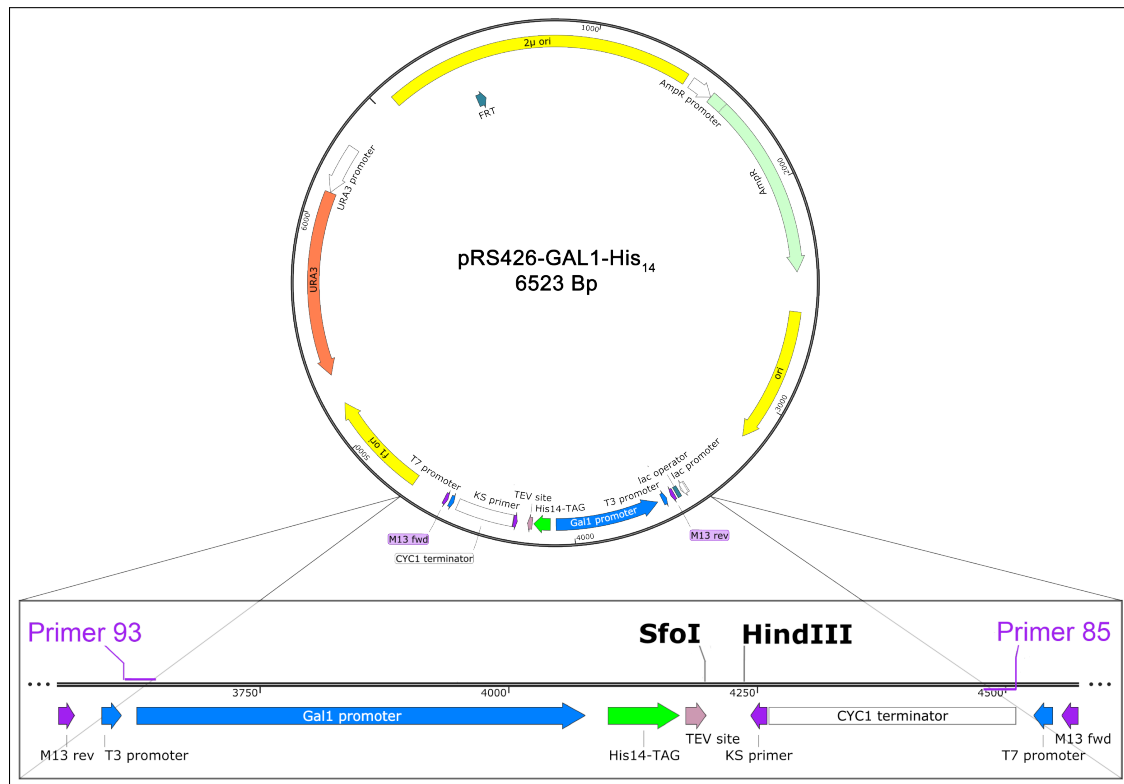


Figure 2.12: His₁₄-tagging Vector. Map of the pRS426-GAL-His₁₄-TEV vector used for N-terminal His₁₄-tagging of Sec61 and sec61S353C. The lower panel represent a zoom of the vector's area of interest (GAL1, TEV restriction site, 14His tag and MCS available). Also to be noted that priming locations for Primer 85 and 95 are labeled in the figure.

The first step in this endeavor was to N-terminally tag Sec61 and Sec61S353C with a 14His-tag. A 6His-tag would be inadequate, since yeast proteome is rich in histidines [89, 446], and a short 6His-tag might have resulted in too much of a background in the purification setup, as the binding and elution conditions could not be so stringent. An N-terminal tagging instead of a C-terminal one was chosen because previous data showed that N-terminal tagging did not impair Sec61 function at the optimal growth temperature [288].

For the 14His N-terminal tagging of Sec61, I used the pRS426-GAL1-14His (*URA*) generously supplied by Alexander Stein [380] (Figure 2.12). As can be seen in the schemes presented in Figure 2.12, this vector has an ORF that includes a 14His tag, followed by a TEV restriction site, with a convenient SfoI restriction site after it, to allow easy in frame cloning of any target gene. Since SfoI is a restriction enzyme that generates blunt ends, and its restriction site is already in frame with the 14His-tag and the *GAL1* promoter encoded in the vector, by cloning into this position I was able to generate an ORF that was under the control of the *GAL1* promoter and that included all the mentioned features. Using a primer complementary to the START codon region of *SEC61* (Primer 63) and another that primed downstream of the STOP codon (and also included a HindIII restriction site - Primer 64) I was able to generate a fragment that had a SfoI compatible end (blunt) and a overhang that permitted a directed cloning. This fragment was then cloned into the SfoI/HindIII digested pRS426-GAL1-14His. Correct cloning was confirmed by sequencing. A scheme of the final construct can be seen in Figure 2.13.

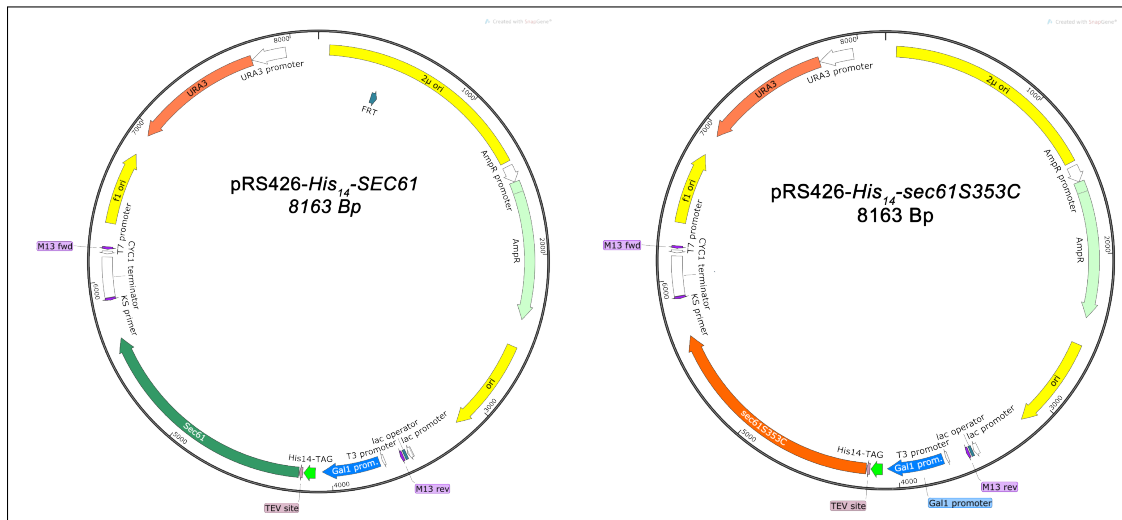


Figure 2.13: Constructs obtained by cloning into pRS426-GAL-His₁₄.. Maps of the construct generated by cloning *SEC61* and *sec61S353C* into pRS426-GAL-14His-TEV. pRS426-His₁₄-*SEC61* on the left and pRS426-His₁₄-*sec61S353C* on the right.

Since *SEC61* is an essential gene, no null mutant strains are available. In order to study the effect of *SEC61* mutations one has to either directly integrate the mutant gene in place of the wild-type gene into the genome, or have a strain in which the genomic copy of the gene is deleted and where a vector containing a functional copy of *SEC61* is present to compensate for the genomic deletion. In the first instance the gene of interest (in a truncated form) has to be cloned into an integrative plasmid. In the second case, the plasmid can be centromeric or 2 μ , only constraint being that it possesses a different auxotrophic marker from the plasmids already in the strain. Unfortunately, pRS426-GAL-14His is neither an integrative plasmid nor has a marker compatible with transformation into the needed strain background. I therefore had to subclone the His-tagged *SEC61* into pRS315. For this purpose, two new primers were designed. One that primed at the beginning of the *GAL1* coding region (Primer 93), and a second one priming at the *CYC1* coding region end (Primer 85) as can be seen in Figure 2.12. Primer 93 contained also a *SacI* restriction site. This primer pair

After successful subcloning of both *GAL1-14His-SEC61-CYC* and *GAL1-14His-sec61S353C-CYC* into pRS315, this constructs were transformed into KRY461. This strain has the genomic *SEC61* deleted and a functional copy being expressed from pGAL-*SEC61* (*URA3*, *CEN*). Selection of transformants with the 14His plasmids was done on minimal solid medium (-LEU / -URA / 2 % Gal / 0,2 % Glu). The transformants were then replated in -LEU / 5'-FOA / 2 % Gal / 0,2 % Glu. Yeast with an active *URA3* gene (*Ura*⁺) convert 5-Fluoroorotic Acid (5-fluorouracil-6-carboxylic acid monohydrate; 5-FOA) to fluorodeoxyuridine, which is toxic to cells [33]. So, if the cell is actively producing *Ura3* (like the KRY461), it dies, unless it loses the plasmid with the *URA3* gene allowing a chase out of the pGAL-*SEC61*. Since the *SEC61* gene is essential, and its only functional copy is also in the inserted plasmid, the cell will only survive if, in addition to losing the pGAL-*SEC61*, it keeps the second plasmid (pRS315-*GAL1-14His-SEC61* or pRS315-*GAL1-14His-sec61S353C*), resulting in an effective plasmid-shuffle [33].

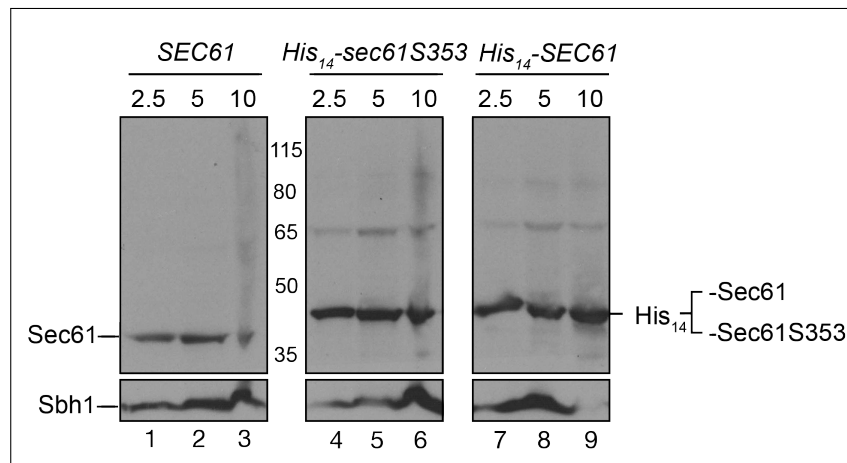


Figure 2.15: His₁₄-tagged constructs expression confirmation. Different volumes of microsomes (at Abs₂₈₀=30) from 3 different strains (*SEC61*, *14His-SEC61*, and *14His-sec61S353C*) were resolved, side by side, by SDS-PAGE and blotted against Sec61. From left to right, 2.5, 5 and 10 µl of microsomes from: *SEC61*, *14His-sec61S353C* and *14His-SEC61*.

After strain construction, expression of the 14His-tagged forms of Sec61 were confirmed by immunoblotting. Different amounts of microsomes prepared from each one of the strains were resolved side by side and compared (Figure 2.15). It is clear that steady state levels of each one of the Sec61 forms is roughly equal. It could be said that they seem even somewhat higher than the one observed in the wild-type strain.

By adding a 14His-tag to Sec61 and Sec61S353C N-termini, I had now the raw material necessary to establish an enrichment of Sec61-crosslinked proteins. Before efforts were channeled to establish such enrichment system, I needed to make sure the 14His-tagging of Sec61 (and Sec61S353C) had no deleterious effects on protein transport across the ER membrane.

2.4.2 Characterization of the 14His-tagged Sec61 forms

Once the strains expressing the *14His-SEC61* (KRY1081) and *14His-sec61S353C* (KRY1061) forms were obtained I had to characterize them, and make sure they did not display any phenotype that would make them inadequate for use in further studies.

To this end I did a standard strain characterization, screening for general growth defects, temperature and tunicamycin sensitivity, as well as any UPR induction.

To screen for generalized growth defects I determined the specific doubling time of each strain. To this end, strains *GAL-SEC61*, *GAL-14His-SEC61*, and *GAL-14His-sec61S353C61* were grown overnight in YPGal (2% Gal / 0.2% Glu), diluted to an OD₆₀₀ of 0.02 in the same medium, applied onto a Biolector Flower plate (1 ml per well, 5 wells per strain), and grown for 24h in the microbioreactor BioLector, monitoring the biomass (measured at 620 nm) every 15 min (growth at 30°C, with shaking at 1200 rpm, 85% humidity, and 20.95% O₂). The specific growth curves of each strain

can be seen in Figure 2.16. None of the mutants grew slower than the wild-type, indicating that the 14His-tagging did not have an impact on general cell growth. By rough estimation through graph analysis I could determine that in the conditions used the tested strains have, respectively, a doubling time of 9h for *SEC61* and *14His-SEC61*, and 7.5h for *14His-sec61S353C*. These values, however, are quite different from the usual yeast doubling times of approximately 2h in YPGal. This might indicate that this setup might be suboptimal for yeast. It should be said that the *14His-sec61S353C* mutant, although showing normal growth in YPGal, shows a slower, bi-phasic growth curve when grown in minimal medium (Supplemental Figure A.10)

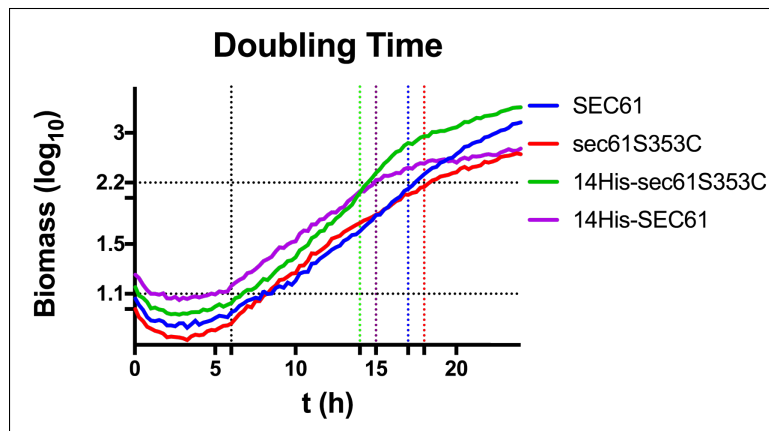


Figure 2.16: Growth rate of 14His-tagged mutants. Cells were grown overnight in liquid YPGal (Gal 2%, 0.2% Glu), diluted in the same type of medium to an OD_{600} of 0.02 and 1 ml of culture applied per well (5 x 1 ml per strain) in a FlowerPlate. The plate was then incubated in the microreactor Biolector at 30°C, with 1200 rpm, 85% humidity and 20.95% O_2 , for 24h. Calibration was done at 320 nm, and biomass determination at 620 nm using Filter 15. Readings were done every 15 min. In the figure the plotted results (after averaging) are shown. *SEC61* in blue, *sec61S353C* in red, *14His-SEC61* in green, and *14His-sec61S353C* in purple. Shown biomass values are in the log scale. Horizontal dotted line serving as guiding for doubling time determination. Vertical dotted lines represent the time points where a biomass of 2.4 units was reached. The coloring of the dotted line corresponds to the data set being intersected by it at 2.4 units of biomass. The black vertical dotted line represents the time point when the least lagged strain reaches the biomass of 1.2 units.

The next step was to determine whether these mutants showed any temperature or tunicamycin sensitivity. Sensitivity to either higher (37°C) or lower (20°C) temperature when compared to the standard growth temperature (30°C) is a common indicator

used to characterize yeast strains with ER translocation defects as transport into the ER is essential [325]. Tunicamycin (Tm) sensitivity is also a useful indicator, informing about the capacity of the mutants to clear misfolded proteins. Tunicamycin interferes with N-linked glycosylation in the ER which often is a prerequisite for protein folding. Hence tunicamycin-sensitivity is often indicative of perturbations in ER homeostasis [395, 349]. For this purpose, sequential dilutions of each strain were prepared (including isogenic controls) and grown on solid media (YPGal 2% Gal, 0.2% Glu). For temperature sensitivity determination, each set was plated in triplicate, in which each replica was grown either at 20, 30 or 37°C for at least 3 days. For tunicamycin sensitivity determination, each set was also plated in triplicate either in the absence or presence of tunicamycin (0.25 or 0.5 µg/ml). All three replicas were then incubated at 30°C for at least 3 days (Figure 2.17).

In Figure 2.17 A the results of the temperature sensitivity are shown. The *sec61-3* mutant shows a growth defect at 20°C and 37°C, and *sec61-32* sensitivity at 20°C, as expected [289, 382]. The *sec61S353C* mutant was also included to screen for any sensitivity characteristic of the point mutation, opposed to any sensitivity caused by the tagging. This untagged mutant, in the conditions used, shows a sensitivity at 37°C but a normal growth at 20°C, as reported [186]. None of our 14His-tagged mutants, however, showed a significant temperature sensitivity, either at 20 or 37°C.

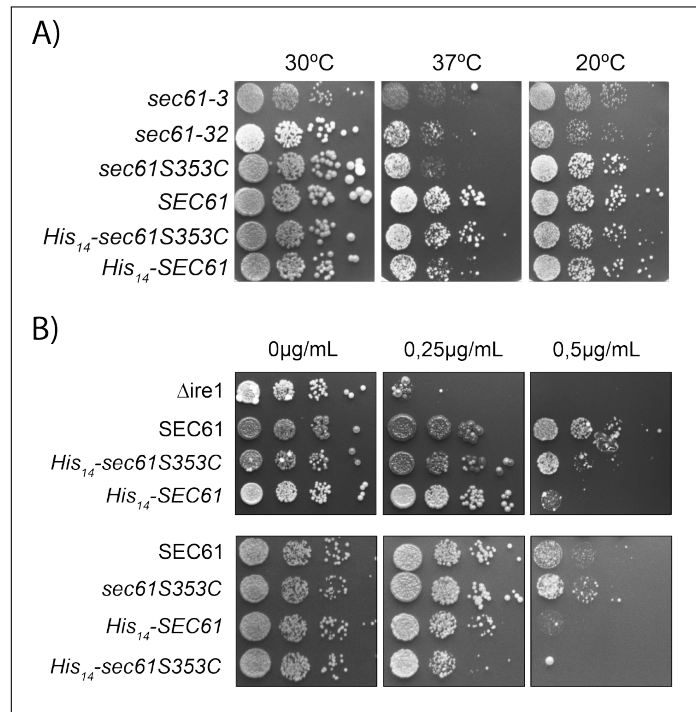


Figure 2.17: Temperature and tunicamycin sensitivity of 14His-tagged strains. Cells were grown overnight in YPD, counted using a Neubauer chamber and sequentially diluted (10^4). Samples of each dilution (5 μ l) were then plated side by side, in solid YPD (2% Gal / 0.2% Glu) and grown for at least 3 days. Each set was replicated 3 times in different plates. **A)** Plates for temperature sensitivity were incubated at 20, 30 or 37 °C (one replica per temperature). **B)** For tunicamycin sensitivity, all plates were grown at 30 °C, but two of the plates were supplemented with 0.25 and 0.5 μ g/ml of Tunicamycin, respectively.

As for the tunicamycin sensitivity (Figure 2.17 B), one can see that for the positive control I used a $\Delta ire1$ mutant, for which strong tunicamycin sensitivity has been widely reported [265, 58, 397]. *IRE1*, encoding Ire1, is the signal transducer for the UPR [409]. Upon accumulation of misfolded proteins in the ER, it is vital as a central component of the UPR [66]. As expected, the growth of this mutant in the presence of 0.25 μ g/ml of tunicamycin was almost null, and completely abolished in the presence of 0.5 μ g/ml of tunicamycin (Figure 2.17 B; top). The *sec61S353C* mutant was also included in the assay for the same reason as described above. In its case, a significant growth compromise is seen only in the presence of 0.5 μ g/ml of tunicamycin, as

is the case of the wild-type strain, that seems to have its viability at least as affected as the *sec61S353C* mutant (Figure 2.17 B; bottom). Our 14His-tagged Sec61 and Sec61S353C, however, show a very slight growth impairment in the presence of 0.25 µg/ml of tunicamycin, but a serious growth impairment in the presence of 0.5 µg/ml of tunicamycin. Since the effect of the same concentrations on the wild-type strain is also strong, it seems fair to assume that no significantly increased tunicamycin-sensitivity is associated with the His₁₄- tag in the conditions tested.

To rule out any UPR induction caused by the tagging of Sec61, an *HAC1* splicing assay was done. In yeast, misfolded-protein accumulation in the ER activates the UPR. This can be experimentally induced by treatment with inhibitors of ER protein folding, like tunicamycin [24]. The UPR triggers an adaptive response to restore ER homeostasis through the action of a transcription-factor, *HAC1* [396, 343]. This transcription factor is only active after alternative mRNA splicing [24, 364, 191]. By quantifying the amount of spliced versus the unspliced forms of the *HAC1* mRNA I could determine, at the RNA level, whether the UPR was or not induced.

To this end, wild-type and mutant strains were grown in minimal medium to a maximum OD₆₀₀ of 1 at 30°C, 220 rpm and incubated for 3h in either the presence or absence of 200 µg/ml of tunicamycin (30°C, 220 rpm), point at which total RNA was isolated, and retrotranscribed into cDNA that was used afterwards for a quantitative PCR reaction using *HAC1* specific primer as well as *ACT1* specific primers. The amplified *ACT1* worked as internal control while the amplified *HAC1* informed about the UPR induction state of the cells.

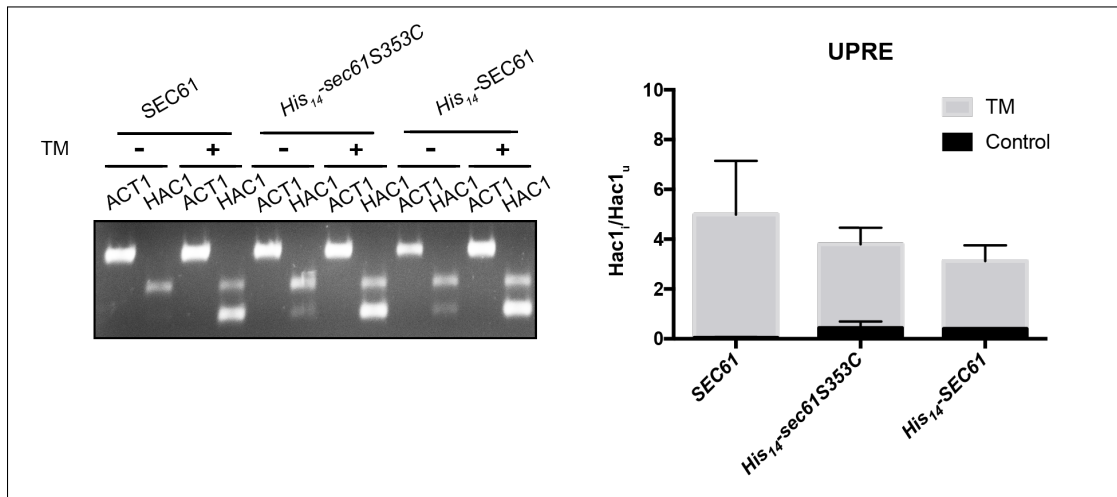


Figure 2.18: UPR activation in the 14His-tagged mutants. To this end, wild-type and mutant strains were grown in minimal medium to a maximum OD₆₀₀ of 1 at 30°C, 220rpm and incubated for 3 h in either the presence (+) or absence (-) of 200 µg/ml of tunicamycin (30°C, 220rpm). Total RNA (0.1 µg) retrotranscribed to cDNA by RT-PCR using MaximaRT and a Oligo(dT18)-dT primer. The resulting cDNA (1 µg) was subjected to quantitative PCR with a set of primers targeting *HAC1* to monitor the UPR. PCR fragments derived from *HAC1_u* mRNA (*HAC1_u* = uninduced; ~ 720 bp) and *HAC1_i* mRNA (*HAC1_i* = induced; ~ 470 bp) are indicated. Primer for *ACT1* were also used with same cDNA to serve as a loading control. Samples were resolved on a 1% agarose gel.

As can be seen in Figure 2.18, for each strain, two sets of reactions are shown: one was grown in the absence of tunicamycin (-), the other set was grown in the presence of tunicamycin (+). It can be observed that in both tagged-mutants, even in the absence of tunicamycin, some spliced form of the *HAC* mRNA can be detected, unlike what happens in the wild-type strain (black bars). This induction, however, is very slight. Although this was not the optimal scenario, this level of induction did not seem significant enough to compromise results obtained in the generated backgrounds, since such induction did not seem to cause any growth defect (Figure 2.16) or significant tunicamycin sensitivity (Figure 2.17 B), pointing to an almost normal ER protein homeostasis.

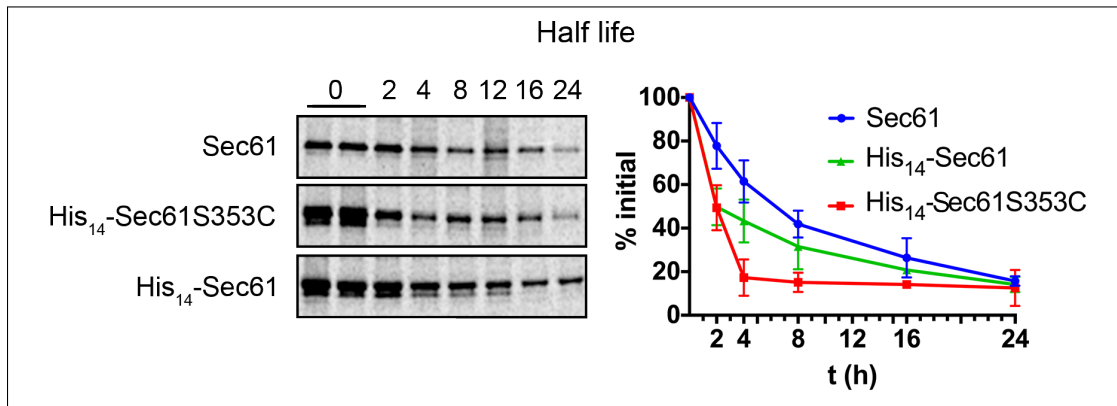


Figure 2.19: 14His-tagged Sec61 forms half life determination. wild-type, *14His-SEC61* and *14His-sec61S353C* cells were grown to a maximum OD₆₀₀ of 1, washed in Labeling Medium, and concentrated to 6 OD₆₀₀/ml in the same medium. Samples were then starved for 30 min and labeled with 6.5 MBq of [³⁵S]-cys/met for 30 min at 30 °C, 220 rpm. After labeling, the zero time point was taken (1.5 OD) and cells immediately killed with sodium-azide, pellet collected and flash frozen in liquid nitrogen. To the remaining culture Chase Mix was added, and the culture was kept growing at 30 °C, 220 rpm. At the designated time points, samples were collected (1.5 ODs) and treated as the zero time point. After all time points had been collected, samples were thawed on ice, lysed by bead-beating (BeadBeatter 16), pre-cleared for 30 min with Protein A Sepharose, and incubated overnight with Protein A Sepharose and 10 µl of a Sec61 N-terminal specific antibody. Samples were then resolved by SDS-PAGE on 4-12 % Bis-Tris gels (NuPAGE® Novex® Pre-Cast gels, Invitrogen). Gels were dried, the signal detected in phosphorplates and acquired in the Typhoon Phosphorimager. Bands were also quantified using ImageQuant software and the relative band intensities (against the zero time point intensity) were plotted. On the left panels the acquired signals for each strain and each time point are shown. On the right, the plotted averaged intensities of each time point when compared with the zero. Sec61: Blue; His₁₄-Sec61: Green; His₁₄-secS353C61: Red.

Even though no significant growth impairment had been detected in the constructed mutants, I decided to verify whether the His₁₄-tag affected the half-life of Sec61.

To this end, I did 24h pulse chases with cells from wild-type, *14His-SEC61* and *14His-sec61S353C* backgrounds. Each culture was pulse-labeled with [³⁵S]-cys/met for 30 min, the indicated time points samples were taken (1.5 OD), lysed, and Sec61 immunoprecipitated. After SDS-PAGE, the signal was acquired by phosphoimaging (Typhoon Phosphoimager) and band intensities were quantified (ImageQuant). The relative band intensities (against the zero time point intensity) were then plotted (Figure 2.19).

As can be seen in Figure 2.19, Sec61 shows an half life of approximately 7h (up-

per slice; blue line). From the analysis of both the band intensities as from the band quantitations, one can see that Sec61 suffers a steady degradation at a constant pace, with $\sim 20\%$ of the initial amount present after 24h. The His₁₄-tagged forms, are degraded faster with $t_{1/2}$ of ~ 2 h (His₁₄-Sec61 - bottom slice, green line; His₁₄-Sec61S353C - bottom slice, green line). It should be noted, however, that in both cases after this initial plummet, the degradation slows down, becoming at least as slow as that of the wild-type protein. Although the absolute amounts of the tagged forms at the zero time points seem much higher than that of the wild-type form, the amounts after this initial decline are very similar to that of Sec61, and keep being so to the end of the experiment.

After studying the growth behavior and temperature sensitivity of the generated strains, it was obvious that no significant growth defect was caused by N-terminally tagging Sec61. It was also obvious that neither the ER protein homeostasis was compromised nor the UPR significantly activated. Although the tagged Sec61-forms showed a shorter half life than the wild-type, I have shown that the steady state levels of the 14His-tagged Sec61 forms were similar to the wild-type strain (Section 2.4.1, Figure 2.15). Faced with this set of results, the 14His tagged constructs were deemed appropriate for further characterization of Sec61 interactions.

2.4.3 Crosslink to His₁₄-tagged Sec61 and Sec61S353C

After successfully tagging Sec61 and Sec61S353C and verifying that such tagging does not cause significant defects in the mutants in question, I could proceed to the purification setup. But, before going down that road, it was paramount to verify if this tagged forms generated the same crosslink patterns as their untagged counterparts. Also, since the idea was to analyze the purified complexes by mass spectrometry,

and after discussing the subject with a mass spectrometry expert, it was deemed that having a setup where the crosslinked complexes were separated (cleaved) before analysis might increase protease access to both the interactor and Sec61, and consequently, help in their detection. Since the sulfhydryl-reactive crosslinker I had been using was uncleavable, an alternative had to be found.

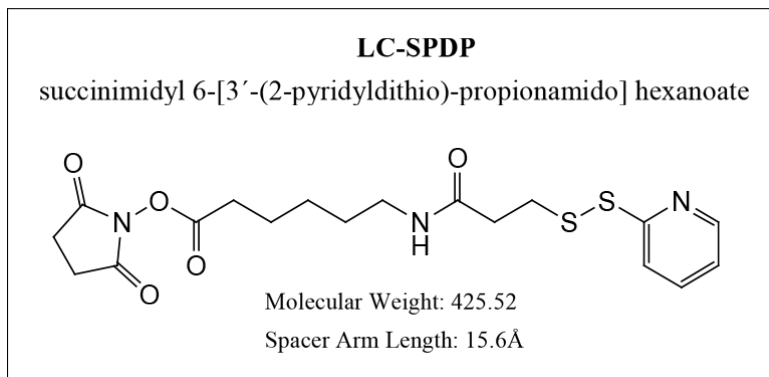


Figure 2.20: LC-SPDP structure. Scheme representing SPDP structure. Molecular formula, molecular weight, and spacer arm length also shown in figure

In order to build a setup equivalent to the SMPH crosslink that allowed the cleavage of the crosslinked complexes before mass spectrometry, a suitable cleavable alternative for SMPH needed to be chosen. After thorough crosslinker review, I chose the crosslinker succinimidyl 6-[3'-(2-pyridyldithio)-propionamido] hexanoate (LC-SPDP)(Figure 2.20). As SMPH, LC-SPDP is water-insoluble, membrane permeable and possesses both an amine- and a sulfhydryl-reactive group. Although the amine reactive group in LC-SPDP is the same as in SMPH (NHS-ester), the sulfhydryl reactive group is different: in SMPH this group is a maleimide, while in LC-SPDP it's a 2-pyridyldithiol group. Despite their different chemical identity, the reactivity of both groups is equivalent [287]. Since LC-SPDP was the only crosslinker with the desired reactivities, cleavability, and spacer-arm length, it looked like the most appropriate choice.

Having settled on the cleavable alternative for SMPH, a comparison of the crosslink pattern between SMPH and LC-SPDP was necessary, as well as the confirmation that the crosslinked complexes could indeed be cleaved.

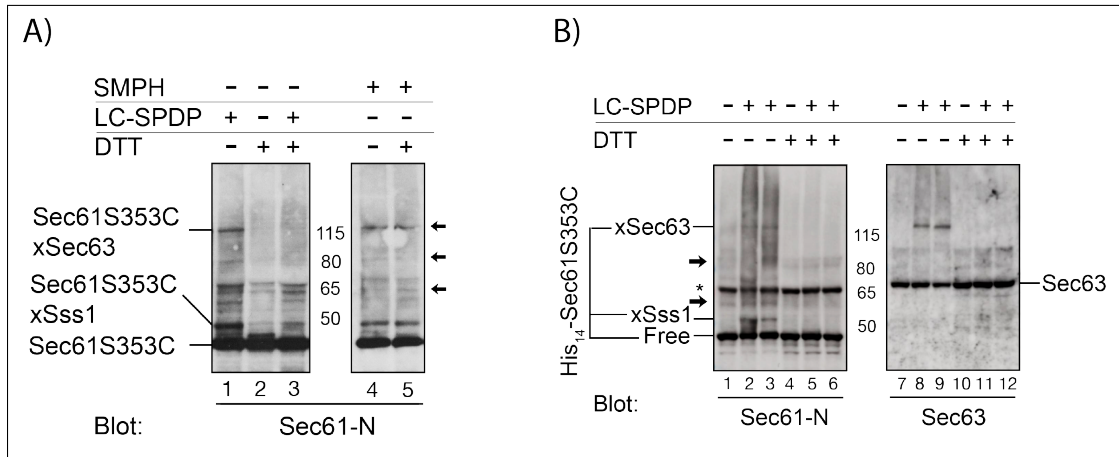


Figure 2.21: LC-SPDP crosslink pattern determination. Comparison of the crosslink pattern of both SMPH and LC-SPDP in a *sec61S353C* background. Microsomes from *sec61S353C* were crosslinked with 1 mM of either SMPH or LC-SPDP for 30 min on ice, quenched for 15 min and solubilized in 2xLaemmli Buffer either with or without 200 mM DTT. Samples were resolved by SDS-PAGE on 4-12% Bis-Tris gels (NuPAGE® Novex® Pre-Cast gels, Invitrogen) and submitted to Western Blotting. Signal acquired in an Amersham Imager 680 blot and gel imager. Arrows represent crosslinked-complexes. Unspecific bands are labeled with an asterisk (*). **A)** Proteins detected using a Sec61 N-terminal antibody. **B)** Determination of the LC-SPDP crosslink pattern on a 14His-*sec61S353C* background. Proteins detected using either a Sec61 N-terminal (left panel) or Sec63 (right panel) antibody.

For this purpose, *sec61S353C* microsomes were crosslinked either with SMPH or LC-SPDP (1 mM, for 30 min on ice, with 15 min of quenching) in the presence or absence of DTT. Samples were then analyzed by immunoblotting using an anti-Sec61 antibody for protein detection.

As can be seen in Figure 2.21 A, in the *sec61S353C* background, I could detect the same crosslinked forms (arrows) in samples treated with either SMPH or LC-SPDP (lane 1 versus lane 4), including the Sec61S353CxSss1 and Sec61S353CxSec63 crosslinked forms (at around 50 and 120 kD, respectively). It can also be seen that upon sample reduction, the crosslinked bands disappear (lane 3 versus lane 5). In

this way it could be confirmed that LC-SPDP was an adequate cleavable counterpart of SMPH for the purpose of this project.

Further confirmation that the crosslink behaviour observed in the *sec61S353C* background was mirrored in the *14His-sec61S353C* background was needed to ensure that this tagged form was a suitable tool for interaction identification in the established setup. To confirm such adequacy, *14His-sec61S353C* microsomes were crosslinked with LC-SPDP (1 mM, for 30 min on ice, with 15 min of quenching), sample solubilized either in the presence or the absence of DTT, and analyzed by immunoblotting. Protein detection was done with either the Sec61 antibody or with the Sec63 antibody. The Sec63 detection was meant not only to further confirm the crosslink pattern of LC-SPDP, but also to evaluate the suitability of using Sec63 and Sec61S353CxSec63 as markers for crosslink and purification efficacy.

In Figure 2.21 B, it can be seen that not only the same Sec61 crosslink pattern as the one obtained in the *sec61S353C* background can be detected in the *14His-sec61S353C* background upon LC-SPDP treatment (left panel, lane 2 and 3) but also that, as established before, the crosslinks are DTT-sensitive (left panel, lane 5 and 6). Also, when using an anti-Sec63 antibody for detection, it can be observed that the crosslinked band at around 130 kD not only has Sec63 in its composition (right panel, lane 2 and 3) but is also DTT sensitive (right panel, lane 5 and 6), as the 120 kD counterpart in the *sec61S353C* background (Figure 2.7).

Being assured that the 14His-tagged strains behaved similarly to the untagged ones regarding the interactions detected by crosslink, the establishment of the purification setup could be undertaken.

2.4.4 14His-tagged Crosslink Purification Setup

Having successfully tagged the different forms of Sec61, a choice of purification method had to be made. Since the tag to be used was a polyhistine one, the choice of Immobilized Metal Affinity Chromatography (IMAC) as the purification system was a given. In this type of chromatography, a matrix charged with a transition metal (usually Ni^{2+}) can selectively bind with good selectivity strongly positively charged peptides, as the polyhistidine tags. This binding can be reversed upon addition of a competing and in excess binding molecule, such as imidazole [31].

Before starting with the establishment of the purification setup, a solubilization strategy that was compatible with downstream purification had to be settled upon. I had to maximize Sec61 solubilization, while keeping it from aggregating and maintaining working conditions that did not compromise subsequent matrix-binding of the tag. Since I knew from previous experience that Sec61 solubilization in IP Buffer (150 mM NaCl / 1 % (v/v) Triton X-100 / 15 mM Tris-HCl, pH 7.5 / 2 mM Sodium Azide / 0.1 % (w/v) SDS) was adequate, I tested solubilization in said buffer under different conditions: 4°C for 30 min, 42°C for 20 min or 65 °C for 10 min. As can be seen in Figure 2.22, the best condition for solubilization of Sec61 was the 4°C incubation (lane 2). To be noted that, even in the best condition tested, the solubilization yield it is not as high as the one obtained in Laemmli Buffer.

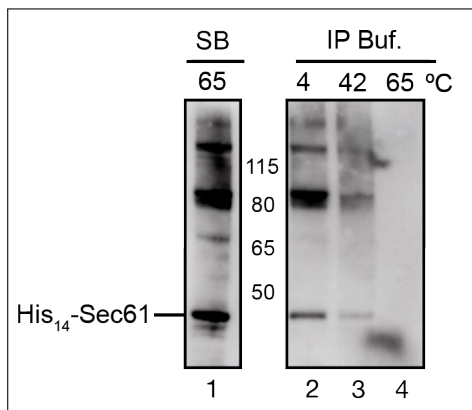


Figure 2.22: His₁₄-Sec61 solubilization test. Microsomes (17eq) from 14His-SEC61 were resuspended in 50 μ l of IP Buffer and incubated either at 4 °C for 30 min, 42 °C for 20 min or 65 °C for 10 min. Sample was centrifuged for 1 min at 16.000 x g, half the volume was mixed with 2xLaemmli Buffer, and samples were resolved by SDS-PAGE on 4-12 % Bis-Tris gels (NuPAGE® Novex® Pre-Cast gels, Invitrogen). Proteins were detected by Western Blot using a Sec61 N-terminal antibody. Control sample was resuspended in 50 μ l of 2xLaemmli Buffer (SB) and denatured for 10 min at 65 °C.

Solubilization in similar or derived buffer, however, would have proven difficult, since the characteristic that caused the increased solubility in Laemmli Buffer was most probably the high amount of SDS. Unfortunately, most IMAC appropriate matrices have low SDS compatibility [336]. SDS is also prone to precipitate at low temperatures, which were necessary in my purification setup to minimize protein degradation during purification process. Also, I deemed that higher concentration of SDS would contribute to a more thorough sample denaturation that might cause aggregation issues during purification. Therefore, I opted for the use of a milder, less precipitation prone detergent in the purification buffers (TritonX-100).

As shown in Supplemental Figure A.12 A and B, different buffers were tested. Starting with a basic buffer for Niqel based IMAC inspired by the buffer used in the work described in a publication where a similar construct was used (B1 - 50 mM Tris-HCl, pH 7.4 / 300 mM KCl / 40 mM Imidazole) [380], I tried different buffer compositions (Table 2.1). In Figure A.12 A, the effect of the addition of 0.5 % TritonX-100 (either by

itself or in combination with 4 M urea) to the buffer was evaluated. It became obvious that the purification buffer must have TritonX-100 in its composition, as only in samples where it was present was I able to detect any purified Sec61 (B2). The presence of urea (B3), however, prevented column retention, when compared to the yields obtained when TritonX-100 was used by itself. The same effect was seen when either the same amount of urea was used in combination with 1 % SDS (B5) or where it was increased to 8M (B6), while reducing, in both cases, the amount of KCl to 150 mM (Figure A.12 B, bottom two panels). However, addition of SDS seemed to improve column retention when compared with the same conditions in its absence (B4 and B5 versus B2 and B6, respectively). Nevertheless, I noticed that, besides resulting in lower yield than Buffer B2, these buffers were also very prone to precipitate and to cause column clogging .

Table 2.1: Tested purification Buffers. Composition of the buffers that were tested during IMAC purification setup.

Buffer Name	Composition					
	Tris-HCl, pH 7.4 (mM)	KCl (mM)	Imidazole (mM)	TritonX-100 (%)	Urea (mM)	SDS (%)
B1	50	300	40	-	-	-
B2	50	300	40	0.5	-	-
B3	50	300	40	0.5	4	-
B4	50	150	40	0.5	-	1
B5	50	150	40	0.5	4	1
B6	50	150	40	0.5	8	-

Based on the information above, I decided to settle on using Buffer B2 (50 mM Tris-HCl, pH 7.4 / 300 mM KCl / 40 mM Imidazole / 0.5 % TritonX-100) as the purification buffer for the remaining of the project.

Due to the intrinsic difficulties of purifying multi-spanning transmembrane proteins like Sec61 (10 TMs), several purification approaches were tested. Not only the buffer composition and native vs denaturing conditions were tested, but also batch vs column purification, manual vs automatic setup, and Ni²⁺ vs Co²⁺ charging of the matrix. All data from the optimization process can be seen in Figure A.13. Shortly, it was determined, that while batch purification worked (Supplemental Figure A.13 A), nickel functioned as a better charging element for the purification matrix than cobalt (lane 5 versus 6) since both generated the same level of background, but a better yield was obtained from the the nickel-charged one (Supplemental Figure A.13 A). Also, upon crosslink and upscaling, the efficiency of purification dropped drastically (Supplemental Figure A.13 B, upper panel) while the amount of background increased (lower panel). Variations of the batch system were made where the sample was either denatured or not prior to purification, and where a gradient of imidazole was used for elution. In all these cases I observed significant loss of His₁₄-Sec61 along the several steps (Supplemental Figure A.13 C, lane 1 to 26). As can be seen, conversely, the usage of an automated purification system in association to a pre-packed HisTrap FF crude column, resulted in a proper column retention of His₁₄-Sec61 (Supplemental Figure A.13 C). This was true for both native and denaturing condition (Supplemental Figure A.12 C). Although the yield of the purification in native conditions seemed to be higher, it also seemed to generate a much greater background, on top of causing elution at slightly lower concentrations of imidazole. Also, since the level of proteolysis in the sample until it could be properly stored for mass spectrometry analy-

sis was a serious concern, I deemed better to denature samples prior to purification, and doing all purification steps at 4°C. The imidazole gradient also seemed to work well for protein elution (Supplemental Figure A.13 C, lane 27 to 40) in this setup. This method also allowed me to follow the purification in real time either by following the absorbance (at 280 nm) or by following the conductance.

After this test phase, all purification conditions had been established. Purification programs were also optimized to allow a more convenient elution pattern and fractioning. A scheme of the final setup can be seen in Figure 2.23.

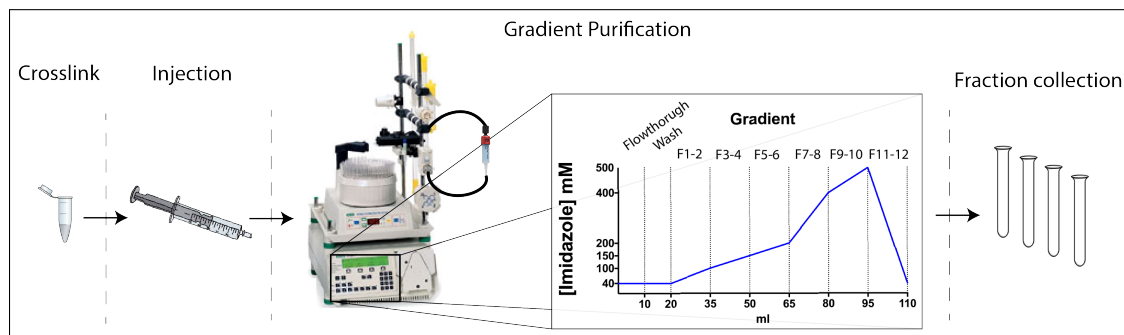


Figure 2.23: Purification system scheme. Microsomes (500 eq) were treated either DMSO (Control), SMPH or LC-SPDP (1 mM), solubilized in 1 ml of IP for 30 min on ice, followed by 10 min at 65°C. Samples were then diluted with 4 ml of cold Purification Buffer, and injected into a Histrap FF (1 ml) pre-packed columns associated to a BioLegend LP purification system. Columns were washed with Binding Buffer (10 ml ; 50 mM Tris-HCl, pH 7.4 / 300 mM KCl / 0.5 % TritonX-100 / 40 mM Imidazole) and with Purification Buffer / 100 mM Imidazole (10 ml). Elution was done along an imidazole gradient (150-500 mM) in 15 ml-long steps. Fractions of 7.5 ml were collected along the imidazole gradient, and DTT (100 mM) were added. Each sample was TCA precipitated, resuspended in 2xLaemmli buffer, and resolved by SDS-PAGE on 4-12 % Bis-Tris gels (NuPAGE® Novex® Pre-Cast gels, Invitrogen).

Briefly, samples were crosslinked (1 ml reactions, using 500 eq of microsomes), solubilized in IP Buffer on ice for 30 min, followed by a 10 min denaturing step at 65 °C. After pre-clearing, sample was diluted with 4 ml of cold Binding Buffer (50 mM Tris-HCl, pH 7.4 / 300 mM KCl / 0.5 % TritonX-100 / 40 mM Imidazole). Sample was then injected into the system. The purification was set on an automatic gradient program. A description of the purification program can be seen in Table 2.2 . Collected fractions were then incubated with DTT, TCA precipitated, resuspended in

50 μ l 2XLaemmli Buffer, and resolved by SDS-PAGE. Each fraction was loaded (10 μ l) in two different acrylamide gels. Detection was done by Western Blot, using the N-Terminal Sec61 antibody for one replica of each purification set, and the Sec63 antibody for the other replica. The remaining sample was resolved on a third gel, which was stained with Coomassie G-250 (Supplemental Figure A.11).

Table 2.2: Purification program Description of the steps programmed into the automatic purification system.

Phase	Amount Imidazole (mM)	Start (ml)	End (ml)	Length (ml)	Fraction
Sample injection	40	0	10	10	Flowthrough
Column Wash	40	10	20	10	Wash
Imidazole gradient	100	20	35	15	F1-2
	150	35	50	15	F3-4
	200	50	65	15	F5-6
	400	65	80	15	F7-8
	500	80	95	15	F9-10
Column Wash	40	95	110	15	F11-12

As can be seen in Figure 2.24 A, independently of the treatment, elution of His₁₄-Sec61S353C was achieved in an acceptably narrow interval of the elution gradient and in easily detectable amounts (upper panels). Loss of protein in the flowthrough was negligible (Figure 2.24 A; upper panel, Flow and Wash). In the lower panels, the results of the Sec63 detection can be seen. Here, it can be observed that there are no overlapping of Sec63 and Sec61 elution from the column in the control condi-

tions (i.e absence of crosslinker), while in crosslinked samples, Sec63 elution overlaps, at least partly, with the Sec61 elution (Figure 2.24 A; compare lanes 4-8 in both upper and lower panels). In sample treated with SMPH, this elution is detected as Sec61S353CxSec63 complex (Figure 2.24 A; bottom central panel, lanes 18 to 20), while in the LC-SPDP treated sample, since the sample was reduced, and the crosslinker cleaved, Sec63 elution is detected in its free form (Figure 2.24 A; bottom right panel, lanes 31 to 33). To further confirm the quality of the purified samples and also as a way of roughly estimating the total amount of purified protein, fractions 3 to 10 from a different set of purifications were pooled, TCA precipitated, resuspended in 2xLaemmli Buffer and resolved by SDS-PAGE. In the same acrylamide gel were also loaded different amounts of BSA to serve as loading control. The gel was then stained with G-250 and the intensity of total amount of protein estimated based on the BSA loading controls used. An example of one of these stainings is showed in Figure 2.24 B. Here, it can be seen that I was able to purify, roughly, around 2 µg of protein from each sample, and that the amount of background was acceptably low.

After data analysis, I deemed that the full crosslink/purification setup was indeed suitable for crosslinked Sec61 complex enrichment, and also suitable for a potentially successful mass spectrometry analysis.

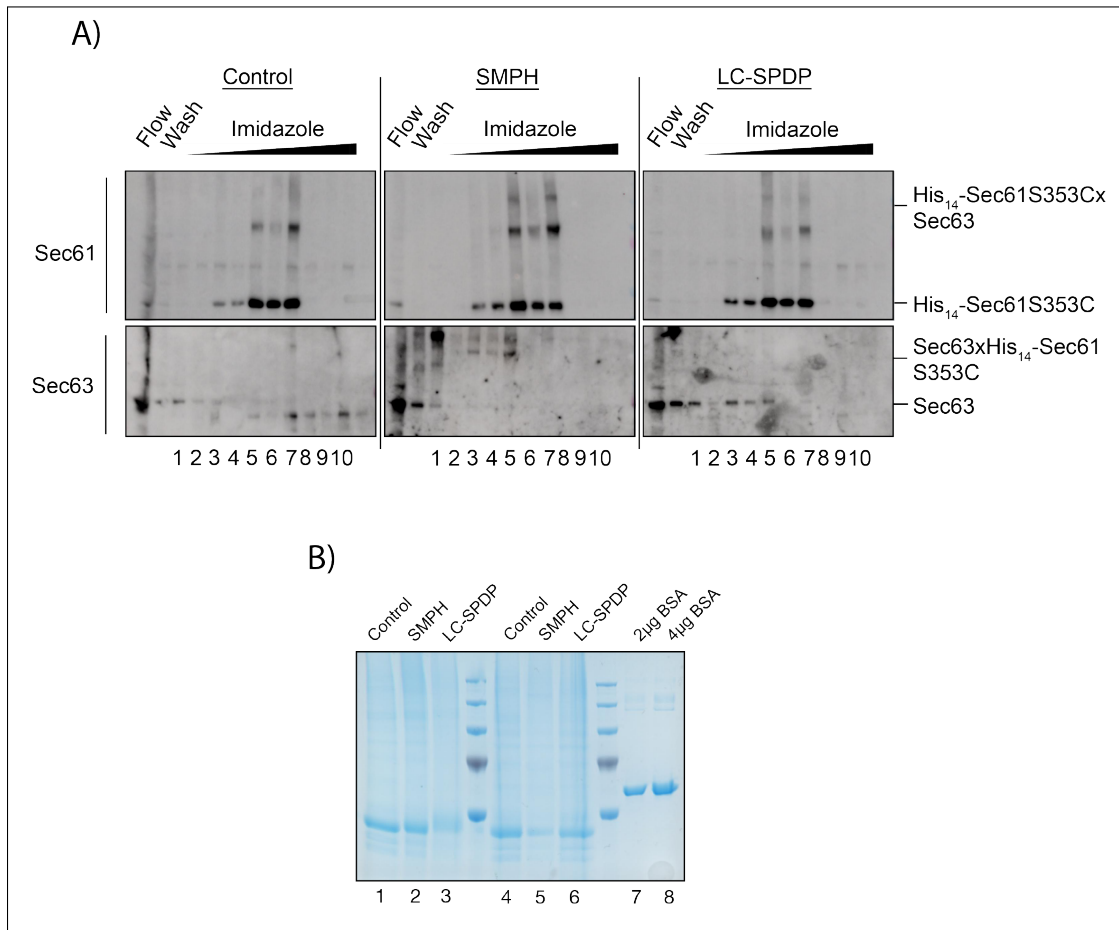


Figure 2.24: Immunoblot and gel staining analysis of purified fractions Microsomes (500 eq) were treated either DMSO (Control), SMPH or LC-SPDP (1 mM), solubilized in 1 ml of IP for 30 min on ice, followed by 10 min at 65 °C. Samples were then diluted with 4 ml of cold Purification Buffer, and injected into a Histrap FF (1 ml) pre-packed columns associated to a BioLegend LP purification system. Columns was washed with Binding Buffer (10 ml; 50 mM Tris-HCl, pH 7.4 / 300 mM KCl / 0.5 % TritonX-100 / 40 mM Imidazole) and with Purification Buffer/ 100 mM Imidazole(10 ml). Elution was done along an imidazole gradient (150-500 mM) in 15 ml-long steps. Fraction of 7.5 ml were collected along the imidazole gradient, and DTT (100 mM) was added. Each sample was TCA precipitated, fraction of interest (3 to 10) were all resuspended in the same 50 µl of 2xLaemmli Buffer, and resolved by SDS-PAGE on 4-12 % Bis-Tris gels (NuPAGE® Novex® Pre-Cast gels, Invitrogen). **A)** Immunoblot analysis of the elution pattern when both a Sec61 and a Sec63 antibody was used for protein detection. **B** Coomassie G-25 stained gel of the pooled His₁₄-Sec61S353C-containing fractions (3-10) to ascertain both purification yield and co-purification levels.

2.5 Liquid Chromatography-tandem Mass Spectrometry and Statistical Analysis

With a successful scheme for crosslink followed by target-form purification established, I was in position of proceeding with the mass spectrometry analysis. My first attempt at mass spectrometry analysis was done in collaboration with Klaus Hollenmeyer in the Chemistry department of the Saarland University using an AB Sciex 4800 Plus MALDI tandem TOF mass spectrometer. Sample was crosslinked, purified, and resolved by SDS-PAGE. After Coomassie staining, visible bands present in the crosslinked samples were excised from the gel, as were the same gel positions of the non-crosslinked sample. Proteins were extracted from the gel slices, trypsin digested and analyzed by mass spectrometry. This analysis was also limited to only LC-SPDP samples, as Dr. Klaus Hollenmeyer did not feel confident on the probability of a detection of Sec61 in the crosslinked form. Unfortunately this approach proved to be unsuccessful, as I was only able to detect Sec61 itself (results supplied as Supplement File MassSpecUds in the annexed virtual media - i.e USB-stick "Dissertation Supp.").

A mass spectrometry analysis in collaboration with Dr. Rod Chalk, of the Structural Genomics Consortium (SGC) Oxford was also attempted. To this end, affinity purified samples and crosslinked samples solubilized with a range of different detergents (n-Dodecyl- β -D-Maltoside - DDM, Octyl Glucose Neopentyl Glycol - OGNG, digitonin, and TritonX-100) were separated by reverse phase chromatography and analyzed by mass spectrometry. The reasoning behind using different detergents and concentrations was that these detergents have different strengths and chemistry, preferentially solubilizing different classes of proteins. In using them, I might be able to solubilize only a sub-population in which Sec61 was included, serving as a rough purification step. Analysis showed that the differential solubilizations were unsuccessful in enrich-

ing Sec61 (data not shown). Analysis of the affinity purified samples returned no hits, not even Sec61 being detected (data not shown). At the time, I thought that such lack of signal was due to a co-precipitation of KCl during TCA precipitation, which inhibited trypsin digestion and compromised the full analysis. Because a lot more effort was necessary for the optimization of this setup, the collaborator lost interest in the project.

I was then given access to the EMBL Core Proteomics facility as my supervisor is an EMBL alumna. The head of the facility, Dr. Mikhail Savitski, and Mandy Rettel, a PhD student, agreed to work with me. They suggested a new approach to analyze my crosslinked samples.

Table 2.3: List of samples analysed by LC-MS/MS

Sample name	Description	N° of samples
Control	Purification from non-crosslinked <i>14His-sec61S353C</i> microsomes	3
Sec61_SMPH	Purification from SMPH crosslinked <i>14His-Sec61</i> microsomes	3
Sec61_LC-SPDP	Purification from LC-SPDP crosslinked <i>14His-Sec61</i> microsomes	3
sec61S353C_SMPH	Purification from SMPH crosslinked <i>14His-sec61S353C</i> microsomes	3
sec61S353C_LC-SPDP	Purification from LC-SPDP crosslinked <i>14His-sec61S353C</i> microsomes	3

For this new approach, samples were purified as described in Section 2.4.4, re-suspended in 50 μ l of 2xLaemmli buffer and resolved for 5 cm on an acrylamide gel. Gels were then shipped to EMBL for analysis. Purifications were done sequentially, making sure to purify the Control samples first, using a dedicated column for each treatment type, and including extensive system washing steps in between samples and sets. On site, each lane was cut into multiple bands, these were subjected to in-gel trypsin digestion, the peptides were recovered and analysed by Liquid Chromatography-tandem Mass Spectrometry (LC-MS/MS). In total, 12 samples were analyzed, as listed in Table 2.3.

Peptides were then separated by liquid chromatography (nanoAcquity UPLC system; Waters), and analyzed in a state-of-the-art mass spectrometer (LTQ Orbitrap Velos Pro; Thermo Fisher Scientific).

The raw mass spectrometry data was processed with MaxQuant (v1.5.2.8) [65] and searched against an Uniprot *Saccharomyces cerevisiae* proteome database. For protein identification a minimum of one unique peptide with a peptide length of at least seven amino acids and a false discovery rate (fdr) below 0.01 were required on the peptide and protein level. Label-free quantification was selected using intensity-based absolute quantification (iBAQ - calculated as the sum of the intensities of the identified peptides and divided by the number of observable peptides of a protein) [347] with the log fit function enabled. The raw mass spectrometry data can be found in the Supplement File RawData (MassSpecEMBL/MassSpecData/RawData) in the annexed virtual media (i.e USB-stick "Dissertation Supp."), as well as the excel file Fulldata.xlsx (MassSpecEMBL/MassSpecData/Fulldata.xlsx) with the iBAQ quantifications that resulted from the above described analysis.

Frank Stein, a biostatistician from the EMBL Proteomics Core Facility, analyzed these samples looking for enriched hits in the crosslinked samples (SMPH and LC-SPDP) when compared to the non-crosslinked ones (Control). He processed the raw output data of MaxQuant (proteinGroups.txt file) using the R programming language (ISBN 3-900051-07-0). As a quality filter, a threshold of 2 unique peptides was set for protein identification. Potential batch-effects were removed from the log₂ of the iBAQ values using the Limma package [316]. Batch-cleaned data were normalized with the variance stabilization (*vs*n) package [166]. Missing values were imputed using the MSNbase package [110]. Finally, limma was used again to identify differentially expressed proteins. A protein was called a "hit" with a *fdr* smaller than 5 % and a fold change of at least 3, and a "candidate" with an *fdr* smaller than 20 % and a fold change of at least 3. The MA plot (which reflects significant differences between samples) generated during analysis can be seen in Figure A.14.

In Figure 2.25, the general enrichment pattern can be seen in the volcano plots, where hits are plotted by means of their level of enrichment versus their *p*-values. Due to the large number of enriched proteins, this group was divided into two categories: "hits" and "candidates". Both show log₂FC values (i.e enrichment factor) higher than 1,58 (which represents a minimal fold-change of 3), but "hits" have a *fdr* below 5% while "candidates" present an *fdr* below 20%, but higher than 5%. This threshold is visible in the graphical representation by a vertical purple line. "Hits" and "candidates" are shape-coded in the graph; "hits" are represented as circles and "candidates" as triangles. All non-enriched proteins (i.e below threshold line) are represented by a small, gray circles. The hits of potential interest were colored red, Sec complex subunits were colored green, and other reported interactors (either by online databases, literature, or personal communication with other researchers) were

colored blue. These hits were resumed in Table 2.4, where the same color code was used.

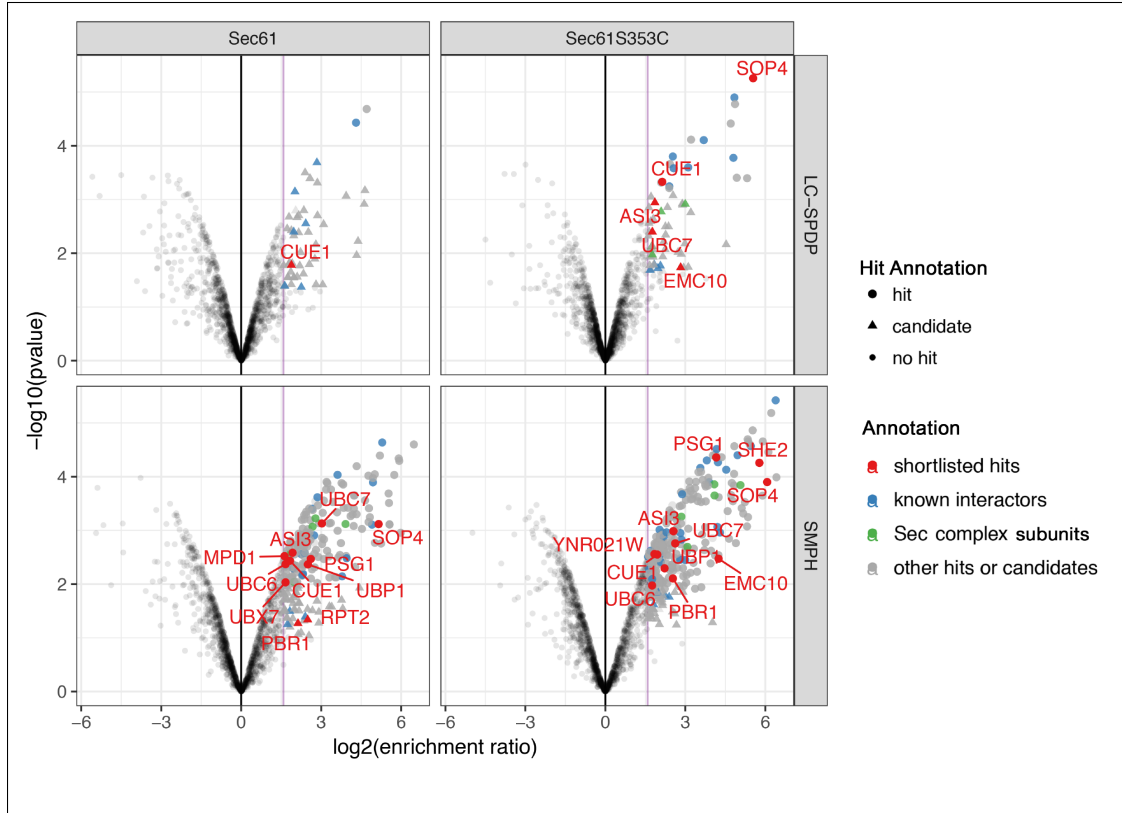


Figure 2.25: Volcano Plot Volcano plots based on the statistically determined protein enrichment in the crosslinked samples (His14-Sec61 and His14-Sec61S353C) when compared to the non-crosslinked samples. The horizontal axis represents log2 fold change (log2FC) reflecting level of enrichment. The vertical axis plots the $-\log_{10}(\text{pValue})$ of enrichment, reflecting significance. Both hits and candidates have a fold change of at least 3. Hits have a false discovery rate (fdr) < 5% and candidates an FDR < 20%. Purple line is at fold-change of 3. Hits shown as colored dots and candidates as triangles. Elements of Sec61 complex in green; known interactors or translation machinery in blue; and shortlisted hits in red and points labeled on graph. Not significant hits below reference line and non-interesting hits above reference line in light grey.

From this protein-enrichment study, a total of 361 enriched proteins were found (204 hits and 155 candidates). The highlighted "hits", with their respective log2FC values and sample representation can be seen in Table 2.4. Some of the "hits" resumed in this table were enriched in more than one treatment/sample (as can be seen in the

"Sample" field for each hit). In those cases, the shown log2FC values are an average of the log2FC values obtained in each sample/treatment. An excel file with the full statistical analysis and resulting data can be found in Supplement File TreatedData.xlsx (MassSpecEMBL/StatisticalAnalysis/TreatedData.xlsx) in the annexed virtual media (i.e USB-stick "Dissertation Supp."). The individual, per sample log2FC values can be consulted there (sheet 3 to 6). Consultation of said list is advisable, since individual log2FC, p-values, and fdr values can be of extreme interest.

Table 2.4: Shortlisted Hits. Listing of shortlisted hits. Presented hits are color coded to match coloring used for volcano plot labeling.

Gene Name	Log2FC	Samples	Gene Name	Log2FC	Samples
SHE2	5,77417	D	EMC2	2,10918	B D C
EMC4	5,06292	A D C B	EMC5	2,10918	D B C
RPL22A	4,53156	D	MNN2	2,10918	C B D
ALG13	4,3982	D C	SEC63	2,10918	D B C
SRP102	4,12642	C D	SEC66	2,10918	C D B
YDR056C	3,53482	D B	SEC72	2,10918	C D B
YKL077W	3,38221	D C	SOP4	2,10918	C B D
SRP72	3,35062	D B	SSS1	2,10918	B D C
IFA38	2,87639	A B D C	UBC7	2,10918	C B D
RPL1B	2,86817	C D	SRP68	2,08099	D
SWP1	2,8159	D	PEX30	2,06552	D C
SRP101	2,79474	C D	RPL30	2,04734	D
TOR1	2,69893	D C	GET3	2,03345	D
RPT2	2,49328	C	SRP21	2,01523	A
OST3	2,49038	A C B D	CUE1	1,91581	C B D A
SEC62	2,36162	D C	ROT2	1,90427	C D
UBP1	2,36082	C D	YNR021W	1,8441	D
YNL181W	2,33121	D C	OST6	1,80838	D
WBP1	2,29404	D	YET3	1,75632	D
PHO88	2,27552	A D B C	UBC6	1,71231	C D
BFR1	2,2493	D	STT3	1,6909	D
SNL1	2,19231	D	UBX7	1,66387	C
ALG11	2,10918	C B D	ALG5	1,65502	C
ALG12	2,10918	C D B	MNN5	1,63337	A
ASI3	2,10918	D C B	MPD1	1,6274	C
EMC1	2,10918	D B C	DPM1	1,60274	D

A LC-SPDP-Sec61
 B LC-SPDP-Sec61S353C
 C SMPH-Sec61
 D SMPH-Sec61S353C

Sec complex subunit
shortlisted "hit"
known interactors

Besides the enrichment pattern of crosslinked samples when compared to the control samples, other combinations of comparison were made (e.g Sec61_SMPH versus Sec61_LC-SPDP, Sec61_SMPH versus sec61S353C_SMP, etc.). Although these

comparisons were not the main objective of the analysis, they might contain some useful information. Therefore a graphical analysis is annexed to this document for future reference (Supplemental Figure A.15 and A.16) and the full data sets (LimmaResults.xlsx) and intermediary graphical analysis are supplied in the Supplement File FullData (MassSpecEMBL/StatisticalAnalysis/FullData) in the annexed virtual media (i.e USB-stick "Dissertation Supp."). There, the file Report.pdf, with a step-by-step description of the data analysis can be consulted.

To have a graphical representation of a possible interaction grid present in this enriched fraction, I tried using network-prediction software and potentially see some pattern. To this end the list of 361 enriched hits (plus Sec61) was fed into the online protein-protein interaction network prediction tool STRING [386]. STRING is a database of known and predicted protein-protein interactions. The interactions include direct (physical) and indirect (functional) associations; they stem from computational prediction, from knowledge transfer between organisms, and from interactions aggregated from other (primary) databases. Before the final graphical representation was obtained, I changed the following settings: network hedges (connecting lines) reflect strength of data support; minimum score to 0.7 required for interaction validation; remove disconnected nodes in the network. All three settings were changed to increase figure clarity and accuracy. I also applied a kmean clustering, where the network was clustered to 7 clusters. The number of clusters was chosen randomly, as it just defines the exact number of clusters the software returns from my network, and only with the intent of highlighting a Sec61-containing cluster. After such setting changes, the following grid was obtained (Figure 2.26).

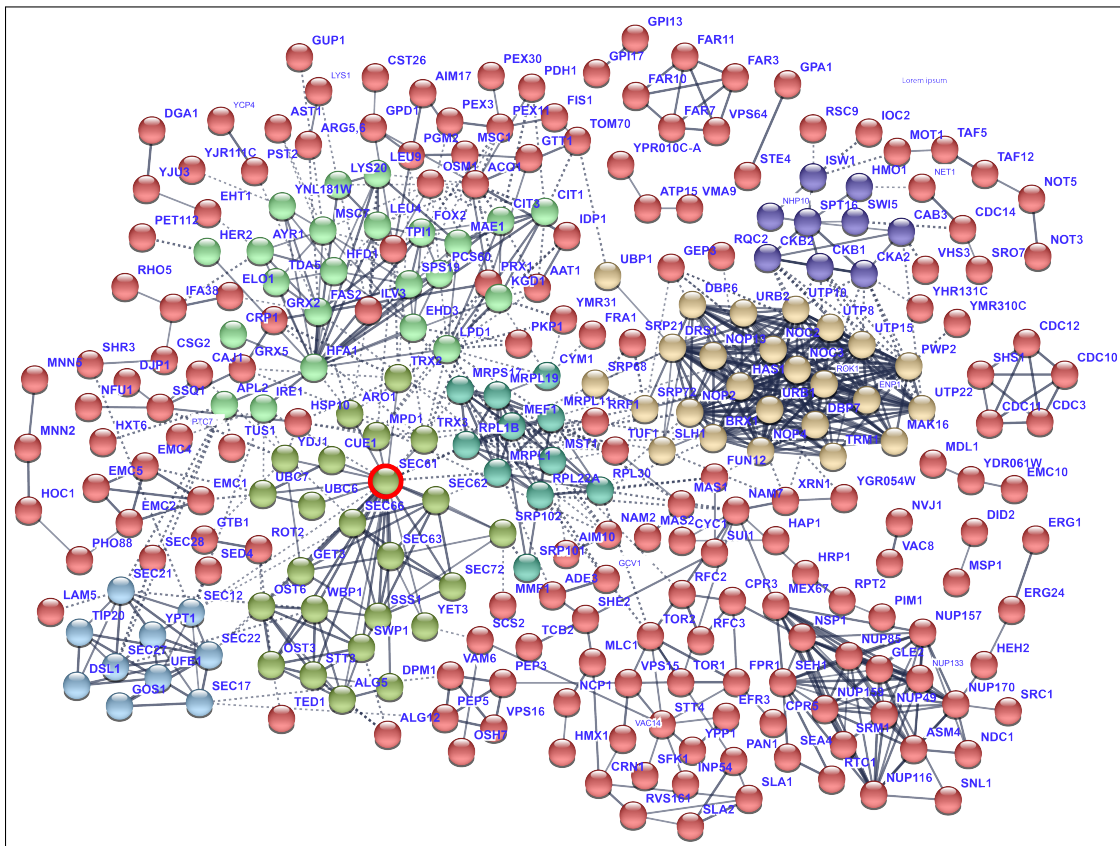


Figure 2.26: Interaction Grid. 361 enriched hits (plus Sec61) were fed into the online protein-protein interaction network prediction tool STRING (database of known and predicted protein-protein interactions). Default settings changed as follow: network hedges (connecting lines) reflect strength of data support; minimum score to 0.7 required for interaction validation; remove disconnected nodes in the network. A kmean clustering, where the network was clustered to 7 clusters was also applied. Sec61 containing cluster in green. Sec61 itself highlighted by a red circle. Non clustered hits shown in red. Other clusters in blue, light green, purple, yellow, and marine blue.

The Sec61-containing cluster is colored green and Sec61 is highlighted by a red circle. It can be seen that in this particular cluster, which represents proteins with close interaction relationship with Sec61, not only other Sec complex elements are present, but also hits like Mpd1, Ubc7, Ubc7, Cue1, Ydj1, among others. It should also be noticed that the EMC complex seems to show close proximity with the Sec61 cluster, which confirms recent data that Sec61 and the EMC complex can cooperate

in protein integration into the ER membrane [362], as well as a cluster that seems of mainly transcription elements (in marine blue). Several other clusters are highlighted (yellow, light green, blue, purple, and the unclustered background in red). The software itself, as soon as the grid was rendered, generated the automatic warning message "your network has significantly more interactions than expected". This was taken as a sign of high probability of a meaningful interaction/graphical representation. The tool allowed also for an analysis of the functional enrichments on our network. The reported results can be seen Supplemental file Functional Analysis. Note that the location of the hits in the grid is not meaningful, the connections between hits and their thickness are.

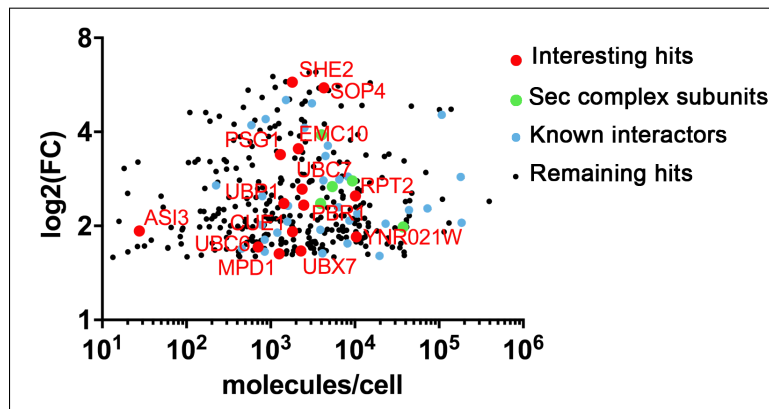


Figure 2.27: Protein abundance/Enrichment Graphical representation of the enrichment level (i.e logFC) of the Sec61 interactors as function of their respective cellular abundance as in [209]. Known interactors blue, Sec61 complex subunits green, interesting interactors red and labeled on the graph. Note absence of correlation between cellular abundance and interaction with Sec61.

While the enrichment pattern was sample- and crosslinker-dependent as can be seen in Figure 2.25, there was the possibility that the detected enrichments might simply reflect the absolute abundance of proteins in the cell. To test this hypothesis, each hit enrichment level was plotted as function of its cellular abundance. The reasoning was that if the enrichments detected reflected the cellular amount of each protein,

then the probability of this representing true interactions was low. In Figure 2.27 we can see that cellular amounts did not correlate with the enrichment levels seen in the mass spectrometric analysis, suggesting that the detected interactions with Sec61 were specific. Files with the data that originated shown figure can be consulted in Supplemental File Kulak cell amounts.xlsx (MassSpecEMBL/StatisticalAnalysis/Kulak cell amounts.xlsx) in the annexed virtual media (i.e USB-stick "Dissertation Supp.").

2.5.1 Crosslinked Peptide Analysis

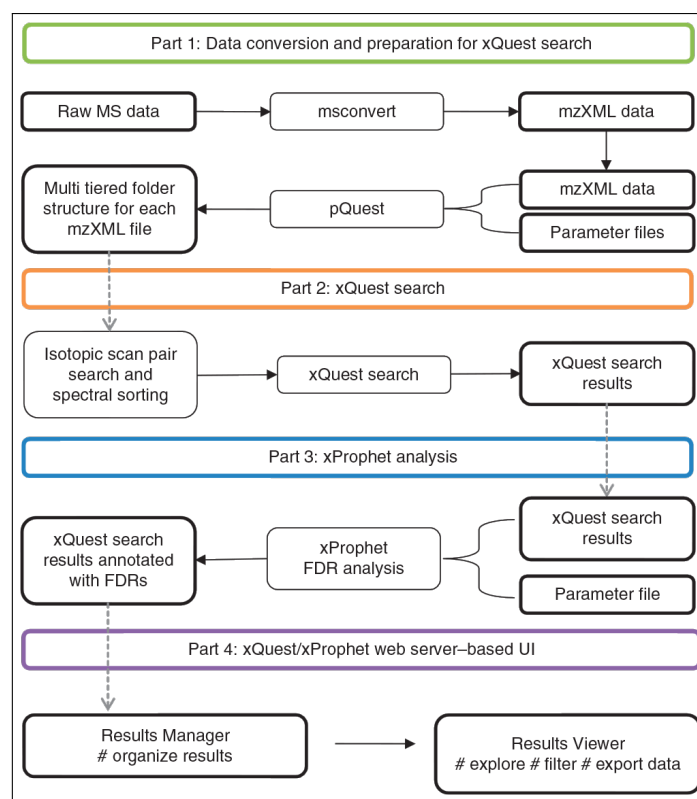


Figure 2.28: xQuest/xProphet pipeline analysis scheme. Workflow of the xQuest/xProphet software pipeline for the identification and statistical validation of cross-linked peptides from XL-MS experiments. The first step includes the conversion of raw MS data to the mzXML format and the preparation of the folder structure for the xQuest search. The second step includes the xQuest search and the identification of cross-linked peptides. The third step describes the statistical validation of the xQuest search results by xProphet, and the fourth step illustrates the web server-based data and result visualization. UI, user interface. Scheme adapted from [217].

Knowing, or even having some hints, of the potential crosslink locations between two crosslinked interactors would be invaluable, so I strived to find a way to infer some information on that from the data. In my search for methods to achieve this end, I came across the xQuest/xProphet software [217]. This software identifies and statistically validates crosslinked peptides from XL-MS experiments. The software was not optimized for our crosslink setup, but I came to understand, that in fact, none of the available software was. There are two main reason for the inadequacy of most software:

- the high complexity of the sample. A total of ~ 1900 different proteins were identified by mass spectrometry in the 12 samples analyzed. This represents a very complex sample, which these softwares are not prepared to handle.
- the crosslinker used. Most software is optimized for the analysis of samples treated with homobifunctional crosslinkers, specially DSS. So, although reactivity with both lysine (K) and cystein (C) could be set, the software was no able to exclude homocrosslinks (K-K or C-C), which meant I had to exclude these manually.

A general schematic from Leitner et al. [217] can be seen in Figure 2.28. Meaningful parameters are described in the Methods section (Section 1.2), and definition files can be found in the Supplement File `deffile.def` (`MassSpecEMBL/xQuest/deffile.def`) in the annexed virtual media (i.e USB-stick "Dissertation Supp.").

Since the software had been reported to behave better when small databases were submitted, I always kept databases below a total number of 30 proteins. This restriction was set not only due to the better behavior of the software with small datasets, but also due to the big data load. For each analysis round I had to screen 12 raw data files for possible combinations. Moreover, the software was used in a virtual machine environment, as it needed to run under the Ubuntu operating system. This caused too much stress on the computer memory, causing not only slow analysis (the

full data set would, in average take 72h to complete the full analysis), but also some crashes of the software during the run, as well as problems with the result loading and export from the server where the data could be read. Since the machine showed itself to be incapable of loading most the results into the server, for whatever reason that neither I, nor the software developer (Alexander Leitner) or the in house IT support that was contacted to try to clarify the subject (Timo Scheller), could determine. To circumvent this issue, data had to be loaded onto a server (ARMv8 system of the HIZ department) that had enough capacity/speed to successfully load the data into the results server. Both the long time needed for each run, as well as the difficulty with the results acquisition, limited the amount of optimization that could be done. I tried, nevertheless, to feed the software bigger databases (175 and 360 proteins).

In all the cases above mentioned, the software was able to identify several crosslinked peptides, not only between Sec61 and interacting proteins, but also between combinations of the other hits. Unfortunately, the maximum score of the hits found in any of the attempts by varying database components and size, was never above 25, which is a low score for a true hit (score should be 40 or higher). Even in the higher score range, I found an even distribution of both hits and decoys. Decoys are random peptides generated by the software based on the sequences on the protein database, and serve as internal controls. This told me that the probability of a given hit being true or false was even. I tried different approaches with the intention of sifting true from false hits: screening for peptide identities and verifying that these were different in control and treated samples, mapping the detected interaction and evaluating the likelihood of it being real (e.g link of cytosolic domain to cytosolic or luminal domain of another protein?, is detected crosslink present in decoy hits?, etc.). These approaches allowed the exclusion of some potential false positives, but not enough.

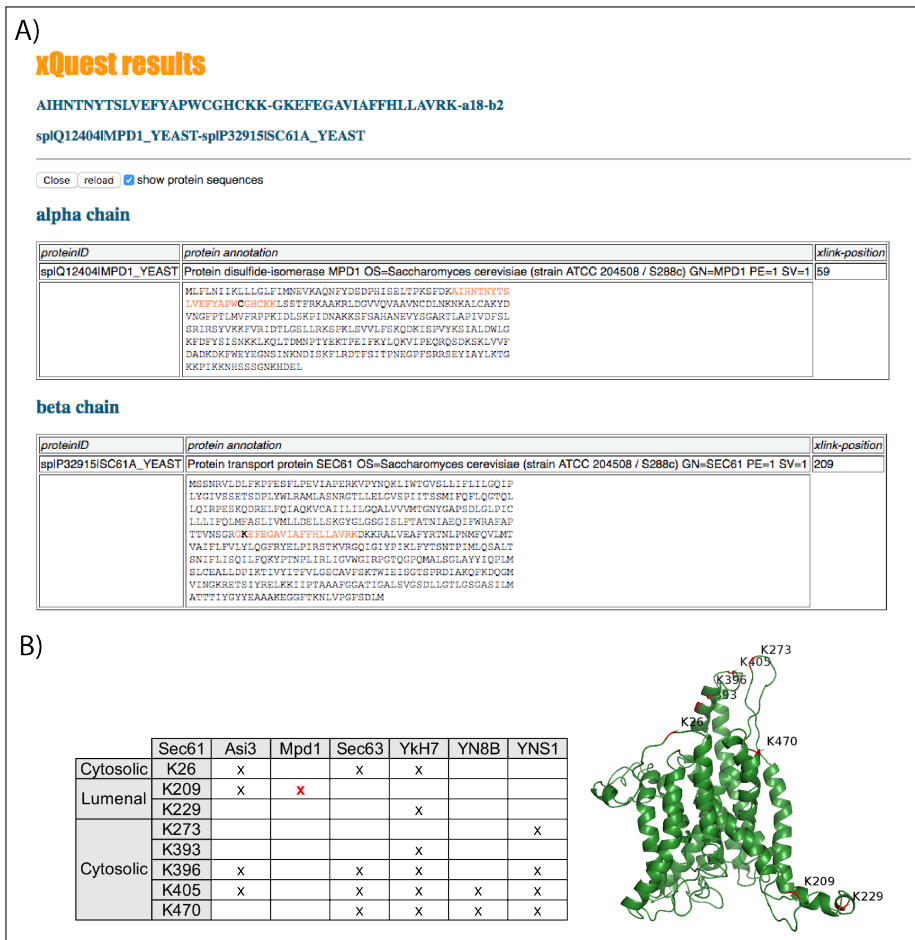


Figure 2.29: xQuest/xProphet Sec61xMpd1 crosslink report. Example of the returned results after xQuest/xProphet analysis. A) Detected Sec61xMpd1 crosslinked site. B) Resume of the detected crosslinked sites detected by the software in a given analysis. A mapping of the detected crosslinked positions onto Sec61 can also be seen.

During these analyses, a specific interaction prediction appeared multiple times, and not only that, but the reported crosslink seemed to be possible and to make sense. This interaction was between Sec61 and Mpd1. The software reported with some regularity a specific crosslink between Mpd1 C59 and Sec61 K209 (K243 in the 14His-Sec61S353C mutant). The reported result can be seen in Figure 2.29 A. The data can be seen in Supplemental File Analysis.xlsx (MassSpecEMBL/xQuest/ Analy-

sis.xlsx) in the annexed virtual media (i.e USB-stick "Dissertation Supp."). This particular analysis was done with a database comprising Sec61, Pbr1 (Yns1), Sec63, YNL021W (Yn8b), Asi3, She2, Psg1 (Ykh7) and Mpd1. In this analysis, like in so many others, several potential Sec63 crosslink sites were also detected, as well as potential interactions with the others tested hits. Reported crosslinks can be seen in Figure 2.29 B.

Another interesting detail is that no crosslink to the unique cystein introduced into L7 was detected by the software, only crosslinked lysines were detected in Sec61.

It should also be said that the xProphet segment of the pipeline did not seem to run properly in any of the analysis, and consequently, no *fdr* values were ever calculated.

With this approach, although some potential crosslink sites had been highlighted, their validity was dubious.

2.6 Sec61 Interactors Analysis

Based on the obtained mass spectrometry data, I chose some Sec61 interactors that seemed functionally interesting for further analysis. These were Asi3, YKL077w (Psg1), YNR021w, She2 and Mpd1.

Asi3 was chosen, although being described as a nuclear protein, involved in Inner Nuclear Membrane (INM) protein quality control, because it not only was strongly present in our samples, but it was also strongly enriched in the crosslinked samples. Asi3, a transmembrane protein that forms the Asi complex with Asi1 and Asi2, is also reported as interacting with Ssh1 in the nucleus, but not with Sec61 [102]. Psg1 and YNR021w are both ER membrane proteins, which are still uncharacterized [115, 168]. Their potential interaction with Sec61 seemed to be of interest since they might represent new ERAD factors. She2 (an RNA binding protein) [264] was also chosen for

further investigation because although it has been reported that She2 binds to the ER, its receptor has never been identified. This has been a long-standing question in the field of RNA-targeting, hence it seemed likely that I could make a valuable contribution here. Mpd1 was also chosen, due to its connection to ERAD [415] and because of the potential crosslink site identified to a luminal domain of Sec61 by the xQuest analysis.

2.6.1 Characterization of Sec61 Interactor Mutants

After narrowing down my list of 361 potential interactors to 5 (Asi3, Psg1, Ynr021w, She2 and Mpd1), the first step was to characterize the strains with deletions in each of the genes encoding Sec61 interactors. I wanted to verify whether they showed any phenotypes that might indicate a role of the potential interaction with Sec61 in ER protein translocation or ERAD. For this purpose, mutant strains were obtained from the Euroscarf strain collection and characterized using basic yeast techniques.

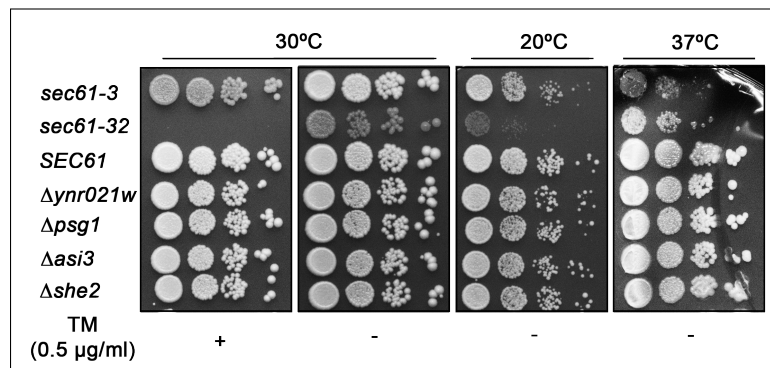


Figure 2.30: Temperature and tunicamycin sensitivity test of $\Delta asi3$, $\Delta ynr021w$, $\Delta psg1$, and $\Delta she2$ mutants. Cell were grown overnight in YPD, counted using a Neubeur chamber and sequentially diluted (10^4). Samples of each dilution ($5 \mu\text{l}$) were then plated side by side, in solid YPD and grown for at least 3 days. Each set was replicated 4 times in different plates. Plates for temperature sensitivity were incubated at 20, 30 or 37 °C (one replica per temperature). For tunicamycin sensitivity, one plate was supplemented with 0.5 $\mu\text{g/ml}$ of tunicamycin and grown at 30 °C.

I started by characterizing these strains with respect to their temperature and tu-

nicamycin sensitivity. Cells were grown overnight, counted and sequential dilutions made (10^4 - 10^7). Dilutions were plated on solid YPD with tunicamycin (0.5 $\mu\text{g/ml}$) or without tunicamycin. The plate with tunicamycin and one of the YPD plates were incubated at 30°C. The two other plates lacking tunicamycin were incubated at either 20 or 37 °C. As shown in Figure 2.30, only the positive controls showed any sensitivity in the tested conditions. The *sec61-3* mutant shows reduced viability both at 20 and 37°C (two right-most panels) and the *sec61-32* at 20°C (second panel from the right) and in the presence of tunicamycin (left-most panel). The *sec61-32* mutant was used as positive control for tunicamycin sensitivity, as this mutant has, at the permissive temperature, the strongest ERAD defect characterized in a *sec61* mutant [289].

The next step was characterizing these strains regarding their ER-import capacity. To that end, I evaluated the translocation of the following proteins:

- wild-type pre-pro- α -factor (pp α F; \sim 18 kDa) which is imported post-translationally into the ER where the signal sequence is cleaved off by signal peptidase [434]. The resulting pro- α -factor (p α F; \sim 16 kDa) is triply glycosylated upon entry into the ER. The glycosylated form is rapidly transported to the Golgi where it is proteolytically cleaved to release the 13 aminoacid long α -factor. Hence the precursor form is only detectable in cells with an ER import or ER-to-Golgi transport defect [382].
- Vacuolar protease carboxypeptidase Y (CPY), a soluble, glycosylated secretory protein is also translocated post-translationally into the ER [201, 258]. It is synthesized as a cytosolic precursor (ppCPY \sim 59 kDa), which has its signal sequence cleaved in the ER, originating the pro CPY form (pCPY, \sim 57 kDa). It then gets N-glycosylated at four sites to p1CPY (67 kDa). CPY is then post-translationally modified in the Golgi to p2CPY (69 kD), and proteolytically processed to mature mCPY (61 kDa) in the vacuole. If cells have a post-translational import defect, then accumulation of the cytosolic ppCPY form can be seen [397, 30]
- Diaminopeptidase B (DPAPB) is a type II membrane protein with an N-terminal

transmembrane domain [288]. Upon co-translational integration into the ER membrane, the precursor protein (pDPAPB - 96 kD) is core-glycosylated to form the mature protein (DPAPB -120 kD) [319]. If DPAPB is efficiently integrated, its precursor form is undetectable, making it a typical substrate to test co-translational translocation impairments.

To evaluate the translocation dynamics of the above mentioned substrates, two approaches were applied: for pp α F, an immunoblotting approach was used, while for CPY and DPAPB, the analysis was done by pulse labeling.

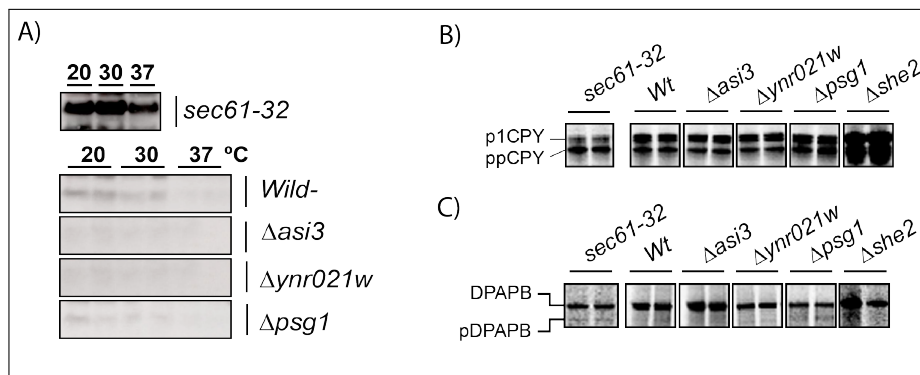


Figure 2.31: Import dynamics in $\Delta asi3$, $\Delta ynr021w$, $\Delta psg1$, and $\Delta she2$. Analysis of the import dynamics of multiple translocation reporters **A)** Analysis of the pp α F translocation profile. Cells were grown to a maximum OD₆₀₀ of 1, and incubated at either 20, 30 or 37°C for a period of 3 hours. After incubation, 1 OD₆₀₀ of cells were collected, washed with Tris-Azide buffer, and an extract prepared. For each sample 0.4 OD₆₀₀ were resolved by SDS-PAGE, and protein detected by Immunoblotting using a pp α F specific antibody. Signal was acquired by chemiluminescence using an Amersham Imager 600. **B)** Analysis of the CPY translocation profile. Cells were labeled with [³⁵S]-met/cys for 5 min, lysed and immunoprecipitated. For each time point 1.5 OD₆₀₀ of cells were lysed and proteins immunoprecipitated using specific antibodies against CPY. After SDS-PAGE, proteins were detected by phosphorimaging. **C)** Analysis of the DPAPB translocation profile. Cells were pulse-labeled with [³⁵S]-met/cys for 15 min, lysed and immunoprecipitated. For each time point 1.5 OD₆₀₀ of cells were lysed and proteins immunoprecipitated using specific antibodies against CPY. After SDS-PAGE, proteins were detected by phosphorimaging. For each experiment, at least three replicas were made.

For the pp α F accumulation, triplicates of the mutants to be analyzed, plus a positive control (*sec61-32*; import defect mutant at 20°C) were grown to an OD₆₀₀ of 1 at 30°C, 220rpm, then one replica of each culture was incubated either at 30, 30 or 37°C for 3 hours. After the incubation, samples were collected from each culture, extracts were made, and resolved by SDS-PAGE. Detection was done by immunoblotting us-

ing a pp α F specific antibody. As can be seen in Figure 2.31 A, none of the mutants, except the positive control *sec61-32*, accumulates ppaF, and so, none of the mutants seems to display any post-translational import defect of soluble substrates.

For the ppCPY and pDPAPB accumulation assay, cells were grown to a maximum OD₆₀₀ of 1, pulse labeled with [³⁵S]-met/cys, cells lysed, and each one of the substrates was immunoprecipitated using specific antibodies. Samples were then resolved by SDS-PAGE, gels dried, signal detected on phosphorimage plates and acquired in a Typhoon phosphorimager. Results can be seen in Figure 2.31 B and C.

For CPY (Figure 2.31 B), which is a post-translational imported, soluble protein only *sec61-32* shows a strong accumulation of this precursor (lanes 1-4). The Δ *she2* mutant (lanes 13-14) showed a curious phenotype, reproducibly expressing much higher amounts of both CPY forms.

In the case of pDPAPB (Figure 2.31 C), we see that, besides the positive control (*sec61-32*; lanes 1-4), only in mutant Δ *ynr021w* (lanes 11-12) is this form detected, indicating that this mutant is import defective for the membranal, co-translationally imported pDPAPB substrate. The intensities of the pDPAPB band, however, are very weak in both *sec61-32* and Δ *ynr021w* even though the *sec61-32* had been shifted to the restrictive temperature where the import defect is strongest (i.e 20 °C). This might have been due to a prolonged lab-cooling problem that could have caused a quicker processing of this form in all backgrounds, including the *sec61-32* mutant, during sample manipulation.

To further characterize the potential translocation defects on the pertinent strains, I did a reporter protein translocation assay using a plasmid encoding a protein substrate for cotranslational ER import (pRS313-*PHO8-URA3*; *HIS*, 2 μ) [262]. This construct encodes a fusion of the sequence coding the first 70 amino acids of Pho8 and

the whole open reading frame (ORF) of *URA3* [262]. *PHO8* encodes alkaline phosphatase, which is involved in the dephosphorylation of phosphotyrosyl peptides in *S. cerevisiae* [81]. *URA3* encodes the Orotidine-5'-phosphate (OMP) decarboxylase which is involved in the *de novo* biosynthesis of pyrimidines in the cytosol [211]. This fusion protein is co-translationally imported into the ER. Since Ura3 needs to be in the cytosol to be used as the only source of Ura3, only in strains with an import defect is this fusion protein able to support growth when no Ura3 is supplied exogenously [262]. This construct has been used to select *sec61* mutants with a co-translational import defect [258].

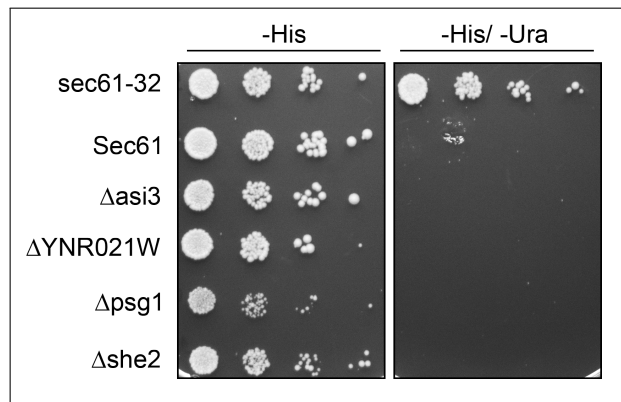


Figure 2.32: Translocation defect assay. Indicated mutants were transformed with the pRS315-*PHO8-URA3* reporter plasmid, cells were grown overnight in liquid minimal medium (2% glucose, -His) at 30°C and 220rpm. Cells were then counted using a Neubauer chamber and serial dilutions (10^4 - 10^1 cells) were made. Serial dilutions were plated in both histidine and histidine/uracil lacking solid minimal medium and grown at 30 °C for 3 days.

Strains were transformed with the plasmid encoding the construct, and selected on minimal solid medium lacking His. After selection, cells were grown overnight in liquid minimal medium also lacking His (30°C, 220rpm), counted using a Neubauer counting chamber, successive dilutions were made (10^4 - 10^1) and plated on solid minimal medium lacking both His and Ura. As can be seen in Figure 2.32, only the import defective *sec61-32* mutant grows on -His/-Ura solid medium (first line of right

panel) suggesting that none of the mutants deleted for Sec61 interactor genes had a co-translational ER import defect.

I next set to characterize these mutants regarding their ERAD capacity. To that end I analyzed the dynamic of two ERAD substrates: KWW and KHN. The ERAD substrate KHN, consists of the signal sequence of *S. cerevisiae* Kar2 fused to the Simian Virus 5 HA Neuraminidase ectodomain [224, 407]. It contains O-linked sugars that are modified upon transport to the Golgi, making it possible to determine the proteins localization. It further contains four N-linked glycosylation sites. This substrate has also internal disulfide bonds [224, 406, 407].

KWW consists of chimeric integral membrane protein in which the luminal domain of Wsc1 was replaced with KHN [406, 407]. The integral membrane protein Wsc1, forming the cytosolic and transmembrane domain of KWW, is a signaling protein (nonessential) with one transmembrane domain [225, 406, 407]. KWW has a misfolded luminal domain leading to its degradation via the ERAD-L pathway [407].

Prior to pulse-chase experiments, all strains were transformed either with the expression plasmid pRS316-KWW-HA (*CEN, URA*) or pRS316-KHN-HA (*CEN, URA*), and selected on minimal sodium medium lacking Ura. Cells were then grown to a maximum OD₆₀₀ of 1, washed in labelling medium, starved for 30 min, and labeled for 15 min. Samples were chased for a total of 90 min, taking samples at the indicated time points. Results can be seen in Figure 2.33.

As can be seen in Figure 2.33, none of the mutants showed any significant delay in the degradation of either KHN or KWW. Thus, none of the tested Sec61 interactors seem to have a role in ERAD of the tested substrates.

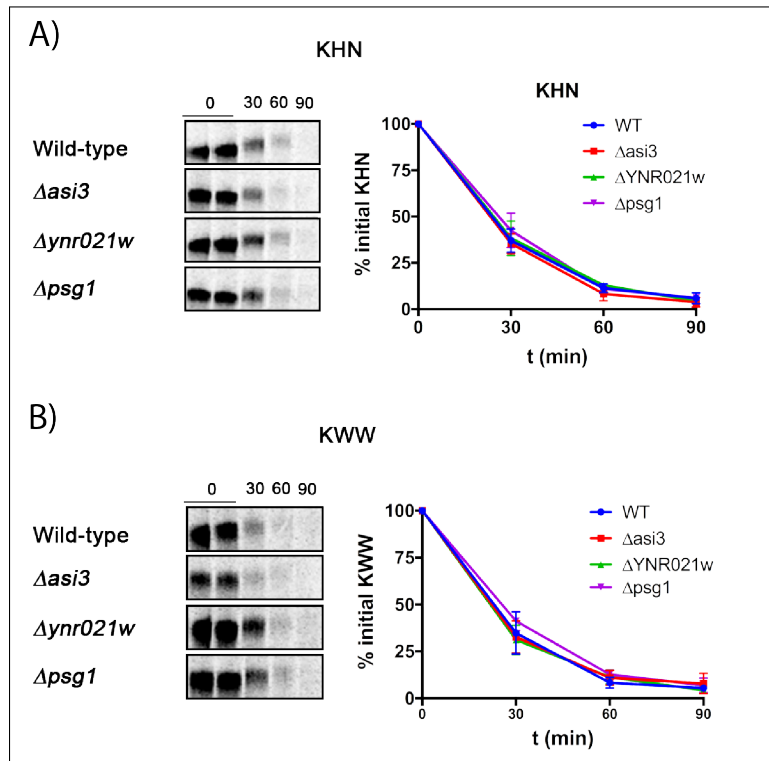


Figure 2.33: Kwn and Khn ERAD dynamics in $\Delta asi3$, $\Delta ynr021w$, and $\Delta psg1$ backgrounds. wild-type and mutant strains were pulse-labeled with [35 S]-met/cys for 15 min, followed by chase incubations for the indicated times. For each time point 1.5 OD₆₀₀ of cells were lysed and proteins immunoprecipitated using an anti-HA antibody (Biomol). After SDS-PAGE, proteins were detected by phosphorimaging. Bands quantified with ImageQuant (GE Healthcare) and averaged values plotted. At least three replicas were made. **A)** Pulse-chase analysis of the KHN ERAD dynamics. **B)** Pulse-chase analysis of the KHN ERAD dynamics

2.6.1.1 She2

Since the data in the literature seemed to strongly suggest that She2 was a real Sec61 interactor, I tried applying the immunoblotting approach to detect such interaction. For that purpose, Prof. Ralf Jansen (Biochemistry, University Tübingen), with whom I collaborated to evaluate the veracity of this interaction, supplied She2 specific antibody. I prepared SMPH crosslink reactions with microsomes from *sec61S353C*, *sec61S353C/Δshe2*, *SEC61* and *SEC61/Δshe2* strains and the SMPH crosslink patterns for both Sec61 and She2 were determined. The *sec61S353C/Δshe2* strain was

generated by integration of the *sec61S353C* mutation into the $\Delta she2$ strain obtained from the Euroscarf strain collection using the pRS306-Trunc.*sec61S353C* construct described in Kaiser & Römisch [186]. Integration was confirmed by sequencing of the target gene after integration. The samples were SMPH crosslinked, resolved by SDS-PAGE and signal detected by Western Blot using both the Sec61 and the She2 antibodies.

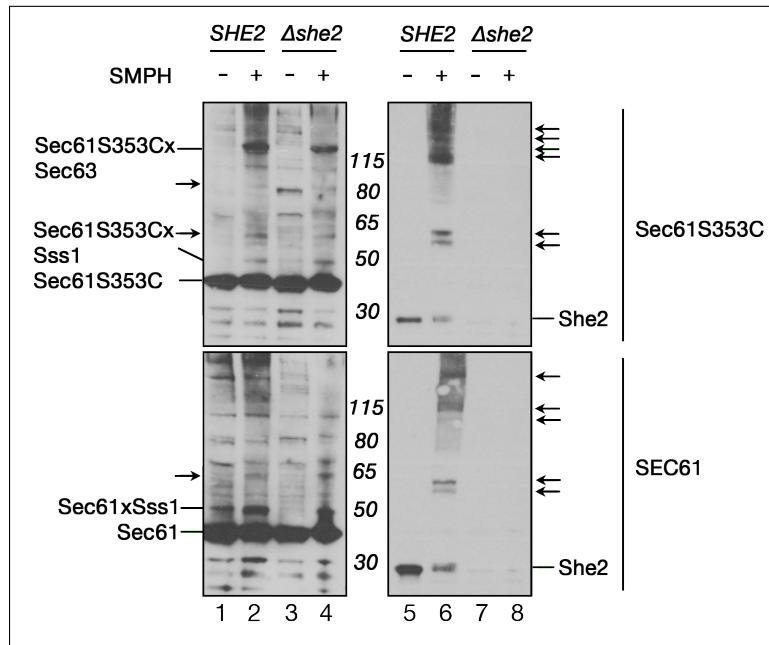


Figure 2.34: SMPH crosslink pattern determination in *sec61S353C/Δshe2* Microsomes from *SEC61/SHE2*, *SEC61/Δshe2*, *sec61S353C/SHE2*, and *sec61S353C/Δshe2* (17eq) were crosslinked with 1 mM SMPH for 30min on ice, quenched for 15min, and analyzed by SDS-PAGE on 4-12 % Bis-Tris gels (NuPAGE® Novex® Pre-Cast gels, Invitrogen). Protein detection was done by Western Blotting using either Sec61 or She2 specific antibodies and signal acquired on ECL film. Crosslinked bands are signaled by a lateral arrow.

As seen in Figure 2.34, the SMPH crosslink pattern observed in both the *sec61S353C* and *sec61S353C/Δshe2* (upper left panel, lanes 2 and 4) are similar to each other and to the one observed before in a *sec61S353C* background (Section 2.3). However, the 120 kD band seems to have its intensity decreased in the *sec61S353C/Δshe2*

(upper left panel, lane 2 versus lane 4). When the She2 antibody was used for detection in the same background (upper right panel), She2 could be detected around 29 kD only in the *SHE2* strain, and no band could be seen in the $\Delta she2$ (lane 5 versus lane 8), as was expected. Also, upon crosslink, She2 presented several crosslinked bands (right arrows). However, no correlation between detected bands (in both *SEC61/SHE2* and *SEC61/ $\Delta she2$*) and the bands seen when Sec61 was detected could be made.

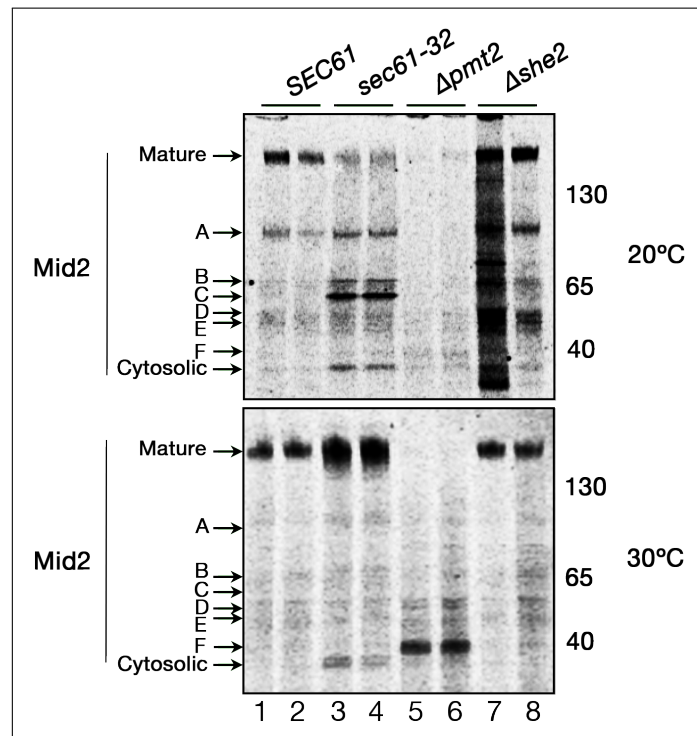


Figure 2.35: Mid2 import and maturation analysis. Cells were pulse-labeled with [³⁵S]-met/cys for 15 min, lysed and immunoprecipitated. For each sample, 1.5 OD₆₀₀ of cells were lysed and proteins immunoprecipitated using specific anti-HA antibody. After SDS-PAGE, proteins were detected by phosphorimaging. Top and bottom panels differ only in the incubation temperature for both starving and labeling of the *sec61 Δ 353C* cells. In the top panel, *sec61 Δ 353C* cells were incubated at 20°C, while in the bottom they were incubated at 30°C.

Since no conclusive answer was obtained from the immunoblotting approach, an alternative one was attempted. I reasoned that if indeed Sec61 and She2 interact, and She2 is needed for targeting of mRNA to Sec61 for co-translational translocation,

then a She2 dependent substrate should be translocation deficient in a $\Delta she2$ strain. I therefore used an HA-tagged form of Mid2: pRS425-MID2-HA (LEU, CEN). Mid2 is a plasma membrane protein, whose RNA targeting depends, on She2 [384]. Mid2 is extensively glycosylated, and when its maturation process is delayed anywhere along the secretory pathway, different sized intermediates accumulate. The translated Mid2 has 28 kD, but its fully glycosylated and mannosylated form has a molecular weight above 200 kD [285, 171]. Several intermediate forms have been detected previously [171]. In this assay two controls were used: the *sec61-32* and the $\Delta pmt2$ mutants. The *sec61-32* mutant was used to assess the effect of an import-defect *sec61* mutant on the Mid2 molecular size. The O-manosyl transferase mutant $\Delta pmt2$ was used as negative control for Mid2 processing, as in this mutant, a total abolishment of maturation had previously been reported [285].

As can be seen in Figure 2.35, in the wild-type strain, although some intermediate forms seem to be detected, the major detected band is that of the fully mature Mid2 at 200 kD (lanes 1 and 2, bottom and top panel; Mature). As expected, in the *sec61-32* mutant, an accumulation of the fully unglycosylated form of Mid2 is detected at around 30 kD (lanes 3 and 4, bottom and top panel; Cytosolic). In the bottom panel a substantial amount of the fully matured form of Mid2 can also be detected in the *sec61-32* lanes. This was also expected, since the restrictive temperature for *sec61-32* is 20°C, whereas the *sec61-32* samples of the bottom panel were incubated at the permissive temperature (30°C), as the remaining of the samples. I could also detect, in the *sec61-32* samples incubated at 20°C, additional intermediates forms (around 65 kD; band B and C). These might result from the delay in the translocation of another protein needed along the Mid2 maturation process. The maturation pattern in the $\Delta pmt2$ mutant is also what was to be expected, as there was no translocation

delay, since the detected Mid2 form presents an higher molecular weight than the untranslocated form (seen in lane 3 and 4, at around 30 kD), which indicates the presence of some post-translational modifications. However, it is still very far from its full matured weight, running at around 40 kD (lane 5 and 6; band F). In the $\Delta she2$ mutant, however, I could observe quite a different pattern (lanes 7 and 8). Although the fully mature form of Mid2 is also detected with intensities comparable to those found in the wild-type, at 20°C I could also detect distinct bands from multiple intermediates (bands B, C, D and E). Nevertheless, such maturation-intermediary pattern does not show either an accumulation of the cytosolic Mid2 form or any other band seen in the *sec61-32* background. Therefore, no correlation between Sec61 and She2 interaction and translocation can be established.

Although She2 presented itself as a strong candidate for Sec61-direct interaction detection, none of the approaches used led to confirmation of a functional role of an interaction. This analysis is being continued in Prof. Jansen's lab, who are investigating the effects of a number of *sec61* mutants on a She2-mediated mRNA targeting to the bud.

2.6.1.2 Asi3

To further probe the potential interaction of Sec61 with Asi3, a functional assay was established. Asi3 has been previously described as part of a nuclear complex (Asi complex) involved in INM protein quality control, promoting the degradation of functional regulators of sterol biosynthesis [102]. Its presence as a potential Sec61 interactor was surprising, but interesting. Several substrates, as Erg11 and Nsg1, have been described as Asi3-dependent for their degradation [102]. I thought that evaluating the degradation dynamics of some of those substrates on the strongest known

ERAD-defective *sec61* mutant (*sec61-32* when grown at 30°C) might give some hints about the overlapping of these two pathways. If any of the Asi3 substrates degradation was also Sec61 dependent, then the probability of the Asi3 interaction with Sec61 being functionally important was strong. I chose Asi3-dependent substrates Erg11 and Nsg1. I transformed constructs with the HA-tagged versions of both substrates into *SEC61* and *sec61-32* backgrounds, and analyzed their degradation dynamic by both cycloheximide chase and pulse-chase. Due to expression issues, evaluation of the degradation process of Nsg1 was not possible, although some degradation delay in the *sec61-32* background seemed to be seen (Supplemental Figure A.17). Erg11 was well expressed and allowed evaluation of its degradation kinetics. Cells were grown to a maximum OD₆₀₀ of 1 and either pulse-labeled with [³⁵S]-met/cys or incubated in the presence of cycloheximide (protein-biosynthesis inhibitor) [141].

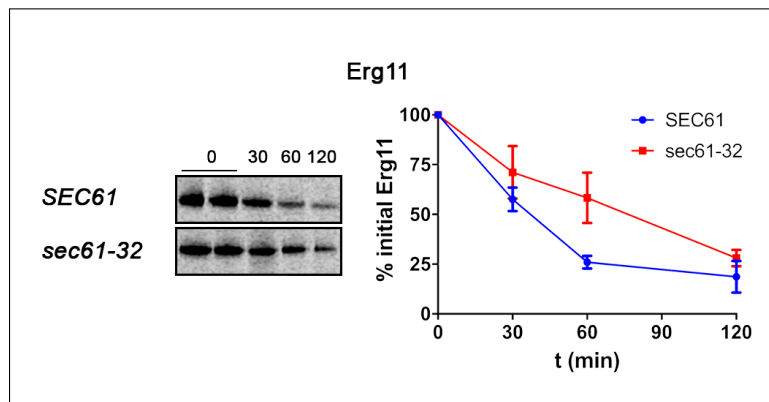


Figure 2.36: Erg11 degradation dynamics analysis. wild-type and mutant strains were pulse-labeled with [³⁵S]-met/cys for 15 min, followed by chase incubations for the indicated times. For each time point 1.5 OD₆₀₀ of cells were lysed and proteins immunoprecipitated using an anti-HA antibody (Biomol). After SDS-PAGE, proteins were detected by phosphorimaging. Bands were quantified using ImageQuant (GE Healthcare) and averaged values plotted. At least three replicas were made.

In Figure 2.36 the pulse-chase results are shown. As can be seen, in a *sec61-32* background, Erg11 showed a considerable slower degradation. While in the *SEC61* background, after 60 min, I could detect only ~25 % of the initial Erg11, in the *sec61-*

32 background, after the same period of time 55 % of the initial Erg11 amount was still detected. Erg11 shows an half life of 35 min in the *SEC61* background and an half life of 90 min in the *sec61-32* background.

The data obtained from cycloheximide chase corroborates the effect seen by pulse-chase (Supplemental Figure A.18).

With this Erg11 degradation analysis, I could establish that Erg11 is indeed also dependent on Sec61 for degradation, suggesting that either Sec61 is the exit channel for nuclear proteins as well as for ERAD, or that Asi3-mediated degradation is not restricted to the INM.

2.7 Sec61 Hinge Mutants to Evaluate Function of Sec61-Mpd1 Interaction

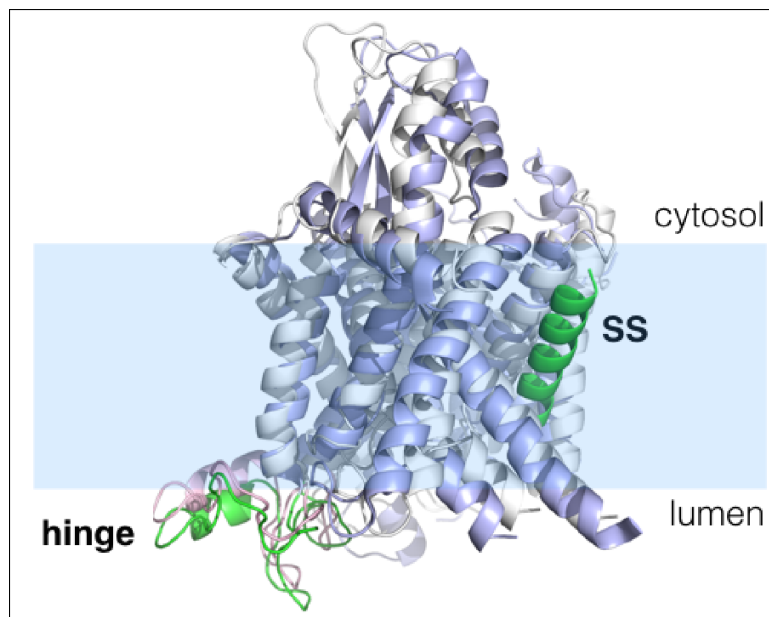


Figure 2.37: Structure of Sec61 channel in closed and opened state. Structure of the Sec61 channel in closed (grey helices, pink hinge) versus open state (blue helices, green hinge, green signal sequence (SS) inserted in lateral gate) (Voorhees and Hegde, 2016) (PDB 3J7Q, PDB3J7R). Note conformational changes in hinge (pink vs green) during channel opening.

My xQuest/xProphet analysis of crosslinked peptides suggested a direct interaction of Mpd1 C59 with K209 in luminal loop5 of Sec61 which constitutes the hinge region around which the N-terminal half of Sec61 swings during channel opening (Figure 2.37) [217, 423]. Comparison of Sec61 loop5 with SecY loop5 of bacteria and archaea by my collaborator, Prof. Ian Collinson (School of Biochemistry, University of Bristol) revealed a substantial extension of loop5 in eukaryotes, which in turn includes the crosslink site of Mpd1 (Figure 2.38, upper panel).

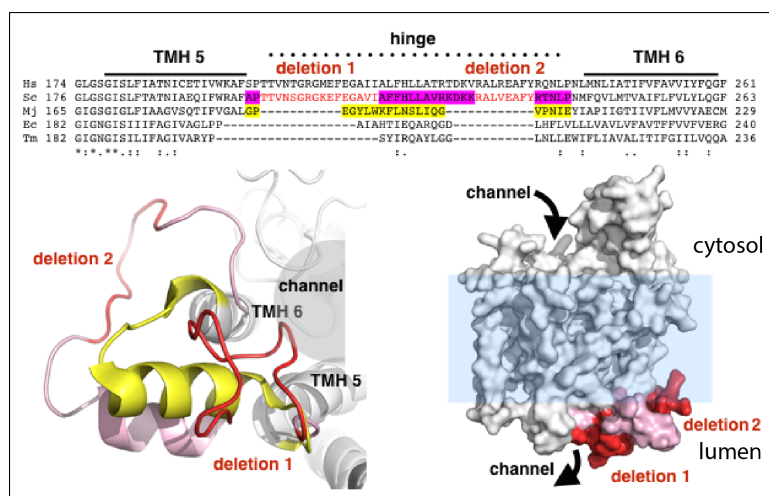


Figure 2.38: Alignment of loop 5 hinge region Top: Alignment of loop5 hinge sequences of eukaryotes (*Homo sapiens*, Hs; *Saccharomyces cerevisiae*, Sc), prokaryotes (*Escherichia coli*, Ec; *Thermotoga maritima*, Tm) and archaea (*Methanococcus jannaschii*). Protein sequences were obtained from Uniprot. Regions coded by deletions in our *sec61* mutants are shown in red. The sequence forming the archaeal hinge region is highlighted in yellow, and the sequence corresponding to the vestigial (post-deletion) eukaryotic counterpart is highlighted in magenta. Bottom left: view of the hinge from the ER lumen (eukaryotic - PDB 3J7Q), showing the protein channel lined by TMHs 5, along with 6 and the intervening hinge (pink) with deletions 1 and 2 in red. The deletions result a shorter hinge akin to the archaeal structure shown in yellow (PDB 1RHZ) (also see middle). Bottom right: space-filling model of Sec61 channel (PDB 3J7Q) in ER membrane indicating positions of deletions 1 and 2. Note that the region deleted in *sec61del1* is accessible for luminal proteins in contrast to *sec61del2* which faces the membrane (lower right).

I hypothesized that the eukaryotic extensions in loop5 might serve as docking sites for ERAD factors to facilitate opening of the Sec61 channel for the lumen for export of ERAD substrates. To test this hypothesis I deleted sections of the Sec61 hinge including the Mpd1 contact site to create a smaller vestigial hinge within Sec61, similar

to the SecY counterpart (Figure 2.38, top and bottom), and investigated the effects on protein transport into the ER and ERAD.

2.7.1 Sec61 Hinge Deletion Mutant Construction

To generate the Sec61 hinge mutant strains, the *SEC61* gene had to be edited. To this purpose a scheme was designed where PCR-driven overlap extension (SOE PCR) was used to delete the target regions indicated in red in Figure 2.38 [3, 164].

During SOE-PCR, overlapping gene fragments are generated. These overlapping fragments will, upon annealing of the homologous regions, generate a continuous unit, that is used as template in a new PCR reaction, generating the fused (full-length) product. By choosing appropriate internal primers that overlap and flank the mutagenesis-targeted sequence, one can either delete, add or exchange a given sequence. The intermediate fragments can then be fused together in a final PCR using flanking primers [164, 161].

The loop5 hinge *sec61* mutants were generated as follow. For the initial SOE-PCR reactions, *SEC61* was amplified from pBW11 [397] (pRS315-*SEC61*;CEN; *LEU*). Deletion 1 and deletion 2 were made separately. Deletion 1/2 was made using deletion 1 construct as template and same primers as used for the generation of deletion 2. For SOE-PCR, the regions upstream and downstream of the deletion sites were amplified using a mutagenic primer and a gene flanking primer. Each mutagenic primer immediately flanks the deletion site and both upstream and downstream deletion-flanking primers have a stretch of complementarity with each other (20 bp) (Figure 2.39 A, bottom panel). After this first round of PCR, products were resolved in a 1 % agarose gel, to both clean and confirm the size of the PCR products (Figure 2.39 B).

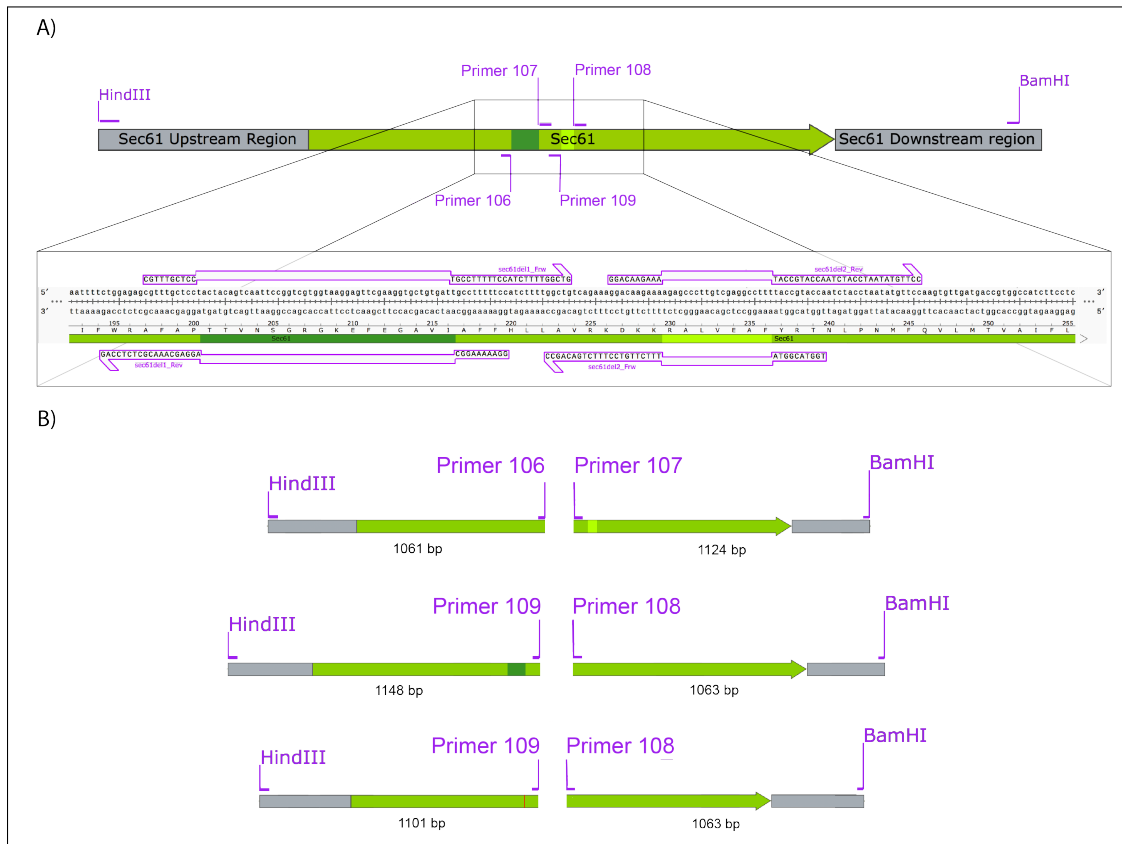


Figure 2.39: Hinge mutants construction scheme. Scheme depicting the strategy used for deletion of the desired loop 5 stretches in order to generate desired Sec61 hinge mutants. Coding region shown in leaf-green. Upstream and downstream regions shown in grey. **A)** Scheme illustrating the Sec61 ORF, with the regions to be deleted highlighted (del1 dark green, del2 light green) as well as the primers used for this purpose. Bottom representations shows a zoom-in of the interest region. **B)** Scheme representing the different fragments originated by SOE-PCR and which ligation originated the desired *sec61del1* (top), *sec61del2* (middle), and *sec61del1/2* (bottom) mutants.

After gel fragment isolation, equal amounts of complementary fragments were used as template for the final amplification with the gene-flanking primer-pair (Primer 64 and 16). Product size was confirmed (Figure 2.40 A) and fragments were then digested HindIII/BamHI, as was the pRS315 vector. Each mutant gene (*sec61del1*, *sec61del2*, and *sec61del1/2*) was ligated into the digested pRS315 (Figure 2.40 B). Positive clones were confirmed by sequencing.

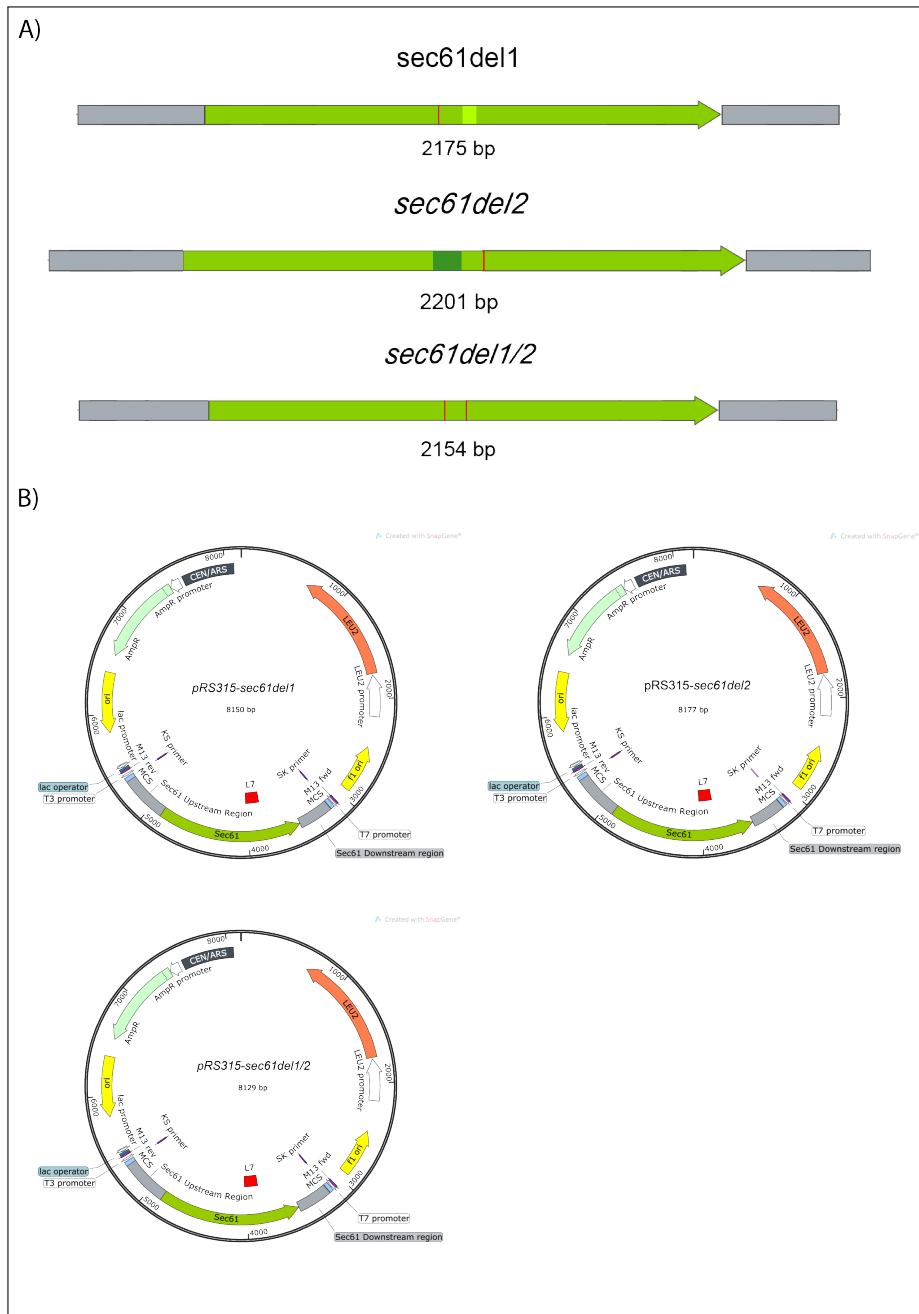


Figure 2.40: Hinge mutants constructs scheme. Scheme depicting the generated *sec61* hinge mutants. *sec61del1* (top), *sec61del2* (middle), and *sec61del1/2* (bottom). **A** Scheme of the fragments generated after ligation of the SOE-PCR generated fragments. **B** Maps of the constructs obtained by cloning of the generated *sec61* mutants into pRS315. pRS315-*sec61del1* (top), pRS315-*sec61del2* (middle), and pRS315-*sec61del1/2* (bottom)

Correct pRS315-*sec61del1*, pRS315-*sec61del2*, and pRS315-*sec61del1/2* were then transformed into KRY461 (*SEC61::HIS* pGAL-*SEC61-URA3*). Transformants were first selected on SC -*URA*-*LEU* medium containing 2% (w/v) galactose and 0.2% (w/v) glucose. The *pGal-SEC61* plasmid shuffle was done on SC 5'-*FOA* plates lacking leucine. Expression of the mutant proteins was confirmed by immunoblotting (Figure 2.41).

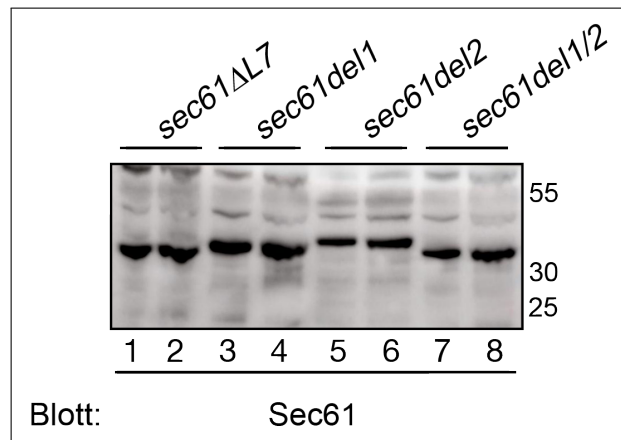


Figure 2.41: Hinge mutants correct expression test. Cells from all the generated hinge mutants (*sec61del1*, *sec61del2*, and *sec61del1/2*), in addition to cells from the *sec61ΔL7* mutant (mutant lacking entire loop 7) [397] were grown in YPD (2% Glu) liquid medium to a maximum OD_{600} of 1, and equal amounts (0.4 OD_{600}) were analyzed by SDS-PAGE on 4-12% Bis-Tris gels (NuPAGE® Novex® Pre-Cast gels, Invitrogen). Protein detection was done by Western Blotting using the Sec61 specific antibody and signal acquired by the Amersham Imager 600 (GE Healthcare).

In the immunoblot shown, the Sec61 Δ L7 form runs at around 35 kDa (lanes 1 and 2), being in accordance with previously seen gel mobility (Section 2.1). With approximately the same mobility, the Sec61del1/2 form was also detected in lanes 7 and 8. In lanes 3 and 4, the Sec61del1 form can be seen at around 37 kD and, showing a slightly lower mobility in gel, the Sec61del2 form in lanes 5 and 6 at around 39kD. In this fashion, I confirmed that the *sec61* mutants forms were being expressed and that their observed gel mobilities were congruent with what was expected from the hinge mutants.

2.7.2 Sec61 Hinge Deletion Mutant Characterization

To determine how the deletions in the loop 5 hinge region affected the cell, the hinge mutants were submitted to a battery of tests.

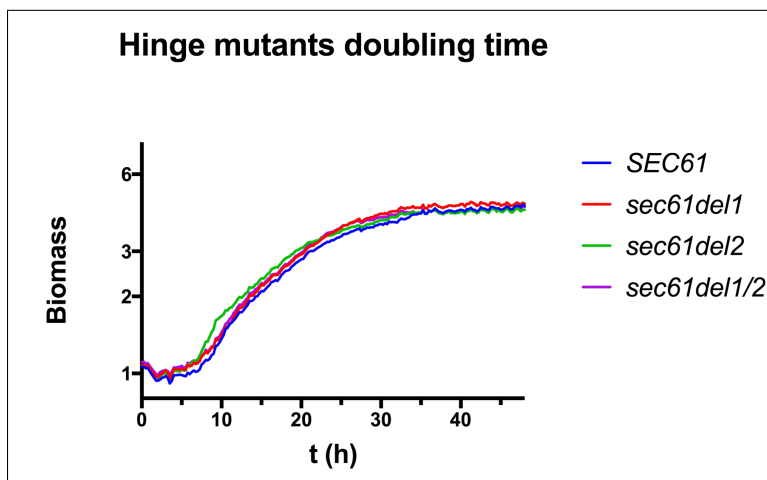


Figure 2.42: Growth rate of *sec61* hinge mutants. Cells were grown overnight in YPD (Gal 2%, 0.2% Glu), diluted to an OD_{600} of 0.02 and 1 ml of culture applied per well (5 x 1 ml per strain) in a FlowerPlate. The plate was then incubated in the microreactor Biolector at 30°C, with 1200rpm, 85% humidity and 20.95% O₂, for 24h. Calibration was done at 320nm, and biomass determination at 620nm using Filter 15. Readings were done every 15 min. In the figure, the plotted results (after averaging) are shown.

I started by evaluating the growth dynamics of the hinge deletion mutants. To this end, overnight grown cultures (YPD, 2% Glu) of *SEC61* (KRY897), *sec61del1* (KRY1116), *sec61del2* (KRY1117) and *sec61del1/2* (KRY1118) were diluted to an OD_{600} of 0.02 (also in YPD, 2% Glu), applied to a Biolector Flower plate (1 ml per well, 12 wells per strain), and grown for 48h in the microbioreactor BioLector, monitoring the biomass (measured at 620nm) at every 15 min (Growth at 30°C, with a shaking of 1200 rpm, 85% humidity and 20.95% O₂). The specific growth curve for each strain can be seen in Figure 2.42.

As can be seen, the hinge mutants show a growth dynamic similar to the wild-type, presenting a growth curve that overlaps almost completely with that of the *SEC61*

background (Figure 2.42).

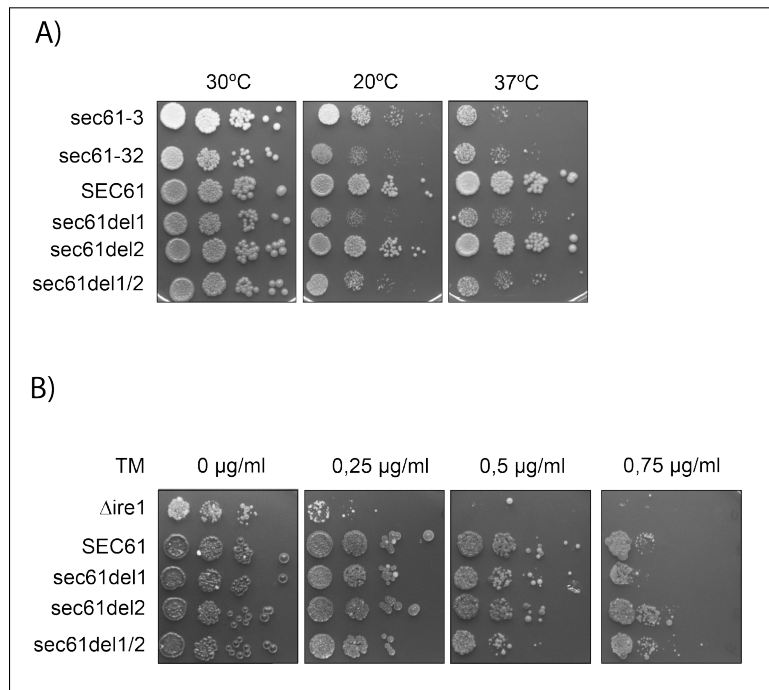


Figure 2.43: Temperature and tunicamycin sensitivity of *sec61* hinge mutants strains. Cells were grown overnight in YPD, counted using a Neubauer chamber and sequentially diluted (10^4). Samples of each dilution ($5 \mu\text{l}$) were then plated side by side, in solid YPD (2% Gal / 0.2% Glu) and grown for at least 3 days. Each set was replicated 3 times in different plates. **A)** Plates for temperature sensitivity were incubated at 20, 30 or 37 °C (one replica per temperature). **B)** For tunicamycin sensitivity, all plates were grown at 30 °C, but three of the plates were supplemented with either 0.25, 0.5, or 0.75 $\mu\text{g/ml}$ of Tunicamycin, respectively.

I also screened these mutants for either cold, heat or tunicamycin sensitivities, as done in previous strain characterizations (Section 2.4.2 and 2.6.1). Cells from wild-type and hinge mutants (together with the appropriate control for each of the assays) were grown overnight, cells counted using a Neubauer counting chamber, sequential dilutions (10^4 - 10^1) prepared and plated in either solid YPD, for temperature sensitivity tests and control conditions of tunicamycin sensitivity test, or in solid YPD supplemented with tunicamycin (0.25, 0.5 or 0.75 $\mu\text{g/ml}$) for the tunicamycin sensitivity assay.

As can be seen in Figure 2.43 A, while deletion1 caused temperature- (right panel) and cold-sensitivity (middle panel) alone and in combination with deletion2, deletion 2 by itself did not affect growth at any of the tested temperatures. As for tunicamycin sensitivity, both the deletion1 and deletion1/2 mutants were mildly affected by the presence of tunicamycin (both 0.25 and 0.5 $\mu\text{g/ml}$) (Figure 2.43 B). At 0.75 $\mu\text{g/ml}$ the tunicamycin effect was more striking, despite its effect being also stronger in the wild-type. Overall, the deletion1 mutant was more sensitive to tunicamycin than the deletion1/2, suggesting that deletion 2 compensates for part of the defect observed in deletion1.

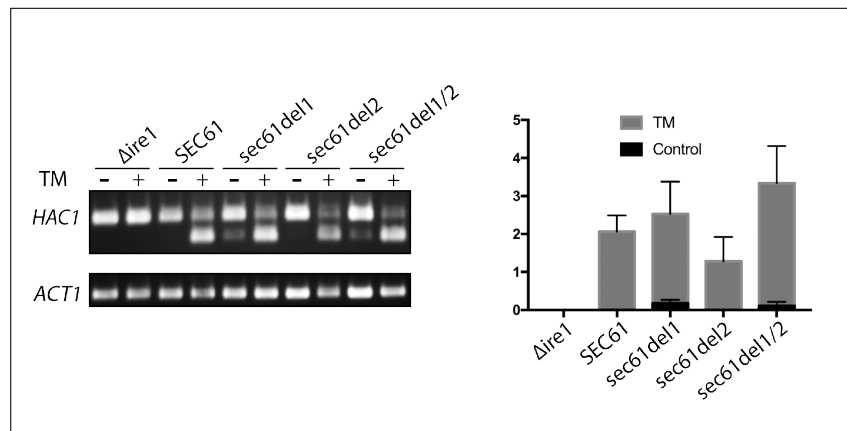


Figure 2.44: UPR activation in the *sec61* hinge mutants. To this end, wild-type and mutant strains were grown in minimal medium to a maximum OD_{600} of 1 at 30°C, 220rpm and incubated for 3 h in either the presence (+) or absence (-) of 200 $\mu\text{g/ml}$ of tunicamycin (30°C, 220rpm). Total RNA (0.1 μg) retrotranscribed to cDNA by RT-PCR using MaximaRT and a Oligo(dT18)-dT primer. The resulting cDNA (1 μg) was subjected to quantitative PCR with a set of primers targeting *HAC1* to monitor the UPR. PCR fragments derived from *HAC1_u* mRNA (*HAC1_u* = uninduced; ~ 720 bp) and *HAC1_i* mRNA (*HAC1_i* = induced; ~ 470 bp) are indicated. Primer for *ACT1* were also used with same cDNA to serve as a loading control. Samples were resolved on a 1% agarose gel.

To probe the proteostasis in Sec61 hinge mutants, I also analyzed their UPR induction by monitoring *HAC1* mRNA splicing. Cells were grown in the presence and absence of tunicamycin, total RNA was extracted, converted to cDNA, and the *HAC1* mRNA splicing induction probed by quantitative PCR (Figure 2.44). The results of this analysis were congruent with those from the tunicamycin sensitivity test, in which

a mild UPR induction was seen in deletion1 and deletion1/2 mutants (Figure 2.44 *versus* Figure 2.43). Interestingly, the basal UPR induction (in the absence of tunicamycin) in the deletion1 mutant was stronger than the one observed in the deletion1/2 mutant (grey columns), although the UPR induction in the presence of tunicamycin was weaker. It should also be noted that deletion2 mutant seems to display a lower basal UPR induction than even the wildtype. This is in congruence with the slightly lower sensitivity shown by the deletion2 mutant in comparison to the wild-type when in the presence of 0.75 $\mu\text{g/ml}$ of tunicamycin (Figure 2.43 B).

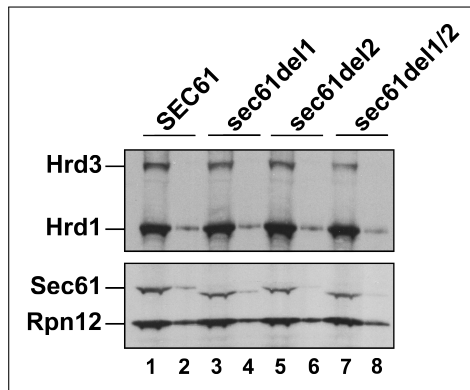


Figure 2.45: Protein steady state levels. Determination of the steady state levels of Sec61, Hrd1 and Hrd3 in the different *sec61* hinge mutants backgrounds. Cells were grown to a maximum OD₆₀₀ of 1 in YPD (2% Glu) and 0.5 and 0.1 OD₆₀₀ of each background was loaded side by side on an acrylamide gel and resolved by electrophoresis. Protein was detected by Immunoblotting using either Sec61, Hrd1 or Hrd3 specific antibodies. Rpn12 was used as loading control.

Two important points in the characterization of the *sec61* mutants are the expression level of the mutant proteins and, of course, whether they cause any defect on protein import into the ER. To address the first point, I evaluated the steady state level of Sec61 in all hinge mutants (Figure 2.45, bottom slice). In addition, to avoid criticism about potential indirect effects of the hinge mutants on ERAD by affecting Hrd1 and Hrd3 biogenesis, the steady state levels of both Hrd1 and Hrd3 were determined (Figure 2.45, top slice). I did both analysis by quantitative immunoblotting. Cells of

the different backgrounds were grown to a maximum OD of 1 in YPD (2% Glu) and 2 different amounts (0.5 and 0.1 OD₆₀₀) of each strain (*SEC61*, *sec61del1*, *sec61del2* and *sec61del1/2*) were resolved by SDS-PAGE and revealed using specific antibodies against the target proteins (Sec61, Hrd1 and Hrd3). Rpn12 was used as loading control.

As is shown by the results in Figure 2.45, steady-state expression levels of all Sec61 hinge mutants were like wild-type, as were the steady state levels of both Hrd1 and Hrd3, showing that they were expressed equally in wild-type and mutant cells.

To evaluate the ER-import capability of these strains, two different translocation reporters were used, as done previously (Section 2.6.1): pDPAPB and pp α F. Cytosolic precursors can only be detected when an import defect is present. While pDPAPB is co-translationally imported into the ER, pp α F is imported post-translationally. As can be seen in Figure 2.46, both pDPAPB and pp α F can only be detected in the *sec61-32*, which has a known import defect when grown at 20°C. Thus none of the hinge mutants displayed any defect in co- or post-translational protein import into the ER.

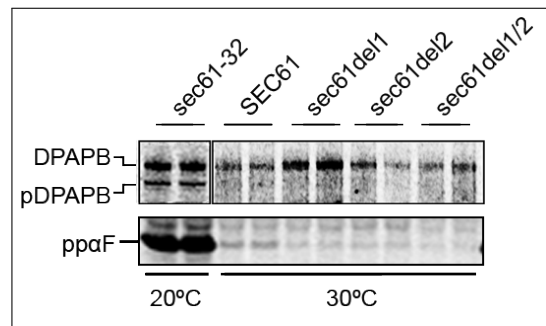


Figure 2.46: Analysis of ER import in *sec61* hinge mutants. Early log-phase cells were pulse labeled with [³⁵S]-met/cys, lysed, and DPAPB (upper; cotranslational import) or prepro alpha-factor (pp α F) (lower; posttranslational import) immunoprecipitated. Starving and labeling were done at 30°C for all strains, except for *sec61-32*, which was incubated at 20°C. Labelling was done for 5 min for pp α F and 15 min for DPAPB. Proteins were detected by phosphorimaging.

As both the *sec61del1* and *sec61del1/2* showed only a moderate tunicamycin-

sensitivity (Figure 2.43) and slightly induced UPR (Figure 2.44), ER-proteostasis was not dramatically compromised in the mutants excluding gross ERAD defects.

Lastly, I set to evaluate the ERAD capacity of the characterized mutants. To do so, I analysed the ERAD dynamics of several well established ERAD substrates: KWW, KHN, p Δ g α F and CPY*.

The ERAD substrate KWW is, as described before, a chimeric integral membrane protein [406, 407]. The luminal domain of KWW, KHN, consists of the signal sequence of *S. cerevisiae* Kar2 fused to the Simian Virus 5 HA Neuraminidase ectodomain. KWW is misfolded in the luminal domain (KHN) leading to its degradation via the ERAD-L pathway [407]. Both proteins are disulfide-bonded. Prior to pulse-chase experiments, the strains were transformed with either the plasmid containing the gene encoding KHN (pSM70, CEN/URA) or KWW (pSM101, CEN/URA). Both forms have a triple HA epitope tag [406].

To evaluate the dynamics of these substrates, cells of wild-type and hinge mutants strains were grown to a maximum OD₆₀₀ of 1, pulse-labeled for 15 min with [³⁵S]-met/cys and chased for the indicated periods. Proteins were then immunoprecipitated with an anti-HA antibody (Biomol), resolved by SDS-PAGE, and signal acquired by phosphorimaging. Band intensities were quantified using the ImageQuant software (GE Healthcare) and relative intensities plotted (GraphPad Prism).

As is obvious in the results shown in Figure 2.47, neither KHN (A; soluble) nor KWW (B; transmembranal) showed significant ERAD defects in any of the Sec61 hinge mutants.

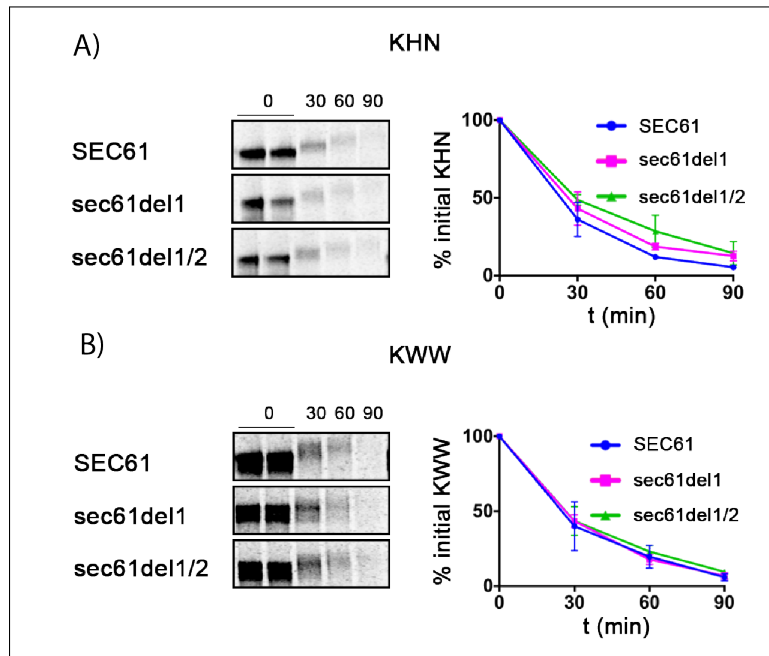


Figure 2.47: KWW and KHN ERAD dynamics determination. The *sec61* hinge mutants were screened for ERAD defects for KWW and KHN. wild-type and mutant strains were pulse-labeled with [³⁵S]-met/cys for 15 min followed by chase incubations for the indicated times. For each time point 1.5 OD₆₀₀ of cells were lysed and proteins immunoprecipitated using specific antibodies against anti-HA. After SDS-PAGE on 4-12 % Bis-Tris gels (NuPAGE® Novex® Pre-Cast gels, Invitrogen), proteins were detected by phosphorimaging. Bands were quantified using ImageQuant (GE Healthcare) and averaged values plotted. For each experiment, at least three replicas were made. **A)** KHN ERAD dynamics. **B)** KWW ERAD dynamics.

Two additional ERAD substrates were also tested: Δ gp α F and CPY*.

The Δ gp α F is a soluble, unglycosylated ERAD substrate, that does not require ubiquitylation for degradation [142, 326, 433]. As the wild-type pre-pro- α -factor (pp α F), the mutant α -factor precursor (p Δ gp α F, ~18 kDa), is efficiently imported into the ER and its signal sequence cleaved [240]. The resulting Δ gp α F (~16 kDa) is an ERAD substrate [54, 238, 240, 437]

For pulse-chase experiments, the *sec61* mutants (*sec61del1*, *sec61del2* and *sec61del1/2*) and the corresponding wild-type (*SEC61*) were transformed with the expression plasmid p416p Δ gp α F (CEN, URA3) carrying a gene encoding p Δ gp α F.

CPY*, a soluble, glycosylated secretory protein that is translocated posttranslation-

ally into the ER [201, 258] was also analyzed. CPY* is a model ERAD (ERAD-L) substrate, being retrotranslocated into the cytosol and degraded by the 26S proteasome [158, 206]. It has multiple disulfide bonds and its ERAD is dependent on reduction of these by Pdi1 [120]. In addition, its ERAD depends on Mpd1 [131], but its exact role is unclear.

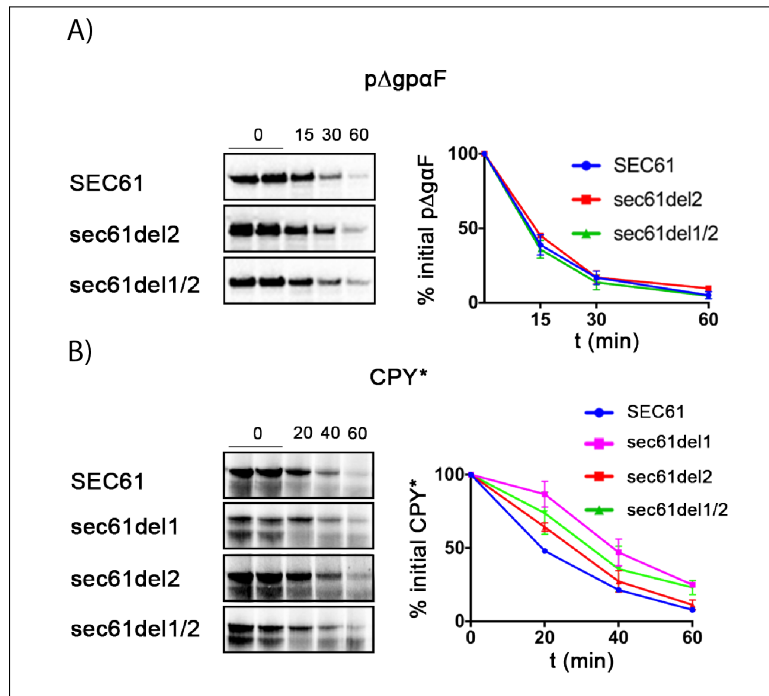


Figure 2.48: $\Delta gp\alpha F$ and Cpy* ERAD dynamics determination. The sec61 hinge mutants were screened for ERAD defects for $\Delta gp\alpha F$ and Cpy*. Wild-type and mutant strains were pulse-labeled with [^{35}S]-met/cys for 5 min followed by chase incubations for the indicated times. For each time point 1.5 OD₆₀₀ of cells were lysed and proteins immunoprecipitated using specific antibodies against either pp αF or CPY. After SDS-PAGE on 4-12 % Bis-Tris gels (NuPAGE® Novex® Pre-Cast gels, Invitrogen), proteins were detected by phosphorimaging. Bands were quantified using ImageQuant (GE Healthcare) and averaged values plotted. For each experiment, at least three replicas were made. A) $\Delta gp\alpha F$ ERAD dynamics. B) CPY* ERAD dynamics.

To analyse the ERAD dynamics of those two substrates, cells of wild-type and Sec61 hinge mutants strains were grown to a maximum OD₆₀₀ of 1, pulse-labeled for 5 min min with [^{35}S]-met/cys and chased for the indicated periods. Proteins were then immuoprecipitated with specific antibodies against either pp αF or CPY, resolved

by SDS-PAGE, and signal acquired by phosphorimaging. Band intensities were quantified using the ImageQuant software (GE Healthcare) and relative intensities plotted (GraphPad Prism).

While the ERAD of $\Delta gp\alpha F$ was unaffected in all Sec61 hinge mutants (Figure 2.48 A), this was not true for the CPY* ERAD (Figure 2.48 B). In Figure 2.48 B, it can be seen that CPY* degradation is compromised in *sec61del1*, which lacks the contact site for Mpd1 (Figure 2.48 B, magenta). In contrast, *sec61del2* barely affects CPY* degradation (Figure 2.48 B, red). The *sec61del1/2* mutant has an intermediate phenotype (Figure 2.48 B, green).

My data suggests that the Sec61 hinge mutants do not have a general ERAD defect, but that the mutant lacking the Mpd1 contact site is specifically defective in ERAD of the substrate whose degradation requires Mpd1 (CPY*).

2.8 Mpd1 interaction

To verify the direct interaction between Sec61 and Mpd1, and the influence of the Sec61 hinge mutants on the interaction, I had to establish a setup that permitted the crosslink and detection of such interaction. One of the problems was my ability to detect Mpd1. Since no specific antibody against it was available, the option presented was of tagging Mpd1 in an effort to have a detection method.

2.8.1 MPD1 HA tagging

For the purpose of tagging Mpd1, I decided to take advantage of a PCR-based tagging setup described in Janke et al. [177], which permits a versatile way of editing yeast genome. It allows easy C- or N-terminal tagging or even gene deletion.

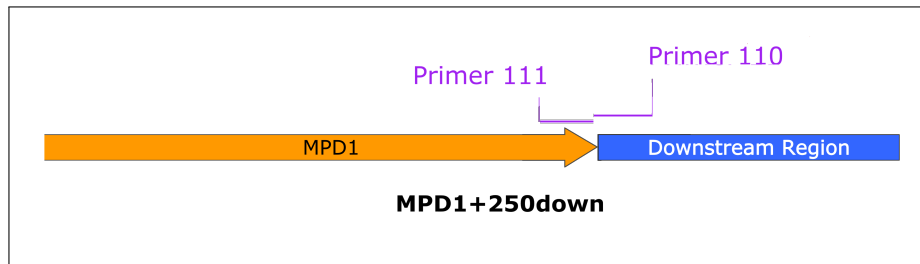


Figure 2.49: *MPD1* gene scheme. Schematic representation of the *MPD1* coding region, including 250bp downstream. The priming regions of the primers used for the latter amplification of the gene HA-tagging cassette and their nomenclature are also represented in the scheme.

I designed two primers (Primer 110 and Primer 111). Primer 111 had homology with the final extension of the target gene (49 bp - excluding the STOP codon; Figure 2.49, in orange) and with the tagging cassette's upstream adaptamer. Primer 110 had homology with the STOP codon and downstream region of the target gene and with the tagging cassettes's downstream adaptamer (50 bp, Figure 2.49, in blue).

The tagging cassette was then amplified from the template plasmid pYM24 (kindly supplied by Dr. Michael Knop) using the above described primers as is schematized in 2.50 A. The adaptamer region of the primers is depicted in grey.

The PCR product was directly used for transformation (Figure 2.50 B). Since the tagging cassette possessed the hphNT1 resistance marker, transformants could be selected on hygromycin supplemented solid YPD. Transformants were then confirmed both by gene amplification and sequencing and by expression test. I was able to have integrants, but the endogenous expression of Mpd1 was so low that its detection was quite difficult (data not shown). Since I needed a setup with high sensitivity in order to allow the determination of an effective interaction of Sec61 and Mpd1, such system was sub-optimal.

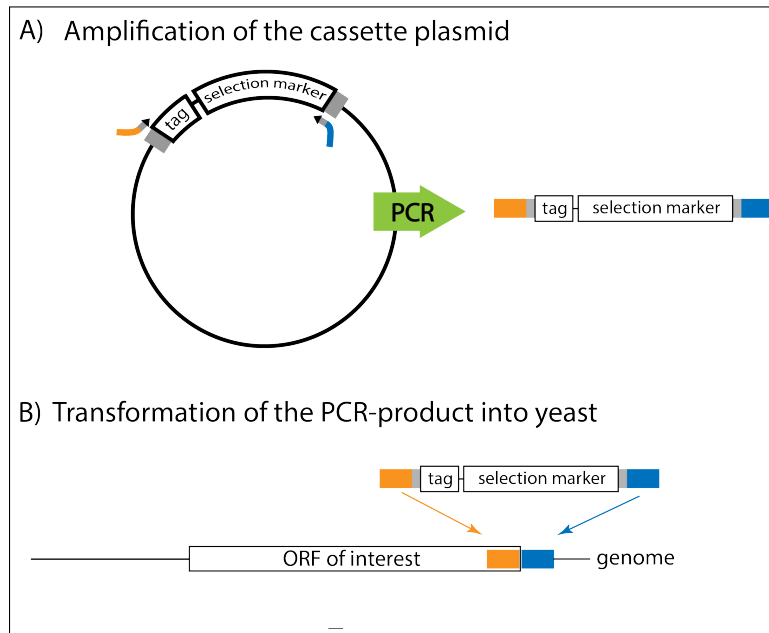


Figure 2.50: MPD1 HA-tagging cassette. Schematic representation of the MPD1 HA-tagging process adapted from [177]. **A)** primers 110 (orange) and 111 (blue) were used in a PCR reactions using as template a plasmid containing the cassette with the HA-tag and a selection marker (*hph*). These primers allow amplification of the cassettes as well as the targeting of the respective PCR product to the desired genomic location. **(B)** Integration of tagging cassette is possible due to the overhangs provided by the Primers 110 and 111 (color-coded primers in the figure A). The same colors indicate homologous sequences as shown in the representation of the genomic region to be altered. Upon transformation, an integration of the cassettes into the yeast genome occurs due to homologous recombination.

Therefore I decided to subclone the tagged MPD1-HA from the genome into a 2 μ plasmid, and in doing so, increase its expression level, and consequently, my capacity for Mpd1 detection.

For this purpose, gene flanking primers were designed (Primer 114 and 115), and used for the amplification of the tagged Mpd1 from the genomic DNA extracted from a genomically MPD1-HA tagged strain. These primers included, respectively, Sall and EcoRI restriction site, which permitted a directed cloning into Sall/EcoRI digested pRS426 (URA, 2 μ M). After confirming a correct cloning by sequencing, this construct was used to transform a *SEC61* strain (KRY897), and also the hinge mutants (KRY1116, KRY1117, and KRY1118). After confirming Mpd1-HA expression and detectability, I

had the conditions to proceed with functional studies.

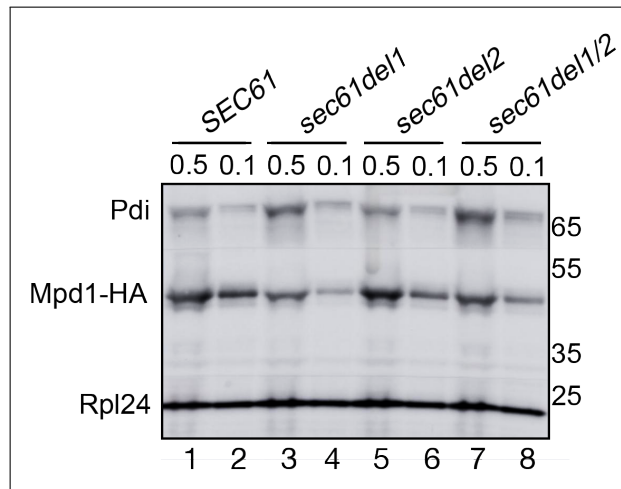


Figure 2.51: Mpd1-HA expression test Analysis of the expression of the tagged form of Mpd1 by Immunoblot. wild-type and hinge mutant cells were grown to a maximum OD₆₀₀ of 1, and equal ODs (0.5 and 0.1) were resolved by SDS-PAGE on 4-12 % Bis-Tris gels (NuPAGE® Novex® Pre-Cast gels, Invitrogen). A commercial anti-Ha antibody (Biomol) was used for the Mpd1-HA. Rpl24 was used as loading control. A specific antibody against Pdi was also used.

In figure 2.51 it can be seen that all mutants were not only expressing Mpd1-HA, but also that its steady state level is similar in all backgrounds.

2.8.2 Mpd1 interaction with Sec61

Having generated a background where Mpd1 could be detected, I was in condition to design a setup that might allow the confirmation of a direct interaction between Sec61 and Mpd1.

To directly confirm that Mpd1 interacted with Sec61, and that this interaction was compromised in the *sec61* hinge mutants, I prepared radiolabelled microsomes from wild-type, *sec61S353C* and *sec61* hinge mutant strains expressing HA-tagged Mpd1 and performed sequential immunoprecipitations with Sec61 and HA-antibodies. Briefly, cells were grown to a maximum OD₆₀₀ of 1 in SC minimal medium (Glu 2% / -Leu / -Ura), pulse labeled for 30 min and crosslinked with either SMPH (1 mM), LC-SPDP (1

mM) or SDAD (1.5 mM). SMPH was chosen because the Sec61-Mpd1 crosslinked peptide was first identified by SMPH crosslinking to Sec61S353C. LC-SPDP, like SMPH, has one cysteine- and one NH₂-reactive group, only LC-SPDP is cleavable. Therefore, in this double immunoprecipitation experiment, and under reducing conditions, the free forms of the Sec61 interactors could be detected. Consequently, SMPH is the negative control for LC-SPDP, because there should be no release of Mpd1 from Sec61 after the first precipitation. SDAD is also cleavable, but with one NH₂-reactive and one photoactivatable reactive group. It was used to efficiently crosslink Mpd1 to Sec61 regardless of the cysteine in loop 7. After quenching, samples were solubilized and submitted to two sequential immunoprecipitation. The first immunoprecipitation was done with an anti-Sec61 N-terminal antibody. Saturation of the immunoprecipitations were confirmed (data not shown). After washing and sample reduction with DTT, samples were submitted to a second immunoprecipitation using the anti-HA antibody. Samples were then resolved by SDS-PAGE and signal acquired by phosphorimaging.

In Figure 2.52 it can be seen that no free Mpd1-HA could be detected in any of the control samples (i.e lacking any crosslinker) (lanes 1, 5, 9, 13, and 17) or in any of the SMPH (i.e non-cleavable) crosslinked samples (lanes 2, 6, 10, 14, and 18). Conversely, as seen in the mass spectrometric analysis, in the LC-SPDP crosslinked *sec61S353C*, a band compatible with Mpd1-HA could be detected at around 45 kDa (lane 19). None of the other backgrounds, however, generated such band (lane 3, 7, 11, and 14). Upon SDAD crosslink, the Mpd1-HA compatible band can be detected in all the tested backgrounds (lane 4, 8, 12, 15, and 20). Nevertheless, its intensity is much higher in the *SEC61* and *sec61S353C* backgrounds (lanes 4 and 20), while in the *sec61* hinge mutants backgrounds its intensity is much weaker (lane 8, 12, and

15).

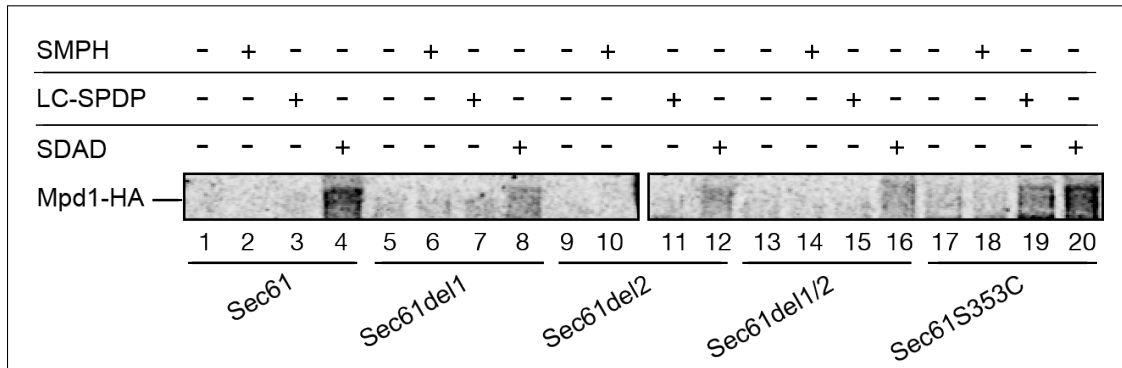


Figure 2.52: Mpd1-Sec61 direct interaction determination. Interaction of Sec61 with Mpd1 was determined by crosslink in [³⁵S]-met/cys-labeled microsomes treated with SMPH (cysteine and NH₂-reactive, non-cleavable), LC-SPDP (cysteine and NH₂-reactive, cleavable) or SDAD (NH₂-reactive and photoactivatable, cleavable) as indicated. For explanations of the crosslinker selection, see Material & Methods. Sec61 and crosslinked proteins were precipitated with anti-Sec61 N-terminal antibodies, followed by reduction of the crosslinker. Subsequently, Mpd1-HA was precipitated using HA-antibodies. After gel electrophoresis, proteins were detected by phosphorimaging. Equal amounts of cells were used for the preparation of each microsomes batch. Protein levels of both Sec61 and Mpd1-HA were similar in all strains. Saturating amounts of antibodies were used for each precipitation.

Collectively, the data suggest that Mpd1 does indeed interact directly with Sec61, and that this interaction is through Sec61 loop 5, since the loop 5 mutations impairs such interaction.

2.9 Genomic Integration of *sec61*ΔL7

In previous work *sec61*ΔL7 (the *sec61* mutant lacking the full luminal loop 7), was shown to have an ERAD impairment, but it also showed some import defects [397]. To understand if the lack of such prominent luminal loop might affect any Sec61 luminal interaction, potentially with ERAD factors, I decided to compare the crosslink pattern of Sec61 *versus* Sec61ΔL7 in my initial work. At the time, the only available mutant strains carrying this mutation were strains where *sec61*ΔL7 was being expressed from a plasmid. I thought that, for future work, the integration of this mutation into the chromosomal DNA of *S.cerevisiae* might contribute to a tighter background.

Therefore I set to generate the above mentioned strain.

For that purpose, I subcloned the *sec61ΔL7* gene from pRS315-*sec61ΔL7* by first digesting the plasmid with BglI. This restriction enzyme cut the vector in three different places: 688 bp upstream of the *sec61ΔL7* ORF, 208 bp downstream of the *sec61ΔL7* START codon, and 2074 bp downstream of the *sec61ΔL7* ORF. This generated three different fragments including a 3144 bp fragment that contained the truncated (lacking the initial -208 bp) *sec61ΔL7* gene. Since the pRS305 (plasmid into which I subcloned *sec61ΔL7*) does not have an available BglI restriction site, an extra blunting step was necessary. To this end, I submitted the BglI digested pRS315-*sec61ΔL7* to an incubation with T4 DNA ligase in the absence of ATP, which resulted in a blunting of the overhang end generated by the BglI digestion. After blunting, I further digested the sample using Sall. The Sall restriction enzyme cuts downstream of the *sec61ΔL7* sequence cloned into pRS315 (including 634 bp of the downstream region of *sec61ΔL7* and 8 bp from the pRS315 plasmid). With this final digestion, I generated a 1705 bp, truncated *sec61ΔL7* gene (*trunc.sec61ΔL7*), with a blunt end and a Sall overhang. Taking advantage of this two ends, I cloned the *trunc.sec61ΔL7* fragment into a SmaI/Sall digested pRS305. After ligation and DH5 α transformation, positive clones were screened by colony PCR and further confirmed by sequencing.

I first tried to integrate the *sec61ΔL7* mutation into an haploid *S.cerevisiae* strain (KRY47). Unfortunately, although many tries were made, I was never able to isolate an integrant. Faced with this challenge, I changed my approach, and tried the integration into a diploid *S.cerevisiae* strain (KRY486), followed by sporulation and tetrad dissection using a MSM Tetrad Dissector (SINGER), with a subsequent characterization of the obtained haploid strains (Figure 2.53).

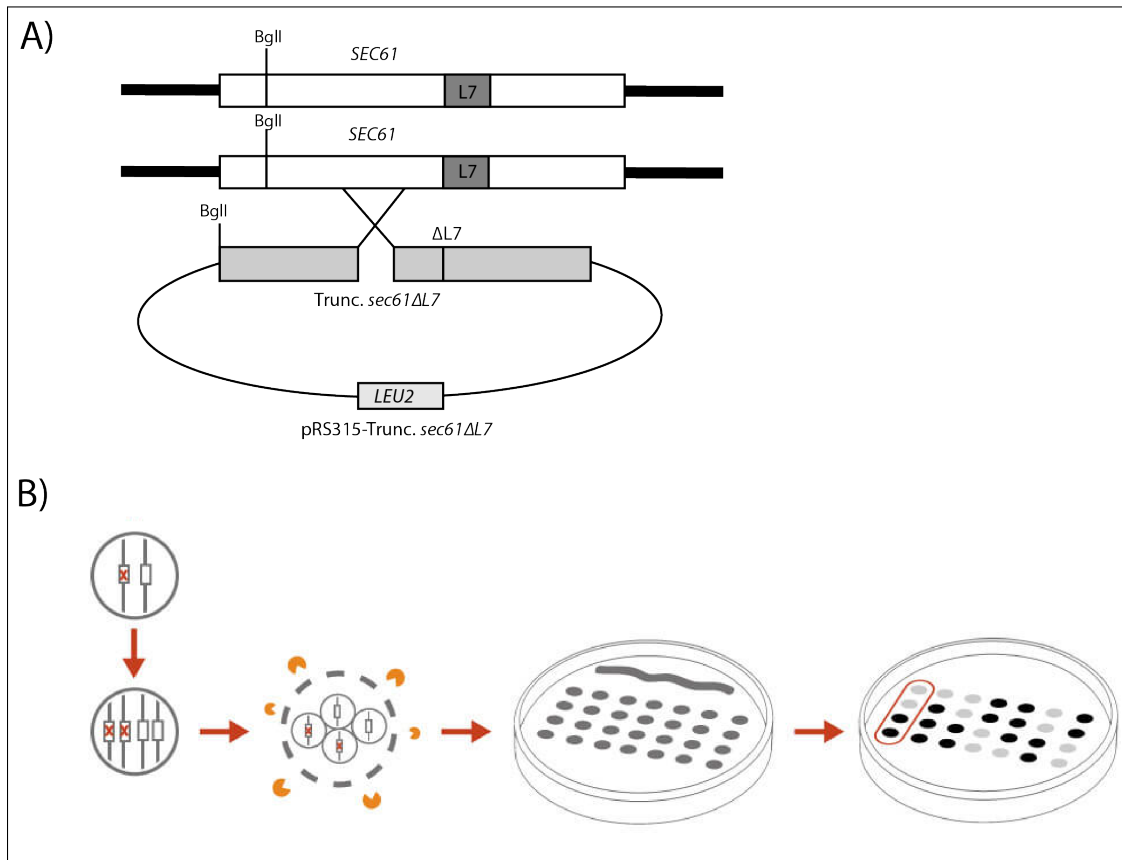


Figure 2.53: Chromosomal integration of *sec61ΔL7*. Schematic illustrating the A) *trunc.sec61ΔL7* integration. B) Sporulation and tetrad dissection process. Figure from www.singerinstruments.com/resource/what-is-yeast-genetics/.

Briefly, integrative vector was linearized, transformed into KRY486 (Figure 2.53 A), and cells selected in solid SC minimal medium (2 % Glu/-LEU). Transformants were then incubated in Sporulation Medium (1% Potassium Acetate / 0.1% Yeast Extract / 0.05% Glucose) for 5 days, tetrads were collected and digested with β -Glucuronidase from *Helix pomatia*. Using a tetrad dissecting microscope (MSM Tetrad Dissector; SINGER) tetrads were dissected and spores gridded as schematized in Figure 2.53 B. To confirm correct integration and expression of our mutant gene, resultant haploid strains were grown overnight in minimal medium, extracts were made and re-

solved by SDS-PAGE. Protein detection was done by Western Blot using a Sec61-specific antibody. Using this approach I was able to isolate one *sec61ΔL7* integrant, as can be seen in Figure 2.54. Here it can be observed that the wild-type Sec61 runs at around 40 kD, as is customary. Sec61 from spores 1-5 and 7 show the same gel migration pattern, showing that all these spores also contain the SEC61 copy of the gene. Spore 6, however, shows a Sec61-specific band at a lower molecular weight, at around 35 kDa, characteristic of Sec61ΔL7 (Section 2.1, Figure 2.1 A)

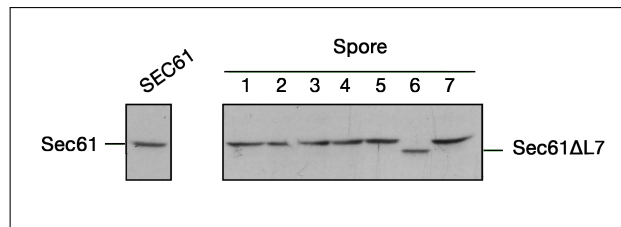


Figure 2.54: Chromosomal integration of *sec61ΔL7*. Immunoblot of spore screen. The wild-type Sec61 can be seen migrating at 40 kD in the wild-type strain, as well as in spore 1-5 and 7. On spore 6, an increased migration of the Sec61 specific band (35 kD) can be easily seen.

It must also be said that to further confirm the correct integration of the *sec61ΔL7* mutation, genomic DNA was isolated, the *sec61ΔL7* was amplified and the fragment sequenced.

This strain was filed and can be used in the future for either crosslink assays or any other purpose (KRY956).

3

Discussion

In the present work I aimed to characterize new Sec61 interactors, both cytosolic and luminal, with special interest in the latter. Sec61 is the pore forming subunit of the ER protein translocation complex. In this role Sec61 interacts closely with Sbh1 and Sss1, the two other components of the Sec61 complex, and is responsible for co-translational translocation [278, 442, 188, 153] (Section 0.2.1). For post-translational translocation to the Sec61 complex joins the Sec63-complex (Sec62, Sec63, Sec71, and Sec72), forming thus the Sec complex [79, 44] (Section 0.2.1). Besides its role in ER protein translocation, Sec61 has also long been one of the candidate retrotranslocons, responsible for transport of ERAD substrates from the ER to the cytosol [289, 288, 120] (Section 0.4.6). Various mutations in the Sec61 protein were reported to impair retrotranslocation and degradation of ERAD substrates like pαF [289, 288, 120], CPY* and Deg1:Sec62ProtA [333], while their anterograde transport into the ER was unaffected [293, 289, 28, 443]. Moreover, blockade of the Sec61 channels with ribosome nascent chain complexes abrogated the retrotranslocation of cholera toxin and amyloid beta-peptide [339, 340]. Also, *SEC61* over-expression alleviates protein import defect during CPY* over-expression in cells unable to induce *SEC61* expression, suggesting Sec61 becomes limiting for import during high export demand [261].

Also supporting the hypothesis of Sec61 involvement on ERAD is the direct interaction of Sec61 with the proteasome [262, 187]. In these studies, a direct interaction between Sec61 and the 19S RP was seen, as well as an impaired ERAD of 19S RP-dependent substrates in *sec61* mutants with decreased affinity for 19S RP [262, 187, 186].

The true identity of the retrotranslocon, however, remains controversial, with Sec61, Hrd1 and Der1 as the three main candidates. All accumulated data seems to suggest that in reality, depending on the substrate and cell conditions, a combination of dif-

ferent elements might work together to form differently structured export complexes [380, 113, 11].

Considerable work has been done before in the effort to identify Sec61 interactors. Thanks to this work we know now of many other Sec61 interactors (Sbh1, Sss1, Sec63, ribosome, SRP, OST complex, etc.) which helped clarify not only Sec61 function and mechanistic action, but also those of other pathways that converge or brush with that of Sec61 [361, 195, 398, 422, 180]. Overall, Sec61 interactors for import are well described. Work in the past, however, has mainly focused on Sec61 cytosolic interactions, or interactions in the protein anterograde import pathway [361, 195, 398, 422, 180]. Here, I undertook an approach that, while not disregarding cytosolic interactions, was focused on new luminal interactions of the Sec61 channel.

In the present work I established a Sec61 chemical crosslink setup (Section 2.1 to 2.3) associated with an affinity purification step (Section 2.4) and mass spectrometry analysis. This setup allowed the identification of several Sec61 interactors as well as multiple candidate interactors (Figure 2.25 and Table 2.4). With data harvested from this setup, I generated specific *sec61* mutants that allowed the identification and characterization of a new luminal Sec61 interaction with Mpd1 (Figure 2.52). Moreover, this interaction seems to be an ERAD-related one, at least for the ERAD substrate CPY* (Figure 2.48 B).

Another interesting interaction reported in this work is the Sec61xAsi3 interaction, that I here established by Erg11 (an Asi3 substrate) ERAD dependency on Sec61.

3.1 Crosslinking Setup

With the objective of identifying Sec61 new interactors I established a crosslinking setup with different crosslinkers. I used DSS (Section 2.1), SDAD (Section 2.2), SMPH

(Section 2.3) and LC-SPDP (Section 2.4.3) to crosslink Sec61 in microsomes *in vitro* and analyzed the resulting Sec61 crosslink pattern. These four different crosslinkers were tested in three different backgrounds: wild-type, *sec61 Δ L7* and *sec61S353C*.

Sec61 Δ L7 is a Sec61 mutant form that lacks the full luminal loop 7 and part of adjacent TMDs (7 and 8) [397]. This mutation causes both ER import and export defects, and a channel distortion that causes Sec61 complex instability [397]. The *Sec61S353C* point mutation, in turn, has a unique luminal cysteine in loop 7. This point mutation induces a conformational change by unfolding the short α -helix of the luminal loop 7, increasing the rigidity of the region [186]. This mutant has no ER import defects, but has a decreased affinity for the 19S regulatory particle of the 26S proteasome, resulting in a specific Δ gpaF ERAD defect, whose export from the ER is dependent on the 19S RP-Sec61 interaction [186].

My initial approach was to crosslink the ER membranes with the above mentioned crosslinkers and detect Sec61-containing complexes by immunoblotting using anti-Sec61 antibodies for protein detection. In all variations of the setup, shifted Sec61-containing bands were detected (DSS:Figure 2.2; SDAD:Figure 2.4; SMPH: Figure 2.8; LC-SPDP:Figure 2.21). By comparing crosslinking patterns obtained when using either a Sec61-specific antibody or antibodies against ER proteins whose molecular weight could account for the detected Sec61-shift, I was able to identify Sec61 interactions with Sss1 (Figure 2.2 B), Sec71 (Figure 2.6) and Sec63 (Figure 2.10 B).

The Sss1 interaction was the most stable of all as it could be detected with all crosslinkers (Figure 2.2 B, 2.4 A, 2.8, 2.21). This interaction was carbonate sensitive (Figure 2.5), which is in accordance to the literature [90]. Moreover, I observed that in the *sec61 Δ L7* background, the Sss1 interaction was impaired. This impairment was observed when crosslinking with DSS (Figure 2.2 A, lanes 2 and 3 versus 5 and 6) or

SDAD (Supplemental Figure A.1 B, lane 3 versus lane 9), but not when SMPH was used (Figure 2.8, lanes 2 and 3). This means that loop 7 deletion either causes an absence or a shift of the amino acids crosslinked by DSS and SDAD. Since loop 7 has no lysines, we know that the DSS crosslinking couldn't be through loop 7, which supported the idea of a distortion. Since SMPH crosslinking of Sec61 Δ L7 to Sss1 is not affected, the amino acids crosslinked here are either in domains that do not move enough to impair crosslinking, or are available for crosslinking due to the conformational change (e.g any of the three natural TMD cysteins of Sec61). Another, simpler, explanation is that SMPH is still able to crosslink to Sss1 despite the distortion just because it is slightly longer than the other two crosslinkers (14.2Å versus 11.4Å and 13.6Å of DSS and SDAD). Nevertheless, this data supports the idea that loop 7 deletion causes a channel distortion that might cause the reported Sec61 complex instability [397].

Interaction of Sec61 with Sec71 was detected when using SDAD (Figure 2.6, lanes 2 and 3 versus lanes 11 and 12). Sec71 identity was supported by Concanavalin A (ConA) complex precipitation (Figure A.3 A, lanes 2 and 3 versus 5), since Sec71 is glycosylated and ConA is a lectin for molecules containing mannose. As Sec71 is an element of the post-translational complex, in which Sec61 is the translocon, such interaction might not be surprising. Before the work of Wu et al. [450] and Itskanov & Park [173], however, very little was known about the interaction of Sec71 with Sec61, or any of other of the elements of the Sec complex. In these works, the authors provided cryo-electron microscopy (cryo-EM) structures of the Sec complex. Although neither of the structures present a perfect coverage of Sec71 and Sec72, when both Sec complex structures are aligned, an almost complete structure of Sec71 and Sec72 can be obtained (Figure 3.1, Sec71 in cyan and teal and Sec71 in bright and dark

green; PyMOL files supplied as Supplement File in the annexed virtual media - i.e USB-stick "Dissertation Supp"- for 3D visualization). As can also be seen in Figure 3.1, both the Sec71 TMD and a cytosolic loop (around amino acid 115-130) are quite close to the TMD4 and the N-terminus (respectively) of Sec61.

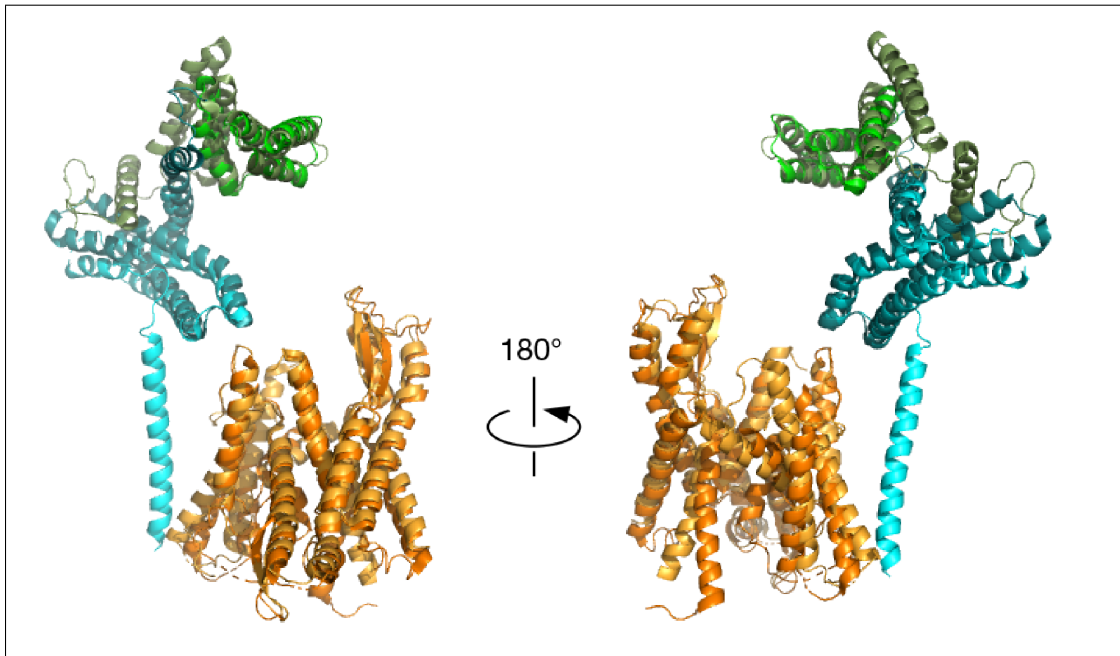


Figure 3.1: Structure of Sec61, Sec71 and Sec72 when in complex. Structures of Sec61, Sec71 and Sec72 reported by Wu et al. [450] (PDB file 6ND1) and by Itskanov & Park [173] (PDB file 6N3Q) where aligned using PyMOL. Sss1, Sbh1 and Sec63 structures were removed for clarity. The structures (i.e Sec61, Sec71, and Sec72) are colored orange, cyan and green in the structure from Wu et al. [450] and yellow, teal and dark green in the structure from Itskanov & Park [173].

This data shows that a crosslink to Sec61 would indeed be possible. Since this information was not available at the time of the experiments, and without other clues to a potential interaction point, I could not pursue this line of research. With the present knowledge, point mutants of both Sec61 and Sec71 could be design and their crosslinking pattern evaluated using my crosslinking setup.

Sec63 also belongs to the Sec complex, where it participates in post-translational translocation. An interaction with Sec61 is therefore, not surprising, perhaps even

less so than Sec71, as Sec61 interaction with Sec63 is known, if not well characterized, for some time [94, 248]. Information about the points of contact between the two proteins were still mainly unknown until recently [450, 173]. Sec63 possesses a luminal J-domain which interacts with Kar2 and it is involved in post-translational import and ERAD [235, 349]. Sec63 interaction was detected in the *sec61S353C* background (Figure 2.8, lanes 8 and 9), but not in *SEC61* (Figure 2.8 lanes 5 and 6) when using a cysteine reactive crosslinker (e.g SMPH). Both Sec61 and Sec63, however, possess other cysteines that could potentially be crosslinked. Sec61 has three natural cysteines (C121, C150 and C373) and Sec63 has seven (C226, C329, C341, C358, C369, C514, C515). Although all of Sec63 cysteines are cytosolic, Sec61 cysteines are localized in TMDs, and consequently, harder to access for crosslinking. The absence of a Sec63 crosslink in the wild-type, suggests that the crosslink is loop 7-cysteine dependent, or at the very least, enhanced, as it could only be strongly detected in the *sec61S353C* background. To further characterize this interaction, different populations of proteins (cytosolic or luminal) were extracted prior to crosslinking by the use of urea or sodium carbonate. The interaction between Sec61 and Sec63 turned out to be carbonate sensitive (Figure 2.9, lanes 2 and 3 versus lanes 10 and 11), indicating that it is either through a luminal partner (since Sec63 is a membrane-protein) or through an extra membrane domain that gets denatured upon carbonate treatment. Since the only luminal loop of Sec63 represents its J-domain, it could be that the interaction detected was through it. We also know that loop 7 cysteine causes an impairment of the affinity of the proteasome for the Sec61 channel [186]. Therefore, it can also be that the enhanced crosslink of *Sec61S353C* to Sec63 is an indirect effect of its impaired 19S RP interaction. If the detected *Sec61S353CxSec63* interaction happens in an ERAD-related role, it could be stabilized or even enhanced

by the accumulation of 19S RP-dependent ERAD substrates. If this would be so, this interaction, as well as this setup, could prove informative. More studies would have to be made to clarify the subject, like screening Sec63 mutants, specifically, J-domains mutants, for Sec61-interaction impairments. Without further data on more precise points of contact, however, I deemed this hard at the time of these experiments. In light of the recent publications [450, 173], however, this could present an alternative line of research.

In further attempt to identify the Sec61 interactors, I applied different immunoblotting approaches. I proceeded with the detection of Sec62, Pdi1, and Kar2 (Figure 2.6 and Figure 2.10 A) but none of these were found crosslinked to Sec61.

I also tried to detect a Hrd3 and Yos9 interaction. This was done by the immunoblotting with specific antibodies (Figure 2.10 A, lanes 3 and 4 versus 15), and by crosslinking in an $\Delta hrd3$ or $\Delta yos9$ background (Figure 2.11 A, lanes 3 and 4 versus 7 and 8). I was unable to detect Hrd3 or Yos9 amongst the Sec61 crosslinked bands.

Lack of an interaction detection however, might not necessarily indicate a lack of interaction. The sensitivity of the immunoblot approach might just not be enough to detect transient or low abundance interactions.

All characterized interactions using this method represented known and relatively stable Sec61 interactions. This bode well for the quality of my crosslinking setup, and on my capacity of crosslinking Sec61 to its interactors. The crosslink setup I established is robust, and could be used in the future to structurally characterize the detected interactions, and perhaps other that were not pursued, after some optimization aiming for a specific target.

For more transient and low abundance interactions, however, this setup was sub-optimal, needing to be associated with downstream steps of enrichment and higher

sensitivity detection for optimization. This can allow detection of more transient and low abundant interactions, that might represent finer steps of Sec61 function and gating control.

From the several variations of the crosslink setup I established, the one that was better targeted for luminal interactions was the SMPH/LC-SPDP based crosslink in the *sec61S353C* background, since the luminal cysteine in this mutant conjugated with the cysteine reactivity of the crosslinker, increased the chances of luminal crosslinks. Consequently, this was the setup that was chosen for Sec61 enrichment and analysis of interactors by mass spectrometry.

3.2 Sec61 Purification

Aiming to achieve sample complexity reduction and Sec61-interactor complexes enrichment, I established a setup for crosslinked-sample purification. This setup required: tagging of Sec61 and Sec61S353C with a 14His-tag; establishment of the crosslink setup in both backgrounds; establishment of a purification setup that allowed Sec61-interactor complex purification.

The *SEC61* and *sec61S353C* genes were tagged by cloning into a plasmid (supplied by Rapaport's lab [380]) that allowed 14His N-terminal-tagging (Figure 2.12). Tagging of the Sec61 N-terminus had already been shown to be possible [289]. The increased size of the tag was used aiming to reduce purification background, as the yeast proteome is rich in histidines. These 14His-tagged constructs were subcloned to a new *CEN* plasmid (pRS315) (Figure 2.14) and construct expression was confirmed (Figure 2.15).

Before proceeding with Sec61 interaction analysis in these backgrounds, the effect of the tagging had to be assessed. These backgrounds displayed doubling times

similar to wild-type (Figure 2.16) and presented no significant temperature nor tunicamycin sensitivity (Figure 2.17 A and B), although a slight UPR induction was detected (Figure 2.18). I also determined the half-life of the 14His-tagged Sec61 forms, which revealed to be much shorter than the wild-type (Figure 2.19). These forms showed a higher initial protein amount when compared to the untagged wild-type form (Figure 2.19, 0 time point), and a quick degradation to levels similar to the observed in the untagged wild-type form (Figure 2.19, 0 to 2h time points). At this point the speed of degradation decreased dramatically, becoming similar to the one observed in the control background (Figure 2.19, 2 to 24h time points). This effect might be due to an higher expression of the tagged constructs, potentially generating a sub-population of Sec61 that does not reach correct membrane topology or does not assemble with Sss1, and suffers quick degradation. Supporting this idea is the fact that steady state levels of the tagged forms are similar to the untagged wild-type form (Figure 2.15).

Besides no significant growth defect or ER protein homeostasis defect being detected, the crosslinking pattern obtained in these backgrounds showed a good overlap with the one obtained in the untagged backgrounds (Figure 2.21 A versus B). Both Sss1 and Sec63 interactions could be detected (Figure 2.21 B, lanes 2, 3, 8 and 9), vouching for the function and stability similarity of the constructs to the untagged counterparts. This showed that this system had potential for the purification of Sec61-crosslinked interactors. Moreover, by resorting to LC-SPDP crosslink, I had a setup in which the crosslinked complexes could be cleaved and the components analyzed individually (Figure 2.21 B, lanes 2 and 3 versus 5 and 6). It must be mentioned that crosslink tests in the *14His-SEC61* background revealed that, unlike the *SEC61* background, some crosslink of Sec63 with His₁₄-Sec61 could be detected (data not

shown), although weaker than in *sec61S353C* or *14His-sec61S353C*. This might indicate that the 14His-tag somehow stabilizes Sec63 interaction. A nonspecific band could also be detected during immunoblotting (Figure 2.21 B, marked with *). This is truly a nonspecific band, obtained with the Sec61 N-terminal antibody, as it appears in blots of both pGal-*SEC61* (Figure 2.4 A, left panel) and *SEC61* backgrounds (Figure 2.4 A, right panel).

The purification process was optimized through a long process, in which different approaches were attempted (Section 2.4.4). In its final version, the setup consisted of solubilizing crosslinked *14His-SEC61* and *14His-sec61353C* ER-vesicles (as well as crosslinker-free samples) and injecting them into an HisTrap column incorporated onto an automated protein purification system (BioLegend LP, Biorad) (Figure 2.23). Sec61 was then eluted along an imidazole gradient (Figure 2.24 A). With this setup I was able to successfully purify Sec61 and its crosslinked interactors in an efficient and clean form (Figure 2.24 B).

This setup could be used in the future, after further optimization, for Sec61 purification in either native or denaturing conditions. If in native conditions, a more biocompatible buffer, like Hepes, should be used instead of Tris, as well as a different pH range. The use of glycerol (instead or in addition to a mild detergent) would also be advisable. For denaturing conditions, the use of minimal amounts of SDS in the buffer may prove beneficial.

Since there is a TEV protease recognition site between the N-terminal His tag and Sec61, an elution by TEV protease digestion might be interesting as it might result in a more specific and clean elution. Size exclusion chromatography (SEC) after IMAC elution might be beneficial for background reduction, since proteins/complexes with molecular weight below 50 kD could be purged, potentially resulting in reduced back-

ground, or even allow an analysis by size range.

Overall, the setup resulted in efficient purification of crosslinked Sec61-containing complexes, with close to maximal Sec61 column binding and a conveniently narrow elution interval. Moreover, Sec63 can be used as marker for process quality control check (i.e crosslink+purification and/or crosslink+purification+cleavage).

3.3 Mass Spectrometry Analysis

Taking advantage of this setup and of the interactions that I was able to characterize by immunoblotting, I crosslinked and purified 14His-tagged Sec61 and 14His-Sec61S353C (Table 2.3), that were then trypsin digested and analyzed by label-free Liquid Chromatography associated high resolution Mass Spectrometry (LC-MS/MS) by Mandy Rettel of the EMBL Core Proteomics Department. The raw mass spectrometry data was processed with MaxQuant (v1.5.2.8) [65] and searched against an Uniprot *Saccharomyces cerevisiae* proteome database. Label free quantitation was used using iBAQ (calculated as the sum of the intensities of the identified peptides and divided by the number of observable peptides of a protein) [347].

For statistical analysis, the raw output data of MaxQuant was processed by Frank Stein, potential batch-effects were removed, the batch-cleaned data was normalized and missing values were imputed. Finally, differentially represented proteins when comparing control conditions (absence of crosslinker) to crosslink conditions (presence of either SMPH or LC-SPDP) were identified. A protein was considered to be enriched if it showed a fold change of at least 3 ($\log_2FC \geq 1.58$). If its false discovery rate (fdr) was smaller than 5 % it was labeled as "hit". If its fdr was lower than 20 % but higher than 5 %, it was labeled as "candidate".

After statistical analysis of the enriched hits on the crosslinked samples, I was able

to identify 361 protein hits that were enriched in the crosslinked samples by at least 3 fold (Figure 2.25; Supplemental File Treated Data.xlsx). After analysis of the enriched hits, I was able to identify a significant number of already reported Sec61 interactors (Figure 2.25 and Table 2.4, blue), including a number of the Sec61 complex subunits (Figure 2.25 and Table 2.4, green).

The variation of patterns between treatments might be due to either the structural differences of SMPH and LC-SPDP or to the structural changes in the loop 7 hinge region, described above. Regarding the structure, SMPH is 1.5 Å shorter than LC-SPDP. This could enable the binding of proteins that experience steric hindrance when using the longer crosslinker, causing a change in the type and number of proteins interacting with Sec61. It could further result in an altered angle at which proteins bind during interaction.

Validating the setup, I found multiple Sec61 known interactors, like the Sec complex subunits (Sec62, Sec71, Sec72, Sss1, but not Sbh1), OST complex subunits (Ost3 and 6, Stt3, Swp1) [226, 428, 334], and almost the full EMC complex. Indeed, recent work has shown that Sec61xEMC interaction is needed for correct topology and insertion of the first transmembrane domain of transmembrane proteins [61]. Moreover, translation and translocation related interactions, like those with Pho88 (or SND3)[9], Srp21, Srp68, Srp101 and Srp102 [180], RPL1B, 22A and 30 were also found. Also vouching for data validity is the fact that the found enrichments did not correlate, in their great majority, with reported cell amounts (Figure 2.27). This indicates that detected enrichments have a high probability of being specific.

When screening the hits for ERAD factors, either reported or postulated, a number of hits stood out: Asi3, Sop4, Emc10, Cue1, Mpd1, Pbr1, Psg1, Rpt2, She2, Ubc6, Ubc7, Ubp1, Ubx7, YNR021W (Figure 2.25 and Table 2.4, red). Among these are

several ERAD-related proteins (e.g. Cue1, Mpd1, Rpt2, Ubc6, Ubc7, Ubx7, Ubp1, Emc10, and Asi3) suggesting a close proximity of the Sec61 channel to the ERAD machinery (Figure 2.26, Sec61 in green highlighted by red circle) and Rpt2, a 19S RP subunit. The detected Ubc6 and Ubc7 interactions, however, might also be due to targeting of Sec61 for degradation as has been reported previously [374, 28]. Rpt2, however, which could also be associated with Sec61-degradation, is only enriched in Sec61 samples, but not in Sec61S353C samples. This is in agreement with the previously reported lower 19S RP affinity of this mutant [186], supporting the notion that it is not a Sec61-degradation related interaction, but a ERAD-relevant interaction.

Upon closer look at gene ontology analysis retrieved by the STRING database of known and predicted protein-protein interactions used to render the predicted interaction grid in Figure 2.26, some points worth discussion came to light. Of the detected enrichments, a good fraction are of cytosolic and mitochondrial proteins. These might represent contaminant ubiquitous proteins, as is likely the case of Tpi1, Fpr1, Cit1, Lys20 or Tom70, which are quite abundant in the cell (Figure 2.27; Supplemental File Kulak cell amounts.xlsx). Most of them, however, must be proteins that cycle to the cytosolic face of the ER either for PTM acquisition or for membrane insertion. Likewise, proteins with a high number of TMDs might also be crosslinked to Sec61 due to slow translocation. This might be the case of hits like Vhc1, which has 12 TMDs according to Uniprot.

Especially striking were the following enrichments:

- Lipid metabolic process factors like Erg1, 24 and 29, Ayr1, Nsg1, Elo1, among others. These might indicate a specific lipid environment for Sec61 which could be interesting and may pose an interesting line of research.
- TOR signalling pathway with an enrichment of Tor1, Tor2, and almost all SEACAT complex (Sea4, Rtc1, Sec13 and Seh1) [263]. This might reveal a connection

between stress signaling and Sec61 availability for remediation.

- COPI subunits (e.g Sec21 and 27, Tip20) and Septin ring (CDC10,CDC11,CDC12,CDC3,SHS1). This is unexpected, as there is no reported physical interaction between Sec61 and the vesicular system.

Although the study of the identity of the enriched hits might be of great interest and usefulness, all projected interactions would have to be functionally confirmed and characterized. Nevertheless, enriched hit analysis might prove extremely useful for future research planning.

3.4 Functional Analysis

Based on the results of the mass spectrometry and its statistical analysis, I decided to functionally characterize mutants of some of the potentially interesting hits. I chose four potential interactors: Asi3, Ynr021w, Psg1 and She2.

Asi3 has been described as a nuclear protein involved in INM protein quality control, promoting the degradation of functional regulators of sterol biosynthesis [102]. It is a transmembrane protein that forms the Asi complex with Asi1 and Asi2, and is reported as interacting with Ssh1 in the nucleus, but not with Sec61 [102]. Both the nuclear localization and the Ssh1 interaction seem to not correlate with my data, since Asi3 was not only strongly present in my samples (which originated from microsomes) (Figure 2.25 and 2.27), but it was also strongly enriched in the crosslinked samples. The fact that Ssh1 was not enriched in my crosslinked samples (Supplemental File Full data set.xlsx), excludes the possibility of enrichment of Ssh1 interactors. Therefore, a characterization of an interaction of Sec61 with Asi3 seemed of high relevance.

Psg1 and Ynr021w are both ER membrane proteins, which are still uncharacter-

ized [115, 168]. Psg1 has been described as interacting with all the Golgi glycosylation machinery including Hoc1 (also one of my enriched hits), and might be involved in quality control of glycosylated proteins[115]. It interacts strongly with the gene product of *YKL063C* [115], which is also uncharacterized and is also enriched in my analysis. Their potential interaction with Sec61 seemed to be of interest since they might represent new ERAD factors.

She2 (an RNA binding protein) [264] was also chosen for further investigation because despite its known targeting to the ER and its genetic interaction with Sec61 (SGD), its ER receptor has never been identified. This has been a long-standing question in the field of RNA-targeting, hence it seemed likely that I could make a valuable contribution.

I tested deletion mutants of all four genes for gross growth defects. They displayed no temperature sensitivity (Figure 2.30, three rightmost panels), and no ER-homeostasis impairment, as I did not detect tunicamycin sensitivity (Figure 2.30, left panel). Moreover, all mutants displayed a normal ER import of pp α F, ppCPY and pDPAPB (Figure 2.31). It must be said, however, that during pDPAPB pulse-chases, the air-conditionair in the lab did not work and that resulted in sub-optimal conditions (as can be seen by the low intensity of the positive control) that might have affected data quality. Since this was the most sensitive import test done to the strains, and some pDPAPB seems to be detected in the Δ *psg1* background, I would suggest not disregarding a potential role of Psg1 in co-translational substrate processing. My characterization, however, excluded any gross import defects in the tested mutants.

To investigate a potential role of these proteins in ERAD, ERAD of two substrates (KHN and KWW) was characterized in Δ *asi3*, Δ *psg1*, and Δ *ynr021w* backgrounds, with no significant effects detected (Figure 2.33), supporting the notion that none of

the mutants displays a grossly impaired proteostasis. To rule out roles with higher degree of specificity of these proteins on ERAD, one would have to screen more substrates and rule out their ERAD impairment. Due to time restrictions I was unable to follow this up during my thesis work.

Next, I decided to investigate the physical interaction between Sec61 and She2. She2 targets RNA to the ER and the bud, but its receptor in the ER is still unknown. If a direct interaction between She2 and Sec61 could be proven, it would support the idea that Sec61 is its ER-receptor. To assess a direct interaction of Sec61 with She2, two strains were generated: *sec61S353C/SHE2* and *sec61S353C/Δshe2*. I used crosslinking to assess if the lack of She2 affected any of the detected shifted bands. When using either the Sec61 or the She2 antibody to detect the interaction, no correlation in the crosslinking pattern was observed (Figure 2.34). This indicated that the interaction was either not a direct one, or I was lacking sufficient sensitivity to detect the She2 interaction in the immunoblotting approach.

I reasoned that if indeed Sec61 and She2 interact, and She2 is needed for targeting of mRNA to Sec61 for co-translational translocation, then a She2 dependent substrate should be translocation deficient in a *Δshe2* strain. Mid2 is a She2 dependent substrate. This means that if the targeting of Mid2 by She2 to the ER is done through She2 interaction with Sec61, in a *Δshe2* background I should be able to detect the same Mid2 cytosolic precursor as in *sec61-32* at restrictive temperature, where Sec61 displays an import defect. This was not the case. Although I detected several Mid2 intermediates in *Δshe2* (Figure 2.35, lanes 7 and 8), none represented the fully unglycosylated cytosolic form detected in *sec61-32* (Figure 2.35, lanes 3 and 4). This might, however, be due to a poor choice of substrate, since Mid2 was also shown to be dependent on Khd1, another mRNA binding protein, for ER targeting [384], and more

substrates should be screened. Due to time and substrate-expression limitations, this was not possible within my study.

Presently, Prof. Prof. Jansen's lab in Tübingen, who has been working on She2 for the past 10 years, is continuing this line of research by investigating the effects of a number of *sec61* mutants on a She2-mediated mRNA targeting to the bud.

To further probe the role of a potential Sec61 interaction with Asi3, I devised a more indirect assay. Several substrates, as Erg11 and Nsg1, have been described as Asi3-dependent for their degradation [102]. I thought that evaluating the degradation dynamics of some of those substrates on the strongest known ERAD-defective *sec61* mutant (*sec61-32* when grown at 30°C) might indicate if an overlapping of these two pathways occurs. If any of the Asi3-substrates degradation was also Sec61-dependent, then the probability of the Asi3 interaction with Sec61 being functionally important was strong. I chose Asi3-dependent substrates Erg11 and Nsg1. I could detect a delay in Erg11 ERAD in a *sec61-32* background grown at the permissive temperature when compared to its degradation in a *SEC61* background (Figure 2.36). Nsg1 expression level, however, was so low that it remains unclear whether this result is meaningful (Figure A.17).

I could establish that Erg11 is indeed also dependent on Sec61 for degradation, suggesting that either Sec61 is the exit channel for nuclear proteins as well as for ERAD, or that Asi3-mediated degradation is not restricted to the INM. Another interesting point to be made is that the Asi complex is described as promoting the degradation of functional regulators of sterol biosynthesis [102], with Erg11 and Nsg1 being two of such regulators. As mentioned above, the enrichment analysis of my crosslinked samples revealed an enrichment of lipid metabolic process factors, including Nsg1, among others. The detected enrichments and interactions suggest that Sec61 might

somehow be involved in this pathway. This result might be of extreme interest, and future research should clarify this interaction.

3.5 Crosslinked Peptides Identification

In any protein-protein interaction study, the knowledge of the potential points of contact between proteins is invaluable, as with this knowledge specific interaction-impairing mutation can be designed. With this in mind, and although it was not the initial plan, I used the xQuest crosslinked-peptide analysis software to identify inter-protein crosslinks in my raw mass spectrometry data, specifically crosslinks to Sec61. In doing so, I attempted to validate my enrichment analysis and gain knowledge for further experimental setup.

There is a number of available software that identifies crosslinked-peptides from raw mass spectrometry data. Among these, xQuest is the most powerful, and was chosen as being the most suitable for analysis of my sample, as many of the other options were not compatible with my crosslinker or did not handle well samples with the complexity of mine. xQuest is optimized for the use of isotopically labeled crosslinkers, but works also (albeit less efficiently) with only a light crosslinker, like the ones used during this study. It is also not optimized for heterobifunctional crosslinkers, like SMPH, thus the impossible homocrosslinks (i.e like K-K or C-C) had to be purged manually. Another limitation is that only one variable amino acid modification (besides of the reactive aminoacids) can be established in the analysis definition file. During identification of peptides by mass spectrometry, some amino acid modifications that cause a shift of their isotopic mass have to be accounted for, as is the case of methionine oxidation and N-terminal acetylation. For peptides identification in my samples, these two modifications were set as variable modification, since they do not occur in

100% of the cases. My samples were also alkylated with iodoacetamide to block cysteines, causing an increase of their isotopic mass. To account for this shift, cysteine alkylation was set as a fixed modification. A high fraction of the peptides, however, would have crosslinked cysteines, which should not be available for alkylation. Cysteines would, then, have two possible forms: alkylated or crosslinked. In this scenario the optimal definition for the xQuest analysis would be setting up three variable modifications: alkylation of cysteines, oxidation of methionines, and N-terminal acetylation. Faced with this choice I opted to prioritize the definition that would conflict less with correct identification of crosslinkable amino acids, and set as variable the alkylation of cysteines.

Upon raw mass spectrometry data analysis with the xQuest software, many crosslinks were detected in each run of the software. The results shown in Figure 2.29 are the results obtained in one such analysis. As can be seen, several crosslinks could be detected between Sec61 and other proteins of the database (Figure 2.29). In all of the runs, however, low score for reported true hits were obtained (10 to 20 instead the 40 that usually indicate true hits) (Supplemental File Analysis.xlsx). Moreover, decoys (nonsense sequence based on the protein database) were scored at same level as hits. This indicates that all my hits were falling into a statistically grey area. This weak statistical confidence should stem from all the software limitations mentioned before and could not be improved despite my best and extensive efforts, as well as support from the software developer (Dr. Alexander Leitner, Zürich)

A common characteristic of all the xQuest detected Sec61 crosslinked peptides was that none represented a crosslink to a cysteine in Sec61, only to lysines. Sec61 has 3 natural cysteines: C121, C150 and C373. All of them are localized in TMDs, so the lack of crosslink to the natural cysteines is not surprising. Even if they do crosslink,

protease digestion might generate peptides that are too apolar, and therefore harder to detect by mass spectrometry. Sec61S353, however, has a fourth cysteine in an extramembrane domain. If this loop 7 cysteine is in close proximity to the place of interaction or sits too close to the membrane, it may happen that it is unavailable for crosslinking as well. Similarly, if the trypsin digestion prior to mass spectrometry analysis generates too big of a peptide (40 amino acids-long in the loop 7 case, considering no miscleaves) software identification becomes also difficult. A double protease digestion prior to the mass spectrometry analysis was considered, but the xQuest software also does not tolerate double-protease digestion.

For individual hit validation one would have to compare some of the known interactions with the described points of contact in the literature. In order to validate the detected hits, a similar analysis would have to be done for each one of the interactions. To be completely thorough, this analysis should be done not only by mapping interaction between Sec61 and its interactors, but also mapping the interactions detected between the interactors, so as to have a multi-plane vision of the complexes. With the obtained scores, that would mean mapping thousand of interactions. This would be impossible in the time given for the present study. Also, not enough information was available for such approach. Many interactions are not characterized and even the structures of many of the detected proteins are not known. The structures of the Sec complex that allow such analysis for Sec63, for example, were just recently available [450, 173]. At the time of the analysis, available information was not enough to allow hit validation.

In light of these new publications the crosslinks of Sec61 to Sec63 detected by the software can now be evaluated. In these works the author set to determine the structure not only of Sec61, but of the entire Sec complex [450, 173]. Both structures re-

ported by Rapoport's (4.1 Å) and Park's (3.7 Å) labs are very similar, as can be seen by the alignment of both structures in Figure 3.2 A (PyMOL files supplied as Supplement Files in the annexed virtual media - i.e USB-stick "Dissertation Supp"- for 3D visualization).

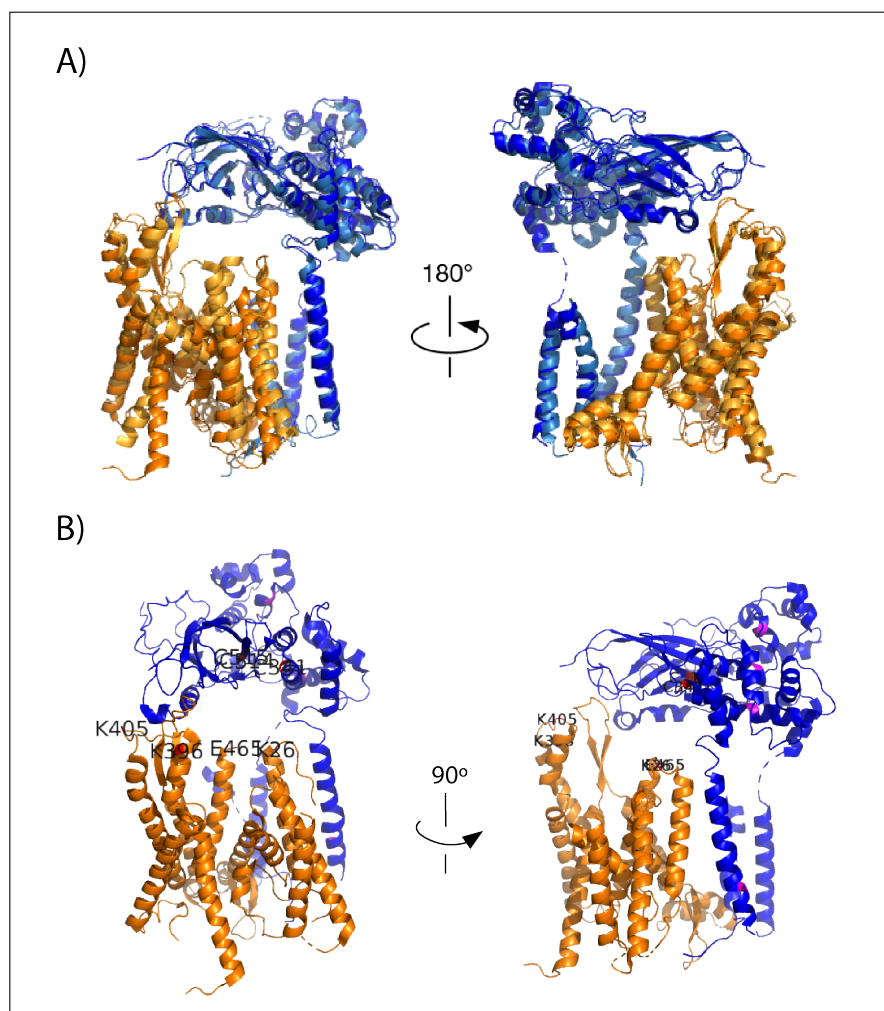


Figure 3.2: Sec61 and Sec63 structure. Structures reported by Wu et al. [450] and Itskanov & Park [173]. Sss1, Sbh1, Sec71, and Sec72 were removed for clarity **A)** Alignment of structures from Wu et al. [450] (PDB file 6ND1) and Itskanov & Park [173] (PDB file 6N3Q). In the structure from Wu et al. [450] Sec61 and Sec63 are in orange and dark blue, respectively. In the structure from Sec61 and Sec63 are in yellow and light blue, respectively. **B)** Structure from Wu et al. [450]. Sec61 and Sec63 in orange and dark blue, respectively. Detected crosslinked amino acids in red and labeled (both in Sec61 as in Sec63). Since structure does not cover Sec61 K470, F465 was marked instead for reference. Remaining Sec63 cysteines in magenta.

Since no crosslinked Sec61 cysteines were identified, whichever true interaction was detected by the software, it happened between a lysine in Sec61 and a cysteine in the interactor. Of the crosslinks detected to Sec63, of its seven cysteines (all cytosolic), three were reported to be crosslinked to Sec61: C341, C514 and C515. If these results were random, crosslinks to any of the cysteines in Sec63 would have been found, and not only crosslinks with the cysteines oriented towards Sec61 (Figure 3.2 B, cysteines in red versus cysteines in magenta). The lysines found to be crosslinked in Sec61, are also in close proximity to the Sec63 cysteines to which they were reported to be crosslinked (Figure 3.2 B, red). The exception might be K405 and K396 (loop 8) which seem somewhat further away from the Sec63 cysteines than the space that the crosslinker was expected to bridge (Figure 3.2 B, red). This area, however, seems flexible and is possible that these areas come closer together during channel opening or closing. Overall, taking into consideration Sec63 cysteine localization, it seems safe to say that the reported crosslinks were, in fact, the most probable ones to occur.

Besides the structures, Rapoport reports also interactions between the Brl domain (a.a 440-490) of Sec63 and loop 6 (a.a 261-290) and 8 (a.a 312-361) of Sec61, the Sec63 TMD3 with TM1 of Sec61, and the N-terminus of Sec63 with the loop 5 of Sec61. Park reports interactions of Sec61 TMD5 (just before loop 5) with Sec63 J-domains (a.a 109-220) and TMD3 (a.a 208-210). Although these locations do not overlap exactly with the detected crosslinks, this is to be expected, since the prerogative for crosslinking is not only spatial closeness of both protein domains, but also the availability of crosslinkable amino acids in a radius compatible with the crosslinker size. The detected crosslinks, however, are close to the domains reported as interacting (e.g K26 close to the beginning of TM1, K405 and K396 close to loop 8). The inter-

action of Sec61 with the Sec63 J-domain would also be in agreement with our data regarding Sec61xSec63 being carbonate sensitive, although no J-domain peptide was found to be crosslinked to a Sec61 peptide. For a more precise analysis, these structures should be rendered in a software that allows drawing of the crosslinks in a size-sensitive form, to verify if the crosslinks would be stereochemically possible.

Overall, as can be seen from the overlap of the crosslinks between Sec61 and Sec63 detected by xQuest and the recently reported Sec complex structure, the reported crosslinks make sense and are definitely possible. This indicates that the probability of the software detecting mainly true interactions is high. Nevertheless, individual validation would be needed. Although time consuming for someone without a bioinformatics background, if hit validation is possible, xQuest analysis may become a powerful tool. Optimization of crosslink setup for analysis with this software, in a machine running Ubuntu operating system natively, would yield quicker and potentially interesting results.

A simple way of trying to validate some of the hits obtained would be to repeat the analysis while crosslinking with an homobifunctional crosslinker. These might generate better scores and allow hit validation. Other variations of the analysis that might yield interesting information would be comparing present results with those obtained when using different crosslinker concentrations, crosslinkers with different characteristics, or even when analyzing different IMAC elution fractions. Analysis of both the enrichment pattern and the crosslinked peptides in Sec61 Δ L7 might also be quite interesting. Hits that are enriched in the current setup but were not in a *sec61* Δ L7 background might prove to be of particular interest. Unfortunately, access to an adequate mass spectrometer was very expensive, and any re-analysis could not be supported by my budget, which was already quite strained in consequence of the present anal-

ysis. In any case, easy and cheap access to state-of-the art MS would be key. To consider as well would be a collaboration with the Aebersold group, whose expertise in this type of analysis would surely allow and quicken a fruitful crosslinked-peptide identification.

3.6 Sec61, Mpd1 and ERAD

During xQuest analysis optimization, a specific crosslink of Sec61 with Mpd1 was especially recurrent (Sec61 K209 to Mpd1 C59; Figure 2.29). Mpd1 had been one of my shortlisted hits, due to its connection to ERAD [415]. It belongs to the protein disulfide isomerase (PDI) family [415], whose members localize mainly to the ER, where they form and isomerize disulfide bonds [269, 86, 401], but also act as chaperones for ERAD relevant substrates [441]. Mpd1 is the only PDI family member that, when under the control of the PDI promotor, can rescue strains deleted for all other PDI homologs [415]. It had previously been shown that the cysteines in the catalytic domain of Pdi1 are essential for reducing the disulfide bonds in CPY* prior to export, making Pdi1 essential for CPY* ERAD [229]. While Pdi1 has two thioredoxin domains with CXXC motifs, Mpd1 contains one active thioredoxin domain with a CGHC motive [269]. The study of Grubb et al. [131] demonstrated that besides Mpd1, the enzymatic activity of Pdi1 is also required for CPY* ERAD, but the reason why both proteins are essential for CPY* ERAD is still unclear.

Upon closer look into the Mpd1 and Sec61 crosslinked peptides I noticed that Mpd1 C59 is the first cysteine in its single redox-active CGHC motif, and Sec61 K209 is in its luminal loop5, which constitutes the hinge region around which the N-terminal half of Sec61 swings during channel opening (Figure 2.37, pink versus green) [217, 423]. Comparison of Sec61 loop5 with SecY loop5 of bacteria and archaea revealed a sub-

stantial extension of loop5 in eukaryotes including the crosslinking site of Mpd1 (Figure 2.38, upper panel). I hypothesized that the eukaryotic extensions in loop5 might serve as docking sites for ERAD factors to facilitate opening of the Sec61 channel from the lumen for export of ERAD substrates (Figure 3.4).

Encouraged by the xQuest detected Mpd1 crosslinking, the Mpd1 role in ERAD [415], and by the structural analysis of Sec61 loop 5, I verified if the Sec61 hinge region was the point of contact for Mpd1, or at least of importance for the ERAD dynamics in yeast.

To achieve this, I deleted the sections of the Sec61 hinge including the Mpd1 contact site that were only present in the eukaryotic channel (Figure 2.38, bottom right). These mutations (*sec61del1*, *sec61del2*, and *sec61del1/2*), as is visible in the topological model, cause a shortening of loop 5, making it similar to the bacterial and archeal channel (Figure 2.38, top and bottom left). I then characterized these strains and investigated the effects of these mutations on protein transport into the ER and on ERAD.

While deletion1 caused temperature- and cold-sensitivity alone and in combination with deletion2 (Figure 2.43 A), steady-state expression levels of all hinge mutants were like wild-type (Figure 2.45), and there was no effect on co- or post-translational protein import into the ER (Figure 2.46). Only the double mutant *sec61del1/2* showed a moderate tunicamycin-sensitivity (Figure 2.43 B) and slightly induced UPR (Figure 2.44).

The temperature-sensitivity could be explained by a temperature dependent protein instability caused by the deleted region 1 and 2, although this was not verified. Another possibility is a deletion-dependent conformational change of the loop 5 hinge region, leading to a defect in the mechanism of the channel-opening. The tunicamycin-

sensitivity points to some misfolded protein response defect, since cells show greater difficulty to deal with misfolded protein clearing. The conclusion that ER-proteostasis was not dramatically compromised in the mutants, excluding gross ERAD defects, is supported by the normal ERAD kinetics for the KHN, KWW, and p Δ gp α F substrates in these backgrounds (Figure 2.47 and 2.48 A) [289, 407].

CPY* degradation, however, was compromised in all Sec61 hinge deletion mutants. Of the three mutants, *sec61del1* (which lacks the contact site for Mpd1) caused the primary defect in ERAD of CPY* (Figure 2.48 B, magenta). The double mutant (*sec61del1/2*) showed an intermediate delay (Figure 2.48 B, green). If both deletions would be responsible for the impact on ERAD, the double deletion should have a higher ERAD impact. This may suggest that it is not just the absence of specific amino acids deleted in *sec61del1*, but also the distortion of the hinge by the deletion that caused the CPY* ERAD defect (Figure 2.38, lower). In *sec61del1/2* this distortion is partially compensated (Figure 2.38, lower), which may account for its weaker phenotype. Since the *sec61del2* mutation is located on the opposite side of loop 5, near the transmembrane domain, the combination of both deletions could thus result in a compensation of the conformational change emanating from *sec61del1*, that translated in a conformation similar to the wild-type.

I have also confirmed that the Mpd1 interaction with Sec61 was compromised in the *sec61* hinge mutants using sequential immunoprecipitations from wildtype, *sec61S353C*, and *sec61* hinge mutant radiolabelled microsomes over-expressing HA-tagged Mpd1. In all hinge mutants less Mpd1 was associated with Sec61 compared to wild-type or *Sec61S353C* (Figure 2.52), but it was not possible to correlate the amount of Mpd1 bound to mutant Sec61 with the degree of the CPY* ERAD defect (compare Figures 2.52 and 2.48 B). The more dramatic effect of the *sec61del2* mutant on Mpd1 crosslink-

ing than on ERAD may be due to the fact that crosslinking is critically dependent on steric proximity of few amino acids whereas protein-protein interaction is usually via a larger surface area. I was, however, unable to co-precipitate sufficient amounts of Mpd1 with Sec61 under native conditions which is why I resorted to crosslinking. Indisputable, however, is that Mpd1 interaction is impaired in the Sec61 hinge mutants, suggesting that loop 5 is important for it, and that these mutants display a CPY* ERAD defect.

The doubling of the $t_{1/2}$ of CPY* that I observed in *sec61del1* (Figure 2.48 B, magenta) is comparable to the effect of a complete deletion of *MPD1* on CPY* degradation [131] suggesting that Mpd1 primarily promotes CPY* ERAD by its interaction with the Sec61 hinge. It has been shown previously that while the oxidoreductase function of Pdi1 is critical for ERAD of disulfide-bonded CPY*, Pdi1's chaperone function - which is decisive for ERAD targeting of other substrates - is not [120, 131]. My data indicates that for CPY*, this targeting role may be fulfilled by the Pdi1 homologue Mpd1 (Figure 3.4).

Mpd1 consists of two thioredoxin modules, a and b [415]. The redox-inactive Mpd1 b module contains an extension similar to, but substantially longer than an extension in the redox-inactive b' module of Pdi1 which serves to bind substrate proteins when it acts as an ERAD targeting chaperone (Figure 3.3) [415, 120]. The Mpd1 b domain may therefore be responsible for substrate binding whereas the a domain - containing C59 that I crosslinked to Sec61 loop5 - interacts with the Sec61 channel.

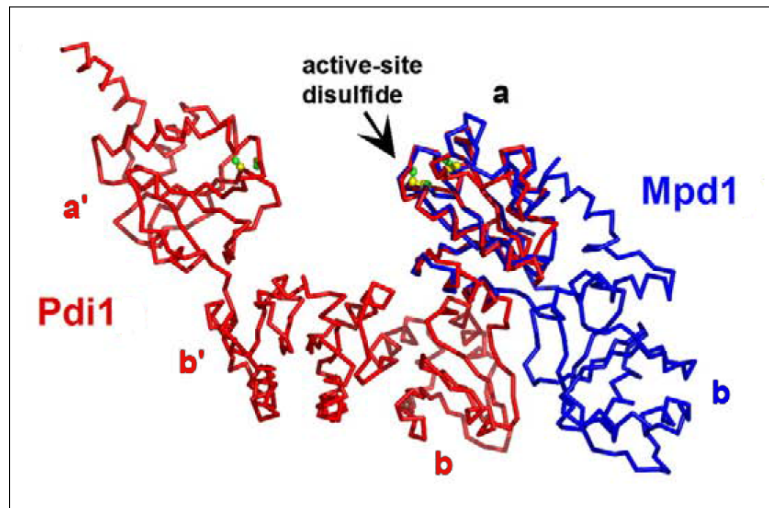


Figure 3.3: Structure of Mpd1 compared to Pdi1. The approximate twofold rotation relating the Mpd1 (blue) and Pdi1 (red) b domains when the a domains are superposed. The rest of the a domain is omitted for clarity. Figure from Vitu et al. [415].

Other studies support the idea that the ubiquitin ligase Hrd1 is the retrograde translocation channel for ERAD [380, 11, 451]. Schoebel et al. [341] solved the structure of the Hrd1/Hrd3 complex by cryo-EM and proposed that it is the ERAD retrograde translocation channel. Baldrige & Rapoport [11] also reconstituted *in vitro* the ERAD pathway using proteoliposomes and purified Hrd1. They crosslinked CPY* with Hrd1 and observed its translocation. This setup was, however, sub-optimal and completely non-physiological, since there was no Hrd3 present (which is necessary for Hrd1 activity control) and CPY* was very aggregation-prone in it.

To exclude that the *sec61* hinge mutants reduced biogenesis of the ER ubiquitin ligase Hrd1 and its cofactor Hrd3 I performed quantitative immunoblots for both proteins and found that they were expressed equally in wild-type and Sec61 hinge mutant cells (Figure 2.45). Moreover, as can be seen in Figure 2.11 B, the $\Delta hrd1$ and $\Delta hrd3$ mutants displayed only a slight delay in $\Delta gpaF$ degradation, which may or may not be indirectly due to the accumulation of ubiquitin-dependent ERAD substrates

in the mutants, but it definitely excludes the Hrd1/Hrd3 complex as ERAD channel for $\Delta gp\alpha F$. This fits with the description of $\Delta gp\alpha F$ being dependent on Sec61 for export [289] and strengthens the idea that at the very least, Hrd1 is not a general ERAD channel.

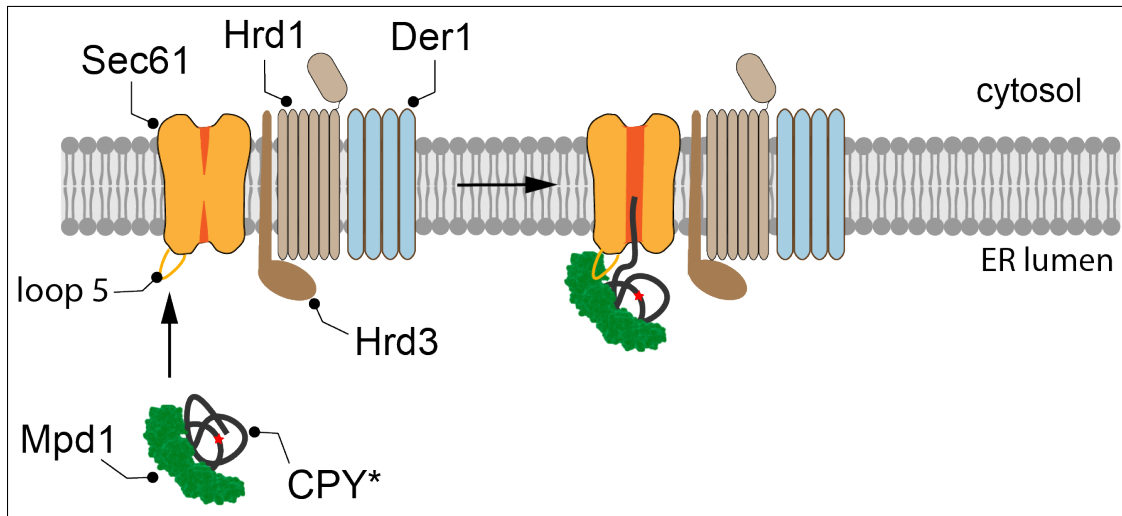


Figure 3.4: Mpd1-Sec61 interaction model. Model for initiation of CPY* ERAD mediated by Mpd1 interaction with luminal hinge of Sec61. Mpd1 (green) binds CPY* and targets. Mpd1 then binds to Sec61 (yellow) through loop 5 and induces channel opening from the luminal side and promotes CPY* export. Sec61, in complex with Hrd3 (dark brown), Hrd1 (light brown) and Der1 (blue) promote

One possibility is that Sec61 and Hrd1 might operate together in retrograde translocation of misfolded proteins to the cytosol. This hypothesis was also stated by Stein et al. [380] and Gauss et al. [113], and Baldrige & Rapoport [11] do not exclude other components to be involved in a physiologic system. Further crosslinking studies showed that Der1 is also a part of the Hrd1/Hrd3 complex [243]. My data on the Mpd1 interaction with Sec61 together with the data from the literature may suggest that Sec61, Der1, and Hrd1/Hrd3 act together in the protein export or form an export channel with varying multiple subunits dependent on the substrate, as shown in Figure 3.4. This assumption is supported by the fact that other known ERAD components, extensively

characterized and which interaction with Hrd1/Hrd3, Der1 and Doa10 is well established [391], were shown to be enriched in our crosslinked samples (Ubc6, Ubc7, Ubx7, Ubp1, Cue1, Rpt2).

3.7 Concluding Remarks

In this study I have successfully established a crosslinking setup that allowed:

- chemical crosslinking of Sec61 to new and known interactors
- purification of Sec61-crosslinked complexes
- Identification of interactors by mass spectrometry.

This setup allowed characterization of several Sec61 interactors, including several newly discovered ones. Besides the enrichment analysis that will surely prove to be a trove of information about Sec61 interactions, I have established interactions between Sec61 and several of the Sec channels subunits (Sss1, Sec71 and Sec63), the nuclear envelope protein Asi3, described as being involved in inner nuclear membrane (INM) protein quality control, and Mpd1, a Pdi1 homologue.

I have shown that Sec61 interacts with Mpd1 through its hinge region and that such interaction is important for ERAD of a specific substrate. My results can now serve as a basis for investigating the exact sequence of events of substrate binding and a Sec61 mediated export.

Collectively, my data suggest that interaction of the CPY* ERAD factor Mpd1 with the Sec61 hinge region in loop5 contributes to export and degradation of this substrate. My results are consistent with the view that Sec61 forms part of an export complex in the ER membrane for misfolded protein transport to the cytosol (Figure 3.4). The extended hinge in Sec61 compared to SecY (Figure 2.38) may serve to activate

and open the channel from the lumen for intercalation and subsequent transport of CPY* to the cytosol (Figure 3.4).

I propose that Mpd1 targets CPY* to an export complex in the ER membrane that likely consists of Sec61, the Hrd complex, and Der1 as shown in Figure 3.4, and that these proteins cooperate in export of CPY* for degradation in the cytosol.

The results obtained during this work are consistent with the view that Sec61 forms part of an export complex in the ER membrane for misfolded protein transport to the cytosol (Figure 3.4).

References

- [1] Agarwal, D., Caillouet, C., Coudert, D., & Cazals, F. (2015). Unveiling contacts within macromolecular assemblies by solving minimum weight connectivity inference (mwc) problems. *Mol Cell Proteomics*, 14(8), 2274–84.
- [2] Ahner, A., Nakatsukasa, K., Zhang, H., Frizzell, R. A., & Brodsky, J. L. (2007). Small heat-shock proteins select deltaf508-cftr for endoplasmic reticulum-associated degradation. *Mol Biol Cell*, 18(3), 806–14.
- [3] Aiyar, A., Xiang, Y., & Leis, J. (1996). Site-directed mutagenesis using overlap extension pcr. *Methods Mol Biol*, 57, 177–91.
- [4] Aloy, P. & Russell, R. B. (2006). Structural systems biology: modelling protein interactions. *Nat Rev Mol Cell Biol*, 7(3), 188–97.
- [5] Antonin, W., Meyer, H. A., & Hartmann, E. (2000). Interactions between spc2p and other components of the endoplasmic reticulum translocation sites of the yeast *saccharomyces cerevisiae*. *J Biol Chem*, 275(44), 34068–72.
- [6] Appenzeller-Herzog, C. (2011). Glutathione- and non-glutathione-based oxidant control in the endoplasmic reticulum. *J Cell Sci*, 124(Pt 6), 847–55.
- [7] Araki, K. & Nagata, K. (2011). Protein folding and quality control in the er. *Cold Spring Harb Perspect Biol*, 3(11), a007526.
- [8] Ast, T., Cohen, G., & Schuldiner, M. (2013). A network of cytosolic factors targets srp-independent proteins to the endoplasmic reticulum. *Cell*, 152(5), 1134–45.
- [9] Aviram, N., Ast, T., Costa, E. A., Arakel, E. C., Chuartzman, S. G., Jan, C. H., Haßdenteufel, S., Dudek, J., Jung, M., Schorr, S., Zimmermann, R., Schwappach, B., Weissman, J. S., & Schuldiner, M. (2016). The snd proteins constitute an alternative targeting route to the endoplasmic reticulum. *Nature*, 540(7631), 134–138.
- [10] Back, J. W., de Jong, L., Muijsers, A. O., & de Koster, C. G. (2003). Chemical cross-linking and mass spectrometry for protein structural modeling. *J Mol Biol*, 331(2), 303–13.
- [11] Baldridge, R. D. & Rapoport, T. A. (2016). Autoubiquitination of the hrd1 ligase triggers protein retrotranslocation in erad. *Cell*, 166(2), 394–407.

- [12] Bantscheff, M., Schirle, M., Sweetman, G., Rick, J., & Kuster, B. (2007). Quantitative mass spectrometry in proteomics: a critical review. *Anal Bioanal Chem*, 389(4), 1017–31.
- [13] Barlowe, C., Orci, L., Yeung, T., Hosobuchi, M., Hamamoto, S., Salama, N., Rexach, M. F., Ravazzola, M., Amherdt, M., & Schekman, R. (1994). Copii: a membrane coat formed by sec proteins that drive vesicle budding from the endoplasmic reticulum. *Cell*, 77(6), 895–907.
- [14] Barlowe, C. K. & Miller, E. A. (2013). Secretory protein biogenesis and traffic in the early secretory pathway. *Genetics*, 193(2), 383–410.
- [15] Baxter, B. K., James, P., Evans, T., & Craig, E. A. (1996). Ssi1 encodes a novel hsp70 of the *saccharomyces cerevisiae* endoplasmic reticulum. *Mol Cell Biol*, 16(11), 6444–56.
- [16] Bays, N. W., Wilhovsky, S. K., Goradia, A., Hodgkiss-Harlow, K., & Hampton, R. Y. (2001). Hrd4/npl4 is required for the proteasomal processing of ubiquitinated er proteins. *Mol Biol Cell*, 12(12), 4114–28.
- [17] Becker, T., Bhushan, S., Jarasch, A., Armache, J.-P., Funes, S., Jossinet, F., Gumbart, J., Mielke, T., Berninghausen, O., Schulten, K., Westhof, E., Gilmore, R., Mandon, E. C., & Beckmann, R. (2009). Structure of monomeric yeast and mammalian sec61 complexes interacting with the translating ribosome. *Science*, 326(5958), 1369–73.
- [18] Beckmann, R., Bubeck, D., Grassucci, R., Penczek, P., Verschoor, A., Blobel, G., & Frank, J. (1997). Alignment of conduits for the nascent polypeptide chain in the ribosome-sec61 complex. *Science*, 278(5346), 2123–6.
- [19] Beckmann, R., Spahn, C. M., Eswar, N., Helmers, J., Penczek, P. A., Sali, A., Frank, J., & Blobel, G. (2001). Architecture of the protein-conducting channel associated with the translating 80s ribosome. *Cell*, 107(3), 361–72.
- [20] Behnke, J., Feige, M. J., & Hendershot, L. M. (2015). Bip and its nucleotide exchange factors grp170 and sil1: mechanisms of action and biological functions. *J Mol Biol*, 427(7), 1589–608.
- [21] Ben-Saadon, R., Fajerman, I., Ziv, T., Hellman, U., Schwartz, A. L., & Ciechanover, A. (2004). The tumor suppressor protein p16(ink4a) and the human papillomavirus oncoprotein-58 e7 are naturally occurring lysine-less proteins that are degraded by the ubiquitin system. direct evidence for ubiquitination at the n-terminal residue. *J Biol Chem*, 279(40), 41414–21.

- [22] Bennett, E. J., Rush, J., Gygi, S. P., & Harper, J. W. (2010). Dynamics of cullin-ring ubiquitin ligase network revealed by systematic quantitative proteomics. *Cell*, 143(6), 951–65.
- [23] Berggård, T., Linse, S., & James, P. (2007). Methods for the detection and analysis of protein-protein interactions. *Proteomics*, 7(16), 2833–42.
- [24] Bernales, S., Papa, F. R., & Walter, P. (2006). Intracellular signaling by the unfolded protein response. *Annu Rev Cell Dev Biol*, 22, 487–508.
- [25] Bertolotti, A., Zhang, Y., Hendershot, L. M., Harding, H. P., & Ron, D. (2000). Dynamic interaction of bip and er stress transducers in the unfolded-protein response. *Nat Cell Biol*, 2(6), 326–32.
- [26] Bhamidipati, A., Denic, V., Quan, E. M., & Weissman, J. S. (2005). Exploration of the topological requirements of erad identifies yos9p as a lectin sensor of misfolded glycoproteins in the er lumen. *Mol Cell*, 19(6), 741–51.
- [27] Bi, X., Corpina, R. A., & Goldberg, J. (2002). Structure of the sec23/24-sar1 pre-budding complex of the copii vesicle coat. *Nature*, 419(6904), 271–7.
- [28] Biederer, T., Volkwein, C., & Sommer, T. (1996). Degradation of subunits of the sec61p complex, an integral component of the er membrane, by the ubiquitin-proteasome pathway. *EMBO J*, 15(9), 2069–76.
- [29] Biederer, T., Volkwein, C., & Sommer, T. (1997). Role of cue1p in ubiquitination and degradation at the er surface. *Science*, 278(5344), 1806–9.
- [30] Blachly-Dyson, E. & Stevens, T. H. (1987). Yeast carboxypeptidase y can be translocated and glycosylated without its amino-terminal signal sequence. *J Cell Biol*, 104(5), 1183–91.
- [31] Block, H., Maertens, B., Priestersbach, A., Brinker, N., Kubicek, J., Fabis, R., Labahn, J., & Schäfer, F. (2009). Immobilized-metal affinity chromatography (imac): a review. *Methods Enzymol*, 463, 439–73.
- [32] Bloom, J., Amador, V., Bartolini, F., DeMartino, G., & Pagano, M. (2003). Proteasome-mediated degradation of p21 via n-terminal ubiquitylation. *Cell*, 115(1), 71–82.
- [33] Boeke, J. D., Trueheart, J., Natsoulis, G., & Fink, G. R. (1987). 5-fluoroorotic acid as a selective agent in yeast molecular genetics. *Methods Enzymol*, 154, 164–75.

- [34] Bordallo, J., Plemper, R. K., Finger, A., & Wolf, D. H. (1998). Der3p/hrd1p is required for endoplasmic reticulum-associated degradation of misfolded luminal and integral membrane proteins. *Mol Biol Cell*, 9(1), 209–22.
- [35] Borkovich, K. A., Farrelly, F. W., Finkelstein, D. B., Taulien, J., & Lindquist, S. (1989). hsp82 is an essential protein that is required in higher concentrations for growth of cells at higher temperatures. *Mol Cell Biol*, 9(9), 3919–30.
- [36] Braakman, I. & Bulleid, N. J. (2011). Protein folding and modification in the mammalian endoplasmic reticulum. *Annu Rev Biochem*, 80, 71–99.
- [37] Braakman, I. & Hebert, D. N. (2013). Protein folding in the endoplasmic reticulum. *Cold Spring Harb Perspect Biol*, 5(5), a013201.
- [38] Bragg, P. D. & Hou, C. (1975). Subunit composition, function, and spatial arrangement in the ca^{2+} - and mg^{2+} -activated adenosine triphosphatases of *escherichia coli* and *salmonella typhimurium*. *Arch Biochem Biophys*, 167(1), 311–21.
- [39] Braun, P. & Gingras, A.-C. (2012). History of protein-protein interactions: from egg-white to complex networks. *Proteomics*, 12(10), 1478–98.
- [40] Braun, S., Matuschewski, K., Rape, M., Thoms, S., & Jentsch, S. (2002). Role of the ubiquitin-selective cdc48(ufd1/npl4) chaperone (segregase) in erad of ole1 and other substrates. *EMBO J*, 21(4), 615–21.
- [41] Braunstein, I., Zach, L., Allan, S., Kalies, K.-U., & Stanhill, A. (2015). Proteasomal degradation of preemptive quality control (pqc) substrates is mediated by an airapl-p97 complex. *Mol Biol Cell*, 26(21), 3719–27.
- [42] Briggs, M. S., Cornell, D. G., Dluhy, R. A., & Gierasch, L. M. (1986). Conformations of signal peptides induced by lipids suggest initial steps in protein export. *Science*, 233(4760), 206–8.
- [43] Brodsky, J. L. (1996). Post-translational protein translocation: not all hsc70s are created equal. *Trends Biochem Sci*, 21(4), 122–6.
- [44] Brodsky, J. L. & Schekman, R. (1993). A sec63p-bip complex from yeast is required for protein translocation in a reconstituted proteoliposome. *J Cell Biol*, 123(6 Pt 1), 1355–63.
- [45] Buchberger, A., Bukau, B., & Sommer, T. (2010). Protein quality control in the cytosol and the endoplasmic reticulum: brothers in arms. *Mol Cell*, 40(2), 238–52.

- [46] Bukau, B. & Horwich, A. L. (1998). The hsp70 and hsp60 chaperone machines. *Cell*, 92(3), 351–66.
- [47] Bukau, B., Weissman, J., & Horwich, A. (2006). Molecular chaperones and protein quality control. *Cell*, 125(3), 443–51.
- [48] Buschhorn, B. A., Kostova, Z., Medicherla, B., & Wolf, D. H. (2004). A genome-wide screen identifies yos9p as essential for er-associated degradation of glycoproteins. *FEBS Lett*, 577(3), 422–6.
- [49] Byrd, J. C., Tarentino, A. L., Maley, F., Atkinson, P. H., & Trimble, R. B. (1982). Glycoprotein synthesis in yeast. identification of man8glcnac2 as an essential intermediate in oligosaccharide processing. *J Biol Chem*, 257(24), 14657–66.
- [50] Cadwell, K. & Coscoy, L. (2005). Ubiquitination on nonlysine residues by a viral e3 ubiquitin ligase. *Science*, 309(5731), 127–30.
- [51] Cai, H., Wang, C. C., & Tsou, C. L. (1994). Chaperone-like activity of protein disulfide isomerase in the refolding of a protein with no disulfide bonds. *J Biol Chem*, 269(40), 24550–2.
- [52] Caldwell, S. R., Hill, K. J., & Cooper, A. A. (2001). Degradation of endoplasmic reticulum (er) quality control substrates requires transport between the er and golgi. *J Biol Chem*, 276(26), 23296–303.
- [53] Cao, X. & Barlowe, C. (2000). Asymmetric requirements for a rab gtpase and snare proteins in fusion of copii vesicles with acceptor membranes. *J Cell Biol*, 149(1), 55–66.
- [54] Caplan, S., Green, R., Rocco, J., & Kurjan, J. (1991). Glycosylation and structure of the yeast mf alpha 1 alpha-factor precursor is important for efficient transport through the secretory pathway. *J Bacteriol*, 173(2), 627–35.
- [55] Carvalho, P., Goder, V., & Rapoport, T. A. (2006). Distinct ubiquitin-ligase complexes define convergent pathways for the degradation of er proteins. *Cell*, 126(2), 361–73.
- [56] Carvalho, P., Stanley, A. M., & Rapoport, T. A. (2010). Retrotranslocation of a misfolded luminal er protein by the ubiquitin-ligase hrd1p. *Cell*, 143(4), 579–91.
- [57] Castillon, G. A., Watanabe, R., Taylor, M., Schwabe, T. M. E., & Riezman, H. (2009). Concentration of gpi-anchored proteins upon er exit in yeast. *Traffic*, 10(2), 186–200.

- [58] Chawla, A., Chakrabarti, S., Ghosh, G., & Niwa, M. (2011). Attenuation of yeast upr is essential for survival and is mediated by ire1 kinase. *J Cell Biol*, 193(1), 41–50.
- [59] Chen, Y., Zhang, Y., Yin, Y., Gao, G., Li, S., Jiang, Y., Gu, X., & Luo, J. (2005). Spd—a web-based secreted protein database. *Nucleic Acids Res*, 33(Database issue), D169–73.
- [60] Cheng, Z., Jiang, Y., Mandon, E. C., & Gilmore, R. (2005). Identification of cytoplasmic residues of sec61p involved in ribosome binding and cotranslational translocation. *J Cell Biol*, 168(1), 67–77.
- [61] Chitwood, P. J., Juszkievicz, S., Guna, A., Shao, S., & Hegde, R. S. (2018). Emc is required to initiate accurate membrane protein topogenesis. *Cell*, 175(6), 1507–1519.e16.
- [62] Clerc, S., Hirsch, C., Oggier, D. M., Deprez, P., Jakob, C., Sommer, T., & Aebi, M. (2009). Htm1 protein generates the n-glycan signal for glycoprotein degradation in the endoplasmic reticulum. *J Cell Biol*, 184(1), 159–72.
- [63] Conti, B. J., Devaraneni, P. K., Yang, Z., David, L. L., & Skach, W. R. (2015). Cotranslational stabilization of sec62/63 within the er sec61 translocon is controlled by distinct substrate-driven translocation events. *Mol Cell*, 58(2), 269–83.
- [64] Cosson, P. & Letourneur, F. (1994). Coatamer interaction with di-lysine endoplasmic reticulum retention motifs. *Science*, 263(5153), 1629–31.
- [65] Cox, J. & Mann, M. (2008). Maxquant enables high peptide identification rates, individualized p.p.b.-range mass accuracies and proteome-wide protein quantification. *Nat Biotechnol*, 26(12), 1367–72.
- [66] Cox, J. S., Shamu, C. E., & Walter, P. (1993). Transcriptional induction of genes encoding endoplasmic reticulum resident proteins requires a transmembrane protein kinase. *Cell*, 73(6), 1197–206.
- [67] Cox, J. S. & Walter, P. (1996). A novel mechanism for regulating activity of a transcription factor that controls the unfolded protein response. *Cell*, 87(3), 391–404.
- [68] Craig, E. A., Huang, P., Aron, R., & Andrew, A. (2006). The diverse roles of j-proteins, the obligate hsp70 co-chaperone. *Rev Physiol Biochem Pharmacol*, 156, 1–21.

- [69] Cross, B. C. S., Sinning, I., Luirink, J., & High, S. (2009). Delivering proteins for export from the cytosol. *Nat Rev Mol Cell Biol*, 10(4), 255–64.
- [70] Cyr, D. M. & Hebert, D. N. (2009). Protein quality control—linking the unfolded protein response to disease. conference on 'from unfolded proteins in the endoplasmic reticulum to disease'. *EMBO Rep*, 10(11), 1206–10.
- [71] Dancourt, J. & Barlowe, C. (2010). Protein sorting receptors in the early secretory pathway. *Annu Rev Biochem*, 79, 777–802.
- [72] Darby, N. J., Kemmink, J., & Creighton, T. E. (1996). Identifying and characterizing a structural domain of protein disulfide isomerase. *Biochemistry*, 35(32), 10517–28.
- [73] Dugaard, M., Rohde, M., & Jäättelä, M. (2007). The heat shock protein 70 family: Highly homologous proteins with overlapping and distinct functions. *FEBS Lett*, 581(19), 3702–10.
- [74] Deak, P. M. & Wolf, D. H. (2001). Membrane topology and function of der3/hrd1p as a ubiquitin-protein ligase (e3) involved in endoplasmic reticulum degradation. *J Biol Chem*, 276(14), 10663–9.
- [75] Deane, C. M., Salwiński, Ł., Xenarios, I., & Eisenberg, D. (2002). Protein interactions: two methods for assessment of the reliability of high throughput observations. *Mol Cell Proteomics*, 1(5), 349–56.
- [76] Delic, M., Valli, M., Graf, A. B., Pfeffer, M., Mattanovich, D., & Gasser, B. (2013). The secretory pathway: exploring yeast diversity. *FEMS Microbiol Rev*, 37(6), 872–914.
- [77] Denic, V., Quan, E. M., & Weissman, J. S. (2006). A luminal surveillance complex that selects misfolded glycoproteins for er-associated degradation. *Cell*, 126(2), 349–59.
- [78] Deshaies, R. J. & Joazeiro, C. A. P. (2009). Ring domain e3 ubiquitin ligases. *Annu Rev Biochem*, 78, 399–434.
- [79] Deshaies, R. J., Sanders, S. L., Feldheim, D. A., & Schekman, R. (1991). Assembly of yeast sec proteins involved in translocation into the endoplasmic reticulum into a membrane-bound multisubunit complex. *Nature*, 349(6312), 806–8.
- [80] Dobson, C. M. (2001). The structural basis of protein folding and its links with human disease. *Philos Trans R Soc Lond B Biol Sci*, 356(1406), 133–45.

- [81] Donella-Deana, A., Ostojić, S., Pinna, L. A., & Barbarić, S. (1993). Specific dephosphorylation of phosphopeptides by the yeast alkaline phosphatase encoded by *pho8* gene. *Biochim Biophys Acta*, 1177(2), 221–8.
- [82] Duttler, S., Pechmann, S., & Frydman, J. (2013). Principles of cotranslational ubiquitination and quality control at the ribosome. *Mol Cell*, 50(3), 379–93.
- [83] E, H. (2012). Chemical crosslinking of proteins: A review. *Journal of Pharmaceutical and Scientific Innovation*, 1(1), 22–26.
- [84] Egea, P. F. & Stroud, R. M. (2010). Lateral opening of a translocon upon entry of protein suggests the mechanism of insertion into membranes. *Proc Natl Acad Sci U S A*, 107(40), 17182–7.
- [85] Ellgaard, L. & Helenius, A. (2003). Quality control in the endoplasmic reticulum. *Nat Rev Mol Cell Biol*, 4(3), 181–91.
- [86] Ellgaard, L. & Ruddock, L. W. (2005). The human protein disulphide isomerase family: substrate interactions and functional properties. *EMBO Rep*, 6(1), 28–32.
- [87] Emr, S., Glick, B. S., Linstedt, A. D., Lippincott-Schwartz, J., Luini, A., Malhotra, V., Marsh, B. J., Nakano, A., Pfeffer, S. R., Rabouille, C., Rothman, J. E., Warren, G., & Wieland, F. T. (2009). Journeys through the golgi-taking stock in a new era. *J Cell Biol*, 187(4), 449–53.
- [88] Enenkel, C., Lehmann, A., & Kloetzel, P. M. (1998). Subcellular distribution of proteasomes implicates a major location of protein degradation in the nuclear envelope-er network in yeast. *EMBO J*, 17(21), 6144–54.
- [89] Eng, J. K., McCormack, A. L., & Yates, J. R. (1994). An approach to correlate tandem mass spectral data of peptides with amino acid sequences in a protein database. *J Am Soc Mass Spectrom*, 5(11), 976–89.
- [90] Esnault, Y., Feldheim, D., Blondel, M. O., Schekman, R., & Képès, F. (1994). Sss1 encodes a stabilizing component of the sec61 subcomplex of the yeast protein translocation apparatus. *J Biol Chem*, 269(44), 27478–85.
- [91] Fagarasanu, A. & Rachubinski, R. A. (2007). Orchestrating organelle inheritance in *saccharomyces cerevisiae*. *Curr Opin Microbiol*, 10(6), 528–38.
- [92] Fagioli, C., Mezghrani, A., & Sitia, R. (2001). Reduction of interchain disulfide bonds precedes the dislocation of ig- μ chains from the endoplasmic reticulum to the cytosol for proteasomal degradation. *J Biol Chem*, 276(44), 40962–7.

- [93] Fath, S., Mancias, J. D., Bi, X., & Goldberg, J. (2007). Structure and organization of coat proteins in the copii cage. *Cell*, 129(7), 1325–36.
- [94] Feldheim, D., Rothblatt, J., & Schekman, R. (1992). Topology and functional domains of sec63p, an endoplasmic reticulum membrane protein required for secretory protein translocation. *Mol Cell Biol*, 12(7), 3288–96.
- [95] Feldheim, D., Yoshimura, K., Admon, A., & Schekman, R. (1993). Structural and functional characterization of sec66p, a new subunit of the polypeptide translocation apparatus in the yeast endoplasmic reticulum. *Mol Biol Cell*, 4(9), 931–9.
- [96] Feldman, M. & van der Goot, F. G. (2009). Novel ubiquitin-dependent quality control in the endoplasmic reticulum. *Trends Cell Biol*, 19(8), 357–63.
- [97] Ferrari, D. M. & Söling, H. D. (1999). The protein disulphide-isomerase family: unravelling a string of folds. *Biochem J*, 339 (Pt 1), 1–10.
- [98] Ferro-Novick, S. & Brose, N. (2013). Nobel 2013 physiology or medicine: Traffic control system within cells. *Nature*, 504(7478), 98.
- [99] Fields, S. & Song, O. (1989). A novel genetic system to detect protein-protein interactions. *Nature*, 340(6230), 245–6.
- [100] Finley, D. (2009). Recognition and processing of ubiquitin-protein conjugates by the proteasome. *Annu Rev Biochem*, 78, 477–513.
- [101] Finley, D., Ulrich, H. D., Sommer, T., & Kaiser, P. (2012). The ubiquitin-proteasome system of *saccharomyces cerevisiae*. *Genetics*, 192(2), 319–60.
- [102] Foresti, O., Rodriguez-Vaello, V., Funaya, C., & Carvalho, P. (2014). Quality control of inner nuclear membrane proteins by the asi complex. *Science*, 346(6210), 751–5.
- [103] Fra, A. M., Fagioli, C., Finazzi, D., Sitia, R., & Alberini, C. M. (1993). Quality control of er synthesized proteins: an exposed thiol group as a three-way switch mediating assembly, retention and degradation. *EMBO J*, 12(12), 4755–61.
- [104] Freedman, R. B., Dunn, A. D., & Ruddock, L. W. (1998). Protein folding: a missing redox link in the endoplasmic reticulum. *Curr Biol*, 8(13), R468–70.
- [105] Fu, L. & Sztul, E. (2003). Traffic-independent function of the sar1p/copii machinery in proteasomal sorting of the cystic fibrosis transmembrane conductance regulator. *J Cell Biol*, 160(2), 157–63.

- [106] Fujiki, Y., Hubbard, A. L., Fowler, S., & Lazarow, P. B. (1982). Isolation of intracellular membranes by means of sodium carbonate treatment: application to endoplasmic reticulum. *J Cell Biol*, 93(1), 97–102.
- [107] Gardner, B. M., Pincus, D., Gotthardt, K., Gallagher, C. M., & Walter, P. (2013). Endoplasmic reticulum stress sensing in the unfolded protein response. *Cold Spring Harb Perspect Biol*, 5(3), a013169.
- [108] Gardner, B. M. & Walter, P. (2011). Unfolded proteins are ire1-activating ligands that directly induce the unfolded protein response. *Science*, 333(6051), 1891–4.
- [109] Gardner, R. G., Swarbrick, G. M., Bays, N. W., Cronin, S. R., Wilhovsky, S., Seelig, L., Kim, C., & Hampton, R. Y. (2000). Endoplasmic reticulum degradation requires lumen to cytosol signaling. transmembrane control of hrd1p by hrd3p. *J Cell Biol*, 151(1), 69–82.
- [110] Gatto, L. & Lilley, K. S. (2012). Msnbase-an r/bioconductor package for isobaric tagged mass spectrometry data visualization, processing and quantitation. *Bioinformatics*, 28(2), 288–9.
- [111] Gauss, R., Jarosch, E., Sommer, T., & Hirsch, C. (2006a). A complex of yos9p and the hrd ligase integrates endoplasmic reticulum quality control into the degradation machinery. *Nat Cell Biol*, 8(8), 849–54.
- [112] Gauss, R., Kanehara, K., Carvalho, P., Ng, D. T. W., & Aebi, M. (2011). A complex of pdi1p and the mannosidase htm1p initiates clearance of unfolded glycoproteins from the endoplasmic reticulum. *Mol Cell*, 42(6), 782–93.
- [113] Gauss, R., Sommer, T., & Jarosch, E. (2006b). The hrd1p ligase complex forms a linchpin between er-lumenal substrate selection and cdc48p recruitment. *EMBO J*, 25(9), 1827–35.
- [114] Gething, M. J., McCammon, K., & Sambrook, J. (1986). Expression of wild-type and mutant forms of influenza hemagglutinin: the role of folding in intracellular transport. *Cell*, 46(6), 939–50.
- [115] Geva, Y., Crissman, J., Arakel, E. C., Gómez-Navarro, N., Chuartzman, S. G., Stahmer, K. R., Schwappach, B., Miller, E. A., & Schuldiner, M. (2017). Two novel effectors of trafficking and maturation of the yeast plasma membrane h⁺-atpase. *Traffic*, 18(10), 672–682.
- [116] Gidalevitz, T., Stevens, F., & Argon, Y. (2013). Orchestration of secretory protein folding by er chaperones. *Biochim Biophys Acta*, 1833(11), 2410–24.

- [117] Gietz, R. D., Schiestl, R. H., Willems, A. R., & Woods, R. A. (1995). Studies on the transformation of intact yeast cells by the liac/ss-dna/peg procedure. *Yeast*, 11(4), 355–60.
- [118] Gietz, R. D. & Woods, R. A. (2002). Transformation of yeast by lithium acetate/single-stranded carrier dna/polyethylene glycol method. *Methods Enzymol*, 350, 87–96.
- [119] Gilbert, H. F. (1998). Protein disulfide isomerase. *Methods Enzymol*, 290, 26–50.
- [120] Gillece, P., Luz, J. M., Lennarz, W. J., de La Cruz, F. J., & Römisch, K. (1999). Export of a cysteine-free misfolded secretory protein from the endoplasmic reticulum for degradation requires interaction with protein disulfide isomerase. *J Cell Biol*, 147(7), 1443–56.
- [121] Gilmore, R. & Blobel, G. (1983). Transient involvement of signal recognition particle and its receptor in the microsomal membrane prior to protein translocation. *Cell*, 35(3 Pt 2), 677–85.
- [122] Gilmore, R. & Blobel, G. (1985). Translocation of secretory proteins across the microsomal membrane occurs through an environment accessible to aqueous perturbants. *Cell*, 42(2), 497–505.
- [123] Gilmore, R., Walter, P., & Blobel, G. (1982). Protein translocation across the endoplasmic reticulum. ii. isolation and characterization of the signal recognition particle receptor. *J Cell Biol*, 95(2 Pt 1), 470–7.
- [124] Gingras, A.-C., Gstaiger, M., Raught, B., & Aebersold, R. (2007). Analysis of protein complexes using mass spectrometry. *Nat Rev Mol Cell Biol*, 8(8), 645–54.
- [125] Glickman, M. H. & Ciechanover, A. (2002). The ubiquitin-proteasome proteolytic pathway: destruction for the sake of construction. *Physiol Rev*, 82(2), 373–428.
- [126] Glickman, M. H., Rubin, D. M., Fried, V. A., & Finley, D. (1998). The regulatory particle of the *saccharomyces cerevisiae* proteasome. *Mol Cell Biol*, 18(6), 3149–62.
- [127] Gogala, M., Becker, T., Beatrix, B., Armache, J.-P., Barrio-Garcia, C., Berninghausen, O., & Beckmann, R. (2014). Structures of the sec61 complex engaged in nascent peptide translocation or membrane insertion. *Nature*, 506(7486), 107–10.

- [128] Goldberg, A. L. (2003). Protein degradation and protection against misfolded or damaged proteins. *Nature*, 426(6968), 895–9.
- [129] Gomez-Navarro, N. & Miller, E. (2016). Protein sorting at the er-golgi interface. *J Cell Biol*, 215(6), 769–778.
- [130] Griesemer, M., Young, C., Robinson, A. S., & Petzold, L. (2014). Bip clustering facilitates protein folding in the endoplasmic reticulum. *PLoS Comput Biol*, 10(7), e1003675.
- [131] Grubb, S., Guo, L., Fisher, E. A., & Brodsky, J. L. (2012). Protein disulfide isomerases contribute differentially to the endoplasmic reticulum-associated degradation of apolipoprotein b and other substrates. *Mol Biol Cell*, 23(4), 520–32.
- [132] Guerrero, C., Tagwerker, C., Kaiser, P., & Huang, L. (2006). An integrated mass spectrometry-based proteomic approach: quantitative analysis of tandem affinity-purified in vivo cross-linked protein complexes (qtax) to decipher the 26 s proteasome-interacting network. *Mol Cell Proteomics*, 5(2), 366–78.
- [133] Günther, R., Bräuer, C., Janetzky, B., Förster, H. H., Ehbrecht, I. M., Lehle, L., & Küntzel, H. (1991). The *saccharomyces cerevisiae* *trg1* gene is essential for growth and encodes a luminal endoplasmic reticulum glycoprotein involved in the maturation of vacuolar carboxypeptidase. *J Biol Chem*, 266(36), 24557–63.
- [134] Habeck, G., Ebner, F. A., Shimada-Kreft, H., & Kreft, S. G. (2015). The yeast *erad-c* ubiquitin ligase *doa10* recognizes an intramembrane degron. *J Cell Biol*, 209(2), 261–73.
- [135] Hale, S. J., Lovell, S. C., de Keyzer, J., & Stirling, C. J. (2010). Interactions between *kar2p* and its nucleotide exchange factors *sil1p* and *lhs1p* are mechanistically distinct. *J Biol Chem*, 285(28), 21600–6.
- [136] Halic, M. & Beckmann, R. (2005). The signal recognition particle and its interactions during protein targeting. *Curr Opin Struct Biol*, 15(1), 116–25.
- [137] Hammond, C., Braakman, I., & Helenius, A. (1994). Role of n-linked oligosaccharide recognition, glucose trimming, and calnexin in glycoprotein folding and quality control. *Proc Natl Acad Sci U S A*, 91(3), 913–7.
- [138] Hampton, R. Y. (2002). Er-associated degradation in protein quality control and cellular regulation. *Curr Opin Cell Biol*, 14(4), 476–82.
- [139] Hampton, R. Y. & Sommer, T. (2012). Finding the will and the way of *erad* substrate retrotranslocation. *Curr Opin Cell Biol*, 24(4), 460–6.

- [140] Hanahan, D. (1983). Studies on transformation of escherichia coli with plasmids. *J Mol Biol*, 166(4), 557–80.
- [141] Hanna, J., Leggett, D. S., & Finley, D. (2003). Ubiquitin depletion as a key mediator of toxicity by translational inhibitors. *Mol Cell Biol*, 23(24), 9251–61.
- [142] Hansen, W., Garcia, P. D., & Walter, P. (1986). In vitro protein translocation across the yeast endoplasmic reticulum: Atp-dependent posttranslational translocation of the prepro-alpha-factor. *Cell*, 45(3), 397–406.
- [143] Hara-Kuge, S., Kuge, O., Orci, L., Amherdt, M., Ravazzola, M., Wieland, F. T., & Rothman, J. E. (1994). En bloc incorporation of coatamer subunits during the assembly of cop-coated vesicles. *J Cell Biol*, 124(6), 883–92.
- [144] Hartl, F. U. (1996). Molecular chaperones in cellular protein folding. *Nature*, 381(6583), 571–9.
- [145] Haßdenteufel, S., Johnson, N., Paton, A. W., Paton, J. C., High, S., & Zimmermann, R. (2018). Chaperone-mediated sec61 channel gating during er import of small precursor proteins overcomes sec61 inhibitor-reinforced energy barrier. *Cell Rep*, 23(5), 1373–1386.
- [146] Hebert, D. N., Foellmer, B., & Helenius, A. (1995). Glucose trimming and reglycosylation determine glycoprotein association with calnexin in the endoplasmic reticulum. *Cell*, 81(3), 425–33.
- [147] Hegde, R. S. & Bernstein, H. D. (2006). The surprising complexity of signal sequences. *Trends Biochem Sci*, 31(10), 563–71.
- [148] Hegde, R. S. & Keenan, R. J. (2011). Tail-anchored membrane protein insertion into the endoplasmic reticulum. *Nat Rev Mol Cell Biol*, 12(12), 787–98.
- [149] Heinrich, S. U., Mothes, W., Brunner, J., & Rapoport, T. A. (2000). The sec61p complex mediates the integration of a membrane protein by allowing lipid partitioning of the transmembrane domain. *Cell*, 102(2), 233–44.
- [150] Helenius, A. & Aebi, M. (2004). Roles of n-linked glycans in the endoplasmic reticulum. *Annu Rev Biochem*, 73, 1019–49.
- [151] Helenius, A., Trombetta, E., Hebert, D., & Simons, J. (1997). Calnexin, calreticulin and the folding of glycoproteins. *Trends Cell Biol*, 7(5), 193–200.
- [152] Hellman, R., Vanhove, M., Lejeune, A., Stevens, F. J., & Hendershot, L. M. (1999). The in vivo association of bip with newly synthesized proteins is dependent on the rate and stability of folding and not simply on the presence of sequences that can bind to bip. *J Cell Biol*, 144(1), 21–30.

- [153] Helmers, J., Schmidt, D., Glavy, J. S., Blobel, G., & Schwartz, T. (2003). The beta-subunit of the protein-conducting channel of the endoplasmic reticulum functions as the guanine nucleotide exchange factor for the beta-subunit of the signal recognition particle receptor. *J Biol Chem*, 278(26), 23686–90.
- [154] Hennessy, F., Nicoll, W. S., Zimmermann, R., Cheetham, M. E., & Blatch, G. L. (2005). Not all j domains are created equal: implications for the specificity of hsp40-hsp70 interactions. *Protein Sci*, 14(7), 1697–709.
- [155] Herzog, F., Kahraman, A., Boehringer, D., Mak, R., Bracher, A., Walzthoeni, T., Leitner, A., Beck, M., Hartl, F.-U., Ban, N., Malmström, L., & Aebersold, R. (2012). Structural probing of a protein phosphatase 2a network by chemical cross-linking and mass spectrometry. *Science*, 337(6100), 1348–52.
- [156] Hessa, T., Kim, H., Bihlmaier, K., Lundin, C., Boekel, J., Andersson, H., Nilsson, I., White, S. H., & von Heijne, G. (2005). Recognition of transmembrane helices by the endoplasmic reticulum translocon. *Nature*, 433(7024), 377–81.
- [157] Hetz, C., Chevet, E., & Harding, H. P. (2013). Targeting the unfolded protein response in disease. *Nat Rev Drug Discov*, 12(9), 703–19.
- [158] Hiller, M. M., Finger, A., Schweiger, M., & Wolf, D. H. (1996). Er degradation of a misfolded luminal protein by the cytosolic ubiquitin-proteasome pathway. *Science*, 273(5282), 1725–8.
- [159] Hirsch, C., Gauss, R., Horn, S. C., Neuber, O., & Sommer, T. (2009). The ubiquitylation machinery of the endoplasmic reticulum. *Nature*, 458(7237), 453–60.
- [160] Hizlan, D., Robson, A., Whitehouse, S., Gold, V. A., Vonck, J., Mills, D., Kühlbrandt, W., & Collinson, I. (2012). Structure of the secy complex unlocked by a preprotein mimic. *Cell Rep*, 1(1), 21–8.
- [161] Ho, S. N., Hunt, H. D., Horton, R. M., Pullen, J. K., & Pease, L. R. (1989). Site-directed mutagenesis by overlap extension using the polymerase chain reaction. *Gene*, 77(1), 51–9.
- [162] Ho, Y., Gruhler, A., Heilbut, A., Bader, G. D., Moore, L., Adams, S.-L., Millar, A., Taylor, P., Bennett, K., Boutilier, K., Yang, L., Wolting, C., Donaldson, I., Schandorff, S., Shewnarane, J., Vo, M., Taggart, J., Goudreault, M., Muskat, B., Alfarano, C., Dewar, D., Lin, Z., Michalickova, K., Willems, A. R., Sassi, H., Nielsen, P. A., Rasmussen, K. J., Andersen, J. R., Johansen, L. E., Hansen, L. H., Jaspersen, H., Podtelejnikov, A., Nielsen, E., Crawford, J., Poulsen, V., Sørensen, B. D., Matthiesen, J., Hendrickson, R. C., Gleeson, F., Pawson, T., Moran, M. F., Durocher, D., Mann, M., Hogue, C. W. V., Figeys, D., & Tyers,

- M. (2002). Systematic identification of protein complexes in *saccharomyces cerevisiae* by mass spectrometry. *Nature*, 415(6868), 180–3.
- [163] Holding, A. N. (2015). XI-ms: Protein cross-linking coupled with mass spectrometry. *Methods*, 89, 54–63.
- [164] Horton, R. M., Hunt, H. D., Ho, S. N., Pullen, J. K., & Pease, L. R. (1989). Engineering hybrid genes without the use of restriction enzymes: gene splicing by overlap extension. *Gene*, 77(1), 61–8.
- [165] Hou, J., Tyo, K. E. J., Liu, Z., Petranovic, D., & Nielsen, J. (2012). Metabolic engineering of recombinant protein secretion by *saccharomyces cerevisiae*. *FEMS Yeast Res*, 12(5), 491–510.
- [166] Huber, W., von Heydebreck, A., Sülthmann, H., Poustka, A., & Vingron, M. (2002). Variance stabilization applied to microarray data calibration and to the quantification of differential expression. *Bioinformatics*, 18 Suppl 1, S96–104.
- [167] Hughes, H. & Stephens, D. J. (2008). Assembly, organization, and function of the copii coat. *Histochem Cell Biol*, 129(2), 129–51.
- [168] Huh, W.-K., Falvo, J. V., Gerke, L. C., Carroll, A. S., Howson, R. W., Weissman, J. S., & O’Shea, E. K. (2003). Global analysis of protein localization in budding yeast. *Nature*, 425(6959), 686–91.
- [169] Hurlley, S. M., Bole, D. G., Hoover-Litty, H., Helenius, A., & Copeland, C. S. (1989). Interactions of misfolded influenza virus hemagglutinin with binding protein (bip). *J Cell Biol*, 108(6), 2117–26.
- [170] Husnjak, K., Elsasser, S., Zhang, N., Chen, X., Randles, L., Shi, Y., Hofmann, K., Walters, K. J., Finley, D., & Dikic, I. (2008). Proteasome subunit rpn13 is a novel ubiquitin receptor. *Nature*, 453(7194), 481–8.
- [171] Hutzler, F., Gerstl, R., Lommel, M., & Strahl, S. (2008). Protein n-glycosylation determines functionality of the *saccharomyces cerevisiae* cell wall integrity sensor mid2p. *Mol Microbiol*, 68(6), 1438–49.
- [172] Huyer, G., Piluek, W. F., Fansler, Z., Kreft, S. G., Hochstrasser, M., Brodsky, J. L., & Michaelis, S. (2004). Distinct machinery is required in *saccharomyces cerevisiae* for the endoplasmic reticulum-associated degradation of a multispanning membrane protein and a soluble luminal protein. *J Biol Chem*, 279(37), 38369–78.
- [173] Itskanov, S. & Park, E. (2019). Structure of the posttranslational sec protein-translocation channel complex from yeast. *Science*, 363(6422), 84–87.

- [174] Jahn, R. & Scheller, R. H. (2006). Snares—engines for membrane fusion. *Nat Rev Mol Cell Biol*, 7(9), 631–43.
- [175] Jakob, C. A., Bodmer, D., Spirig, U., Battig, P., Marcil, A., Dignard, D., Bergeron, J. J., Thomas, D. Y., & Aebi, M. (2001). Htm1p, a mannosidase-like protein, is involved in glycoprotein degradation in yeast. *EMBO Rep*, 2(5), 423–30.
- [176] Jakob, C. A., Burda, P., Roth, J., & Aebi, M. (1998). Degradation of misfolded endoplasmic reticulum glycoproteins in *saccharomyces cerevisiae* is determined by a specific oligosaccharide structure. *J Cell Biol*, 142(5), 1223–33.
- [177] Janke, C., Magiera, M. M., Rathfelder, N., Taxis, C., Reber, S., Maekawa, H., Moreno-Borchart, A., Doenges, G., Schwob, E., Schiebel, E., & Knop, M. (2004). A versatile toolbox for pcr-based tagging of yeast genes: new fluorescent proteins, more markers and promoter substitution cassettes. *Yeast*, 21(11), 947–62.
- [178] Jarosch, E., Taxis, C., Volkwein, C., Bordallo, J., Finley, D., Wolf, D. H., & Sommer, T. (2002). Protein dislocation from the er requires polyubiquitination and the aaa-atpase cdc48. *Nat Cell Biol*, 4(2), 134–9.
- [179] Jentsch, S. & Rumpf, S. (2007). Cdc48 (p97): a "molecular gearbox" in the ubiquitin pathway? *Trends Biochem Sci*, 32(1), 6–11.
- [180] Jiang, Y., Cheng, Z., Mandon, E. C., & Gilmore, R. (2008). An interaction between the srp receptor and the translocon is critical during cotranslational protein translocation. *J Cell Biol*, 180(6), 1149–61.
- [181] Josefsson, L. G. & Randall, L. L. (1981). Different exported proteins in *e. coli* show differences in the temporal mode of processing in vivo. *Cell*, 25(1), 151–7.
- [182] Julius, D., Schekman, R., & Thorner, J. (1984). Glycosylation and processing of prepro-alpha-factor through the yeast secretory pathway. *Cell*, 36(2), 309–18.
- [183] Junne, T., Schwede, T., Goder, V., & Spiess, M. (2006). The plug domain of yeast sec61p is important for efficient protein translocation, but is not essential for cell viability. *Mol Biol Cell*, 17(9), 4063–8.
- [184] Junne, T., Schwede, T., Goder, V., & Spiess, M. (2007). Mutations in the sec61p channel affecting signal sequence recognition and membrane protein topology. *J Biol Chem*, 282(45), 33201–9.

- [185] Kabani, M., Kelley, S. S., Morrow, M. W., Montgomery, D. L., Sivendran, R., Rose, M. D., Gierasch, L. M., & Brodsky, J. L. (2003). Dependence of endoplasmic reticulum-associated degradation on the peptide binding domain and concentration of bip. *Mol Biol Cell*, 14(8), 3437–48.
- [186] Kaiser, M.-L. & Römisch, K. (2015). Proteasome 19s rp binding to the sec61 channel plays a key role in erad. *PLoS One*, 10(2), e0117260.
- [187] Kalies, K.-U., Allan, S., Sergeyenko, T., Kröger, H., & Römisch, K. (2005). The protein translocation channel binds proteasomes to the endoplasmic reticulum membrane. *EMBO J*, 24(13), 2284–93.
- [188] Kalies, K. U., Rapoport, T. A., & Hartmann, E. (1998). The beta subunit of the sec61 complex facilitates cotranslational protein transport and interacts with the signal peptidase during translocation. *J Cell Biol*, 141(4), 887–94.
- [189] Kanehara, K., Kawaguchi, S., & Ng, D. T. W. (2007). The edem and yos9p families of lectin-like erad factors. *Semin Cell Dev Biol*, 18(6), 743–50.
- [190] Katiyar, S., Till, E. A., & Lennarz, W. J. (2001). Studies on the function of yeast protein disulfide isomerase in renaturation of proteins. *Biochim Biophys Acta*, 1548(1), 47–56.
- [191] Kawahara, T., Yanagi, H., Yura, T., & Mori, K. (1997). Endoplasmic reticulum stress-induced mrna splicing permits synthesis of transcription factor hac1p/ern4p that activates the unfolded protein response. *Mol Biol Cell*, 8(10), 1845–62.
- [192] Kelleher, D. J. & Gilmore, R. (2006). An evolving view of the eukaryotic oligosaccharyltransferase. *Glycobiology*, 16(4), 47R–62R.
- [193] Kemmink, J., Dijkstra, K., Mariani, M., Scheek, R. M., Penka, E., Nilges, M., & Darby, N. J. (1999). The structure in solution of the b domain of protein disulfide isomerase. *J Biomol NMR*, 13(4), 357–68.
- [194] Khmelinskii, A., Blaszczyk, E., Pantazopoulou, M., Fischer, B., Omnus, D. J., Le Dez, G., Brossard, A., Gunnarsson, A., Barry, J. D., Meurer, M., Kirrmaier, D., Boone, C., Huber, W., Rabut, G., Ljungdahl, P. O., & Knop, M. (2014). Protein quality control at the inner nuclear membrane. *Nature*, 516(7531), 410–3.
- [195] Kida, Y. & Sakaguchi, M. (2018). Interaction mapping of the sec61 translocon identifies two sec61 α regions interacting with hydrophobic segments in translocating chains. *J Biol Chem*, 293(44), 17050–17060.

- [196] Kim, I., Ahn, J., Liu, C., Tanabe, K., Apodaca, J., Suzuki, T., & Rao, H. (2006). The png1-rad23 complex regulates glycoprotein turnover. *J Cell Biol*, 172(2), 211–9.
- [197] Kim, W., Spear, E. D., & Ng, D. T. W. (2005). Yos9p detects and targets misfolded glycoproteins for er-associated degradation. *Mol Cell*, 19(6), 753–64.
- [198] Kim, Y. T., Tabor, S., Churchich, J. E., & Richardson, C. C. (1992). Interactions of gene 2.5 protein and dna polymerase of bacteriophage t7. *J Biol Chem*, 267(21), 15032–40.
- [199] Kimura, T., Hosoda, Y., Sato, Y., Kitamura, Y., Ikeda, T., Horibe, T., & Kikuchi, M. (2005). Interactions among yeast protein-disulfide isomerase proteins and endoplasmic reticulum chaperone proteins influence their activities. *J Biol Chem*, 280(36), 31438–41.
- [200] Klappa, P., Ruddock, L. W., Darby, N. J., & Freedman, R. B. (1998). The b' domain provides the principal peptide-binding site of protein disulfide isomerase but all domains contribute to binding of misfolded proteins. *EMBO J*, 17(4), 927–35.
- [201] Knop, M., Finger, A., Braun, T., Hellmuth, K., & Wolf, D. H. (1996a). Der1, a novel protein specifically required for endoplasmic reticulum degradation in yeast. *EMBO J*, 15(4), 753–63.
- [202] Knop, M., Hauser, N., & Wolf, D. H. (1996b). N-glycosylation affects endoplasmic reticulum degradation of a mutated derivative of carboxypeptidase yscy in yeast. *Yeast*, 12(12), 1229–38.
- [203] Koegl, M., Hoppe, T., Schlenker, S., Ulrich, H. D., Mayer, T. U., & Jentsch, S. (1999). A novel ubiquitination factor, e4, is involved in multiubiquitin chain assembly. *Cell*, 96(5), 635–44.
- [204] Kohlmann, S., Schäfer, A., & Wolf, D. H. (2008). Ubiquitin ligase hul5 is required for fragment-specific substrate degradation in endoplasmic reticulum-associated degradation. *J Biol Chem*, 283(24), 16374–83.
- [205] Koo, E. H., Lansbury, Jr, P. T., & Kelly, J. W. (1999). Amyloid diseases: abnormal protein aggregation in neurodegeneration. *Proc Natl Acad Sci U S A*, 96(18), 9989–90.
- [206] Kostova, Z. & Wolf, D. H. (2003). For whom the bell tolls: protein quality control of the endoplasmic reticulum and the ubiquitin-proteasome connection. *EMBO J*, 22(10), 2309–17.

- [207] Kota, J., Gilstring, C. F., & Ljungdahl, P. O. (2007). Membrane chaperone shr3 assists in folding amino acid permeases preventing precocious erad. *J Cell Biol*, 176(5), 617–28.
- [208] Kruse, K. B., Brodsky, J. L., & McCracken, A. A. (2006). Characterization of an erad gene as vps30/atg6 reveals two alternative and functionally distinct protein quality control pathways: one for soluble z variant of human alpha-1 proteinase inhibitor (a1piz) and another for aggregates of a1piz. *Mol Biol Cell*, 17(1), 203–12.
- [209] Kulak, N. A., Pichler, G., Paron, I., Nagaraj, N., & Mann, M. (2014). Minimal, encapsulated proteomic-sample processing applied to copy-number estimation in eukaryotic cells. *Nat Methods*, 11(3), 319–24.
- [210] Kurjan, J. & Herskowitz, I. (1982). Structure of a yeast pheromone gene (mf alpha): a putative alpha-factor precursor contains four tandem copies of mature alpha-factor. *Cell*, 30(3), 933–43.
- [211] Lacroute, F. (1968). Regulation of pyrimidine biosynthesis in *saccharomyces cerevisiae*. *J Bacteriol*, 95(3), 824–32.
- [212] Lakkaraju, A. K. K., Thankappan, R., Mary, C., Garrison, J. L., Taunton, J., & Strub, K. (2012). Efficient secretion of small proteins in mammalian cells relies on sec62-dependent posttranslational translocation. *Mol Biol Cell*, 23(14), 2712–22.
- [213] Lam, Y. A., Lawson, T. G., Velayutham, M., Zweier, J. L., & Pickart, C. M. (2002). A proteasomal atpase subunit recognizes the polyubiquitin degradation signal. *Nature*, 416(6882), 763–7.
- [214] Lang, S., Benedix, J., Fedeles, S. V., Schorr, S., Schirra, C., Schäuble, N., Jalal, C., Greiner, M., Hassdenteufel, S., Tatzelt, J., Kreutzer, B., Edelmann, L., Krause, E., Rettig, J., Somlo, S., Zimmermann, R., & Dudek, J. (2012). Different effects of sec61 α , sec62 and sec63 depletion on transport of polypeptides into the endoplasmic reticulum of mammalian cells. *J Cell Sci*, 125(Pt 8), 1958–69.
- [215] Lang, S., Pfeffer, S., Lee, P.-H., Cavalié, A., Helms, V., Förster, F., & Zimmermann, R. (2017). An update on sec61 channel functions, mechanisms, and related diseases. *Front Physiol*, 8, 887.
- [216] Lee, R. J., Liu, C.-W., Harty, C., McCracken, A. A., Latterich, M., Römisch, K., DeMartino, G. N., Thomas, P. J., & Brodsky, J. L. (2004). Uncoupling retrotranslocation and degradation in the er-associated degradation of a soluble protein. *EMBO J*, 23(11), 2206–15.

- [217] Leitner, A., Walzthoeni, T., & Aebersold, R. (2014). Lysine-specific chemical cross-linking of protein complexes and identification of cross-linking sites using lc-ms/ms and the xquest/xprophet software pipeline. *Nat Protoc*, 9(1), 120–37.
- [218] Leitner, A., Walzthoeni, T., Kahraman, A., Herzog, F., Rinner, O., Beck, M., & Aebersold, R. (2010). Probing native protein structures by chemical cross-linking, mass spectrometry, and bioinformatics. *Mol Cell Proteomics*, 9(8), 1634–49.
- [219] Li, G., Zhao, G., Zhou, X., Schindelin, H., & Lennarz, W. J. (2006). The aaa atpase p97 links peptide n-glycanase to the endoplasmic reticulum-associated e3 ligase autocrine motility factor receptor. *Proc Natl Acad Sci U S A*, 103(22), 8348–53.
- [220] Li, H., Korennykh, A. V., Behrman, S. L., & Walter, P. (2010). Mammalian endoplasmic reticulum stress sensor ire1 signals by dynamic clustering. *Proc Natl Acad Sci U S A*, 107(37), 16113–8.
- [221] Lilley, B. N. & Ploegh, H. L. (2004). A membrane protein required for dislocation of misfolded proteins from the er. *Nature*, 429(6994), 834–40.
- [222] Liu, F., Rijkers, D. T. S., Post, H., & Heck, A. J. R. (2015). Proteome-wide profiling of protein assemblies by cross-linking mass spectrometry. *Nat Methods*, 12(12), 1179–84.
- [223] Liu, Y., Choudhury, P., Cabral, C. M., & Sifers, R. N. (1999). Oligosaccharide modification in the early secretory pathway directs the selection of a misfolded glycoprotein for degradation by the proteasome. *J Biol Chem*, 274(9), 5861–7.
- [224] Loayza, D., Tam, A., Schmidt, W. K., & Michaelis, S. (1998). Ste6p mutants defective in exit from the endoplasmic reticulum (er) reveal aspects of an er quality control pathway in *saccharomyces cerevisiae*. *Mol Biol Cell*, 9(10), 2767–84.
- [225] Lodder, A. L., Lee, T. K., & Ballester, R. (1999). Characterization of the wsc1 protein, a putative receptor in the stress response of *saccharomyces cerevisiae*. *Genetics*, 152(4), 1487–99.
- [226] Loibl, M., Wunderle, L., Hutzler, J., Schulz, B. L., Aebi, M., & Strahl, S. (2014). Protein o-mannosyltransferases associate with the translocon to modify translocating polypeptide chains. *J Biol Chem*, 289(12), 8599–611.
- [227] Lomant, A. J. & Fairbanks, G. (1976). Chemical probes of extended biological structures: synthesis and properties of the cleavable protein cross-linking reagent [35s]dithiobis(succinimidyl propionate). *J Mol Biol*, 104(1), 243–61.

- [228] Lowe, M. (2011). Structural organization of the golgi apparatus. *Curr Opin Cell Biol*, 23(1), 85–93.
- [229] Luz, J. M. & Lennarz, W. J. (1998). The nonactive site cysteine residues of yeast protein disulfide isomerase are not required for cell viability. *Biochem Biophys Res Commun*, 248(3), 621–7.
- [230] Lyman, S. K. & Schekman, R. (1995). Interaction between bip and sec63p is required for the completion of protein translocation into the er of *saccharomyces cerevisiae*. *J Cell Biol*, 131(5), 1163–71.
- [231] Macer, D. R. & Koch, G. L. (1988). Identification of a set of calcium-binding proteins in reticuloplasm, the luminal content of the endoplasmic reticulum. *J Cell Sci*, 91 (Pt 1), 61–70.
- [232] Madés, A., Gotthardt, K., Awe, K., Stieler, J., Döring, T., Füsér, S., & Prange, R. (2012). Role of human sec63 in modulating the steady-state levels of multi-spanning membrane proteins. *PLoS One*, 7(11), e49243.
- [233] Makowski, M. M., Willems, E., Jansen, P. W. T. C., & Vermeulen, M. (2016). Cross-linking immunoprecipitation-ms (xip-ms): Topological analysis of chromatin-associated protein complexes using single affinity purification. *Mol Cell Proteomics*, 15(3), 854–65.
- [234] Mandon, E. C., Trueman, S. F., & Gilmore, R. (2013). Protein translocation across the rough endoplasmic reticulum. *Cold Spring Harb Perspect Biol*, 5(2).
- [235] Matlack, K. E., Misselwitz, B., Plath, K., & Rapoport, T. A. (1999). Bip acts as a molecular ratchet during posttranslational transport of prepro-alpha factor across the er membrane. *Cell*, 97(5), 553–64.
- [236] Mayer, M. P. & Bukau, B. (2005). Hsp70 chaperones: cellular functions and molecular mechanism. *Cell Mol Life Sci*, 62(6), 670–84.
- [237] Mayer, T. U., Braun, T., & Jentsch, S. (1998). Role of the proteasome in membrane extraction of a short-lived er-transmembrane protein. *EMBO J*, 17(12), 3251–7.
- [238] Mayinger, P. & Meyer, D. I. (1993). An atp transporter is required for protein translocation into the yeast endoplasmic reticulum. *EMBO J*, 12(2), 659–66.
- [239] McCaffrey, K. & Braakman, I. (2016). Protein quality control at the endoplasmic reticulum. *Essays Biochem*, 60(2), 227–235.

- [240] McCracken, A. A. & Brodsky, J. L. (1996). Assembly of er-associated protein degradation in vitro: dependence on cytosol, calnexin, and atp. *J Cell Biol*, 132(3), 291–8.
- [241] McKnight, C. J., Stradley, S. J., Jones, J. D., & Gierasch, L. M. (1991). Conformational and membrane-binding properties of a signal sequence are largely unaltered by its adjacent mature region. *Proc Natl Acad Sci U S A*, 88(13), 5799–803.
- [242] Medicherla, B., Kostova, Z., Schaefer, A., & Wolf, D. H. (2004). A genomic screen identifies dsk2p and rad23p as essential components of er-associated degradation. *EMBO Rep*, 5(7), 692–7.
- [243] Mehnert, M., Sommer, T., & Jarosch, E. (2014). Der1 promotes movement of misfolded proteins through the endoplasmic reticulum membrane. *Nat Cell Biol*, 16(1), 77–86.
- [244] Melcher, K. (2004). New chemical crosslinking methods for the identification of transient protein-protein interactions with multiprotein complexes. *Curr Protein Pept Sci*, 5(4), 287–96.
- [245] Melnyk, A., Rieger, H., & Zimmermann, R. (2015). Co-chaperones of the mammalian endoplasmic reticulum. *Subcell Biochem*, 78, 179–200.
- [246] Meusser, B., Hirsch, C., Jarosch, E., & Sommer, T. (2005). Erad: the long road to destruction. *Nat Cell Biol*, 7(8), 766–72.
- [247] Meyer, D. I., Krause, E., & Dobberstein, B. (1982). Secretory protein translocation across membranes—the role of the "docking protein". *Nature*, 297(5868), 647–50.
- [248] Meyer, H. A., Grau, H., Kraft, R., Kostka, S., Prehn, S., Kalies, K. U., & Hartmann, E. (2000). Mammalian sec61 is associated with sec62 and sec63. *J Biol Chem*, 275(19), 14550–7.
- [249] Mezzacasa, A. & Helenius, A. (2002). The transitional er defines a boundary for quality control in the secretion of tso45 vsv glycoprotein. *Traffic*, 3(11), 833–49.
- [250] Misselwitz, B., Staack, O., Matlack, K. E., & Rapoport, T. A. (1999). Interaction of bip with the j-domain of the sec63p component of the endoplasmic reticulum protein translocation complex. *J Biol Chem*, 274(29), 20110–5.
- [251] Molinari, M., Calanca, V., Galli, C., Lucca, P., & Paganetti, P. (2003). Role of edem in the release of misfolded glycoproteins from the calnexin cycle. *Science*, 299(5611), 1397–400.

- [252] Mori, K., Ma, W., Gething, M. J., & Sambrook, J. (1993). A transmembrane protein with a cdc2+/cdc28-related kinase activity is required for signaling from the er to the nucleus. *Cell*, 74(4), 743–56.
- [253] Mumberg, D., Müller, R., & Funk, M. (1994). Regulatable promoters of *Saccharomyces cerevisiae*: comparison of transcriptional activity and their use for heterologous expression. *Nucleic Acids Res*, 22(25), 5767–8.
- [254] Nakatsukasa, K. & Brodsky, J. L. (2008). The recognition and retrotranslocation of misfolded proteins from the endoplasmic reticulum. *Traffic*, 9(6), 861–70.
- [255] Nakatsukasa, K., Huyer, G., Michaelis, S., & Brodsky, J. L. (2008). Dissecting the er-associated degradation of a misfolded polytopic membrane protein. *Cell*, 132(1), 101–12.
- [256] Neduva, V. & Russell, R. B. (2005). Linear motifs: evolutionary interaction switches. *FEBS Lett*, 579(15), 3342–5.
- [257] Neuber, O., Jarosch, E., Volkwein, C., Walter, J., & Sommer, T. (2005). Ubx2 links the cdc48 complex to er-associated protein degradation. *Nat Cell Biol*, 7(10), 993–8.
- [258] Ng, D. T., Brown, J. D., & Walter, P. (1996). Signal sequences specify the targeting route to the endoplasmic reticulum membrane. *J Cell Biol*, 134(2), 269–78.
- [259] Ng, D. T., Hiebert, S. W., & Lamb, R. A. (1990). Different roles of individual n-linked oligosaccharide chains in folding, assembly, and transport of the simian virus 5 hemagglutinin-neuraminidase. *Mol Cell Biol*, 10(5), 1989–2001.
- [260] Ng, D. T., Randall, R. E., & Lamb, R. A. (1989). Intracellular maturation and transport of the sv5 type ii glycoprotein hemagglutinin-neuraminidase: specific and transient association with grp78-bip in the endoplasmic reticulum and extensive internalization from the cell surface. *J Cell Biol*, 109(6 Pt 2), 3273–89.
- [261] Ng, D. T., Spear, E. D., & Walter, P. (2000). The unfolded protein response regulates multiple aspects of secretory and membrane protein biogenesis and endoplasmic reticulum quality control. *J Cell Biol*, 150(1), 77–88.
- [262] Ng, W., Sergeyenko, T., Zeng, N., Brown, J. D., & Römisch, K. (2007). Characterization of the proteasome interaction with the sec61 channel in the endoplasmic reticulum. *J Cell Sci*, 120(Pt 4), 682–91.
- [263] Nicastro, R., Sardu, A., Panchaud, N., & De Virgilio, C. (2017). The architecture of the rag gtpase signaling network. *Biomolecules*, 7(3).

- [264] Niessing, D., Hüttelmaier, S., Zenklusen, D., Singer, R. H., & Burley, S. K. (2004). She2p is a novel rna binding protein with a basic helical hairpin motif. *Cell*, 119(4), 491–502.
- [265] Nikawa, J., Akiyoshi, M., Hirata, S., & Fukuda, T. (1996). *Saccharomyces cerevisiae* ire2/hac1 is involved in ire1-mediated kar2 expression. *Nucleic Acids Res*, 24(21), 4222–6.
- [266] Nishikawa, S. & Endo, T. (1997). The yeast jem1p is a dnaj-like protein of the endoplasmic reticulum membrane required for nuclear fusion. *J Biol Chem*, 272(20), 12889–92.
- [267] Nishikawa, S. I., Fewell, S. W., Kato, Y., Brodsky, J. L., & Endo, T. (2001). Molecular chaperones in the yeast endoplasmic reticulum maintain the solubility of proteins for retrotranslocation and degradation. *J Cell Biol*, 153(5), 1061–70.
- [268] Noiva, R., Freedman, R. B., & Lennarz, W. J. (1993). Peptide binding to protein disulfide isomerase occurs at a site distinct from the active sites. *J Biol Chem*, 268(26), 19210–7.
- [269] Nørgaard, P., Westphal, V., Tachibana, C., Alsøe, L., Holst, B., & Winther, J. R. (2001). Functional differences in yeast protein disulfide isomerases. *J Cell Biol*, 152(3), 553–62.
- [270] Nyathi, Y., Wilkinson, B. M., & Pool, M. R. (2013). Co-translational targeting and translocation of proteins to the endoplasmic reticulum. *Biochim Biophys Acta*, 1833(11), 2392–402.
- [271] Ogg, S. C., Barz, W. P., & Walter, P. (1998). A functional gtpase domain, but not its transmembrane domain, is required for function of the srp receptor beta-subunit. *J Cell Biol*, 142(2), 341–54.
- [272] Oliver, J. D., Roderick, H. L., Llewellyn, D. H., & High, S. (1999). Erp57 functions as a subunit of specific complexes formed with the er lectins calreticulin and calnexin. *Mol Biol Cell*, 10(8), 2573–82.
- [273] Oliver, J. D., van der Wal, F. J., Bulleid, N. J., & High, S. (1997). Interaction of the thiol-dependent reductase erp57 with nascent glycoproteins. *Science*, 275(5296), 86–8.
- [274] Olzmann, J. A., Kopito, R. R., & Christianson, J. C. (2013). The mammalian endoplasmic reticulum-associated degradation system. *Cold Spring Harb Perspect Biol*, 5(9).

- [275] Ou, W. J., Cameron, P. H., Thomas, D. Y., & Bergeron, J. J. (1993). Association of folding intermediates of glycoproteins with calnexin during protein maturation. *Nature*, 364(6440), 771–6.
- [276] Oveland, E., Muth, T., Rapp, E., Martens, L., Berven, F. S., & Barsnes, H. (2015). Viewing the proteome: how to visualize proteomics data? *Proteomics*, 15(8), 1341–55.
- [277] Panzner, S., Dreier, L., Hartmann, E., Kostka, S., & Rapoport, T. A. (1995a). Posttranslational protein transport in yeast reconstituted with a purified complex of sec proteins and kar2p. *Cell*, 81(4), 561–70.
- [278] Panzner, S., Dreier, L., Hartmann, E., Kostka, S., & Rapoport, T. A. (1995b). Posttranslational protein transport into the endoplasmic reticulum. *Cold Spring Harb Symp Quant Biol*, 60, 31–40.
- [279] Park, E., Ménétret, J.-F., Gumbart, J. C., Ludtke, S. J., Li, W., Whynot, A., Rapoport, T. A., & Akey, C. W. (2014). Structure of the secy channel during initiation of protein translocation. *Nature*, 506(7486), 102–6.
- [280] Park, E. & Rapoport, T. A. (2011). Preserving the membrane barrier for small molecules during bacterial protein translocation. *Nature*, 473(7346), 239–42.
- [281] Park, E. & Rapoport, T. A. (2012). Mechanisms of sec61/secy-mediated protein translocation across membranes. *Annu Rev Biophys*, 41, 21–40.
- [282] Park, S.-H., Bolender, N., Eisele, F., Kostova, Z., Takeuchi, J., Coffino, P., & Wolf, D. H. (2007). The cytoplasmic hsp70 chaperone machinery subjects misfolded and endoplasmic reticulum import-incompetent proteins to degradation via the ubiquitin-proteasome system. *Mol Biol Cell*, 18(1), 153–65.
- [283] Parodi, A. J. (2000). Protein glucosylation and its role in protein folding. *Annu Rev Biochem*, 69, 69–93.
- [284] Pfeffer, S., Burbaum, L., Unverdorben, P., Pech, M., Chen, Y., Zimmermann, R., Beckmann, R., & Förster, F. (2015). Structure of the native sec61 protein-conducting channel. *Nat Commun*, 6, 8403.
- [285] Philip, B. & Levin, D. E. (2001). Wsc1 and mid2 are cell surface sensors for cell wall integrity signaling that act through rom2, a guanine nucleotide exchange factor for rho1. *Mol Cell Biol*, 21(1), 271–80.
- [286] Phizicky, E. M. & Fields, S. (1995). Protein-protein interactions: methods for detection and analysis. *Microbiol Rev*, 59(1), 94–123.

- [287] Pierce, T. S. (2009). Crosslinking technical handbook. *Thermo Fisher Scientific, Rockford, IL, USA*.
- [288] Pilon, M., Römisch, K., Quach, D., & Schekman, R. (1998). Sec61p serves multiple roles in secretory precursor binding and translocation into the endoplasmic reticulum membrane. *Mol Biol Cell*, 9(12), 3455–73.
- [289] Pilon, M., Schekman, R., & Römisch, K. (1997). Sec61p mediates export of a misfolded secretory protein from the endoplasmic reticulum to the cytosol for degradation. *EMBO J*, 16(15), 4540–8.
- [290] Pincus, D., Chevalier, M. W., Aragón, T., van Anken, E., Vidal, S. E., El-Samad, H., & Walter, P. (2010). Bip binding to the er-stress sensor ire1 tunes the homeostatic behavior of the unfolded protein response. *PLoS Biol*, 8(7), e1000415.
- [291] Pind, S., Riordan, J. R., & Williams, D. B. (1994). Participation of the endoplasmic reticulum chaperone calnexin (p88, ip90) in the biogenesis of the cystic fibrosis transmembrane conductance regulator. *J Biol Chem*, 269(17), 12784–8.
- [292] Plath, K., Mothes, W., Wilkinson, B. M., Stirling, C. J., & Rapoport, T. A. (1998). Signal sequence recognition in posttranslational protein transport across the yeast er membrane. *Cell*, 94(6), 795–807.
- [293] Plemper, R. K., Böhmler, S., Bordallo, J., Sommer, T., & Wolf, D. H. (1997). Mutant analysis links the translocon and bip to retrograde protein transport for er degradation. *Nature*, 388(6645), 891–5.
- [294] Plemper, R. K., Bordallo, J., Deak, P. M., Taxis, C., Hitt, R., & Wolf, D. H. (1999). Genetic interactions of hrd3p and der3p/hrd1p with sec61p suggest a retro-translocation complex mediating protein transport for er degradation. *J Cell Sci*, 112 (Pt 22), 4123–34.
- [295] Plemper, R. K., Egner, R., Kuchler, K., & Wolf, D. H. (1998). Endoplasmic reticulum degradation of a mutated atp-binding cassette transporter pdr5 proceeds in a concerted action of sec61 and the proteasome. *J Biol Chem*, 273(49), 32848–56.
- [296] Plemper, R. K. & Wolf, D. H. (1999). Endoplasmic reticulum degradation. reverse protein transport and its end in the proteasome. *Mol Biol Rep*, 26(1-2), 125–30.
- [297] Ploegh, H. L. (2007). A lipid-based model for the creation of an escape hatch from the endoplasmic reticulum. *Nature*, 448(7152), 435–8.

- [298] Plumb, R., Zhang, Z.-R., Appathurai, S., & Mariappan, M. (2015). A functional link between the co-translational protein translocation pathway and the upr. *Elife*, 4.
- [299] Politis, A., Stengel, F., Hall, Z., Hernández, H., Leitner, A., Walzthoeni, T., Robinson, C. V., & Aebersold, R. (2014). A mass spectrometry-based hybrid method for structural modeling of protein complexes. *Nat Methods*, 11(4), 403–406.
- [300] Preuss, D., Mulholland, J., Franzusoff, A., Segev, N., & Botstein, D. (1992). Characterization of the *Saccharomyces* golgi complex through the cell cycle by immunoelectron microscopy. *Mol Biol Cell*, 3(7), 789–803.
- [301] Puig, A. & Gilbert, H. F. (1994). Protein disulfide isomerase exhibits chaperone and anti-chaperone activity in the oxidative refolding of lysozyme. *J Biol Chem*, 269(10), 7764–71.
- [302] Puig, O., Caspary, F., Rigaut, G., Rutz, B., Bouveret, E., Bragado-Nilsson, E., Wilm, M., & Séraphin, B. (2001). The tandem affinity purification (tap) method: a general procedure of protein complex purification. *Methods*, 24(3), 218–29.
- [303] Quan, E. M., Kamiya, Y., Kamiya, D., Denic, V., Weibezahn, J., Kato, K., & Weissman, J. S. (2008). Defining the glycan destruction signal for endoplasmic reticulum-associated degradation. *Mol Cell*, 32(6), 870–7.
- [304] Raasi, S. & Wolf, D. H. (2007). Ubiquitin receptors and erad: a network of pathways to the proteasome. *Semin Cell Dev Biol*, 18(6), 780–91.
- [305] Rabinovich, E., Kerem, A., Fröhlich, K.-U., Diamant, N., & Bar-Nun, S. (2002). Aaa-atpase p97/cdc48p, a cytosolic chaperone required for endoplasmic reticulum-associated protein degradation. *Mol Cell Biol*, 22(2), 626–34.
- [306] Ramachandran, N., Hainsworth, E., Bhullar, B., Eisenstein, S., Rosen, B., Lau, A. Y., Walter, J. C., & LaBaer, J. (2004). Self-assembling protein microarrays. *Science*, 305(5680), 86–90.
- [307] Ramírez, M. P., Rivera, M., Quiroga-Roger, D., Bustamante, A., Vega, M., Baez, M., Puchner, E. M., & Wilson, C. A. M. (2017). Single molecule force spectroscopy reveals the effect of bip chaperone on protein folding. *Protein Sci*, 26(7), 1404–1412.
- [308] Rape, M., Hoppe, T., Gorr, I., Kalocay, M., Richly, H., & Jentsch, S. (2001). Mobilization of processed, membrane-tethered spt23 transcription factor by cdc48(ufd1/npl4), a ubiquitin-selective chaperone. *Cell*, 107(5), 667–77.

- [309] Rapoport, T. A. (2007). Protein translocation across the eukaryotic endoplasmic reticulum and bacterial plasma membranes. *Nature*, 450(7170), 663–9.
- [310] Rapoport, T. A., Li, L., & Park, E. (2017). Structural and mechanistic insights into protein translocation. *Annu Rev Cell Dev Biol*, 33, 369–390.
- [311] Rappsilber, J. (2011). The beginning of a beautiful friendship: cross-linking/mass spectrometry and modelling of proteins and multi-protein complexes. *J Struct Biol*, 173(3), 530–40.
- [312] Rashid, K. A., Hevi, S., Chen, Y., Le Cahérec, F., & Chuck, S. L. (2002). A proteomic approach identifies proteins in hepatocytes that bind nascent apolipoprotein b. *J Biol Chem*, 277(24), 22010–7.
- [313] Reithinger, J. H., Yim, C., Kim, S., Lee, H., & Kim, H. (2014). Structural and functional profiling of the lateral gate of the sec61 translocon. *J Biol Chem*, 289(22), 15845–55.
- [314] Richly, H., Rape, M., Braun, S., Rumpf, S., Hoegel, C., & Jentsch, S. (2005). A series of ubiquitin binding factors connects cdc48/p97 to substrate multiubiquitylation and proteasomal targeting. *Cell*, 120(1), 73–84.
- [315] Rigaut, G., Shevchenko, A., Rutz, B., Wilm, M., Mann, M., & Séraphin, B. (1999). A generic protein purification method for protein complex characterization and proteome exploration. *Nat Biotechnol*, 17(10), 1030–2.
- [316] Ritchie, M. E., Phipson, B., Wu, D., Hu, Y., Law, C. W., Shi, W., & Smyth, G. K. (2015). limma powers differential expression analyses for rna-sequencing and microarray studies. *Nucleic Acids Res*, 43(7), e47.
- [317] Rivett, A. J. (1993). Proteasomes: multicatalytic proteinase complexes. *Biochem J*, 291 (Pt 1), 1–10.
- [318] Rivett, A. J. (1998). Intracellular distribution of proteasomes. *Curr Opin Immunol*, 10(1), 110–4.
- [319] Roberts, C. J., Pohlig, G., Rothman, J. H., & Stevens, T. H. (1989). Structure, biosynthesis, and localization of dipeptidyl aminopeptidase b, an integral membrane glycoprotein of the yeast vacuole. *J Cell Biol*, 108(4), 1363–73.
- [320] Römisch, K. (2004). A cure for traffic jams: small molecule chaperones in the endoplasmic reticulum. *Traffic*, 5(11), 815–20.
- [321] Römisch, K. (2005). Endoplasmic reticulum-associated degradation. *Annu Rev Cell Dev Biol*, 21, 435–56.

- [322] Römisch, K. (2017). A case for sec61 channel involvement in erad. *Trends Biochem Sci*, 42(3), 171–179.
- [323] Rossanese, O. W., Reinke, C. A., Bevis, B. J., Hammond, A. T., Sears, I. B., O'Connor, J., & Glick, B. S. (2001). A role for actin, cdc1p, and myo2p in the inheritance of late golgi elements in *saccharomyces cerevisiae*. *J Cell Biol*, 153(1), 47–62.
- [324] Rossanese, O. W., Soderholm, J., Bevis, B. J., Sears, I. B., O'Connor, J., Williamson, E. K., & Glick, B. S. (1999). Golgi structure correlates with transitional endoplasmic reticulum organization in *pichia pastoris* and *saccharomyces cerevisiae*. *J Cell Biol*, 145(1), 69–81.
- [325] Rothblatt, J. A., Deshaies, R. J., Sanders, S. L., Daum, G., & Schekman, R. (1989). Multiple genes are required for proper insertion of secretory proteins into the endoplasmic reticulum in yeast. *J Cell Biol*, 109(6 Pt 1), 2641–52.
- [326] Rothblatt, J. A. & Meyer, D. I. (1986). Secretion in yeast: reconstitution of the translocation and glycosylation of alpha-factor and invertase in a homologous cell-free system. *Cell*, 44(4), 619–28.
- [327] Rubin, D. M., Glickman, M. H., Larsen, C. N., Dhruvakumar, S., & Finley, D. (1998). Active site mutants in the six regulatory particle atpases reveal multiple roles for atp in the proteasome. *EMBO J*, 17(17), 4909–19.
- [328] Ruggiano, A., Foresti, O., & Carvalho, P. (2014). Quality control: Er-associated degradation: protein quality control and beyond. *J Cell Biol*, 204(6), 869–79.
- [329] Saibil, H. (2000). Molecular chaperones: containers and surfaces for folding, stabilising or unfolding proteins. *Curr Opin Struct Biol*, 10(2), 251–8.
- [330] Sanger, F., Nicklen, S., & Coulson, A. R. (1977). Dna sequencing with chain-terminating inhibitors. *Proc Natl Acad Sci U S A*, 74(12), 5463–7.
- [331] Savitski, M. M., Reinhard, F. B. M., Franken, H., Werner, T., Savitski, M. F., Eberhard, D., Martinez Molina, D., Jafari, R., Dovega, R. B., Klaeger, S., Kuster, B., Nordlund, P., Bantscheff, M., & Drewes, G. (2014). Tracking cancer drugs in living cells by thermal profiling of the proteome. *Science*, 346(6205), 1255784.
- [332] Schächter, V. (2002). Bioinformatics of large-scale protein interaction networks. *Biotechniques*, Suppl, 16–8, 20–4, 26–7.
- [333] Schäfer, A. & Wolf, D. H. (2009). Sec61p is part of the endoplasmic reticulum-associated degradation machinery. *EMBO J*, 28(19), 2874–84.

- [334] Scheper, W., Thaminy, S., Kais, S., Stagljar, I., & Römisch, K. (2003). Coordination of n-glycosylation and protein translocation across the endoplasmic reticulum membrane by sss1 protein. *J Biol Chem*, 278(39), 37998–8003.
- [335] Schibich, D., Gloge, F., Pöhner, I., Björkholm, P., Wade, R. C., von Heijne, G., Bukau, B., & Kramer, G. (2016). Global profiling of srp interaction with nascent polypeptides. *Nature*, 536(7615), 219–23.
- [336] Schlager, B., Straessle, A., & Hafen, E. (2012). Use of anionic denaturing detergents to purify insoluble proteins after overexpression. *BMC Biotechnol*, 12, 95.
- [337] Schlenstedt, G., Harris, S., Risse, B., Lill, R., & Silver, P. A. (1995). A yeast dnaj homologue, scj1p, can function in the endoplasmic reticulum with bip/kar2p via a conserved domain that specifies interactions with hsp70s. *J Cell Biol*, 129(4), 979–88.
- [338] Schmidt, C., Lenz, C., Grote, M., Lührmann, R., & Urlaub, H. (2010). Determination of protein stoichiometry within protein complexes using absolute quantification and multiple reaction monitoring. *Anal Chem*, 82(7), 2784–96.
- [339] Schmitz, A., Herrgen, H., Winkeler, A., & Herzog, V. (2000). Cholera toxin is exported from microsomes by the sec61p complex. *J Cell Biol*, 148(6), 1203–12.
- [340] Schmitz, A., Schneider, A., Kummer, M. P., & Herzog, V. (2004). Endoplasmic reticulum-localized amyloid beta-peptide is degraded in the cytosol by two distinct degradation pathways. *Traffic*, 5(2), 89–101.
- [341] Schoebel, S., Mi, W., Stein, A., Ovchinnikov, S., Pavlovicz, R., DiMaio, F., Baker, D., Chambers, M. G., Su, H., Li, D., Rapoport, T. A., & Liao, M. (2017). Cryo-em structure of the protein-conducting erad channel hrd1 in complex with hrd3. *Nature*, 548(7667), 352–355.
- [342] Schrader, E. K., Harstad, K. G., & Matouschek, A. (2009). Targeting proteins for degradation. *Nat Chem Biol*, 5(11), 815–22.
- [343] Schröder, M. (2008). Endoplasmic reticulum stress responses. *Cell Mol Life Sci*, 65(6), 862–94.
- [344] Schubert, U., Antón, L. C., Gibbs, J., Norbury, C. C., Yewdell, J. W., & Bennink, J. R. (2000). Rapid degradation of a large fraction of newly synthesized proteins by proteasomes. *Nature*, 404(6779), 770–4.

- [345] Schuberth, C. & Buchberger, A. (2005). Membrane-bound ubx2 recruits cdc48 to ubiquitin ligases and their substrates to ensure efficient er-associated protein degradation. *Nat Cell Biol*, 7(10), 999–1006.
- [346] Schwaller, M., Wilkinson, B., & Gilbert, H. F. (2003). Reduction-reoxidation cycles contribute to catalysis of disulfide isomerization by protein-disulfide isomerase. *J Biol Chem*, 278(9), 7154–9.
- [347] Schwanhäusser, B., Busse, D., Li, N., Dittmar, G., Schuchhardt, J., Wolf, J., Chen, W., & Selbach, M. (2011). Global quantification of mammalian gene expression control. *Nature*, 473(7347), 337–42.
- [348] Scott, D. C. & Schekman, R. (2008). Role of sec61p in the er-associated degradation of short-lived transmembrane proteins. *J Cell Biol*, 181(7), 1095–105.
- [349] Servas, C. & Römisch, K. (2013). The sec63p j-domain is required for erad of soluble proteins in yeast. *PLoS One*, 8(12), e82058.
- [350] Sevilla, L. M., Comstock, S. S., Swier, K., & Miller, J. (2004). Endoplasmic reticulum-associated degradation-induced dissociation of class ii invariant chain complexes containing a glycosylation-deficient form of p41. *J Immunol*, 173(4), 2586–93.
- [351] Shamu, C. E. & Walter, P. (1996). Oligomerization and phosphorylation of the ire1p kinase during intracellular signaling from the endoplasmic reticulum to the nucleus. *EMBO J*, 15(12), 3028–39.
- [352] Shan, S.-o. & Walter, P. (2005). Co-translational protein targeting by the signal recognition particle. *FEBS Lett*, 579(4), 921–6.
- [353] Shao, S. & Hegde, R. S. (2011). Membrane protein insertion at the endoplasmic reticulum. *Annu Rev Cell Dev Biol*, 27, 25–56.
- [354] Shaw, A. S., Rottier, P. J., & Rose, J. K. (1988). Evidence for the loop model of signal-sequence insertion into the endoplasmic reticulum. *Proc Natl Acad Sci U S A*, 85(20), 7592–6.
- [355] Shen, S. H., Chrétien, P., Bastien, L., & Slilaty, S. N. (1991). Primary sequence of the glucanase gene from oerskovia xanthineolytica. expression and purification of the enzyme from escherichia coli. *J Biol Chem*, 266(2), 1058–63.
- [356] Shen, X., Ellis, R. E., Lee, K., Liu, C. Y., Yang, K., Solomon, A., Yoshida, H., Morimoto, R., Kurnit, D. M., Mori, K., & Kaufman, R. J. (2001). Complementary signaling pathways regulate the unfolded protein response and are required for c. elegans development. *Cell*, 107(7), 893–903.

- [357] Shi, Y., Pellarin, R., Fridy, P. C., Fernandez-Martinez, J., Thompson, M. K., Li, Y., Wang, Q. J., Sali, A., Rout, M. P., & Chait, B. T. (2015). A strategy for dissecting the architectures of native macromolecular assemblies. *Nat Methods*, 12(12), 1135–8.
- [358] Shimizu, Y., Okuda-Shimizu, Y., & Hendershot, L. M. (2010). Ubiquitylation of an erad substrate occurs on multiple types of amino acids. *Mol Cell*, 40(6), 917–26.
- [359] Shindiapina, P. & Barlowe, C. (2010). Requirements for transitional endoplasmic reticulum site structure and function in *saccharomyces cerevisiae*. *Mol Biol Cell*, 21(9), 1530–45.
- [360] Shorter, J. & Warren, G. (2002). Golgi architecture and inheritance. *Annu Rev Cell Dev Biol*, 18, 379–420.
- [361] Shrimal, S., Cherepanova, N. A., & Gilmore, R. (2017). Dc2 and kcp2 mediate the interaction between the oligosaccharyltransferase and the er translocon. *J Cell Biol*, 216(11), 3625–3638.
- [362] Shurtleff, M. J., Itzhak, D. N., Hussmann, J. A., Schirle Oakdale, N. T., Costa, E. A., Jonikas, M., Weibezahn, J., Popova, K. D., Jan, C. H., Sinitcyn, P., Vembar, S. S., Hernandez, H., Cox, J., Burlingame, A. L., Brodsky, J. L., Frost, A., Borner, G. H., & Weissman, J. S. (2018). The er membrane protein complex interacts cotranslationally to enable biogenesis of multipass membrane proteins. *Elife*, 7.
- [363] Sidrauski, C., Cox, J. S., & Walter, P. (1996). trna ligase is required for regulated mrna splicing in the unfolded protein response. *Cell*, 87(3), 405–13.
- [364] Sidrauski, C. & Walter, P. (1997). The transmembrane kinase ire1p is a site-specific endonuclease that initiates mrna splicing in the unfolded protein response. *Cell*, 90(6), 1031–9.
- [365] Sikorski, R. S. & Hieter, P. (1989). A system of shuttle vectors and yeast host strains designed for efficient manipulation of dna in *saccharomyces cerevisiae*. *Genetics*, 122(1), 19–27.
- [366] Silberstein, S., Schlenstedt, G., Silver, P. A., & Gilmore, R. (1998). A role for the dnaj homologue scj1p in protein folding in the yeast endoplasmic reticulum. *J Cell Biol*, 143(4), 921–33.
- [367] Singh, A., Chen, E. Y., Lugovoy, J. M., Chang, C. N., Hitzeman, R. A., & Seeburg, P. H. (1983). *Saccharomyces cerevisiae* contains two discrete genes coding for the alpha-factor pheromone. *Nucleic Acids Res*, 11(12), 4049–63.

- [368] Sinz, A. (2006). Chemical cross-linking and mass spectrometry to map three-dimensional protein structures and protein-protein interactions. *Mass Spectrom Rev*, 25(4), 663–82.
- [369] Sinz, A., Arlt, C., Chorev, D., & Sharon, M. (2015). Chemical cross-linking and native mass spectrometry: A fruitful combination for structural biology. *Protein Sci*, 24(8), 1193–209.
- [370] Smith, M. H., Ploegh, H. L., & Weissman, J. S. (2011). Road to ruin: targeting proteins for degradation in the endoplasmic reticulum. *Science*, 334(6059), 1086–90.
- [371] Smits, A. H., Jansen, P. W. T. C., Poser, I., Hyman, A. A., & Vermeulen, M. (2013). Stoichiometry of chromatin-associated protein complexes revealed by label-free quantitative mass spectrometry-based proteomics. *Nucleic Acids Res*, 41(1), e28.
- [372] Smits, A. H. & Vermeulen, M. (2016). Characterizing protein-protein interactions using mass spectrometry: Challenges and opportunities. *Trends Biotechnol*, 34(10), 825–834.
- [373] Sogaard, M., Tani, K., Ye, R. R., Geromanos, S., Tempst, P., Kirchhausen, T., Rothman, J. E., & Söllner, T. (1994). A rab protein is required for the assembly of snare complexes in the docking of transport vesicles. *Cell*, 78(6), 937–48.
- [374] Sommer, T. & Jentsch, S. (1993). A protein translocation defect linked to ubiquitin conjugation at the endoplasmic reticulum. *Nature*, 365(6442), 176–9.
- [375] Song, J. L. & Wang, C. C. (1995). Chaperone-like activity of protein disulfide-isomerase in the refolding of rhodanese. *Eur J Biochem*, 231(2), 312–6.
- [376] Song, W., Raden, D., Mandon, E. C., & Gilmore, R. (2000). Role of sec61alpha in the regulated transfer of the ribosome-nascent chain complex from the signal recognition particle to the translocation channel. *Cell*, 100(3), 333–43.
- [377] Spear, E. D. & Ng, D. T. W. (2005). Single, context-specific glycans can target misfolded glycoproteins for er-associated degradation. *J Cell Biol*, 169(1), 73–82.
- [378] Stagg, S. M., Gürkan, C., Fowler, D. M., LaPointe, P., Foss, T. R., Potter, C. S., Carragher, B., & Balch, W. E. (2006). Structure of the sec13/31 copii coat cage. *Nature*, 439(7073), 234–8.
- [379] Steel, G. J., Fullerton, D. M., Tyson, J. R., & Stirling, C. J. (2004). Coordinated activation of hsp70 chaperones. *Science*, 303(5654), 98–101.

- [380] Stein, A., Ruggiano, A., Carvalho, P., & Rapoport, T. A. (2014). Key steps in erad of luminal er proteins reconstituted with purified components. *Cell*, 158(6), 1375–1388.
- [381] Stevenson, J., Huang, E. Y., & Olzmann, J. A. (2016). Endoplasmic reticulum-associated degradation and lipid homeostasis. *Annu Rev Nutr*, 36, 511–42.
- [382] Stirling, C. J., Rothblatt, J., Hosobuchi, M., Deshaies, R., & Schekman, R. (1992). Protein translocation mutants defective in the insertion of integral membrane proteins into the endoplasmic reticulum. *Mol Biol Cell*, 3(2), 129–42.
- [383] Strahl-Bolsinger, S., Immervoll, T., Deutzmann, R., & Tanner, W. (1993). Pmt1, the gene for a key enzyme of protein o-glycosylation in *Saccharomyces cerevisiae*. *Proc Natl Acad Sci U S A*, 90(17), 8164–8.
- [384] Syed, M. I., Moorthy, B. T., Jenner, A., Fetka, I., & Jansen, R.-P. (2018). Signal sequence-independent targeting of mid2 mRNA to the endoplasmic reticulum by the yeast RNA-binding protein Khd1p. *FEBS Lett*, 592(11), 1870–1881.
- [385] Szathmary, R., Biemann, R., Nita-Lazar, M., Burda, P., & Jakob, C. A. (2005). Yos9 protein is essential for degradation of misfolded glycoproteins and may function as lectin in erad. *Mol Cell*, 19(6), 765–75.
- [386] Szklarczyk, D., Gable, A. L., Lyon, D., Junge, A., Wyder, S., Huerta-Cepas, J., Simonovic, M., Doncheva, N. T., Morris, J. H., Bork, P., Jensen, L. J., & Mering, C. v. (2019). STRING v11: protein-protein association networks with increased coverage, supporting functional discovery in genome-wide experimental datasets. *Nucleic Acids Res*, 47(D1), D607–D613.
- [387] Tang, X. & Bruce, J. E. (2009). Chemical cross-linking for protein-protein interaction studies. *Methods Mol Biol*, 492, 283–93.
- [388] Tannous, A., Pisoni, G. B., Hebert, D. N., & Molinari, M. (2015). N-linked sugar-regulated protein folding and quality control in the ER. *Semin Cell Dev Biol*, 41, 79–89.
- [389] Taxis, C., Hitt, R., Park, S.-H., Deak, P. M., Kostova, Z., & Wolf, D. H. (2003). Use of modular substrates demonstrates mechanistic diversity and reveals differences in chaperone requirement of erad. *J Biol Chem*, 278(38), 35903–13.
- [390] Taxis, C., Vogel, F., & Wolf, D. H. (2002). ER-golgi traffic is a prerequisite for efficient ER degradation. *Mol Biol Cell*, 13(6), 1806–18.
- [391] Thibault, G. & Ng, D. T. W. (2012). The endoplasmic reticulum-associated degradation pathways of budding yeast. *Cold Spring Harb Perspect Biol*, 4(12).

- [392] Thomas, P. J., Qu, B. H., & Pedersen, P. L. (1995). Defective protein folding as a basis of human disease. *Trends Biochem Sci*, 20(11), 456–9.
- [393] Tortorella, D., Story, C. M., Huppa, J. B., Wiertz, E. J., Jones, T. R., Bacik, I., Bennink, J. R., Yewdell, J. W., & Ploegh, H. L. (1998). Dislocation of type I membrane proteins from the ER to the cytosol is sensitive to changes in redox potential. *J Cell Biol*, 142(2), 365–76.
- [394] Trakselis, M. A., Alley, S. C., & Ishmael, F. T. (2005). Identification and mapping of protein-protein interactions by a combination of cross-linking, cleavage, and proteomics. *Bioconjug Chem*, 16(4), 741–50.
- [395] Tran, J. R., Tomsic, L. R., & Brodsky, J. L. (2011). A cdc48p-associated factor modulates endoplasmic reticulum-associated degradation, cell stress, and ubiquitinated protein homeostasis. *J Biol Chem*, 286(7), 5744–55.
- [396] Travers, K. J., Patil, C. K., Wodicka, L., Lockhart, D. J., Weissman, J. S., & Walter, P. (2000). Functional and genomic analyses reveal an essential coordination between the unfolded protein response and ER-associated degradation. *Cell*, 101(3), 249–58.
- [397] Tretter, T., Pereira, F. P., Ulucan, O., Helms, V., Allan, S., Kalies, K.-U., & Römisch, K. (2013). Erad and protein import defects in a sec61 mutant lacking ER-luminal loop 7. *BMC Cell Biol*, 14, 56.
- [398] Tripathi, A., Mandon, E. C., Gilmore, R., & Rapoport, T. A. (2017). Two alternative binding mechanisms connect the protein translocation sec71-sec72 complex with heat shock proteins. *J Biol Chem*, 292(19), 8007–8018.
- [399] Trombetta, E. S. & Parodi, A. J. (2003). Quality control and protein folding in the secretory pathway. *Annu Rev Cell Dev Biol*, 19, 649–76.
- [400] Tsukazaki, T., Mori, H., Fukai, S., Ishitani, R., Mori, T., Dohmae, N., Perederina, A., Sugita, Y., Vassilyev, D. G., Ito, K., & Nureki, O. (2008). Conformational transition of sec machinery inferred from bacterial SecY structures. *Nature*, 455(7215), 988–91.
- [401] Turano, C., Coppari, S., Altieri, F., & Ferraro, A. (2002). Proteins of the PDI family: unpredicted non-ER locations and functions. *J Cell Physiol*, 193(2), 154–63.
- [402] Turriziani, B., von Kriegsheim, A., & Pennington, S. R. (2016). Protein-protein interaction detection via mass spectrometry-based proteomics. *Adv Exp Med Biol*, 919, 383–396.

- [403] Van, P. N., Peter, F., & Söling, H. D. (1989). Four intracisternal calcium-binding glycoproteins from rat liver microsomes with high affinity for calcium. no indication for calsequestrin-like proteins in inositol 1,4,5-trisphosphate-sensitive calcium sequestering rat liver vesicles. *J Biol Chem*, 264(29), 17494–501.
- [404] Van den Berg, B., Clemons, Jr, W. M., Collinson, I., Modis, Y., Hartmann, E., Harrison, S. C., & Rapoport, T. A. (2004). X-ray structure of a protein-conducting channel. *Nature*, 427(6969), 36–44.
- [405] Varshavsky, A. (2012). The ubiquitin system, an immense realm. *Annu Rev Biochem*, 81, 167–76.
- [406] Vashist, S., Kim, W., Belden, W. J., Spear, E. D., Barlowe, C., & Ng, D. T. (2001). Distinct retrieval and retention mechanisms are required for the quality control of endoplasmic reticulum protein folding. *J Cell Biol*, 155(3), 355–68.
- [407] Vashist, S. & Ng, D. T. W. (2004). Misfolded proteins are sorted by a sequential checkpoint mechanism of er quality control. *J Cell Biol*, 165(1), 41–52.
- [408] Vasilescu, J. & Figeys, D. (2006). Mapping protein-protein interactions by mass spectrometry. *Curr Opin Biotechnol*, 17(4), 394–9.
- [409] Vembar, S. S. & Brodsky, J. L. (2008). One step at a time: endoplasmic reticulum-associated degradation. *Nat Rev Mol Cell Biol*, 9(12), 944–57.
- [410] Vembar, S. S., Jin, Y., Brodsky, J. L., & Hendershot, L. M. (2009). The mammalian hsp40 erdj3 requires its hsp70 interaction and substrate-binding properties to complement various yeast hsp40-dependent functions. *J Biol Chem*, 284(47), 32462–71.
- [411] Vembar, S. S., Jonikas, M. C., Hendershot, L. M., Weissman, J. S., & Brodsky, J. L. (2010). J domain co-chaperone specificity defines the role of bip during protein translocation. *J Biol Chem*, 285(29), 22484–94.
- [412] Verma, R., Chen, S., Feldman, R., Schieltz, D., Yates, J., Dohmen, J., & Deshaies, R. J. (2000). Proteasomal proteomics: identification of nucleotide-sensitive proteasome-interacting proteins by mass spectrometric analysis of affinity-purified proteasomes. *Mol Biol Cell*, 11(10), 3425–39.
- [413] Verma, R., Oania, R., Graumann, J., & Deshaies, R. J. (2004). Multiubiquitin chain receptors define a layer of substrate selectivity in the ubiquitin-proteasome system. *Cell*, 118(1), 99–110.
- [414] Viotti, C. (2016). Er to golgi-dependent protein secretion: The conventional pathway. *Methods Mol Biol*, 1459, 3–29.

- [415] Vitu, E., Gross, E., Greenblatt, H. M., Sevier, C. S., Kaiser, C. A., & Fass, D. (2008). Yeast mpd1p reveals the structural diversity of the protein disulfide isomerase family. *Journal of Molecular Biology*, 384(3), 631 – 640.
- [416] von Heijne, G. (1984). How signal sequences maintain cleavage specificity. *J Mol Biol*, 173(2), 243–51.
- [417] von Heijne, G. (1985). Signal sequences. the limits of variation. *J Mol Biol*, 184(1), 99–105.
- [418] von Heijne, G. (1986). Towards a comparative anatomy of n-terminal topogenic protein sequences. *J Mol Biol*, 189(1), 239–42.
- [419] von Heijne, G. (1990). The signal peptide. *J Membr Biol*, 115(3), 195–201.
- [420] von Heijne, G. & Gavel, Y. (1988). Topogenic signals in integral membrane proteins. *Eur J Biochem*, 174(4), 671–8.
- [421] von Mering, C., Krause, R., Snel, B., Cornell, M., Oliver, S. G., Fields, S., & Bork, P. (2002). Comparative assessment of large-scale data sets of protein-protein interactions. *Nature*, 417(6887), 399–403.
- [422] Voorhees, R. M., Fernández, I. S., Scheres, S. H. W., & Hegde, R. S. (2014). Structure of the mammalian ribosome-sec61 complex to 3.4 Å resolution. *Cell*, 157(7), 1632–43.
- [423] Voorhees, R. M. & Hegde, R. S. (2016a). Structure of the sec61 channel opened by a signal sequence. *Science*, 351(6268), 88–91.
- [424] Voorhees, R. M. & Hegde, R. S. (2016b). Toward a structural understanding of co-translational protein translocation. *Curr Opin Cell Biol*, 41, 91–9.
- [425] Walsh, P., Bursać, D., Law, Y. C., Cyr, D., & Lithgow, T. (2004). The j-protein family: modulating protein assembly, disassembly and translocation. *EMBO Rep*, 5(6), 567–71.
- [426] Walter, P., Ibrahimi, I., & Blobel, G. (1981). Translocation of proteins across the endoplasmic reticulum. i. signal recognition protein (srp) binds to in-vitro-assembled polysomes synthesizing secretory protein. *J Cell Biol*, 91(2 Pt 1), 545–50.
- [427] Wang, C. C. & Tsou, C. L. (1993). Protein disulfide isomerase is both an enzyme and a chaperone. *FASEB J*, 7(15), 1515–7.

- [428] Wang, L. & Dobberstein, B. (1999). Oligomeric complexes involved in translocation of proteins across the membrane of the endoplasmic reticulum. *FEBS Lett*, 457(3), 316–22.
- [429] Wang, Q. & Chang, A. (2003). Substrate recognition in er-associated degradation mediated by eps1, a member of the protein disulfide isomerase family. *EMBO J*, 22(15), 3792–802.
- [430] Wang, Q., Groenendyk, J., & Michalak, M. (2015). Glycoprotein quality control and endoplasmic reticulum stress. *Molecules*, 20(8), 13689–704.
- [431] Wang, X. Z., Harding, H. P., Zhang, Y., Jolicoeur, E. M., Kuroda, M., & Ron, D. (1998). Cloning of mammalian ire1 reveals diversity in the er stress responses. *EMBO J*, 17(19), 5708–17.
- [432] Ware, F. E., Vassilakos, A., Peterson, P. A., Jackson, M. R., Lehrman, M. A., & Williams, D. B. (1995). The molecular chaperone calnexin binds glc1man9glcnac2 oligosaccharide as an initial step in recognizing unfolded glycoproteins. *J Biol Chem*, 270(9), 4697–704.
- [433] Waters, M. G. & Blobel, G. (1986). Secretory protein translocation in a yeast cell-free system can occur posttranslationally and requires atp hydrolysis. *J Cell Biol*, 102(5), 1543–50.
- [434] Waters, M. G., Evans, E. A., & Blobel, G. (1988). Prepro-alpha-factor has a cleavable signal sequence. *J Biol Chem*, 263(13), 6209–14.
- [435] Weiel, J. & Hershey, J. W. (1982). The binding of fluorescein-labeled protein synthesis initiation factor 2 to escherichia coli 30 s ribosomal subunits determined by fluorescence polarization. *J Biol Chem*, 257(3), 1215–20.
- [436] Wepf, A., Glatter, T., Schmidt, A., Aebersold, R., & Gstaiger, M. (2009). Quantitative interaction proteomics using mass spectrometry. *Nat Methods*, 6(3), 203–5.
- [437] Werner, E. D., Brodsky, J. L., & McCracken, A. A. (1996). Proteasome-dependent endoplasmic reticulum-associated protein degradation: an unconventional route to a familiar fate. *Proc Natl Acad Sci U S A*, 93(24), 13797–801.
- [438] Wiertz, E. J., Jones, T. R., Sun, L., Bogyo, M., Geuze, H. J., & Ploegh, H. L. (1996a). The human cytomegalovirus us11 gene product dislocates mhc class i heavy chains from the endoplasmic reticulum to the cytosol. *Cell*, 84(5), 769–79.

- [439] Wiertz, E. J., Tortorella, D., Bogyo, M., Yu, J., Mothes, W., Jones, T. R., Rapoport, T. A., & Ploegh, H. L. (1996b). Sec61-mediated transfer of a membrane protein from the endoplasmic reticulum to the proteasome for destruction. *Nature*, 384(6608), 432–8.
- [440] Wild, K., Halic, M., Sinning, I., & Beckmann, R. (2004). Srp meets the ribosome. *Nat Struct Mol Biol*, 11(11), 1049–53.
- [441] Wilkinson, B. & Gilbert, H. F. (2004). Protein disulfide isomerase. *Biochim Biophys Acta*, 1699(1-2), 35–44.
- [442] Wilkinson, B. M., Esnault, Y., Craven, R. A., Skiba, F., Fieschi, J., K'epès, F., & Stirling, C. J. (1997). Molecular architecture of the er translocase probed by chemical crosslinking of sss1p to complementary fragments of sec61p. *EMBO J*, 16(15), 4549–59.
- [443] Willer, M., Forte, G. M. A., & Stirling, C. J. (2008). Sec61p is required for erad-I: genetic dissection of the translocation and erad-I functions of sec61p using novel derivatives of cpy. *J Biol Chem*, 283(49), 33883–8.
- [444] Willer, T., Valero, M. C., Tanner, W., Cruces, J., & Strahl, S. (2003). O-mannosyl glycans: from yeast to novel associations with human disease. *Curr Opin Struct Biol*, 13(5), 621–30.
- [445] Wirth, A., Jung, M., Bies, C., Frien, M., Tyedmers, J., Zimmermann, R., & Wagner, R. (2003). The sec61p complex is a dynamic precursor activated channel. *Mol Cell*, 12(1), 261–8.
- [446] Wohlschlegel, J. A., Johnson, E. S., Reed, S. I., & Yates, 3rd, J. R. (2004). Global analysis of protein sumoylation in *saccharomyces cerevisiae*. *J Biol Chem*, 279(44), 45662–8.
- [447] Wolin, S. L. & Walter, P. (1989). Signal recognition particle mediates a transient elongation arrest of preprolactin in reticulocyte lysate. *J Cell Biol*, 109(6 Pt 1), 2617–22.
- [448] Wormald, M. R. & Dwek, R. A. (1999). Glycoproteins: glycan presentation and protein-fold stability. *Structure*, 7(7), R155–60.
- [449] Wu, H., Ng, B. S. H., & Thibault, G. (2014). Endoplasmic reticulum stress response in yeast and humans. *Biosci Rep*, 34(4).
- [450] Wu, X., Cabanos, C., & Rapoport, T. A. (2019). Structure of the post-translational protein translocation machinery of the er membrane. *Nature*, 566(7742), 136–139.

- [451] Wu, X. & Rapoport, T. A. (2018). Mechanistic insights into er-associated protein degradation. *Curr Opin Cell Biol*, 53, 22–28.
- [452] Wu, Y., Swulius, M. T., Moremen, K. W., & Sifers, R. N. (2003). Elucidation of the molecular logic by which misfolded alpha 1-antitrypsin is preferentially selected for degradation. *Proc Natl Acad Sci U S A*, 100(14), 8229–34.
- [453] Xie, W., Kanehara, K., Sayeed, A., & Ng, D. T. W. (2009). Intrinsic conformational determinants signal protein misfolding to the hrd1/htm1 endoplasmic reticulum-associated degradation system. *Mol Biol Cell*, 20(14), 3317–29.
- [454] Xie, W. & Ng, D. T. W. (2010). Erad substrate recognition in budding yeast. *Semin Cell Dev Biol*, 21(5), 533–9.
- [455] Xing, S., Wallmeroth, N., Berendzen, K. W., & Grefen, C. (2016). Techniques for the analysis of protein-protein interactions in vivo. *Plant Physiol*, 171(2), 727–58.
- [456] Xu, C. & Ng, D. T. W. (2015). Glycosylation-directed quality control of protein folding. *Nat Rev Mol Cell Biol*, 16(12), 742–52.
- [457] Ye, Y., Meyer, H. H., & Rapoport, T. A. (2001). The aaa atpase cdc48/p97 and its partners transport proteins from the er into the cytosol. *Nature*, 414(6864), 652–6.
- [458] Ye, Y., Meyer, H. H., & Rapoport, T. A. (2003). Function of the p97-ufd1-npl4 complex in retrotranslocation from the er to the cytosol: dual recognition of nonubiquitinated polypeptide segments and polyubiquitin chains. *J Cell Biol*, 162(1), 71–84.
- [459] Ye, Y., Shibata, Y., Yun, C., Ron, D., & Rapoport, T. A. (2004). A membrane protein complex mediates retro-translocation from the er lumen into the cytosol. *Nature*, 429(6994), 841–7.
- [460] Youker, R. T., Walsh, P., Beilharz, T., Lithgow, T., & Brodsky, J. L. (2004). Distinct roles for the hsp40 and hsp90 molecular chaperones during cystic fibrosis transmembrane conductance regulator degradation in yeast. *Mol Biol Cell*, 15(11), 4787–97.
- [461] Young, C. L. & Robinson, A. S. (2014). Protein folding and secretion: mechanistic insights advancing recombinant protein production in *s. cerevisiae*. *Curr Opin Biotechnol*, 30, 168–77.
- [462] Young, M. M., Tang, N., Hempel, J. C., Oshiro, C. M., Taylor, E. W., Kuntz, I. D., Gibson, B. W., & Dollinger, G. (2000). High throughput protein fold identification

by using experimental constraints derived from intramolecular cross-links and mass spectrometry. *Proc Natl Acad Sci U S A*, 97(11), 5802–6.

- [463] Zattas, D., Adle, D. J., Rubenstein, E. M., & Hochstrasser, M. (2013). N-terminal acetylation of the yeast derlin der1 is essential for hrd1 ubiquitin-ligase activity toward luminal er substrates. *Mol Biol Cell*, 24(7), 890–900.
- [464] Zhang, H., Tang, X., Munske, G. R., Tolic, N., Anderson, G. A., & Bruce, J. E. (2009). Identification of protein-protein interactions and topologies in living cells with chemical cross-linking and mass spectrometry. *Mol Cell Proteomics*, 8(3), 409–20.
- [465] Zhao, X. & Jääntti, J. (2009). Functional characterization of the trans-membrane domain interactions of the sec61 protein translocation complex beta-subunit. *BMC Cell Biol*, 10, 76.
- [466] Zhou, M., Li, Q., & Wang, R. (2016). Current experimental methods for characterizing protein-protein interactions. *ChemMedChem*, 11(8), 738–56.
- [467] Zhu, H. & Snyder, M. (2003). Protein chip technology. *Curr Opin Chem Biol*, 7(1), 55–63.
- [468] Zielinska, D. F., Gnad, F., Wiśniewski, J. R., & Mann, M. (2010). Precision mapping of an in vivo n-glycoproteome reveals rigid topological and sequence constraints. *Cell*, 141(5), 897–907.
- [469] Zimmermann, R., Eyrisch, S., Ahmad, M., & Helms, V. (2011). Protein translocation across the er membrane. *Biochim Biophys Acta*, 1808(3), 912–24.
- [470] Zybailov, B. L., Glazko, G. V., Jaiswal, M., & Raney, K. D. (2013). Large scale chemical cross-linking mass spectrometry perspectives. *J Proteomics Bioinform*, 6(Suppl 2), 001.

Publications

Pereira, F., Rettel, M., Stein, F., Savitski, M., Collinson, I., & Römisch, K. (2019). Effect of Sec61 interaction with Mpd1 on endoplasmic reticulum-associated degradation. *PLoS One*

Tretter, T., **Pereira, F. P.**, Ulucan, O., Helms, V., Allan, S., Kalies, K.-U., & Römisch, K. (2013). ERAD and protein import defects in a *sec61* mutant lacking ER-luminal loop 7. *BMC Cell Biol*, 14, 56.

Barbieri, G., **Pereira, F.**, Elia, F., Simon, J., Babarit, A., Lupusella, C., Schuldiner, M., & Römisch, K. Sec61 channel phosphorylation selectively enhances protein import into the endoplasmic reticulum. In preparation.

Pereira, F., & Römisch, K. (2017). "Identification of Sec61p interactors by crosslinking and Mass Spectrometry" 13th ER & Redox Club Meeting, Hombourg (Germany) (*POSTER*)

Pereira, F., & Römisch, K. (2016). "Identification of Sec61p interacting partners in the ER lumen" EMBO Meeting, Manheim (Germany) (*POSTER*)

Pereira, F., & Römisch, K. (2014). "Identification of the Sec61p Loop 7 interactors by crosslinking" FEBS-EMBO Meeting, Paris (France) (*POSTER*)

Acknowledgments

First of all, I would like to thank my PhD supervisor Prof. Dr. Karin Römisch for giving me the opportunity to work in her lab, allowing me to grow as a scientist, and for ensuring that I always had conditions to undertake my research. Her philosophy of allowing students to conduct research independently, allowing me to follow my own ideas, helped me grow not only as a scientist, but as an individual as well, as it contributed immensely for my personal and self-confidence growth. Her advice on research and scientific writing has been of great value for me. Thank you for all your support and patience.

I would also like to thank my second PhD supervisor Prof. Dr. Richard Zimmermann, for accepting this charge and for the interest in my work and the valuable suggestions he gave me during our meetings.

I thank Dr. Alexander Stein for all his support in the setting up of the xQuest/xProphet pipeline, and for never getting exasperated with my incessant and basic questions.

I thank Timo Scheller from the Saarland University IT department who kindly helped me with some technical difficulties during xQuest/xProphet analysis setup and who granted me access to the ARM system, without which I would have not been able to access data that turnout to be very important in this work.

I must also thank Prof. Dr. Schmitt and his group, who kindly shared equipment and reagents with us whenever needed. I thank especially Sara, Björn, Andrea, Steffi, and Yutaka, who were always friendly and ready to help whenever I needed their help

Many thanks to Prof. Dr. Wittman for allowing access to the Biolector, and Mirjam as well as the other elements of the group who trained me in the use of the machine and helped me in multiple issues along my internship.

I thank also Francesco Elia and Guido Barbieri for sharing this adventure with me, and with whom I shared many good and bad moments, happy and stressful periods. Thank you for being there through it all. Great coworkers, even better friends.

Many thanks to Prof. Dr. Gert-Wieland Kohring for his words of encouragement, help setting up the BioLogic and AKTA Purification system, and overall, for all the technical, scientific and moral support he always supplied. Great person, great co-worker, AMAZING chef. I must also thank Susanne Kohring in that respect, as well as for always treating me with such kindness. My house is always opened for both of you.

Many thanks also to Carmen Clemens, my beloved Frau Clemens. Thank you for your energy and good humor. Thank you for becoming a good friend. Thank you for all the help with...well just about everything. My life in Germany would have been quite different, and definitely much sadder, without knowing you. My home is always

opened to you, being it in Germany, Portugal, or Timbuktu!

I thank Birgit Hasper for being the calm, organized and extremely competent person she is. Thank you for being my buddy during practicals, having things ready even before I thought about them, and for ALWAYS knowing where EVERYTHING is. If it wasn't for you, I would be lost looking for erlenmeyer corks to this day.

I also want to express my gratitude to Juncal Z. González for her patience and help provided with various administrative matters, which more often than not were beyond her job responsibilities. Above all, I thank her for her good humor and latin blood, that made me feel that much more at home.

To all my research group I thank the good moments we spent together. I aimed for 3 years, we ended up sharing 5. I won't lie saying they were the best 5 years of my life, but I can guarantee that without you all, I wouldn't have grown as I have, I wouldn't be the person I am now, and these 5 years would be unbearable. Thank you for helping me reach the finish line.

I must also thank all the students I supervised along my internship, both during their internships and during practical classes. Thank you for always reminding me how was to look at Science with fresh eyes, how to always be curious, and above all, for helping me (and especially my patience) grow. Despite all my whining, I will miss you all.

At a very personal level I want to thank four very important individuals in my life and without whom this thesis would never have been possible: my aunt Mariana Rosa Esteves, my better half Joana Godinho, my mother Luisa Pereira, and my sister Cláudia Pereira. To my aunt I thank everything. I thank her for being the amazing person she is, for her unconditional love, and for giving me such a rich and happy childhood. Without her unconditional support, at all levels imaginable, I would never have become the person I am today. Without her determination as an example, mine would have been a meager thing. Hope I can have you for many more years, 97 are not enough. I love you. To Joana, my partner, and above all else, my best friend, I thank for the beautiful person she is, for the extraordinary patience she has to put up with me, and for the courage and love she showed me when she accepted changing all her life, leave all her family and friends, her whole world, for me. I cannot say it will be forever, but I can say I cannot picture my life without you. I love you. To my mother I thank all the sacrifices she has done in her life in order to give me and my sister the best life possible, the life she didn't had. Without her strength, both me and my sister would not be the same. I love you. To my sister, my old old sister, I thank being who she is, for taking care of me since I can remember, for her unconditional love, and above all else, for helping modeling who I am today. Gosto tanto de ti que até faz doer o coração. I love you



Supplements

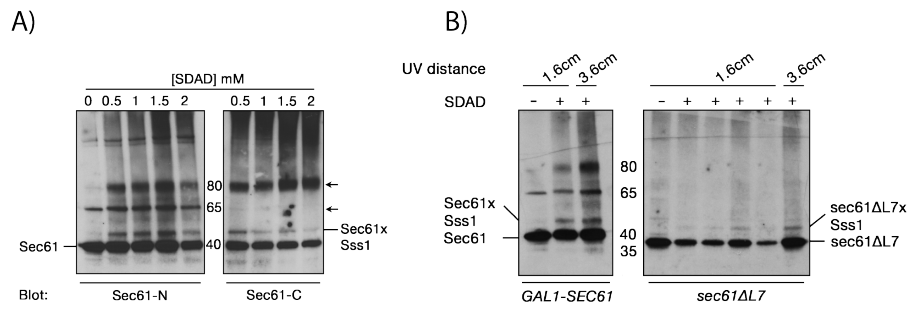


Figure A.1: Sec61 SDAD crosslinking pattern determination. Immunoblot analysis of the SDAD crosslinking pattern after titrating crosslinker concentration and UV irradiation distance. ER vesicles (17eq) were crosslinked with 1.5 mM SDAD for 30 min on ice, quenched for 15 min, UV-irradiated (356 nm) and analyzed by SDS-PAGE on 4-12 % Bis-Tris gels (NuPAGE® Novex® Pre-Cast gels, Invitrogen). Protein detection was done by western blotting and signal acquired in ECL film. **A)** SDAD concentration titration in wildtype microsomes (KRY461; GAL1-SEC61). Two different anti-Sec61 antibodies were used: an N-Terminal and an C-Terminal. The UV irradiation distance used was 3.6 cm. **B)** Distance of UV irradiation test. Microsomes from GAL1-SEC61 (left panel) *sec61ΔL7* (right panel) were used. Two different distances were used: 1.6cm and 3.6 cm.

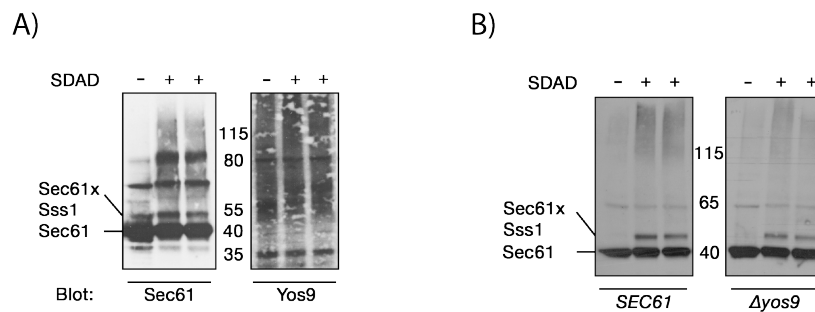


Figure A.2: SDAD conditions titration. Immunoblot analysis of the Sec61 SDAD crosslinking pattern versus the Yos9 one. ER vesicles (17eq) were crosslinked with 1.5 mM SDAD for 30 min on ice, quenched for 15 min, UV-irradiated (356 nm; 3.6 cm) and analyzed by SDS-PAGE on 4-12 % Bis-Tris gels (NuPAGE® Novex® Pre-Cast gels, Invitrogen). Protein detection was done by western blotting and signal acquired in ECL film. **A)** Comparison of the SDAD crosslinking pattern when two different antibodies are used for protein detection: anti-Sec61 and anti-Yos9. **B)** Comparison of the SDAD crosslinking pattern obtained in a SEC61 (Left panel) or Δyos9 (left panel) background.

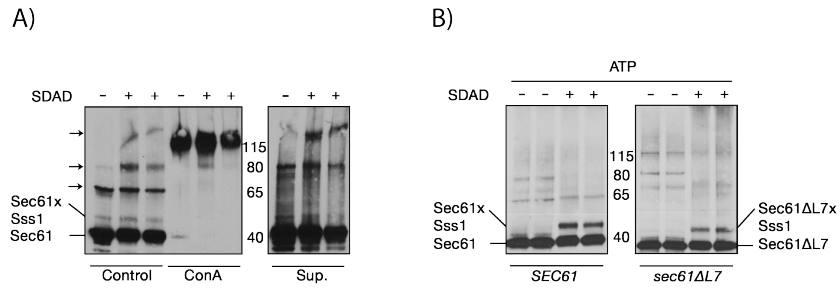


Figure A.3: Sec61 SDAD crosslinking pattern determination. Immunoblot analysis of the SDAD crosslinking pattern after different treatments. ER vesicles (17eq) were crosslinked with 1.5 mM SDAD for 30 min on ice, quenched for 15 min, UV-irradiated (356 nm; 3.6 cm) and analyzed by SDS-PAGE on 4-12 % Bis-Tris gels (NuPAGE® Novex® Pre-Cast gels, Invitrogen). Protein detection was done by western blotting and signal acquired in ECL film. **A)** Concanavalin-A precipitation of SDAD crosslinked samples. Samples were solubilized in IP Buffer after crosslinking and incubated under rotation with 20 μ l Concanavalin A for 2h at room temperature. Supernatant was removed and TCA precipitated, and beads were washed and sample was eluted in 2xLaemmli Buffer. After denaturing the samples were resolved in SDS-PAGE. Lanes 1 to 3 (right panel) show a control set of reactions where two samples were crosslinked with SDAD (lanes 2 and 3) and one where the sample was treated only with DMSO (lane 1). Lanes 4 to 6 show a similar set, but in which the samples were incubated with Concanavalin-A and proteins bound to it were eluted and resolved by SDS-PAGE. The left panel (lanes 7 to 9) show the TCA precipitations of the supernatants of the Concanavalin A incubations. Sec61 antibody was used for protein detection. **B)** SDAD crosslinking pattern in the presence of exogenous ATP (5 mM) in SEC61 and sec61ΔL7 backgrounds.

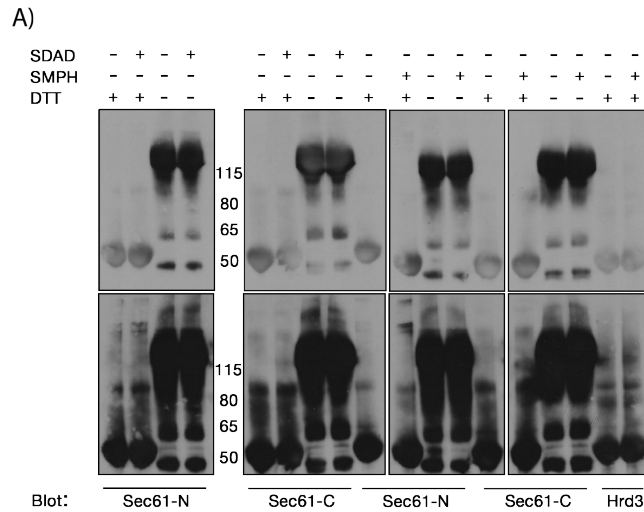


Figure A.4: Immunoprecipitation of SMPH crosslinking samples. Samples were crosslinked either with SDAD (1.5 mM) or SMPH (1 mM) and immunoprecipitated with a range of antibodies (10 μ l): α -Sec61-N, α -Sec61-C and α -Hrd3. Protein was then detected by immunoblotting using a Sec61 specific antibody. Two exposures are shown (shorter: upper panel; longer: bottom panel). For each different immunoprecipitation, two replicas were made: one where the sample was reduced before SDS-PAGE (DTT) and another where it was not.

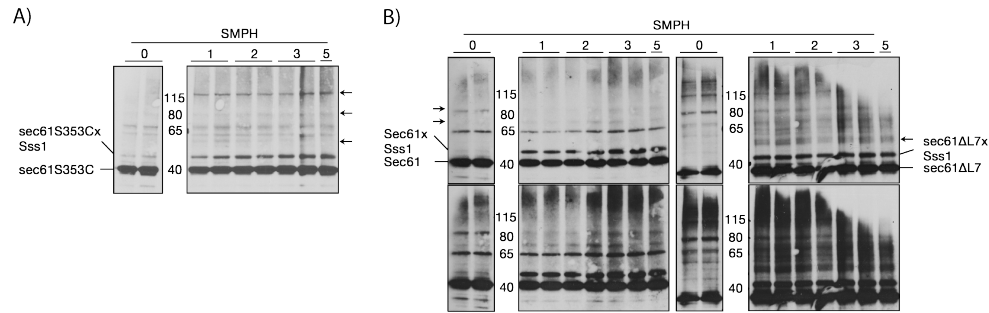


Figure A.5: Sec61 SMPH concentration titration. ER vesicles (17eq) were crosslinked with different amounts of SMPH for 30 min on ice, quenched for 15 min, and analyzed by SDS-PAGE on 4-12 % Bis-Tris gels (NuPAGE® Novex® Pre-Cast gels, Invitrogen). Protein detection was done by western blotting and signal acquired in ECL film. **A)** SMPH concentration titration on a *sec61S353C* background. **B)** SMPH concentration titration on a *SEC61* (leftmost panels) and a *sec61ΔL7* (rightmost panels) background. Both top and lower panels shows the same gel slices, just with different exposure times. Lower panels represents longer exposure.

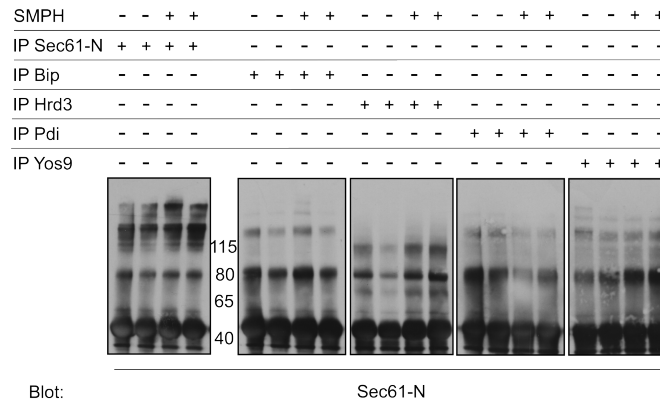


Figure A.6: SMPH crosslinking pattern determination by multi-antibody immunoprecipitation. ER vesicles (17eq) were crosslinked with 1 mM of SMPH for 30 min on ice, and quenched for 15 min. After solubilization, the samples were submitted to an immunoprecipitation with one of the following antibodies: α -Sec61-N, α -Bip, α -Hrd3, α -Pdi, or α -Yos9. For this purpose, solubilizations were incubated for either 2 h at room temperature or over night at 4 °C, under rotation, with 10 μ L of the specific antibody and 60 μ L of ProteinA-Sepharose. Sepharose beads were washed, sample eluted with 2xLaemmli Buffer, and analyzed by SDS-PAGE on 4-12 % Bis-Tris gels (NuPAGE® Novex® Pre-Cast gels, Invitrogen). Protein detection was done by western blotting using the Sec61 antibody, and signal acquired in ECL film.

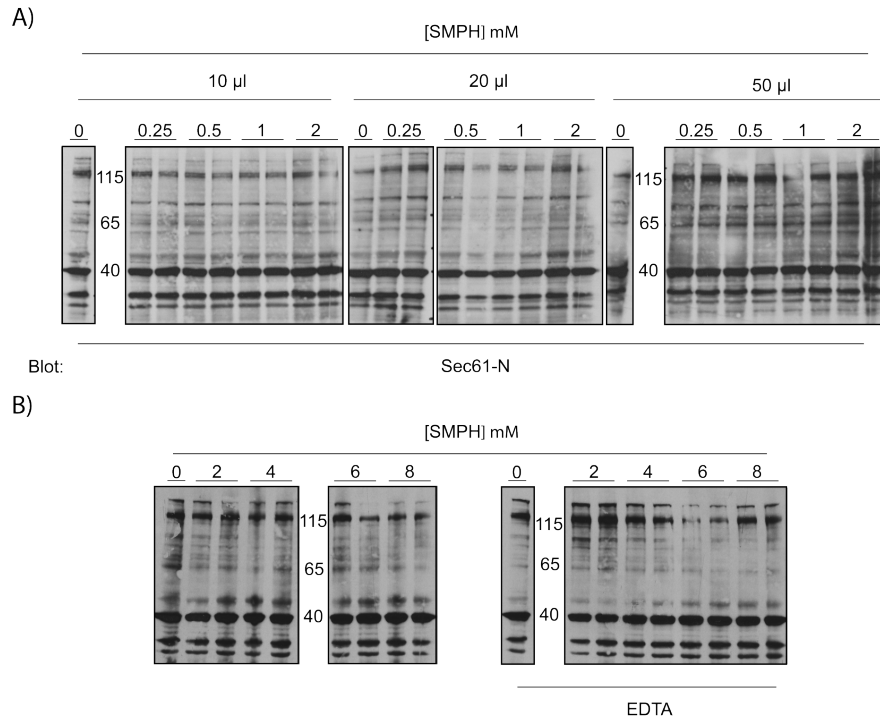


Figure A.7: Sec61 SMPH crosslinking pattern determination in permeated cells. Cells were permeabilized by liquid Nitrogen lysis, and crosslinked with different amounts of SMPH, solubilized and resolved by SDS-PAGE on 4-12 % Bis-Tris gels (Nu-PAGE® Novex® Pre-Cast gels, Invitrogen). A) Crosslinking of semi-permeated cells. Reactions were done in a total volume of 100 μ l and 10, 20 or 50 μ l of permeated cells were used. B) SMPH crosslinking of semi-permeated cells in the presence of EDTA.

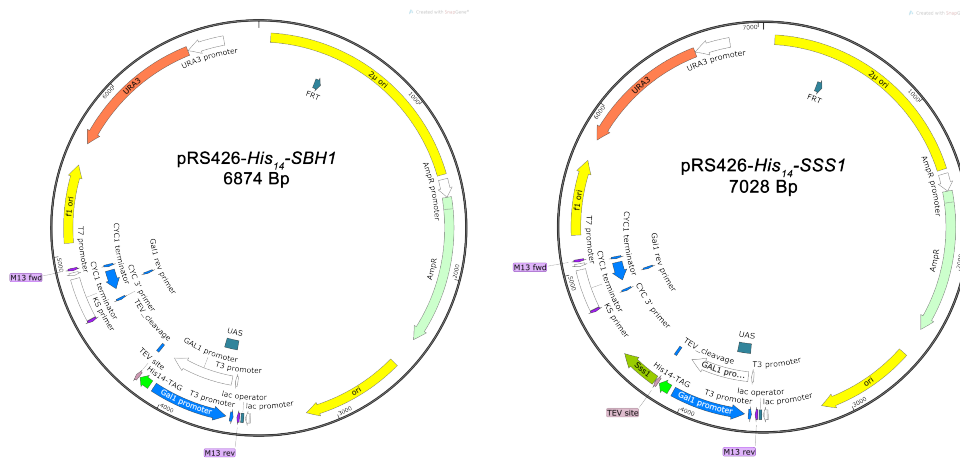


Figure A.8: Constructs obtained by cloning into pRS426-GAL-*His*₁₄. Maps of the construct generated by cloning *SBH1* and *SSS1* into pRS426-GAL-14*His*-TEV. pRS426-*His*₁₄-*SEC61* on the left and pRS426-*His*₁₄-*sec61S353C* on the right.

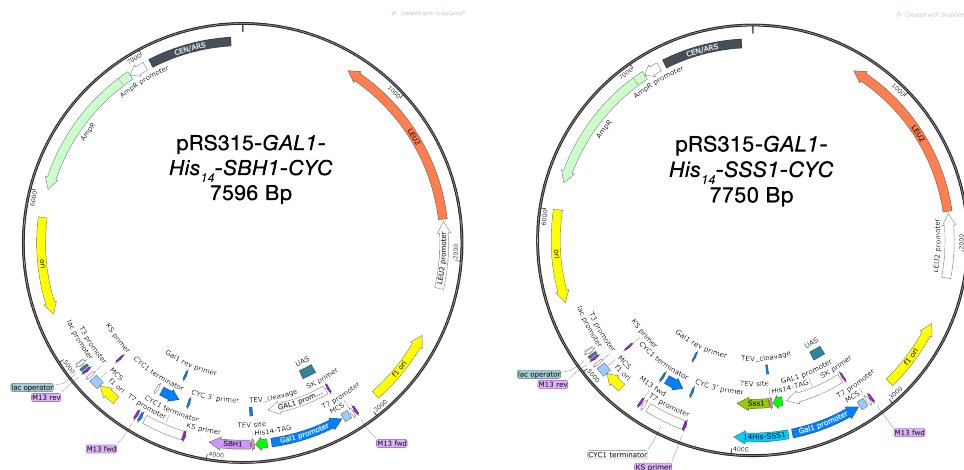


Figure A.9: Constructs obtained by subcloning 14His-tagged constructs into pRS315. Maps of the construct generated by subcloning GAL1-14His-SBH1-CYC1 (left) and GAL1-14His-SSS1-CYC1 (right) into pRS315.

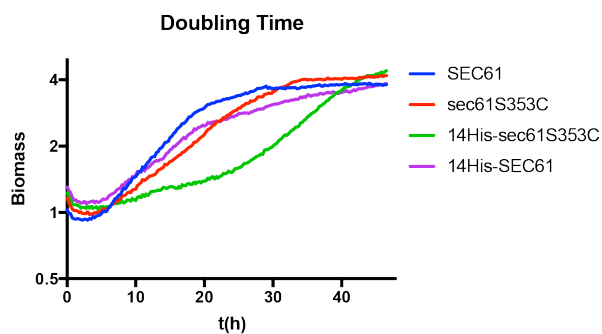


Figure A.10: Growth rate of 14His-tagged mutants in minimal medium. Cells were grown overnight in liquid SC -LEU medium (Gal 2%, 0.2% Glu), diluted in the same type of medium to an OD_{600} of 0.02 and 1 ml of culture applied per well (5 x 1 ml per strain) in a FlowerPlate. The plate was then incubated in the microreactor Biolector at 30°C, with 1200rpm, 85% humidity and 20.95% O_2 , for 48h. Calibration was done at 320nm, and biomass determination at 620nm using Filter 15. Readings were done each 15 min. In the figure we can see the plotted results, after averaging. Shown biomass values are in the log scale. SEC61 in blue, sec61S353C in red, 14His-SEC61 in green, and 14His-sec61S353C in magenta.

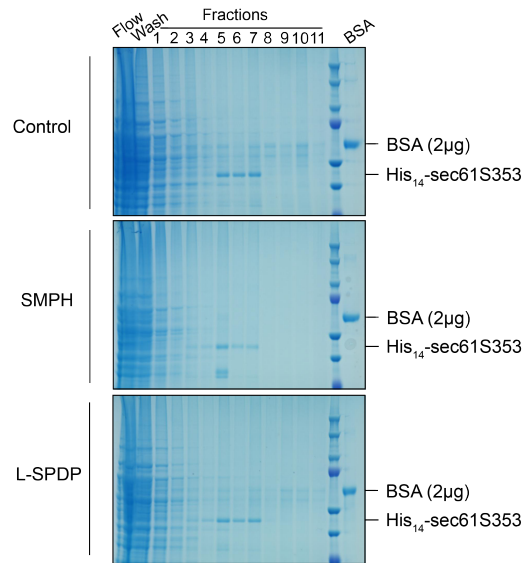


Figure A.11: Protein total amount after purification. Purification of His₁₄-sec61S353c after different treatments: Control (upper panel), SMPH crosslinking (middle panel), and LC-SPDP (bottom panel). For each set, 500 eq of microsomes were treated either with DMSO (control) or 1 mM crosslinker (SMPH or LC-SPDP), quenched, solubilized and Purified using the bofere described system (BioLogic; Biorad) along an imidazole gradient. The different fractions were TCA precipitated, incubated with DTT and resolved by SDS-PAGE on 4-12 % Bis-Tris gels (NuPAGE® Novex® Pre-Cast gels, Invitrogen). For protein detection, gels were stained with Coomassie G-250. Besides the different fraction a loading control of 2 µg of BSA was also loaded in each gel (lane 15).

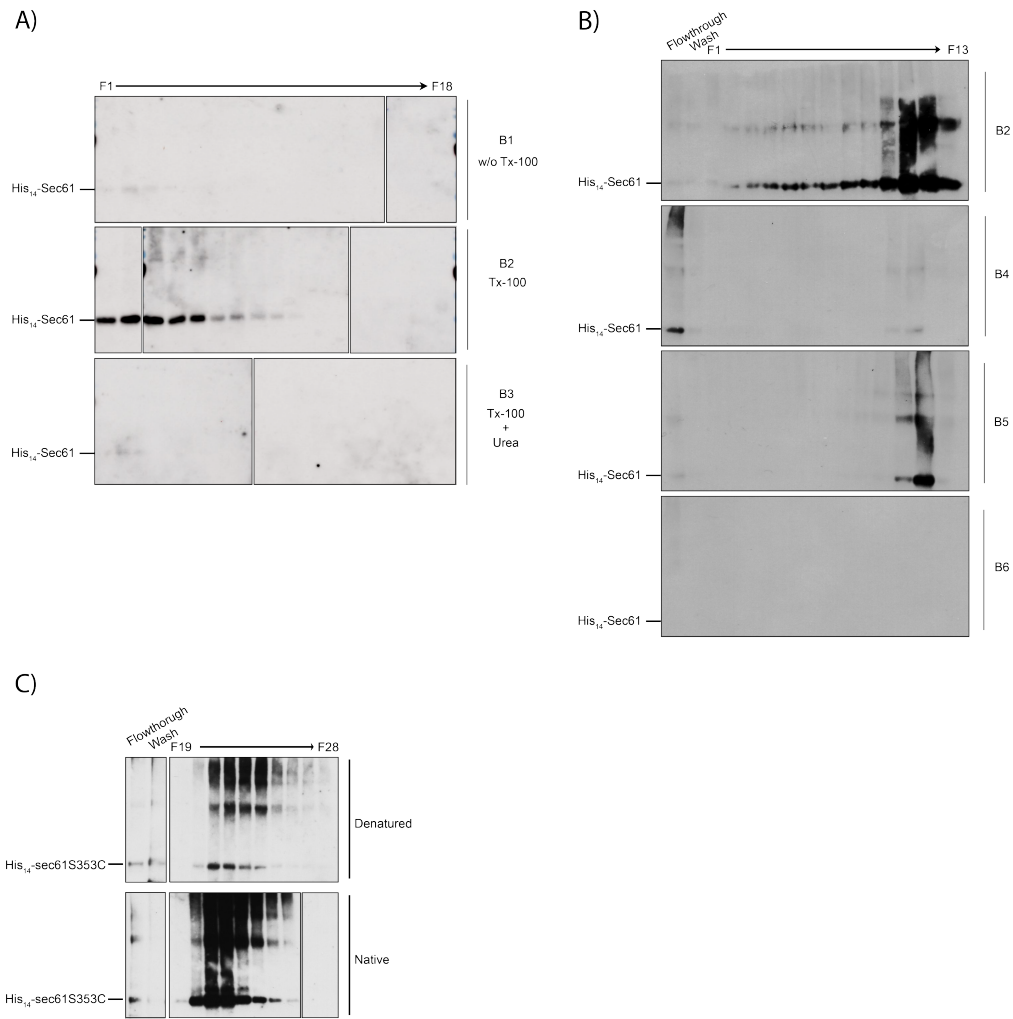


Figure A.12: Purification buffers test. On an automated purifications system, several buffer compositions (Binding Buffer/Elution Buffer) were tested. The default 50 mM Tris-HCl, pH 7.4 / 300 mM KCl / 40 mM Imidazole (B1) buffer was used as the baseline conditions. Samples were eluted along a imidazole gradient (100-500mM) using the same base-buffer as the correspondent Binding Buffer being tested. Samples were TCA precipitated and resolved by SDS-PAGE on 4-12 % Bis-Tris gels (NuPAGE® Novex® Pre-Cast gels, Invitrogen). Protein detection was done using an anti-Sec61 antibody. **A)** Comparison of the purification pattern obtained when using either the default buffer (B1; upper panel), the same buffer supplemented with 0.5 % of TritonX-100 (B2; middle panel), or with 0.5 % of TritonX-100 and 4 M Urea (B3; bottom panel). **B)** Comparison of the purification pattern obtained when using either the TritonX-100 supplemented buffer (0.5 %)(B2; upper panel), a B2-based buffer further supplemented with 1 % (B4; second panel from the top), and buffer based on B4 further supplemented with 4 M (B5; Second panel from the bottom) or 8M (B6; bottom panel) of urea, while in both cases reducing the KCl to 150 mM. **C)** Comparison of the purification pattern obtained using B2-like buffers for purification either under denaturing (upper panel) or native (bottom panel) conditions.

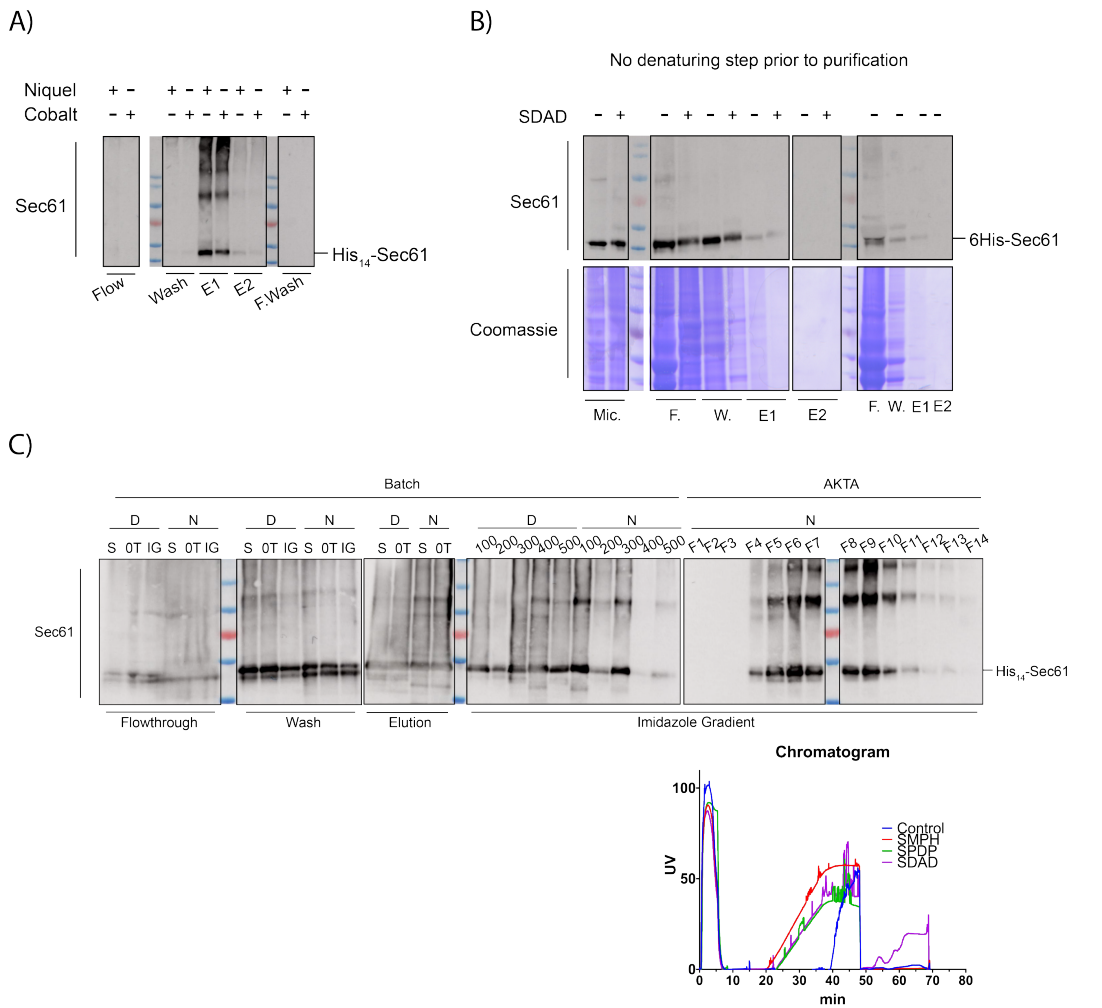


Figure A.13: Purification system test. Several affinity purification systems and strategies were tested. **A)** Test of the better resin charging cation in a batch setup. Two different cations were tested: Ni^{2+} and Co^{2+} . Samples (microsomes; 50 eq) were solubilized and incubated with either a Ni^{2+} (Ni Sepharose) or Co^{2+} (Talon® Superflow) charged resins and eluted with Elution Buffer (50 mM Tris-HCl, pH 7.4 / 300 mM KCl / 0.5 % TritonX-100 / 500 mM Imidazole). **B)** The purification efficiency of the batch setup in crosslinking conditions was also tested. Microsomes (50 eq) were either treated with DMSO (control) or SDAD, and submitted to the batch purification setup. Flow through (F), Wash (W), first Elution (E1), and second Elution (E2) fractions were TCA precipitated and resolved by SDS-PAGE. A set of standard SDAD crosslinking reactions (17 eq) were also solubilized and TCA precipitated (Mic.) to serve as the baseline for sample complexity. The sample was either immunoblotted against Sec61 (upper panel) or stained with Coomassie Brilliant Blue (bottom panel). **C)** The use of denaturing or native conditions for sample preparation was also tested. For the batch purification setup (Batch), sample was purified using either deanturing (D) or native (N) conditions. Purification was done either by simple elution (500 mM Imidazole (Elution) or along an Imidazole gradient (100-500 mM). Each fraction was resolved by SDS-PAGE and immunoblotted against Sec61. For the automated purification setup (AKTA) only native conditions (N) were used and elutions was doen only along an imidazole gradient (100-500 mM; rightmost panels) An typical chromatogram obtained during a automated purification setup is shown below the immunoblot panel.

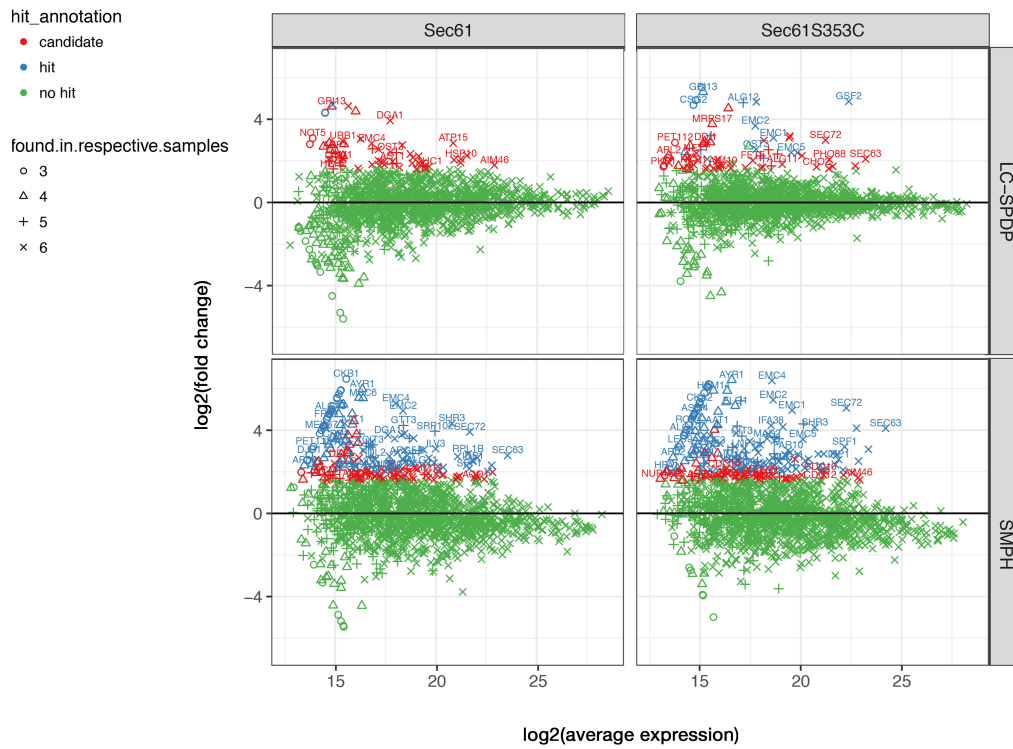


Figure A.14: Mass spectrometry statistical analysis MA plot. An MA plot (plot displaying a difference in expression patterns between the average intensities of two samples) was done by plotting each hit enrichment (\log_2 fold change) in function of its sample absolute amounts in the sample (\log_2 average expression). The above plots represent the difference of enrichment when the differently crosslinked samples (Sec61 and sec61S353C) were compared to the control samples (uncrosslinked sec61S353C).

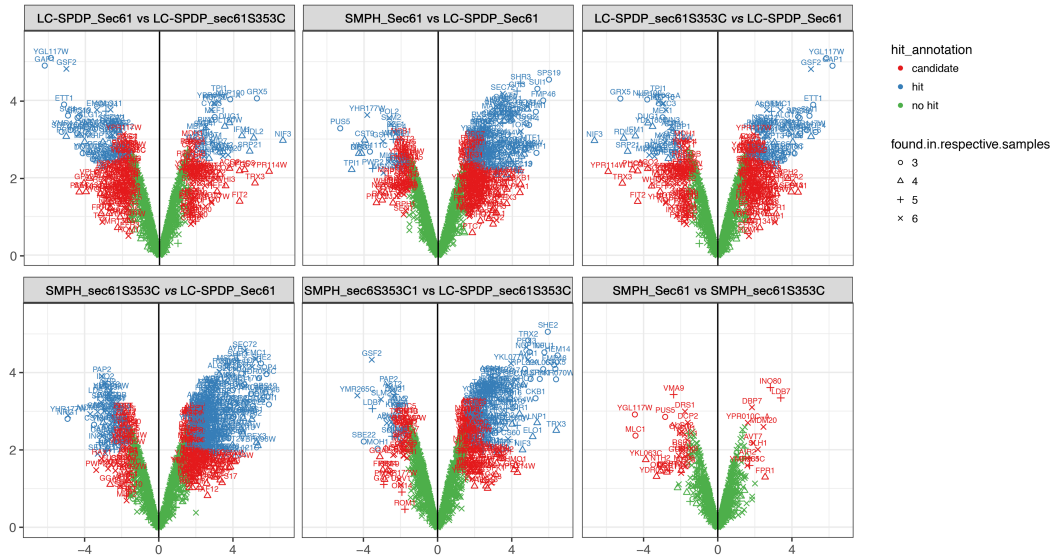


Figure A.15: Secondary comparisons Volcano plots. Volcano plots based on the statistically determined protein enrichment in the crosslinked samples (His14-Sec61 and His14-Sec61S353C) when compared between each other. The horizontal axis represents \log_2 fold change (\log_2FC) reflecting level of enrichment. The vertical axis plots the $-\log_{10}(pValue)$ of enrichment, reflecting significance. Both hits (blue) and candidates (red) have a fold change of at least 3. Hits have a false discovery rate (fdr) < 5 % and candidates an FDR < 20 %. Purple line is at fold-change of 3. Not significant hits below threshold in green.

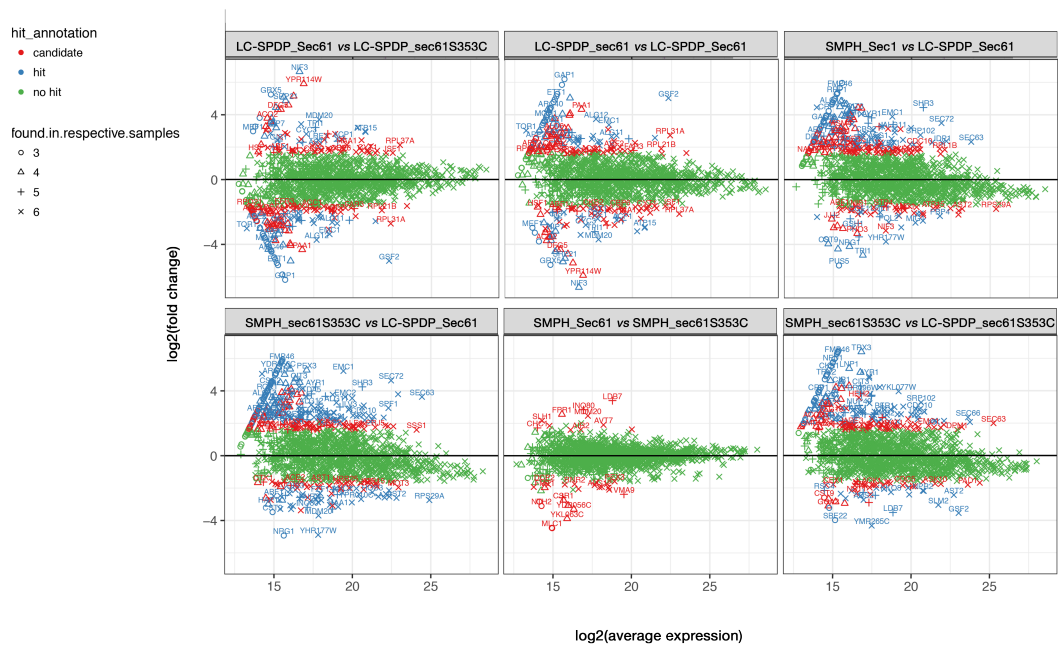


Figure A.16: Secondary comparisons MA plots. An MA plot (plot displaying a difference in expression patterns between the average intensities of two samples) was done by plotting each hit enrichment (\log_2 fold change) in function of its sample absolute amounts in the sample (\log_2 average expression). The above plots represent the difference of enrichment when the differently crosslinked samples (Sec61 and sec61S353C) were compared to each other in different combinations.

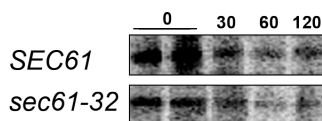


Figure A.17: Nsg1 degradation dynamics analysis. Wildtype and mutant strains were pulse-labeled with $[^{35}\text{S}]$ -met/cys for 15 min, followed by chase incubations for the indicated times. For each time point 1.5 OD₆₀₀ of cells were lysed and proteins immunoprecipitated using an anti-HA antibody (Biomol). After SDS-PAGE, proteins were detected by phosphorimaging.

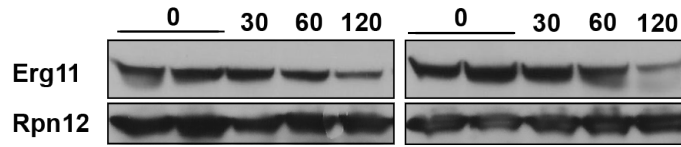


Figure A.18: Erg11 degradation dynamics analysis by cycloheximide chase. Wildtype and mutant strains were grown to a maximum OD₆₀₀ of 1, cycloheximide (100 µg/ml) was added, zero time point taken washed with Tri-Azide. Cultures were incubated at 30°C, 220 rpm and shown time point taken and treated as the zero time points. Each time point was lysed and resolved by SDS-PAGE. Proteins were detected by immunoblotting using an anti-HA antibody (Biomol) and signal was acquired in ECL film.